The role of inflammation in retinal ischaemia

Senthil Selvam

UCL

Thesis submitted in fulfilment of the requirements for the degree of

Doctor of Philosophy

Supervised by Professor Marcus Fruttiger

2018

I, Senthil Selvam confirm that the work presented in this thesis is my own. Where information has been derived from other sources, I confirm that this has been indicated in the thesis.

Dr Senthil Selvam 7th August 2018

Acknowledgements:

I would like to thank my supervisor Marcus Fruttiger for allowing me the opportunity to undertake my PhD in his laboratory at The UCL Institute of Ophthalmology, as well as for his support, guidance and mentoring.

Thanks go to Dr Michael Powner who has acted as my post-doc throughout the duration of my PhD offering guidance, advice and tuition.

Thanks also go to members of the lab group and the associated clinical team at Moorfield's Eye Hospital for their support and guidance.

Dr Sidath Liyanage is acknowledged for his help and advice performing and analysing the flow cytometry experiments presented in this report.

RNA sequencing presented in this report was performed by Tony Brooks at the UCL Institute of Child Health and the created files were sent to Monte Radeke, at the Neuroscience Research Institute (NRI), University of California Santa Barbara for alignment.

And finally I'd like to thank my family and my fiancée for all their support.

Abstract:

Purpose: The immune cascade is known to contribute to the pathology seen in oxygen induced retinopathy (OIR), however its exact role is poorly defined. We hypothesised that immune cell activation worsens hypoxia and exacerbates the neovascular sequelae seen in ischaemic retinopathy.

Methods: We assess the effect of intraperitoneal lipopolysaccharide (IP LPS) injection in OIR mice. Neovascularisation was assessed by measuring the avascular area and neovascular tuft area at P17. Hypoxia was assessed using vessel tortuosity and EF5 hypoxia staining at P14. The activated retinal inflammatory cell population was characterised using immunohistochemistry and flow cytometry. Transgenic mice were bred to delete different subpopulations of inflammatory cells to define their role in hypoxia modulation. RNA sequencing performed on retinal tissue analysed the effect of systemic LPS on retinal cytokines and angiogenesis markers.

Results: IP LPS injection at P12 in OIR mice significantly reduced neovascularisation at P17 and hypoxia at P14. Immunohistochemistry revealed an influx of round, CD11b+, lectin stained cells into the retina of LPS treated mice, which on flow cytometry were identified as myeloid cells, being predominantly Cd11b+Ly6Ghi neutrophils. Experimental depletion of the myeloid lineage was achieved using ROSA26eGFP-DTALysMcre, CCL2 and CCR2 knockout mouse lines and anti-CCR2 antibody MC21. However, when these mice were LPS treated, the effects on hypoxia readouts caused by LPS were still seen. Transcriptional profiling of the retina (using RNAseq) revealed a large upregulation in IL1β in the central, hypoxic retina of LPS treated mice. Injection

of IL1β at P12 also mimicked the effects of LPS, suggesting that IL1β is a key mediator of the hypoxia reducing effect LPS has in the OIR model.

Conclusions: These findings are counterintuitive to the current literature and provide new insight into the role the immune system has on regulating oxygen demand in the retina. This novel approach to reducing hypoxia has the potential to lead to novel therapies targeting hypoxia and preventing neovascularisation in ischaemic eye disease.

Impact Statement:

I believe that the research presented in this thesis can provide a platform for a fundamentally novel therapeutic approach for vascular complications in ischemic eye disease.

This approach is based on reducing the amount of nutrients and oxygen that are consumed in the retina, rather than targeting the supply problem of insufficient vascularisation. This will achieve a reduction of angiogenic factors such as VEGF indirectly. The insights gained on the effect of IL1β on retinal metabolism and VEGF production can be used as a model system from which we can learn how retinal metabolism can be manipulated.

This endeavour will be aided by progress made in the cancer field. There, targeting cellular metabolism has emerged as a promising therapeutic strategy in recent years. Because retinal metabolism resembles that of tumours (both are dominated by glycolysis) we can benefit from insights and tools (e.g. chemical inhibitors of glycolytic enzymes) that have been developed in cancer biology but that might also be useful in ophthalmology. Moreover, this approach might impact in fields beyond ischemic eye disease, such as cerebral vascular disease, ischemic heart disease and peripheral vascular disease.

Clinical benefits will be indirect, as the presented work here is basic scientific research. Nevertheless, once the underlying mechanisms have been identified in future work derived from this project, translational work aiming to manipulate metabolic activity can start.

Work from this thesis has been presented at international ophthalmic research conferences and planned for planned for publication in peer reviewed journals.

Contents

The Role of Inflammation in Retinal Ischaemia 1

Acknowledgements:.....3

Abstract:.....4

Impact Statement:.....6

Contents.....8

List of tables.....14

List of figures.....16

Abbreviations:.....20

1. Introduction.....22

1.1 Vascular Development.....22

1.1.1 Angiogenesis versus Vasculogenesis.....22

1.2 Development of the retinal vasculature.....24

1.2.1 Physiological Development of the Retinal Astrocyte Foundation.....24

1.2.2 Pathological Development of the Retinal Astrocyte Foundation.....28

1.2.3. Physiological Development of the Primary Plexus.....29

1.2.3.1 Sprouting Angiogenesis.....29

1.2.3.2 Role of Vasculature Endothelial Growth Factor in Angiogensis.....30

1.2.3.3 Vascular Remodelling.....35

1.2.4.2 Vessel Maturity and Susceptibility to Hyperoxia.....36

1.2.4. Pathological Development of the Primary Plexus.....37

1.2.4.1 The oxygen induced retinopathy model.....37

1.2.4.3 Pathological neovascularisation versus physiological angiogenesis.....39

1.3. Inflammation.....41

1.3.1 Innate versus adaptive Immunity.....41

1.3.2 Toll-like receptor 4 activation by Lipopolysaccharide.....43

1.3.3 Phagocytic cells of the innate immune response.....46

1.3.3.1 Monocytes and Macrophages.....46

1.3.3.2 M1/M2 Polarisation of Macrophages.....47

1.3.3.3 Neutrophils.....50

1.3.4 Inflammation in ischaemia retinopathy.....51

1.4 Thesis Aims.....52

2. Materials and Methods:.....53

2.1 - Mice.....53

2.2 – Oxygen Induced Retinopathy Model.....55

2.3 – Intraperitoneal Injections.....56

2.3.1 - Lipopolysaccharide Injections.....57

2.3.2 – Interleukin 1 Beta Injections.....57

2.3.3 – MC21 (anti mouse CCR2) Injections.....57

2.4 – Intraocular Injections.....58

2.4.1 – Interleukin 1 Beta Injections.....58

2.4.2 – CCL5 Injections.....59

2.4.2 – Vehicle Injections 59

2.5 – Retinal Wholemount Preparation 59

2.6 - Immunohistochemistry 60

2.6.1 – EF5 Hypoxia Staining 61

2.6.2 – BrDU Proliferation Staining 61

2.7 – Retinal Wholemount Imaging 63

2.8 – Image J Retinal Wholemount Analysis 63

2.8.1 – Avascular Area Analysis 64

2.8.2 – Vessel Tortuosity Analysis: Tortuosity Index and Integrated Curvature 64

2.8.3 – Hypoxia Analysis: EF5 Hypoxic Area, Hypoxic Intensity and Hypoxic Density 66

2.8.4 – Neovascular Area 66

2.8.5 – Cell Counting 67

2.8.6 – Statistical Analysis 67

2.9 – Flow Cytometry 68

2.9.1 – Mice 68

2.9.2 – Tissue Preparation 68

2.9.3 – Flow Cytometry Staining 68

2.9.4 – Data Acquisition 69

2.9.5 – Data Analysis 70

2.10 – RNA Sequencing 70

2.10.1 - Mice 70

2.10.1 – Retinal RNA and Wholemount Preparation.....71

2.10.2 – RNA Extraction 71

2.10.3 – RNA Sequencing.....72

3. Results: 74

3.1 The effect of inflammation in ischaemic retinopathy on hypoxia and neovascularisation.....74

3.1.1 The effect of systemic LPS injection on neovascularisation at P17 in OIR ...74

3.1.2 The effect of systemic LPS injection on hypoxia at P14 in OIR.....81

3.1.3 - Systemic LPS injection appears to reduce proliferation at P14 in OIR.....87

3.1.4 – The effect of systemic LPS injection on hypoxia in TLR4 deficient mice at P14 in OIR.....93

3.2 Systemic Inflammation induces an invasion of inflammatory cells into hypoxic areas of ischaemic retina..... 104

3.2.1 Inflammatory cells which invade into hypoxic retinas of mice treated systemically with LPS are of myeloid origin..... 104

3.2.2 Myeloid cells which invade into hypoxic retinas of mice treated systemically with LPS are predominantly neutrophils 114

3.3 The role of invading myeloid population on hypoxia in ischaemic retina 118

3.3.1 The effect of depleting invading myeloid population seen in LPS treated OIR retinas on hypoxia in LysmCreDTA mice 118

3.3.2 The effect of depletion of the invading immune cell population seen in LPS treated OIR retinas on hypoxia in CCL2 and CRR2 knockout mice 130

3.3.3 The effect of depletion of invading CCR2+ cells seen in LPS treated OIR retinas on hypoxia in anti-CRR2 treated mice 142

3.4 Systemic LPS injection modulates retinal hypoxia and metabolism through cytokine signalling 154

3.4.1 Systemic LPS injection as a modulator of retinal hypoxia. 155

3.4.2 Systemic LPS Injection as a modulator of retinal metabolism. 157

3.4.3 Systemic LPS Injection as a modulator of cytokine expression in the retina. 158

3.5 The effect of IL1β in ischaemic retinopathy on hypoxia and neovascularisation 159

3.5.1 The effect of intraocular injections of IL1β, CCL5 and vehicle on hypoxia at P14 in OIR..... 159

3.5.2 Intraocular injections of IL1β and vehicle reduce neovascularisation at P17 in OIR..... 174

3.5.3 Systemic injection of IL1β reduces hypoxia at P14 in OIR..... 184

4. Discussion: 190

4.1 Inflammation in ischaemic retinopathy reduces hypoxia and neovascularisation 190

4.2 Systemic Inflammation induces an invasion of myeloid derived neutrophils and monocyte/macrophages into hypoxic areas of retina. 197

4.3 The invasion of myeloid derived neutrophils and monocyte/macrophages are not responsible for the reduction in hypoxia 199

4.4 Systemic LPS injection modulates retinal hypoxia and metabolism through cytokine signalling..... 203

4.5 IL1β in ischaemic retinopathy reduces hypoxia and neovascularisation 206

4.6 Future Work..... 212

4.7 Outlook 213

4.8 Conclusion..... 214

8. References..... 216

List of tables

Table 2.1. Mice strains used with details of suppliers and phenotypes. 55

Table 2.2. List of antibodies, suppliers and dilutions used. 63

Table 3.1 – Statistical Comparison of P17 OIR PBS vs LPS treatment groups.....77

Table 3.2 – Statistical Comparison of P14 OIR PBS vs LPS treatment groups.....83

Table 3.2.1 – Statistical Comparison of P14 OIR PBS vs LPS treatment groups.....92

Table 3.3 – Statistical Comparison of TLR4 deficient P14 OIR PBS vs LPS treatment groups.....95

Table 3.4 – Statistical Comparison of C3H Rd1 mice P14 OIR PBS vs LPS treatment groups..... 100

Table 3.5 Statistical comparison of inflammatory cell populations at P14 OIR in PBS vs LPS treatment groups..... 112

Table 3.6 – Statistical Comparison of P14 LysMCreDTA P14 OIR & LPS WT vs Tg groups 121

Table 3.7 – Statistical Comparisons of P14 LysMCreDTA Tg OIR PBS vs LPS treatment groups..... 126

Table 3.8 – Statistical Comparisons of P14 $CCR2^{-/-}$ OIR PBS vs LPS treatment groups 132

Table 3.9 – Statistical Comparisons of P14 $CCL2^{-/-}$ OIR PBS vs LPS treatment groups138

Table 3.10 – Statistical Comparisons of P14 OIR & LPS Control vs MC21 treatment groups..... 148

Table 3.11 – Statistical Comparisons of P14 OIR & MC21 PBS vs LPS treatment groups 149

Table 3.12– Statistical Comparisons of P14 CCL5 control vs injected treatment groups 164
Table 3.13 – Statistical Comparisons of P14 IL1β control vs injected treatment groups 169
Table 3.14 – Statistical Comparisons of P14 vehicle control vs injected treatment groups..... 170
Table 3.15 – Statistical Comparisons of P17 IL1β control vs injected treatment groups 179
Table 3.16 – Statistical Comparisons of P17 vehicle control vs injected treatment groups..... 180
Table 3.17 – Statistical Comparisons of P14 vehicle vs IL1β treatment groups 185

List of figures

Figure 1.1 – Angiogenesis versus Vasculogenesis.....23

Figure 1.2 – Role of retinal astrocytes in angiogenesis.....27

Figure 1.3 – The tip stalk phenotype in sprouting endothelial cells.....31

Figure 1.4 – Vascular remodelling.....36

Figure 1.5 - Phases of the OIR model.....38

Figure 1.6 - Neovascularisation.....40

Figure 1.7 - Neovascularisation.....44

Figure 1.8 - Overview of the pattern-recognition receptor system of phagocytes, including the TLR family.....45

Figure 1.9 – M1/M2 Macrophage activation and polarisation.....48

Figure 1.10 – Neutrophil macrophage interaction during the innate immune response 49

Figure 2.1 - Avascular Area Analysis. 64

Figure 2.2 - Vessel Tortuosity Analysis: Tortuosity Index and Integrated Curvature. ..65

Figure 2.3 - Hypoxia Analysis: EF5 Hypoxic Area. 66

Figure 2.4 – Neovascular Area Analysis. 67

Figure 3.1 – Intraocular injection of LPS results in retinal inflammatory reaction and reduced pathological neovascularisation 75

Figure 3.2(a) – Intraperitoneal injection of LPS at P12 after hyperoxia leads to reduced neovascular phenotype at P17 in OIR.....78

Figure 3.2(b) - Intraperitoneal injection of LPS at P12 after hyperoxia leads to reduced neovascular phenotype at P17 in OIR.....79

Figure 3.2(c) - Intraperitoneal injection of LPS at P12 after hyperoxia leads to reduced neovascular phenotype at P17 in OIR. 80
Figure 3.3(a) – Intraperitoneal injection of LPS at P12 after hyperoxia leads to reduced hypoxia at P14 in OIR. 84
Figure 3.3(b) – Intraperitoneal injection of LPS at P12 after hyperoxia leads to reduced hypoxia at P14 in OIR. 85
Figure 3.3(c) - Intraperitoneal injection of LPS at P12 after hyperoxia leads to reduced hypoxia at P14 in OIR. 86
Figure 3.4(a) - Intraperitoneal injection of LPS at P12 after hyperoxia leads to reduced proliferation at P14 in OIR 88
Figure 3.4(b) - Intraperitoneal injection of LPS at P12 after hyperoxia leads to reduced proliferation at P14 in OIR. 89
Figure 3.5(a) - Intraperitoneal injection of LPS at P12 after hyperoxia leads to Erg staining of the retinal ganglion cell axons in the avascular area at P14 in OIR 90
Figure 3.5(b) - Intraperitoneal injection of LPS at P12 after hyperoxia does not affect retinal thickness at P14 in OIR 92
Figure 3.5(c) - Intraperitoneal injection of LPS at P12 after hyperoxia does not affect retinal thickness at P14 in OIR 93
Figure 3.6(a) – Intraperitoneal injection of LPS at P12 in C3H TLR4 deficient mice after hyperoxia does not change hypoxia seen at P14 in OIR. 96
Figure 3.6(b) – Intraperitoneal injection of LPS at P12 in C3H TLR4 deficient mice after hyperoxia does not change hypoxia seen at P14 in OIR. 97
Figure 3.6(c) Intraperitoneal injection of LPS at P12 in C3H TLR4 deficient mice after hyperoxia does not change hypoxia seen at P14 in OIR. 98

Figure 3.7(a) – Intraperitoneal injection of LPS at P12 in C3H mice after hyperoxia does not change hypoxia seen at P14 in OIR. 101
Figure 3.7(b) – Intraperitoneal injection of LPS at P12 in C3H mice after hyperoxia does not change hypoxia seen at P14 in OIR. 102
Figure 3.7(c) Intraperitoneal injection of LPS at P12 in C3H mice after hyperoxia does not change hypoxia seen at P14 in OIR. 103
Figure 3.8(a) – GFP expression in LysMCre Reporter Mice at P6 and during the vaso-obliterative stage of the OIR model at P10 106
Figure 3.8(b) – GFP expression in LysMCre Reporter Mice at P12 following vasobliteration. 107
Figure 3.9(a) - Intraperitoneal injection of LPS at P12 after hyperoxia leads to influx of GFP expressing peripheral myeloid cells in LysMCre reporter mice retina at P14 in OIR 108
Figure 3.9(b) - Intraperitoneal injection of LPS at P12 after hyperoxia leads to influx of GFP expressing peripheral myeloid cells in LysMCre reporter mice retina at P14 in OIR 109
Figure 3.10 - Intraperitoneal injection of LPS at P12 after hyperoxia leads to influx of lectin positive, IBA1 negative cells in the avascular area at P14 in OIR 111
Figure 3.11(a) - Intraperitoneal injection of LPS at P12 after hyperoxia leads to influx of Cd11b, lectin positive, IBA1 negative cells in the avascular area at P14 in OIR 113
Figure 3.11(b) - Intraperitoneal injection of LPS at P12 after hyperoxia leads to influx of Cd11b, lectin positive, IBA1 negative cells in the avascular area at P14 in OIR 114
Figure 3.12 – Flow cytometry using a myeloid panel of cell surface markers highlights a large increase in neutrophils in the retina of OIR mice at P14 in the LPS group. 117

Figure 3.14(c) – No difference in hypoxia is seen at P14 between LysMCreDTA WT and Tg mouse pups injected with LPS at P12 124

Figure 3.15(c) – Intraperitoneal injection of LPS at P12 after hyperoxia leads to reduced hypoxia in LysMCreDTA Tg mouse pups at P14 in OIR 129

Figure 3.17(b) – Intraperitoneal injection of LPS at P12 after hyperoxia leads to reduced hypoxia in CCR2$^{-/-}$ mouse pups at P14 in OIR 134

Figure 3.17(c) – Intraperitoneal injection of LPS at P12 after hyperoxia leads to reduced hypoxia in CCR2$^{-/-}$ mouse pups at P14 in OIR 135

Figure 3.23 – A selection of the RNA sequencing data to show the differences in gene expression between central and peripheral retina in a P14 control, PBS control and LPS treated mouse. 156

Figure 3.25(c) - 168

Figure 3.26(c) - 173

Figure 3.27(c) – Intraocular injection of IL1β at P12 after hyperoxia leads to reduced neovascular phenotype at P17 in OIR. 178

Figure 3.28(c) – Intraocular injection of vehicle at P12 after hyperoxia leads to reduced neovascular phenotype at P17 in OIR..... 183

Figure 3.29(c) –..... 188

Abbreviations:

ALK	activin receptor-like kinase
AMP	antimicrobial peptides
Ang	angiopoietin
AP-1	activating protein-1
Apln	apelin
BMP	bone morphogenetic protein
BrdU	5-bromo-2'-deoxy-uridine
CCL	chemokine ligands
Cdc42	cell division control protein 42
CXCL	chemokine C-X-C motif ligands
DCC	deleted in colorectal cancer
DEPC	diethyl pyrocarbonate
Dll4	delta-like ligand 4
DTA	diphtheria toxin fragment A
G-CSF	granulocyte colony-stimulating factor
GM-CSF	granulocyte–macrophage colony-stimulating factor
GFAP	glial fibrillary acidic protein
HIF	hypoxia-inducible factor
IgG	immunoglobulin G
ICAM-1	intercellular adhesion molecule-1
IFNβ	interferon-beta
IGF1	insulin-like growth factor 1
IL-1β	interleukin 1 beta
IL-6	interleukin 6
IL-8	inteterlukin 8
IVC	individually ventilated cages
KO	knock out
LIF	leukemia inhibitory factor
LIFR	leukemia inhibitory factor receptor
LPS	lipopolysaccharide

M1	microbicidal or inflammatory
M2	anti-inflammatory
MCP-1	monocyte chemoattractant protein-1
MMP	matrix metalloproteinases
mRNA	messenger ribonucleic acid
MyD88	myeloid differentiation primary response protein 88
NF-kB	nuclear factor for the kappa-light chain enhancer in B cells
NRP1	neuropilin-1
OIR	oxygen induced retinopathy
PAMP	pathogen associated molecular patterns
PFA	paraformaldehyde
PBS	phosphate buffered saline
PDGF	platelet derived growth factor
PDGFA	platelet derived growth factor A
PDGFRα	platelet derived growth factor receptor alpha
PlGF	platelet growth factor
PKM2	Pyruvate kinase M2
PRR	pattern recognition receptors
ROBO	roundabout
ROP	retinopathy of prematurity
TGF-β	transforming growth factor beta
TIR	toll/interleukin-1 receptor
TIRAP	toll/interleukin-1 receptor domain-containing adapter protein
TLR	toll-like receptor
TNFα	tumour necrosis factor alpha
TRAM	TRIF-related adapter molecule
TRIF	TIR domain-containing adapter-inducing interferon-beta
UNC 5B	uncoordinated 5B
VCAM-1	vascular cell adhesion molecule-1
VEGF	vascular endothelial growth factor
VEGFR	vascular endothelial growth factor receptor

1. Introduction

1.1 Vascular Development

1.1.1 Angiogenesis versus Vasculogenesis

To alleviate hypoxia, blood vessel formation occurs either via angiogenesis or vasculogenesis. Vasculogenesis is the process by which blood vessels form from angioblasts, which differentiate into endothelial cells once they migrate to the site of future vessels where they begin to form patent vessels **(Figure 1.1)**. This process is seen when the dorsal aorta and cardinal veins are formed during development (Risau and Flamme, 1995).

Angiogenesis is the process by which proliferating endothelial cells from already formed patent vessels proliferate in order to sprout and extend the already exiting vascular network (Risau, 1997). The endothelial cells are attracted by pro-angiogenic signals and in turn develop protruding filodopia which allow them to become mobile. The mobile cells are designated as tip cells and lead the new vessel into the surrounding environment directed by guidance cues **(Figure 1.1)** . On sensing hypoxia, the local environment produces pro-angiogenic signals such as vascular endothelial growth factor (VEGF), platelet growth factor (PlGF), and angiopoietin 1 (Ang1) to promote tip cells guided vessel growth (Carmeliet, 2003). The trailing stalk cells establish a lumen and proliferate to extend the sprouting vessel (Carmeliet and Jain, 2011). On the initiation of blood flow, a basement membrane forms and mural cells are recruited to stabilize the newly formed vessels in a process of vascular remodelling (Potente et al., 2011).

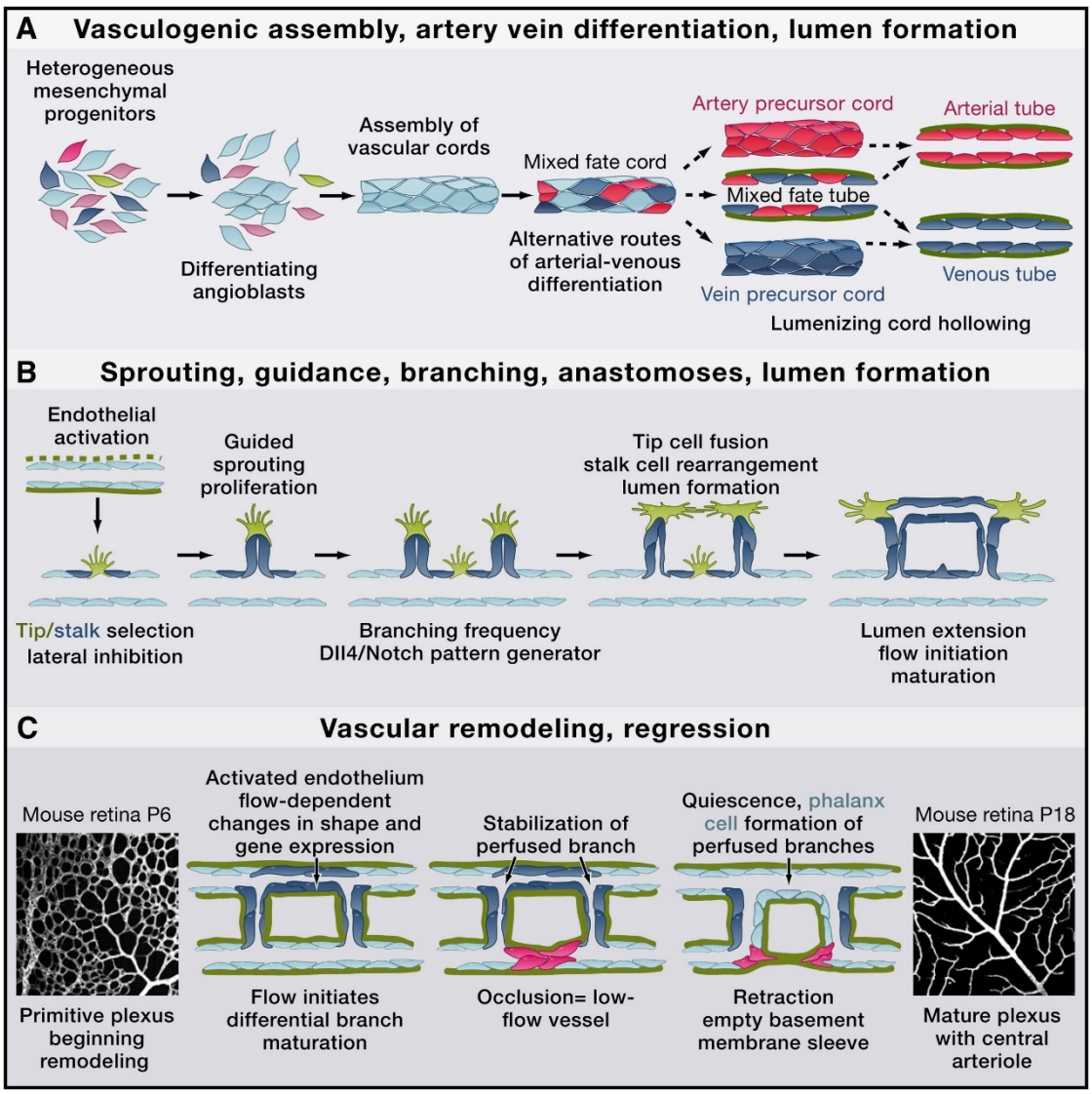

Figure 1.1 – Angiogenesis versus Vasculogenesis (Potente et al., 2011). *(A) Vasculogenesis mechanism. (B) Angiogenesis mechanism.*

The brain is predominantly vascularised through angiogenesis. In the retina, both angiogenesis and vasculogenesis have been reported in vascularisation. It has been suggested that suggested that the primary inner vascular plexus of the retina is formed by vasculogenesis, however more recent work has proved that the primary plexus forms by sprouting angiogenesis (Fruttiger, 2002).

The retinal vasculature functions to metabolically sustain the inner retina. The development of the retinal vasculature relies on highly coordinated signalling between various retinal cell types. During development internal metabolic requirements need

to be integrated with external influences such as oxygen and nutrient supply. When mechanisms such as sprouting angiogenesis, vascular network remodelling and vessel maturation are disrupted they can lead to vascular pathology.

1.2 Development of the retinal vasculature

1.2.1 Physiological Development of the Retinal Astrocyte Foundation

The development of the retinal vasculature is controlled through crucial interactions between retinal neurons, astrocytes and endothelial cells (Fruttiger et al. 1996; Fruttiger 2002; Watanabe & Raff 1988). During the formation of the superficial vascular plexus retinal blood vessels and astrocytes are intimately associated. The importance of this association is highlighted by the fact that retinal astrocytes are only found in the retina of species that possess a retinal vasculature (Schnitzer, 1987; Stone & Dreher, 1987). Furthermore, astrocytes are absent from avascular regions in these species (Engerman, 1976; Schnitzer, 1987; Huxlinet al., 1992), the primate fovea being a prime example (Gariano *et al.*, 1996).

In mice, astrocyte precursor cells from the optic nerve, that express Pax2 and vimentin (Chu, Hughes and Chan-Ling, 2001), develop into retinal astrocytes. These immature, elongated, spindle shaped astrocytes (Fruttiger, 2002) proliferate and migrate from the optic nerve head at around embryonic day 19, by which stage they express platelet derived growth factor receptor alpha (PDGFRα)(Mudhar et al. 1993; Fruttiger et al. 1996).

Platelet derived growth factor A (PDGFA), secreted by retinal ganglion cells, promotes astrocyte proliferation and migration from the optic nerve, along retinal ganglion cell axons in a centrifugal fashion across the inner retinal surface to the retinal periphery

(Fruttiger et al., 2000). Once they reach the retinal periphery, astrocytes continue to proliferate and create a mesh-like network that is fully developed by birth at embryonic day 21. It is this network that provides the template for retinal vascular growth.

Inhibition of platelet derived growth factor (PDGF) at this stage results in the failure of the astrocyte network to form and the absence of proceeding vascular growth. Whereas overexpression of PDGF results in over proliferation of both the astrocyte and vascular networks (Fruttiger et al., 1996; Gariano et al., 1996; Dorrell et al., 2002).

At birth, the mouse retina is avascular and prior to the development of the retinal vasculature the immature, perinatal astrocytes are characterised by low expression of glial fibrillary acidic protein (GFAP) and high expression of vimentin and nestin. The astrocytes and neurons of the retina undergo a physiological hypoxia, resulting in the expression of hypoxia-inducible factors (HIF) HIF-1α and HIF-2α, which in turn lead to the transcription of hypoxia response genes such as erythropoietin (Caprara *et al.*, 2011) and vascular endothelial growth factor (VEGF). Localised gradients of VEGF concentration then guide the invasion and migration of vascular endothelial cells from the optic nerve head over the astrocyte network (Gerhardt *et al.*, 2003).

Several studies have shown that during development retinal astrocytes produce increased levels of VEGF mRNA prior to vascularisation et al., 1996; West, Richardson and Fruttiger, 2005). However, in studies where astrocyte derived VEGF was deleted, only a minor effect was seen on the developing vascular plexus (Scott *et al.*, 2010; Weidemann *et al.*, 2010) suggesting that astrocyte derived growth factors may be dispensable when compared to those secreted by the neuronal cells of the retinal ganglion cell layer (Sapieha *et al.*, 2012). Neuroretinal specific knockouts of HIF-1α

have been shown to significantly impair both the development of the astrocyte network and the vascular plexus (Nakamura-Ishizu *et al.*, 2012).

It is therefore more likely that the importance of astrocytes in the intricate patterning of the retinal vasculature is due to the R-cadherin mediated cell to cell adhesions they form with the endothelial filopodia (Dorrell, Aguilar and Friedlander, 2002; Gerhardt *et al.*, 2003) which act to stabilise vessel sprouts and guide them towards the extracellular fibronectin matrices which astrocytes also mediate the formation of (Uemura *et al.*, 2006).

As endothelial cells migrate over the astrocytes they produce apelin (Apln) which stimulates endothelial apelin receptor (also known as the APJ receptor) and subsequent leukemia inhibitory factor (LIF) production (Sakimoto *et al.*, 2012). LIF is predominantly expressed in developing endothelium and the LIF receptor (LIFR) is expressed in the surrounding retinal astrocytes awaiting vascularisation (Kubota et al. 2008a). LIF induces the differentiation of astrocytes into a mature, stellate morphology. LIF and APJ knockout (KO) mice both demonstrate aberrant overgrowth of immature astrocyte and endothelial networks (Kubota et al. 2008b; Sakimoto et al. 2012), while APJ and Apln KO mice demonstrate delayed retinal angiogenesis (Kasai *et al.*, 2008; del Toro *et al.*, 2010). Mature astrocytes upregulate GFAP expression and downregulate Tlx, vimentin and VEGF.

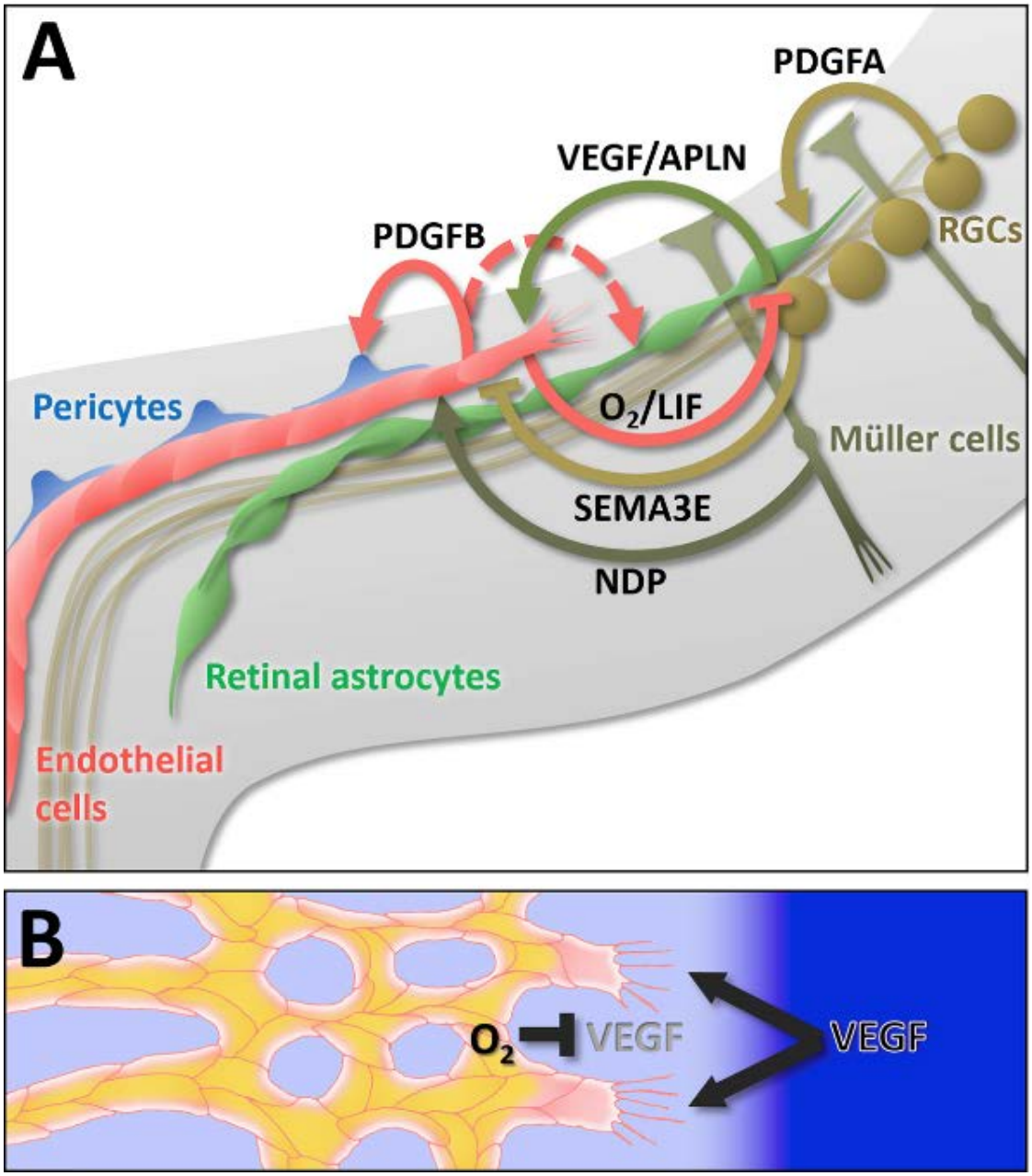

Figure 1.2 – Role of retinal astrocytes in angiogenesis (Selvam et al., 2018) *(A) Cell-cell signalling between retinal astrocytes and developing vessels. (B) VEGF gradient that guides tip cell migration.*

The inhibition of astrocyte VEGF expression prevents further astrocyte proliferation and therefore acts as negative feedback to prevent hyper-proliferation of the astrocyte and vascular networks. When VEGF-Trap is used to supress retinal vessel growth, a

compensatory upregulation of VEGF and downregulation of GFAP is noted in the resulting dense retinal astrocyte network (Uemura *et al.*, 2006).

1.2.2 Pathological Development of the Retinal Astrocyte Foundation

As demonstrated in murine models, disruption to the development of the astrocyte network can result in disruption of normal retinal vessel growth. Although normal development of the astrocyte network occurs in physiological retinal hypoxia when retinal hypoxia becomes pathological, as is seen in oxygen induced retinopathy (OIR), astrocytes degenerate within the vaso-obliterated area (Chan-Ling and Stone, 1992; Stone *et al.*, 1996). In the absence of the astrocyte network there is no template to guide vessel growth during the re-vascularisation phase which results in the formation of the characteristic, pathological neovascularisation seen in OIR (Dorrell et al. 2010). Indeed, interventions aimed at reducing the neovascular sequelae of OIR which preserve the astrocyte template have been shown to promote physiological revascularisation after vaso-obliteration (Gu et al. 2002; Downie et al. 2008; Kubota et al. 2008). Intravitreal injection of astrocytes and astrocyte conditioned media was found to rescue both endogenous astrocytes and microglia from hypoxic degeneration. Protection of retinal astrocytes and microglia directly correlated with the reduction in neovascularisation seen in OIR (Dorrell et al. 2010).

Microglia are thought to play a role in the development of the retinal vasculature as they have been shown to be present in the developing retina prior to the migration of astrocytes from the optic nerve and the development of the astrocyte network (Checchin *et al.*, 2006). Astrocytes can behave similarly to myeloid derived microglia and can work synergistically to mediate retinal inflammatory damage (González *et al.*, 2014). Reactive astrocytes produce both inflammatory cytokines (interleukin 1 beta

(IL-1β), interleukin 6 (IL-6) and interleukin 8 (IL-8)) and chemokines (chemokine ligands (CCL): CCL2, CCL5, CCL20; chemokine C-X-C motif ligands (CXCL): CXCL10, CXCL12, CXCL1, CXCL2 and CX3CL1) which recruit microglial cells (de Hoz *et al.*, 2016).

In tumour necrosis factor alpha (TNFα) knockout (KO) mice undergoing OIR significantly more microglial cells were found to be recruited to the inner nuclear layer and the astrocyte network was found to be better preserved in comparison to wild type controls. The authors hypothesised that microglial cells, recruited to the vaso-obliterated area in response to ischaemia, secrete neurotrophic factors that protect the astrocytes from hypoxic injury (Stevenson *et al.*, 2010). Intravitreal injection of myeloid progenitor cells has also been found to be protective of retinal astrocytes and to promote normal revascularisation of the hypoxic retina (Dorrell et al. 2010; Ritter et al. 2006). As well as being neuroprotective, microglia are also capable of releasing pro-angiogenic factors (such as basic fibroblast growth factor, metalloproteinases and TNFα) (Fletcher *et al.*, 2010), which would further suggest that they have an important role in retinal angiogenesis.

1.2.3. Physiological Development of the Primary Plexus

1.2.3.1 Sprouting Angiogenesis

The primary plexus of the retina is vascularised by a process of angiogenesis, in which proliferating endothelial cells degrade the extracellular matrix, sprout and migrate to form new vessel sprouts from the existing capillary ring at the optic nerve head at postnatal day P1 (Provis *et al.*, 1997; Pitulescu *et al.*, 2010).

Vessel growth is induced by angiogenic stimuli released by the hypoxic retina, such as VEGF, ANG2 and fibroblast growth factors. These stimuli direct the migration of

specialised endothelial cells found at the distal end of the vascular sprouts at the peripheral edge of the developing vascular plexus (Gerhardt, 2008). In response to VEGF these endothelial tip cells activate cell division control protein 42 (Cdc42) and extend numerous long, motile filopodia which probe to sense growth factors, extracellular matrix and other attractant or repellent guidance cues, allowing them to lead and guide the endothelial sprouts (Adams and Eichmann, 2010). They have a specific molecular signature, characterised by the enriched expression of growth factor (such as VEGF receptor 2 (VEGFR2), VEGF receptor 3 (VEGFR3) and platelet derived growth factor (PDGF)-BB receptor) and guidance cue receptors (such as uncoordinated 5B (UNC 5B), delta-like ligand 4 (Dll4), neuropilin-1 (NRP1), netrins, plexins, neogenin, ephrins, semaphorins, slits and apelin receptors) (Tammela *et al.*, 2008; De Smet *et al.*, 2009; del Toro *et al.*, 2010). Depending on the nature of the guidance cue it encounters tip cells can either advance, stall, turn or retract (Larrivée *et al.*, 2009).

1.2.3.2 Role of Vasculature Endothelial Growth Factor in Angiogensis

VEGF is essential to angiogenesis in the retina and binds to the tyrosine kinase receptors VEGFR1, VEGFR 2 and VEGFR 3. Even though the receptors are found to be present in overlapping spatial and temporal patterns they play different roles in VEGF signalling (Gelfand *et al.*, 2014). VEGFR2 is the main VEGF signal transducing receptor and endothelial cell specific deletion of VEGFR2 results in reduced angiogenic sprouting in the developing mouse retina (Benedito *et al.*, 2012; Zarkada *et al.*, 2015).

VEGF stimulation of tip cell VEGFR2 in turn upregulates Dll4 expression, activating Notch receptors in the more proximal, neighbouring endothelial stalk cells. The Dll4-Notch interaction simultaneously upregulates the decoy receptor VEGFR1 and

downregulates VEGFR2 and VEGFR3 expression on stalk cells, making them less sensitive to VEGF and preventing them from becoming stalk cells **(Figure 1.3)**.

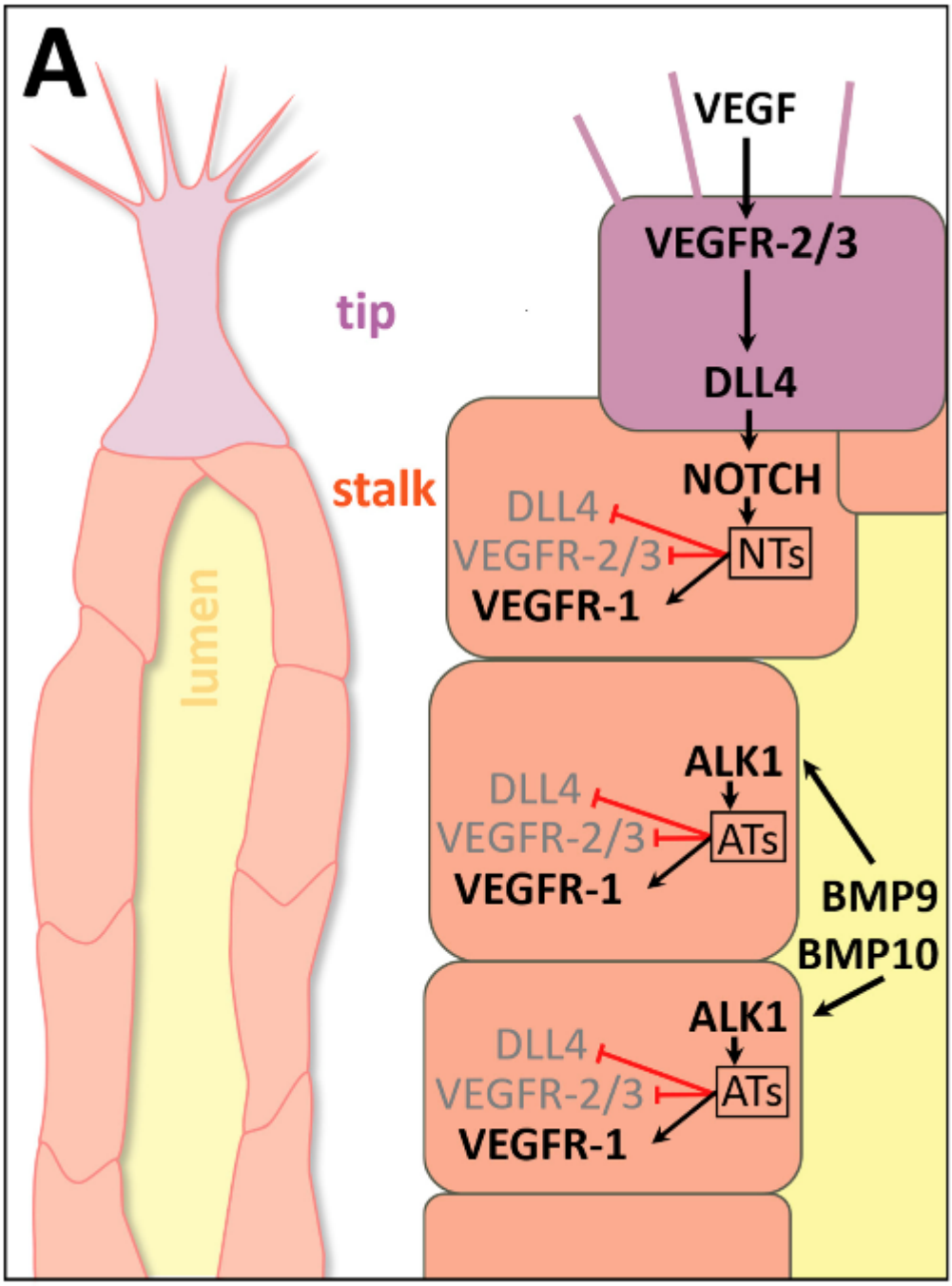

Figure 1.3 – The tip stalk phenotype in sprouting endothelial cells (adapted from Selvam et al., 2018)

Stalk cells in turn promote tip cell formation by expressing the Notch ligand Jagged1 which antagonises Dll4-Notch signalling (Benedito *et al.*, 2009). This notch-mediated lateral inhibition means that in response to VEGF stalk cells will proliferate rather than sprout behind the guidance of the tip cells, allowing for the formation of a coordinated, branching network of vascular lumen while preventing uncoordinated endothelial cell proliferation (Hellström *et al.*, 2007; Lobov *et al.*, 2007; Suchting *et al.*, 2007). Endothelial tip cells selectively express Plexin-D1 in response to VEGF and Sema3E in their differentiation from the stalk cells (Kim *et al.*, 2011).

Alongside Notch, bone morphogenetic protein (Bmp)/transforming growth factor beta (TGF-β)/Smad signalling also affects stalk cell differentiation (Moya *et al.*, 2012). Bmp 9 and Bmp 10 signal through activin receptor-like (ALK)1 and ALK2 to induce Smad 1 phosphorylation, which inhibits endothelial cell migration and proliferation, promoting the stalk cell phenotype. TGF-β can both prevent or promote tip cell differentiation, depending on whether it binds to Alk 1 or Alk5. TGF-β/ALK1/Smad 1/5/8 signalling promotes endothelial cell migration and proliferation whereas TGF-β/Alk5/Smad 2/3 signalling inhibits endothelial cell migration and proliferation (Pardali, Goumans and ten Dijke, 2010). Nrp1 suppresses the stalk cell phenotype by inhibiting Alk 1 and Alk 5 activation of Smad 2/3. Notch in turn inhibits Nrp1, allowing Alk1 and Alk 5 to induce Hey 1, Hey 2 and Hes 1 which down regulate VEGFR2 and Dll4 to promote stalk cell behaviour (Larrivée *et al.*, 2012; Aspalter *et al.*, 2015).

Endothelial cells are plastic in nature with the tip and stalk cell phenotypes being highly transient so that endothelial cells are continuously competing for the tip cell position (Jakobsson *et al.*, 2010). In angiogenic vessels the endothelial cell phenotype is continuously in flux as a result of constant re-evaluation of VEGFR/Notch/Dll4

signalling that occurs when tip cells migrate in response to the hypoxia induced VEGF gradient (Bentley *et al.*, 2009).

As the developing vasculature delivers oxygen to the central retina, VEGF messenger ribonucleic acid (mRNA) is downregulated in comparison to the peripheral, non-vascularised retina where VEGF mRNA is highly expressed in response to hypoxia (Gerhardt *et al.*, 2003; West, Richardson and Fruttiger, 2005; Hellström *et al.*, 2007). Any disturbance to this specific distribution of VEGF will therefore impact upon how the primary plexus grows across the retina. Retinal neurons have also been shown to highly express VEGFR2 and are thought to maintain the VEGF gradient across the retina by engulfing any excess VEGF, thereby restricting primary plexus growth to the inner retina. Genetic deletion of neuronal specific VEGFR2 results in excessive VEGF around neurons which in turns misdirects angiogenesis towards the neurons rather than the astrocytes (Okabe *et al.*, 2014). VEGF-A isoforms differ in their heparin and heparin sulfate binding capacity. The smaller isoforms (VEGF-A_{121} in humans; VEGF-A_{120} in mice) diffuse freely and induce endothelial cell proliferation. Whereas the larger isoforms (VEGF-A_{189} & VEGF-A_{165} in humans; VEGF-A_{188} & VEGF-A_{164} in mice) bind tightly to heparin, remain in the extracellular matrix and promote extension of tip cell filopodia, guiding them towards the extracellular matrix. (Carmeliet, 2003b; Witmer *et al.*, 2003).

However, despite the pivotal role of VEGF in the development of the retinal vascular, the intricate patterning of the retinal vasculature cannot be solely explained by the differential expression of VEGF. Endothelial tip cells share many of the features associated with axonal growth cones and given that they share similar attractive and repulsive guidance cues it is no surprise that blood vessels and nerve fibres run

together in close proximity (Adams and Eichmann, 2010). Four major receptor families have been identified in the guidance of vascular and axonal growth: UNC5 family and deleted in colorectal cancer (DCC) with their Netrin ligands; roundabout (ROBO) with their Slit ligands and EPH and their Ephrin ligands; plexin/NRP complexes with their class 3 Semaphorin ligands (Carmeliet, 2003b; Siemerink *et al.*, 2013).

At the onset of angiogenic sprouting tip cells secrete matrix metalloproteinases (MMPs) in order to breakdown the basement membrane and allow them to detach from neighbouring mural cells. In the degradation of extracellular matrix MMPs further propagate angiogenesis through the liberation of proangiogenic factors, such as VEGF, that are sequestered within the matrix. The extracellular matrix also transmits guidance cues for tip cells via integrins.

Integrins mediate adhesion and cell signalling between vascular endothelial cells and neuroepithelial cells to promote vascular development in the central nervous system. β8 integrin promotes the activation of extracellular matrix bound TGFβ and stimulates endothelial cell TGFβR signalling (McCarty, 2009). Endothelial cell NRP1 balances β8 integrin activated TGFβ signalling to control sprouting angiogenesis by binding to β8 integrin to form intercellular complexes, thereby supressing TGFβ signalling. Cell type specific deletion of either β8 integrin, NRP1 or TGFβ receptors resulted in impaired vascular endothelial cell – neuroepithelial cell adhesion, impaired TGFβ signalling and ultimately pathological angiogenesis (Hirota *et al.*, 2015).

MMPs secreted by tip cells can also release antiangiogenic molecules, such as the semaphorins, from the extracellular matrix to prevent inappropriate sprouting. Secreted class 3 semaphorin protein Sema3C has been shown to impair endothelial tip

cell formation by disrupting endothelial junction integrity and inhibiting the formation of focal adhesions with the extracellular matrix (Yang *et al.*, 2015).

Furthermore, ligation of α2β1 and α2β6 integrins in endothelial cells has been shown to induce Notch/Dll4 signalling further highlighting the role of the extracellular matrix and integrins in the control of endothelial cell migration and proliferation during sprouting angiogenesis (Estrach *et al.*, 2011).

1.2.3.3 Vascular Remodelling

Following vessel development, the area of the vascular network behind the tip cells becomes dense as the capillary plexus begins to form. Through selective pruning and stabilisation of vessels the network is remodelled into the hierarchical vascular tree.

The remodelling process is governed by vessel stabilisation and vessel regression. Vessel maturity, perfusion and endothelial mural cell interactions act as stabilising factors whereas poor perfusion, endothelial cell apoptosis and migration act as destabilising factors.

The primary plexus is dependent on vessel pruning through endothelial cell migration. Behind the growing front of the primary plexus, endothelial cells migrate to neighbouring vessel branches resulting in pruning of capillaries and strengthening of neighbouring vessels **(Figure 1.4)** (Selvam et al., 2018).

In addition to lateral migration, remodelling can also be caused by endothelial cell apoptosis which results in vessel regression. Retinal macrophages have been shown to be play an important part in the pruning process. They are thought to bind to the vascular network and induce endothelial cell death via Fas ligand (Ishida *et al.*, 2003). Mac-1 staining macrophages that express MMP2 and MMP9 have been described in

avascular and vascularised areas in the developing retina. MMP2 and MMP9 are able to digest fibronectin in order to remodel the vasculature and in op/op mice which have decreased expression of these metalloproteinases reduced branching and a lack of arterial-venous patterning is seen at P4 (Kubota *et al.*, 2009). However, when postnatal mouse pups are treated with LPS at P4, retinal vascular density was found to be increased. These mice then go on to show signs of excessive vascular pruning in the later stages of retinal vascular maturation after the initial rise in vascular density (Tremblay, Miloudi, Chaychi, Favret, Binet, KA, *et al.*, 2013).

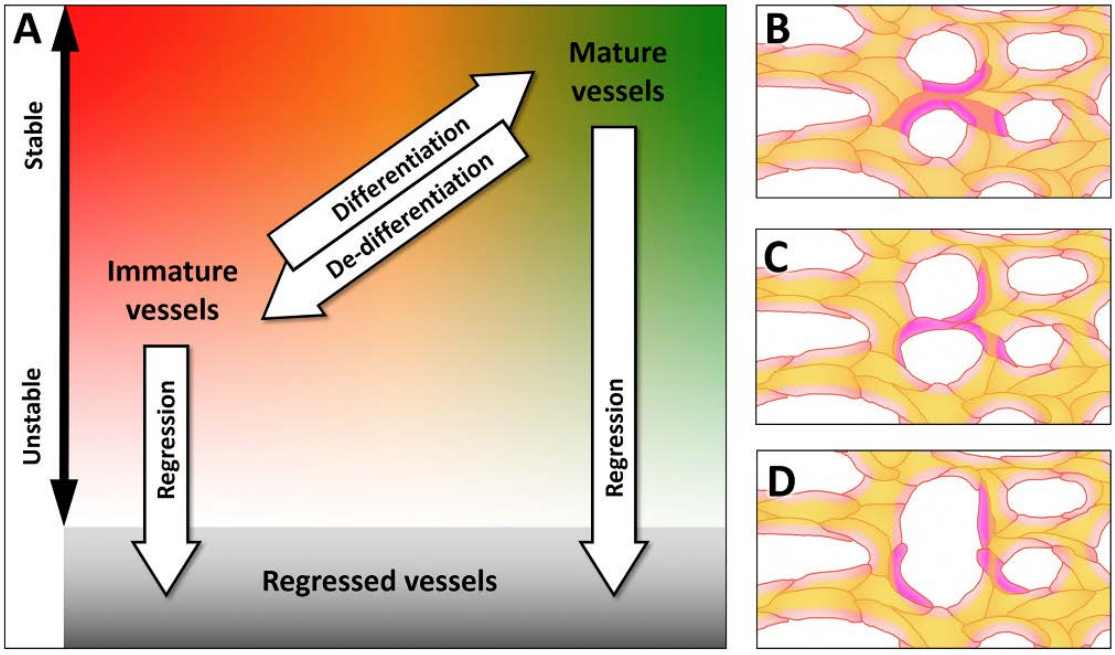

Figure 1.4 – Vascular remodelling (Selvam et al., 2018) *(A) Vessels are differentiated into immature and mature states depending on their stability. (B) Lateral migration of endothelial cells results in vessel pruning.*

1.2.4.2 Vessel Maturity and Susceptibility to Hyperoxia

During the first two postnatal weeks of development the retinal vasculature is immature and thereby is susceptible to ablation by exposure to hyperoxia. However,

after this period as the vessels mature they develop resistance to hyperoxia. The hyperoxia obliterates the central capillaries and the diffusion zones around the arteries. The hyperoxia causes this effect through the resulting retinal VEGF down-regulation which leads to endothelial cell death. The hyperoxia also causes direct damage to endothelial cells through reactive oxygen species. Macrophages then participate in this hyperoxia induced vasculature remodelling (Ishida *et al.*, 2003).

1.2.4. Pathological Development of the Primary Plexus

1.2.4.1 The oxygen induced retinopathy model

The OIR model in mice is the most widely used model for studying pathological angiogenesis in mice retina (Smith et al. 1994). There have been over 35,500 publications relating to OIR to date (Kim, D'Amore and Connor, 2016). In the model P7 mouse pups are placed into a chamber of 75% oxygen with their feeding mothers until P12. During this hyperoxic phase, the central retinal capillaries are depleted so that when the mice are returned to normoxic conditions, the vaso-obliterated area becomes acutely hypoxic. This hypoxic phase triggers pathological angiogenesis resulting in neovascular tufts towards the vitreous. Neovascularisation is at its highest at day 17 (5 days after re-exposure to room air). After P17, the neovascular phenotype then begins to regress. By P25, the vasculature has normalised **(Figure 1.5)**.

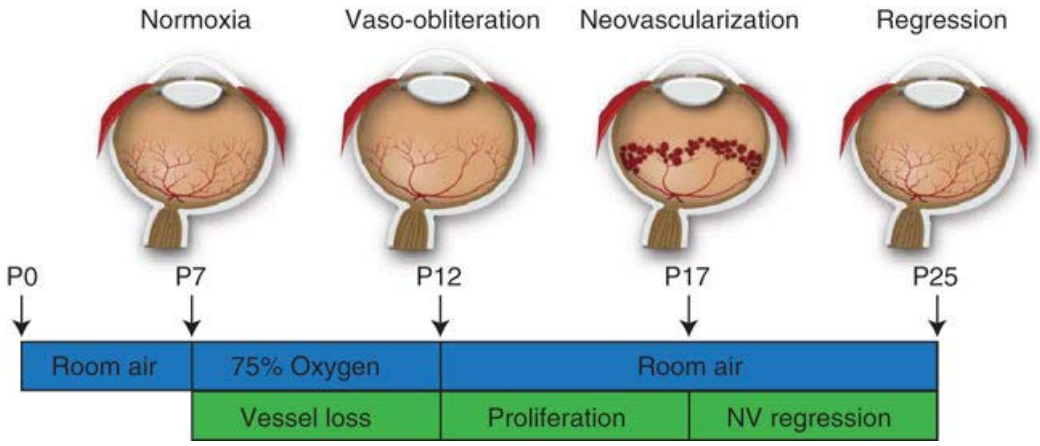

Figure 1.5 - Phases of the OIR model (Connor et al., 2009)**.** *Schematic showing the different phases in a mouse OIR model - the vaso-obliterative phase between P7-P12 in 75% oxygen, the vasoproliferative phase between P12-P17 in normoxia and the regression phase after P17 in normoxia. By P25, a normal retinal vascular network is re-established.*

The mouse model (Smith et al., 1994) of OIR has become the standard protocol because it is both highly quantifiable and easily reproducible (Connor et al., 2009). The ability to digitally map areas of neovascularisation and vaso-obliteration of retinal wholemounts using computer imaging software means that analysis of multiple retinal wholemounts is possible in quick succession. Arterial tortuosity is the earliest change in vessel anatomy that can be detected in response to hypoxia before the appearance of neovascular sprouting and its quantification has been shown to be an early marker of hypoxia in OIR and may predict future pathological neovascularisation (Scott et al., 2014).

In this model, vaso-obliteration is seen in the centre rather than the periphery, which is the opposite to the clinical picture seen in ROP. This is due to the higher concentrations of oxygen being delivered to the central retina by the persistent hyaloid artery radiating out from the centre (Lange et al., 2009). The radial arteries and veins are resistant to hyperoxia and supply the viable vasculature network seen in the retinal periphery (Claxton and Fruttiger, 2003).

At P12 when the mice are returned to normoxic conditions the vaso-proliferative phase commences. The central avascular area where vaso-obliteration has occurred becomes immediately hypoxic except in the diffusion zones surrounding the retinal arteries. The hypoxia causes a VEGF driven angiogenic response. As VEGF levels become pathological vascular sprouts form from the peripheral capillaries and veins and rather than grow across the inner retina surface they grow towards the vitreous, as is seen in proliferative diabetic retinopathy. Arteries become tortuous in response to the hypoxia driven VEGF up-regulation. Arterial vessel tortuosity is a diagnostic criterion of plus disease in ROP.

The neovascularisation seen in the model is representative of the neovascular tufts seen in human ischemic retinopathies such as diabetic retinopathy and retinopathy of prematurity. Although the pathology leading to neovascularisation varies between the different ischemic retinopathies, the final outcome of pathological neovascularisation is always the result of hypoxia induced VEGF overexpression.

1.2.4.3 Pathological neovascularisation versus physiological angiogenesis

It is still not fully understood why hypoxia driven angiogenesis results in pathological neovascularisation rather than physiological revascularisation. The OIR model provides a good model for further investigating this conundrum and for testing interventions aimed at reducing the neovascular consequences of retinal hypoxia.

Neovascularisation is a result of the vascular repair response to the profound hypoxia and ensuing VEGF upregulation seen in the ischaemic, vaso-obliterated areas. In these conditions the mechanisms that govern physiological sprouting angiogenesis of the

primary plexus during normal retinal vascularisation are disrupted. The pathologically high levels of VEGF that ensue in response to inner retinal hypoxia prevent the tip/stalk machinery from functioning correctly (Selvam et al., 2018). The resulting neovascularisation is characterised by the development of abnormal vessels that grow away from the highly organised, physiological layers of the retinal vasculature. These pathological, tortuous and leaky vessels penetrate the inner limiting membrane and grow into the normally avascular vitreous cavity, forming unorganised, small calibre pre-retinal tufts **(Figure 1.6)**. Unlike vessels that re-vascularise the capillary depleted areas through normal sprouting angiogenesis, these don't undergo vessel remodelling or maturation and are therefore susceptible to complications such as bleeding, plasma leakage and may ultimately result in retinal detachment (Stahl *et al.*, 2010). Reducing VEGF levels from P12 in the OIR model has been shown to prevent neovascular tuft formation and promote physiological angiogenesis which revascularizes the vaso-oblitered area (Selvam et al, 2018).

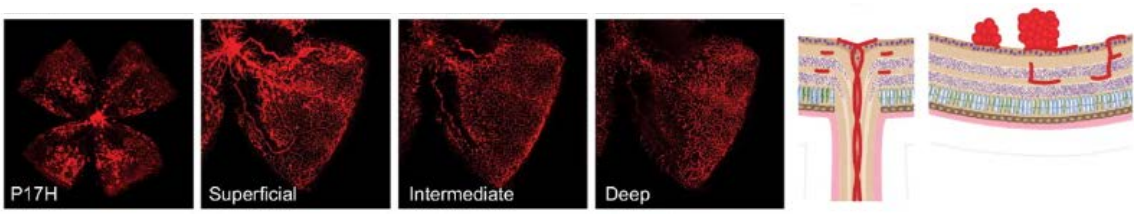

Figure 1.6 - Neovascularisation (Stahl *et al.*, 2010) *At P17 in the OIR model pathological vessels grow into the vitreous cavity as opposed to radially along the inner retina as is seen in the physiological development of the primary plexus.*

Ischaemic retinopathies are usually the result of a deficient retinal vasculature. In ROP this is due to inadequate development of the retinal vasculature, in diabetic retinopathy this is due to vascular degeneration and in retinal artery occlusion this is due to vascular occlusion. The balance between retinal oxygen demand and supply ultimately determines whether retinal angiogenesis will be pathological or physiological. Therapies aim to either increase oxygen supply to the ischaemic tissue or reduce the oxygen demand of the ischaemic tissue in order to address the balance. If the ischaemia is resolved early enough prior to the development of neovascularisation it may be possible to direct angiogenesis towards healthy regeneration.

Insulin-like growth factor (IGF-1), erythropoietin and Il10, have all been shown to influence the formation of neovascular tufts (Dace et al. 2008;). Retinal astrocytes and retinal macrophages have also been linked to neovascularisation (Checchin et al. 2006; Kubota et al. 2009). Depending on their activation status retinal microglia have also been implicated in neovascular tuft formation (Fischer *et al.*, 2011). Given that microglia, lymphocytes and macrophage/monocytes have all been shown to be modulators of angiogenesis in OIR it would suggest that inflammation has a significant role in the determining whether hypoxia induced angiogenesis is pathological or physiological.

1.3. Inflammation

1.3.1 Innate versus adaptive Immunity

The innate immune system is present from birth and acts as the first response to invading pathogens. Upon identification of a pathogen a broad immune response is

mounted to protect the host until the adaptive immune response. Adaptive immunity refers to the continually refined and, “adapted” response of T and B lymphocytes to pathogens in order to provide long lasting protection.

The mechanisms by which both responses are mounted are fundamentally different. Adaptive immunity changes throughout the lifetime of the host. During development every T and B lymphocyte acquires a unique receptor. As they are exposed to pathogens the T and B lymphocytes specific to those pathogenic antigens expand as a clone of cells specifically directed against that particular pathogen. As the cell lines expand the specificity and affinity of the receptors to the pathogenic antigen are continually refined resulting in an improved response in the host over time (Medzhitov and Janeway, 1997).

Whereas innate immunity identifies pathogens via receptors specific to molecular components of pathogens, pathogen associated molecular patterns (PAMP), that are foreign to the host. These are called pattern recognition receptors (PRR). Activation of these receptors in response to foreign pathogens results in a temporary upregulation of the innate immune response but the response remains unchanged over the host’s lifetime.

The host component of the innate immune system comprises of physical barriers that prevent pathological penetration (e.g. tight junctions, mucous and epithelial membranes, and vascular endothelial cells), epithelial and phagocytic enzymes (e.g. lysozyme), inflammatory serum proteins (e.g. c-reactive protein and complement), antimicrobial peptides (e.g. defensins), cytokine releasing cells (e.g. mast cells, natural killer cells and macrophages), phagocytic cells (e.g. moncoytes/macrophages and

neutrophils) and micro-organism sensing cell receptors (e.g. toll-like-receptors (TLR)) (Medzhitov, 2013).

Membrane-bound PRRs are expressed by many innate immune cells as well as antigen-presenting cells (e.g. monocytes/macrophages, dendritic cells, and B lymphocytes). These transmembrane PRRs act as sentinels and once activated induce rapid upregulation of other PRRs.

1.3.2 Toll-like receptor 4 activation by Lipopolysaccharide

Toll-like receptors (TLRs) are transmembrane PRRs expressed on and within cells of the innate immune system (e.g. monocytes/macrophages and neutrophils). TLRs are able to recognise a range of PAMPs, such as microbial cell wall components and proteins. TLR signalling regulates transcription factors responsible for pro-inflammatory cytokine gene expression (O'Neill, 2006; O'Neill, 2008).

TLRs and interleukin-1 (IL-1) receptors share the myeloid differentiation primary response protein 88 (MyD88) dependent signalling pathway that induces the intra-cellular activation of transcription factors activating protein-1 (AP-1) and NF-kappa-B (nuclear factor for the kappa-light chain enhancer in B cells) (Kim *et al.*, 2007). These factors result in the production of several potent proinflammatory cytokines, including TNF, IL-1, IL-6, and pro-IL1 beta, and chemokines intercellular adhesion molecule-1 (ICAM-1), vascular cell adhesion molecule-1 (VCAM-1), and nitric oxide.

There are ten human TLRs, of which the first to be identified was TLR4 . TLR4 is specific for and very sensitive to bacterial endotoxin, lipopolysaccharide (LPS). TLR4 is expressed on the cell surface to allow recognition of extracellular PAMPs released by pathogens (Murdock and Núñez, 2016).

LPS, a component of the outer membrane of all gram-negative bacteria is a prototypical PAMP. LPS contains lipid A, a highly conserved structure of the lipid bilayer of the outer bacterial cell membrane, which specifically interacts with TLR4. The interaction of LPS with TLR4 occurs in a complex with LPS-binding protein (LBP), CD14, and myeloid differentiation factor-2 (MD-2) **(Figure 1.7)** (Kim and Kim, 2017).

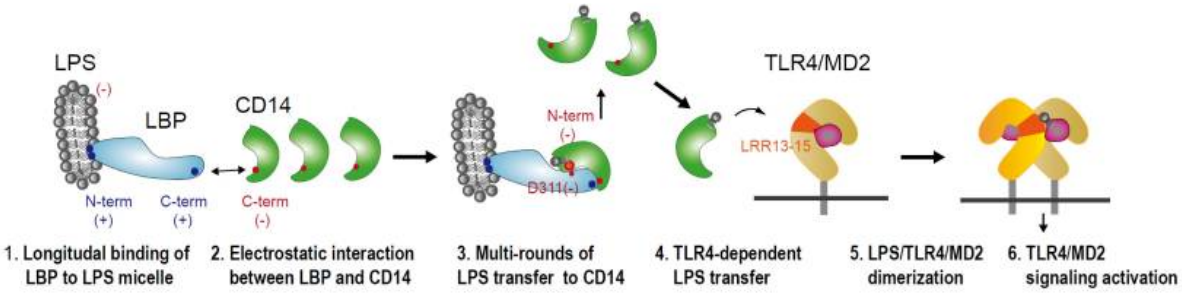

Figure 1.7 - Neovascularisation (adapted from Kim and Kim, 2017) *Interaction of LPS with the LBP/CD14/MD2 complex. .*

Like other TLRs, TLR4, signals via the intermediate MyD88 but with the adapter molecule toll/interleukin-1 receptor (TIR) domain-containing adapter protein (TIRAP) which links the TIR domain with MyD88. TLR4 can also signal independently of MyD88 via the molecule TIR domain-containing adapter-inducing interferon-beta (IFNβ) (TRIF) pathway. TLR4 requires the intermediate TRIF-related adapter molecule (TRAM) to link the TIR domain if TLR4 with TRIF **(Figure 1.8)** (Trinchieri and Sher, 2007)

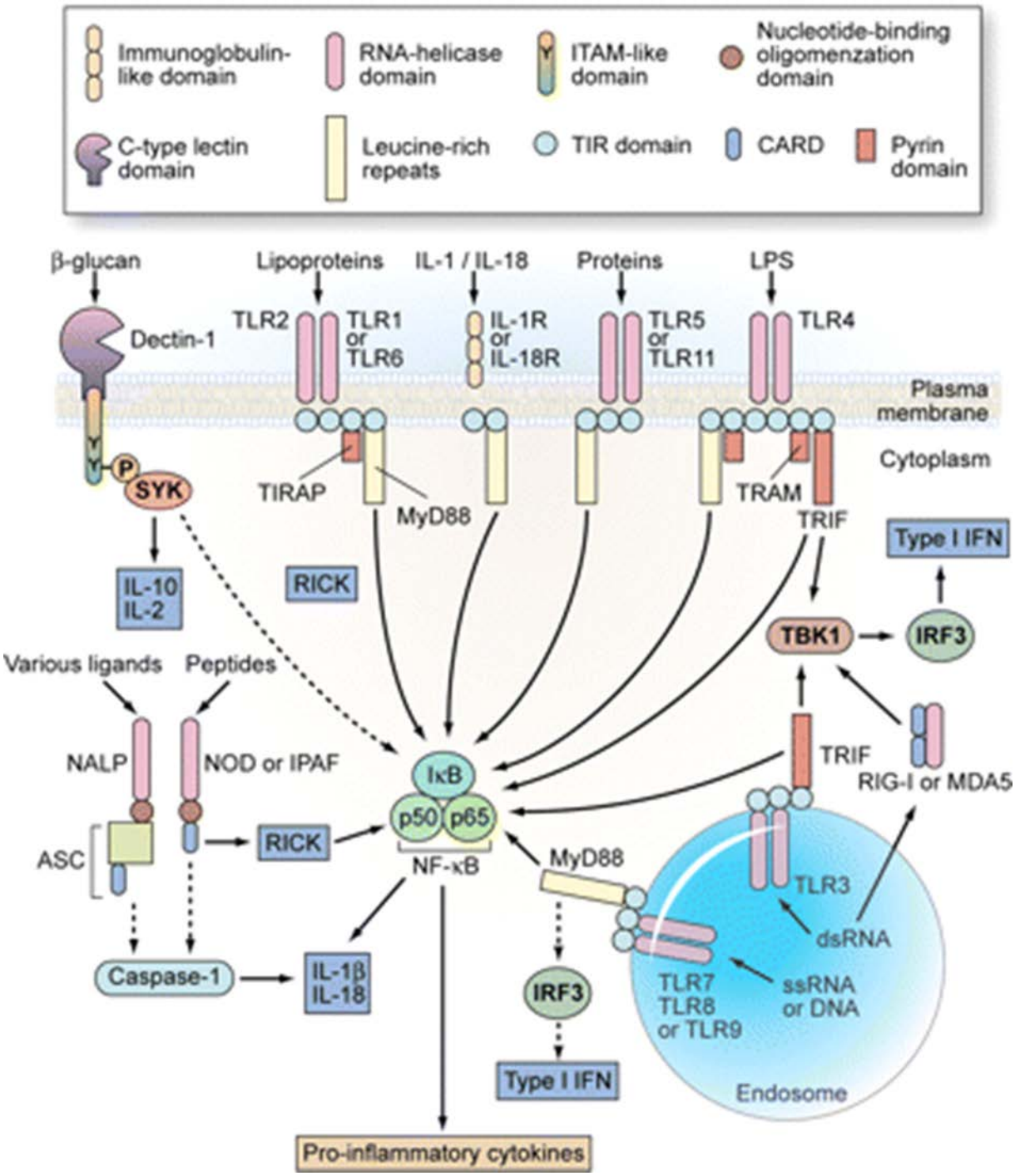

Figure 1.8 - Overview of the pattern-recognition receptor system of phagocytes, including the TLR family (adapted from Trinchieri and Sher, 2007)

TLRs are differentially expressed on different classes of leukocyte cells. Monocytes, macrophages and neutrophils express all TLRs, except TLR3 (Prince *et al.*, 2011). These

phagocytic cells therefore play an important role in LPS activation of the innate immune response.

1.3.3 Phagocytic cells of the innate immune response

Monocytes/macrophages and neutrophils differentiate from common precursors and therefore share common features. Typically, neutrophils are recruited first and have a higher microbicidal activity; with monocytes/macrophages being recruited later in the immune response (Silva, 2010; McCracken and Allen, 2014). As specialised phagocytic cells they have various roles in the innate immune response. This means that they can digest and present antigens to other immune cells, thereby allowing them to interact with the adaptive immune system (Silva and Correia-Neves, 2012). They co-express similar antigens and can produce effector molecules such as chemokines and cytokines (Nauseef, 2007; Daley *et al.*, 2008). Monocytes/macrophages and neutrophils work together to produce an enhanced immune response by regulating other immune cells as well as each other.

1.3.3.1 Monocytes and Macrophages

Monocytes are also produced in the bone marrow and circulate before entering the tissues (Geissmann *et al.*, 2010). Some will take up antigens and transport them to regional lymph nodes without differentiating into macrophages. Unlike neutrophils, macrophages are found to be resident in tissues as they are less immunoreactive; which enables them to survey the tissue for pathogens (Davies and Taylor, 2015). Most monocytes will differentiate into macrophages to renew the resident macrophage population that is characteristic for the tissue in which they reside (e.g. microglia in the brain and retina). Tissue resident macrophages can also develop from yolk sac embryonic progenitors rather than blood monocytes (Katsumoto *et al.*, 2014).

When resident macrophages recognise the presence of a pathogen they produce neutrophil chemoattractants such as interleukin-1α, CXCL1, CXCL2, and monocyte chemoattractant protein-1 (MCP-1). To prolong the survival of the incoming neutrophils macrophages produce a variety of growth factors such as granulocyte colony-stimulating factor (G-CSF), granulocyte–macrophage colony-stimulating factor (GM-CSF), and TNFα. It is this influx of neutrophils that signals the onset of inflammation (De Filippo *et al.*, 2008).

During inflammation, tissue macrophage populations polarise towards either proinflammatory, microbicidal (M1), or anti-inflammatory (M2) subtypes [160].

1.3.3.2 M1/M2 Polarisation of Macrophages

Depending on the microenvironment, macrophages polarise towards a pro-inflammatory "M1" or anti-inflammatory "M2" phenotype **(Figure 1.9)** (Benoit et al., 2008). The M1/M2 distinction is an oversimplification and remains controversial as there is no defined criteria to define the phenotypes. The M1/M2 paradigm is more of a sliding scale (Hamilton *et al.*, 2014). It has been shown that multiple subsets of macrophages exist and can contribute to different processes of inflammation (Geissmann, Jung and Littman, 2003) and that macrophages can reversibly change their polarisation in response to micro-environment signalling. (Stout and Suttles, 2004).

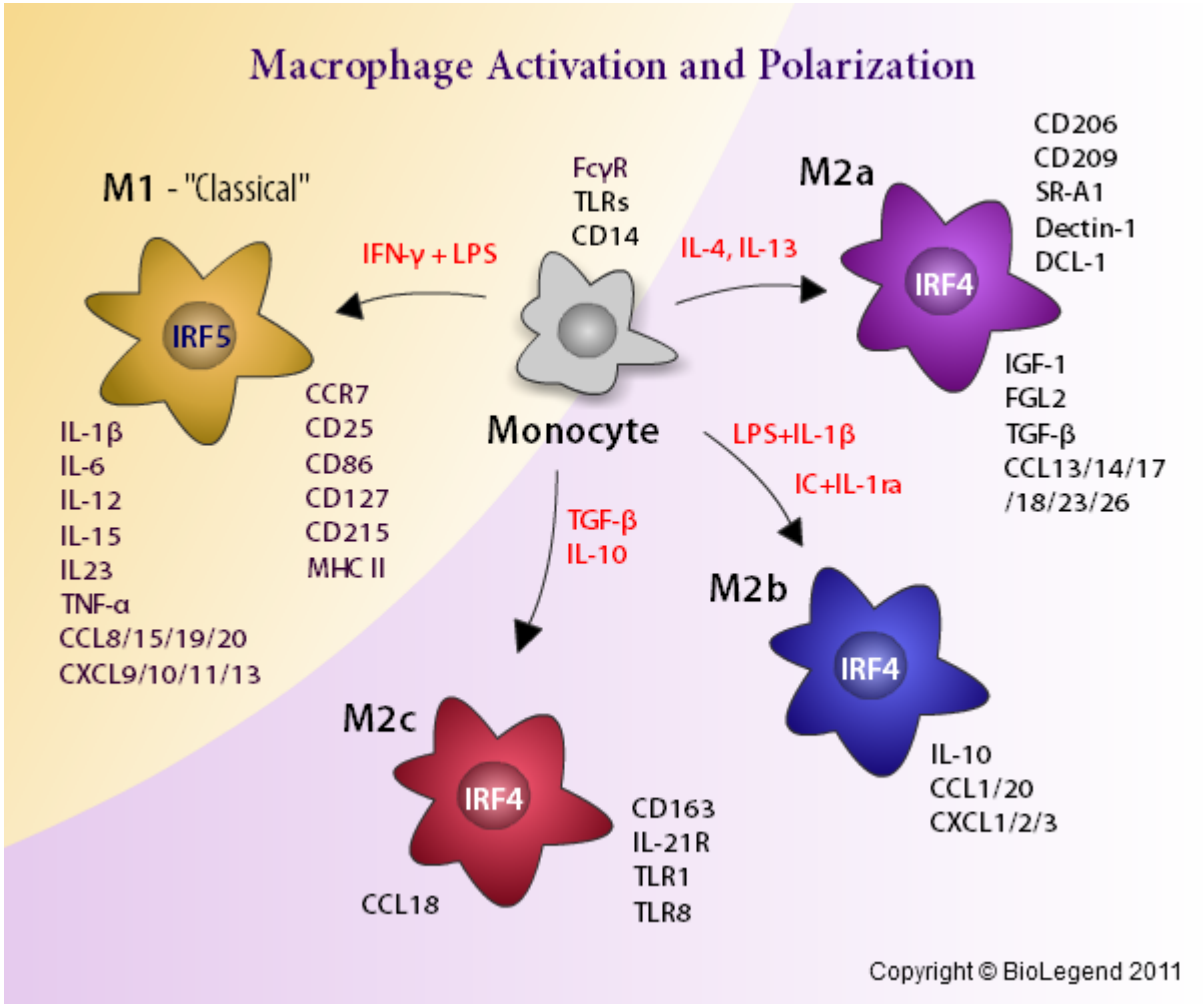

Figure 1.9 – M1/M2 Macrophage activation and polarisation (sourced from www.Biolegend.com)

Pro-inflammatory M1 macrophages express inducible nitric oxide synthase and CD40 while producing TNF-α and IL-6 and act as 'activated' or "classical" macrophages stimulated by injury. M1 macrophages are predominantly seen in inflammatory situations dominating by TLR and interferon signalling. Whereas anti-inflammatory M2 macrophages stimulate a T_H2 response and promote immunosuppression (D'Orazio and Niederkorn, 1998). They express arginase I and CD206 while producing transforming growth factor (TGF)-β and IL-10 to control inflammation and minimize damage by supporting angiogenesis (Balkwill and Mantovani, 2001) and facilitating tissue repair (Wynn and Vannella, 2016).

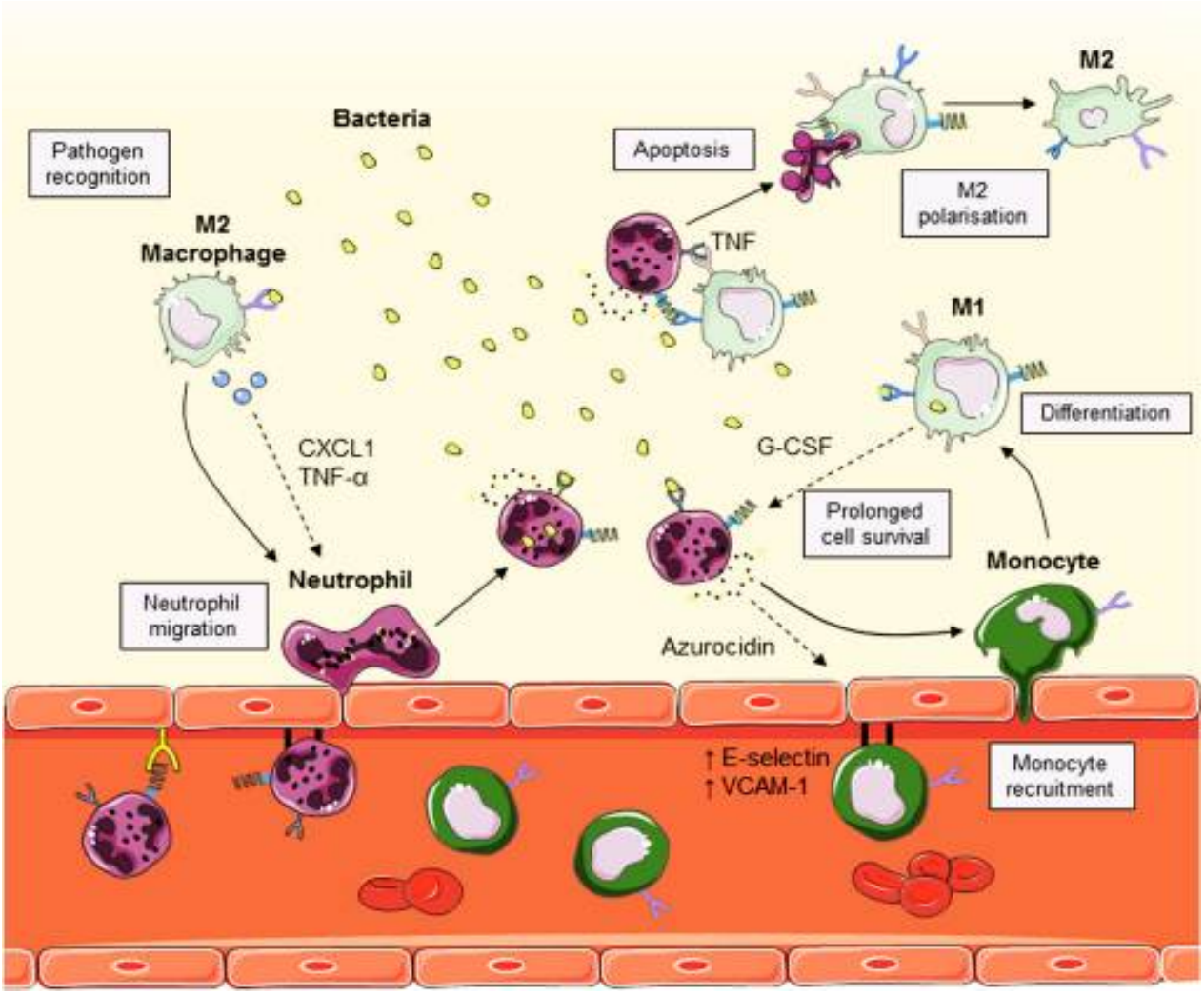

Figure 1.10 – Neutrophil macrophage interaction during the innate immune response (Prame Kumar, Nicholls and Wong, 2018)

During an infection, neutrophils typically induce a M1 phenotype in macrophages to prime their pro-inflammatory activity. One of the mechanisms by which neutrophils mediate macrophage polarization is by their release of azurocidin **(Figure 1.10)**. Neutrophil-derived azurocidin through upregulation of endothelial ICAM-1, VCAM-1 and E-selectin attracts monocytes (Soehnlein *et al.*, 2008). Neutrophils also promote the transmigration of monocytes by altering vascular permeability through induction of changes in endothelial cell cytoskeletal structure (Gautam *et al.*, 2001). In addition, neutrophil-endothelial cell adherence induces the production of reactive oxygen species, lytic enzymes, and vasoactive substances, which can further damage

endothelial cells. LPS, in addition to promoting an M1 macrophage phenotype may also directly disrupt the cytoskeleton and microvascular endothelial barrier integrity, in part, through nitric oxide synthase (NOS), and NF-kB activation (McGown *et al.*, 2011).

1.3.3.3 Neutrophils

Neutrophils are typically not found to be resident in body cavities because of their strong reactivity to pathogens. As a result, they are produced and stored in the large reserves of the bone marrow, allowing them to be readily deployed into circulating blood (Yamashiro *et al.*, 2001). Neutrophils are the most prevalent circulating phagocytes in humans (McCracken and Allen, 2014).

Chemotactic factors generated at sites of inflammation and infection result in neutrophils being the first cells of the immune response to be recruited. Factors recognised by neutrophils include neutrophil chemokine interleukin-8 (IL-8), leukotriene B4, and complement-derived C5a. Neutrophils are also chemoattracted by various antimicrobial peptides (AMPs) which diffuse from the site of injury or infection to provide a chemotactic gradient that allows neutrophil migration and further activation as they transmigrate (Rehaume and Hancock, 2008).

Once activated neutrophils express adhesion molecules that result in aggregation and margination to the vascular endothelium. The endothelium also expresses adherence molecules to attract incoming neutrophils. In order to migrate to the site of injury the neutrophils go through a process of rolling, adhesion, diapedesis, and chemotaxis (Movat *et al.*, 1987). The release of mediators by neutrophils at the site of infection results in the cardinal signs of local inflammation, comprising of erythema due to local vasodilation, hyperaemia, and oedema due to increased microvascular permeability.

On arriving at the site of injury, neutrophils phagocytose invading pathogens that have been opsonized by innate and acquired immune processes (e.g. fixation of immunoglobulin G (IgG) and complement C3 fragment) (Ricklin *et al.*, 2010). It has been shown that certain neutrophils are able to return to the circulation following their initial extravasation resulting in systemic inflammation at sites distant to the initial site of injury (Silvestre-Roig, Hidalgo and Soehnlein, 2016). Inflammatory conditions have been shown to produce neutrophilic survival signals that can extend the life span of neutrophils. Oxygen deprivation in tissue during inflammation has been shown to drive hypoxia-inducible factor dependent activation of neutrophil survival pathways (Thompson *et al.*, 2014).

1.3.4 Inflammation in ischaemia retinopathy

In OIR blocking $VEGF_{164}$ inhibits leukocyte adhesion to neovascular tufts which in turn supresses neovascular tuft formation (Ishida et al. 2003). Depletion of monocytes with clodronate-liposomes results in suppression of neovascular tufts whereas anti-CD2 inhibition of T lymphocytes promoted tuft formation.

Treatments aimed at suppressing inflammation such as dexamethasone or ibuprofen also inhibit neovascular tuft formation (Rotschild *et al.*, 1999; Sharma *et al.*, 2003) Similar results are seen in knockout animals of inflammatory proteins such as TNFα receptor, MCP-1 and macrophage inflammatory protein-1 alpha (Yoshida *et al.*, 2003; Ilg et al, 2005). Inflammatory signalling pathways involving reactive oxygen species, nitric oxide and dietary omega-3-polyunsaturated fatty acids, have been shown to influence angiogenesis in OIR (Connor *et al.*, 2007; Brooks *et al.*, 2001 Dong *et al.*, 2009).

Cells of the immune system have been implicated in both pathological neovascularisation and revascularisation. Depleting resident microglia has been shown to cause pathological neovascularisation (Checchin et al. 2006; Kubota et al. 2009). However at the same time, bone marrow derived cells injected intravitreally have been shown to promote physiological revascularisation and stop pathological neovascularisation (Ritter et al. 2006). Activation status of macrophages seems to be critical to the angiogenesis outcome.

Different subsets of myeloid cells have been shown to have different angiogenic properties. (Checchin et al. 2006). Polarisation status is also critical to the role macrophages play in angiogenesis. In Il10 deficient mice, Il10 has been shown regulate angiogenic potential through up-regulation of VEGF (Dace et al. 2008).

1.4 Thesis Aims

The aim of this thesis is to explore the concept that stimulation of inflammation in ischaemic retinopathy may modulate hypoxia and reduce the neovascular consequences seen in ischaemia. Better understanding of the preliminary findings may produce the scientific basis for a fundamentally novel approach to ischaemia based on reducing oxygen demand rather than increasing oxygen supply.

2. Materials and Methods:

Reagents were purchased from Sigma Aldrich UK, unless stated otherwise.

2.1 - Mice

All animals were handled in accordance with the UK Animals (Scientific Procedures) Act 1986. The project was approved by the UK Home Office and the UCL Institute of Ophthalmology Ethics Sub-Committee (approval ID PPL 70/8648).

Multiple strains of mice were used; C57BL/6J (purchased from Charles River), C3H/HeJOlaHsd-TLR4$^{Lps\text{-}d}$ mice (which possess a mutation at the LPS response locus (mutation in the toll-like receptor 4 gene, TLR4) resulting in resistance to endotoxin (Poltorak *et al.*, 1998); purchased from Harlan Laboratories), C3H/HeNHsd (containing the Pde6b^{rd1}mutation; purchased from Harlan Laboratories).

B6.129P2-Lyz2$^{tm1(cre)Ifo}$/J (also known as LysM Cre) mice (which specifically express nuclear localised Cre recombinase inserted into the first coding ATG of the lysozyme 2 gene, thereby placing Cre expression under control of the Lys2 gene in cells of the myeloid lineage i.e. monocytes, mature macrophages and granulocytes (Clausen et al. 1999); purchased from the Jackson Laboratory), Gt(ROSA)26Sor$^{tm4(ACB\text{-}tdTomato,\text{-}RGFP)Luo}$ (also known as ROSA$^{mT/mG}$) mice (which express cell membrane localised red fluorescence in widespread cells and tissues prior to Cre recombinase exposure, after which cell membranes express green fluorescence (Muzumdar *et al.*, 2007); purchased from the Jackson Laboratory). A LysM reporter strain was created by crossing LysM Cre transgenic mice with homozygote ROSA$^{mT/mG}$ mice to produce ROSA$^{mT/mG}$ heterozygote, LysM Cre transgenic offspring in which myeloid derived cells express green fluorescent protein.

B6.129P-Gt(ROSA)26Sor$^{tm1(DTA)Jpmb}$/J (also known as ROSA26$^{eGFP-DTA}$) homozygote female mice in which diphtheria toxin fragment A (DTA) transcription is prevented by a strong transcriptional stop sequence until crossed with a strain expressing Cre recombinase under the control of a promoter of interest, whereby the loxP-flanked EGFP and STOP cassette are deleted and the Gt(ROSA)26Sor promoter drives expression of diphtheria toxin, resulting in specific ablation of cre expressing cells (Ivanova *et al.*, 2005); purchased from the Jackson Laboratory) were crossed with LysM Cre transgenic male mice to produce ROSA26$^{eGFP-DTA}$ heterozygote, LysM Cre transgenic offspring in which myeloid derived cells were selectively ablated.

B6.129(Cg)-Ccr2$^{tm2.1Ifc}$/J (also known as Ccr2^{RFP}) mice (in which a monomeric red fluorescent protein sequence replaces the coding sequence of the chemokine (C-C motif) receptor 2 (Ccr2) gene, abolishing gene function and thereby reducing monocyte recruitment (Saederup *et al.*, 2010); mice kindly provided by Dr Florian Sennlaub, INSERM, Institut de la Vision, Paris) and B6.129S4-Ccl2 ^{tm1Rol}/J (also known as Ccl2 KO) mice (in which a mutation in the SCYA2 gene encoding for monocyte chemoattractant protein 1 (MCP-1)(also known as chemokine (C-C motif) ligand 2 Ccl2) results in impaired monocyte and macrophage recruitment (Lu *et al.*, 1998); mice kindly provided by Dr Florian Sennlaub, INSERM, Institut de la Vision, Paris) were also used to examine the effect of impaired monocyte and macrophage recruitment.

Mouse Strain	**Purchased From**	**Phenotype**
C57BL/6J	Charles River	Wild type mice – no phenotype
C3H/HeJOlaHsd-TLR4^{Lps-d} mice	Harlan Laboratories	Mutation in TLR4 resulting in resistance to endotoxin/LPS
C3H/HeNHsd	Harlan Laboratories	Mutation in Pde6b^{rd1} resulting in thin retina
B6.129P2-Lyz2$^{tm1(cre)Ifo}$/J (also known as LysM Cre)	Jackson Laboratory	Expresses Cre recombinase in the LysM 2 gene resulting in

		expression in cells of the myeloid lineage
Gt(ROSA)26Sor$^{tm4(ACB-tdTomato,-RGFP)Luo}$ (also known as ROSA$^{mT/mG}$)	Jackson Laboratory	Expresses red fluorescence in cell membranes prior to Cre recombinase exposure, after which expresses green fluorescence
ROSA$^{mT/mG-c/wt}$,LysM Cre^{tg} (also known as LysM Cre reporter)	Bred in house	Expresses green fluorescent protein in myeloid derived cells
B6.129P-Gt(ROSA)26Sor$^{tm1(DTA)Jpmb}$/J (also known as ROSA26$^{eGFP-DTA}$)	Jackson Laboratory	Expresses diphtheria toxin when crossed with cre recombinase expressing cell, resulting in specific ablation of cre expressing cells
ROSA26$^{eGFP-DTA-C/Wt}$,LysMCre^{tg} (also known as LysMCreDTA Tg)	Bred in house	Selective ablation of myeloid derived cells
B6.129(Cg)-Ccr2$^{tm2.1Ifc}$/J (also known as Ccr2^{RFP})	Dr Florian Sennlaub, INSERM, Institut de la Vision, Paris	Abolished Ccr2 gene function resulting in reduced monocyte recruitment
B6.129S4-Ccl2 ^{tm1Rol}/J (also known as Ccl2 KO)	Dr Florian Sennlaub, INSERM, Institut de la Vision, Paris	Mutation in the SCYA2 gene encoding for Ccl2 resulting in impaired monocyte and macrophage recruitment

Table 2.1. Mice strains used with details of suppliers and phenotypes.

2.2 – Oxygen Induced Retinopathy Model

Mice were housed in individually ventilated cages (IVC) in the biological services unit at the UCL Institute of Ophthalmology. The IVC cages provide mice with constant access to dehydrated rodent feed and water, which was topped up regularly. Every four days the mice were transferred to fresh IVCs with fresh bedding.

Date of birth of neonatal mice was recorded as P0. At P7 litters were exposed with their feeding mothers to hyperoxia (75% Oxygen) for 5 days until P12 as described previously (Smith et al., 1994). Oxygen was taken from a gas container (BOC, size F, medical oxygen) and delivered into a perspex oxygen chamber. A sensor inside the cage monitored the oxygen concentration which was maintained constantly at 75% ± 2% by the oxygen controller (PROOX 110; Reming Bioinstruments CO, Redfield USA).

Temperature was kept stable at 25˚C ± 2˚C and humidity within the chamber was monitored. The animals were exposed to 12 hour cycles of broad spectrum light. The filters of the IVC cages were removed to allow free flow of oxygen into and out of the cages. Cages and bedding were changed at P9.

Mothers were exposed to hyperoxia for 22 hours a day and given 2 hour breaks of normoxia to prevent oxygen toxicity during this period (Tan *et al.*, 2013). The oxygen chamber is equipped with an outlet valve to allow the flow of oxygen throughout the system, ensuring that any build-up of carbon dioxide is flushed out of the chamber. Soda-lime crystals are also placed in the chamber to act as a carbon dioxide quencher.

At P12 litters and feeding mothers were then returned to normoxic conditions and housed in IVCs. Pups were weighed at P7, P12, P14 and P17 to ensure that the mice continued to gain weight throughout their development and that malnutrition had not occurred. At the P14 time points any pups weighing less than 5g were excluded and at the P17 time point any pups weighing less than 6g were excluded from the study (Connor *et al.*, 2009). Any pups found to significantly weigh less than their littermates (±0.5g) were also excluded from analysis. Litter sizes were restricted to a maximum of 8 pups per mother to control for the nutritional status of the pups and to limit the feeding demand placed on the mothers. Pups were then culled by decapitation at either P14 to examine hypoxia or at P17 to examine neovascularisation.

2.3 – Intraperitoneal Injections

Intraperitoneal injections were delivered to the mice pups at P12 on removal from the OIR chamber. Mouse pups were scruffed and inverted to allow for the intra-abdominal

organs to move away from the abdominal wall. Injections were given to the right lower abdominal quadrant to avoid injury to the abdominal organs.

2.3.1 - Lipopolysaccharide Injections

In LPS experiments, mice pups in the treatment group were injected with 20µg of LPS (a 20µl injection of 1mg/ml LPS in 1xPBS, LPS from Sigma Aldrich, UK) and mice pups in the control group were injected with 20µl of 1xPBS intraperitoneally using a 50µl glass microliter syringe (Hamilton Company, USA). Separate syringes were used for each group to avoid contamination.

2.3.2 – Interleukin 1 Beta Injections

Mice pups in the treatment group were injected with 0.5µg of IL1β (a 10µl injection of 50µg/ml IL1β in 0.1% bovine serum albumin(BSA) in 1x PBS, IL1β from PeproTech EC Ltd, UK) and mouse pups in the control group were injected with 10µl of vehicle (0.1% BSA in 1x PBS) intraperitoneally using a 50µl glass microliter syringe (Hamilton Company, USA). Once again separate syringes were used for each group to avoid contamination.

2.3.3 – MC21 (anti mouse CCR2) Injections

To block CCR2 and to deplete CCR2+ cells in mice undergoing OIR in both PBS and LPS treatment groups the rat anti mouse MC21 antibody (Mack *et al.*, 2001) (provided by Professor Matthias Mack, University Hospital Regensburg, Germany) was injected systemically. Mouse pups in the control group were injected intraperitoneally with 20µg of MC21 (20µl of 1mg/ml antibody solution) and mouse pups in the control group were injected intraperitoneally with 20µg of rat IgG2b negative control antibody

(1mg/ml antibody solution, from Biorad, UK) using a 50µl glass microliter syringe (Hamilton Company, USA), ensuring separate syringes were used for each group.

After system injection of the MC21 antibody, CCR2+ cells disappear after 6-8 hours and reappear after 48 hours. Prolonged depletion can be achieved by daily injection of 20µg MC21 (Liu *et al.*, 2013). However, 5 days after the initial MC21 injection neutralising antibodies against MC21 develop in the mouse thereby inactivating the effect of injections. Therefore, pups undergoing OIR were injected with either MC21 or IgG2b negative control on days P11, P12, P13, P14 to ensure sufficient depletion throughout the period where the mice are exposed to normoxia.

2.4 – Intraocular Injections

Intraocular injections were delivered to the mice pups at P12 on removal from the OIR chamber. Mouse pups were deeply anaesthetised using isoflurane inhalation (Isoflourane-Vet™, 100% inhalation vapour liquid from Merial, UK). Injections were delivered using a 10µl gastight glass syringe (Hamilton, USA) loaded with a 33 gauge ½ inch needle (STERiJECT needle, TSK Laboratories, Japan). The anaesthetised mice pups and the left eye to be injected were sterilised with 100% ethanol prior to injection to prevent infection. The syringe was loaded to a micromanipulator (Prior Scientific, UK) and the needle tip advanced through the sclera, posterior to the iris and the lens, into the vitreous (Gerhardt *et al.*, 2003).

2.4.1 – Interleukin 1 Beta Injections

Mice pups were injected with 5ng of IL1β (a 0.5µl injection of 10µg/ml IL1β in 0.1% bovine serum albumin(BSA) in 1x PBS, IL1β from PeproTech EC Ltd, UK) into the left eye. The contralateral, non-injected right eye in the same mouse was used as a control.

2.4.2 – CCL5 Injections

Mice pups were injected with 500ng of CCL5 (a 0.5µl injection of 1000µg/ml CCL5 in 0.1% bovine serum albumin(BSA) in 1x PBS, CCL5 from PeproTech EC Ltd, UK) into the left eye. The contralateral, non-injected right eye in the same mouse was used as a control.

2.4.2 – Vehicle Injections

Mice pups were injected with 0.5µl of vehicle (0.1% bovine serum albumin(BSA) in 1x PBS) into the left eye. The contralateral, non-injected right eye in the same mouse was used as a control.

2.5 – Retinal Wholemount Preparation

Mice were culled by decapitation and their eyes were enucleated using curved forceps. The enucleated eyes were fixed in 2% paraformaldehyde for 5 minutes (1:1 solution of 4% PFA and 2xPBS) and then transferred into petri dishes of 2xPBS solution, where they were kept for 10mins to soften the eyes prior to being dissected.

Using a 21 gauge needle an incision was made into the cornea. The cornea and outer sclera were removed in a strip like fashion using fine forceps and spring loaded microdissection scissors (Biology grade 4, dumoxel, Agar Scientific Ltd). The lens, hyaloid vasculature and vitreous body were then removed from the eye cup using forceps ensuring that no remaining vitreous was left attached to the retina. To flatten the eye cup, radial relaxing incisions were cut into the retina up to the mid periphery. The 2xPBS was aspirated and the retinas flattened onto the floor of the petri dish, ensuring that all the retinal leaves were unfolded.

Retinas were then either fixed with 4% paraformaldehyde for 45 minutes at room temperature or cold methanol. Methanol which was kept in the freezer at –20^{o}C was added slowly one drop at a time using a Pasteur pipette on the retinas to prevent the retinas from curling up. Methanol fixed retinas were then stored in 96 well plates at minus 20˚C (Powner et al. 2012).

2.6 - Immunohistochemistry

Methanol fixed retinas were removed from the freezer and blocked for at least one hour at room temperature in retinal wholemount blocking buffer solution (3% triton, 0.5% Tween 20, 0.1% sodium azide in 1% BSA) in the 96 well plate. Paraformaldehyde fixed retinas were also blocked in retinal wholemount blocking buffer solution for at least one hour.

The retinas were then removed from the blocking buffer and incubated in antibody solution made up of the primary antibodies and wholemount buffer where they were left overnight, covered at room temperature. The following day retinas were washed in wholemount blocking buffer for an hour (3 washes of approximately 20 minutes in duration each) and then incubated in secondary antibody solution of a 1:200 concentration in wholemount blocking buffer for 4 hours. The wholemounts were then washed three times in wholemount blocking buffer (the first two washes lasting for approximately 30 minutes each and the final wash being left overnight, covered at room temperature). The following day the wholemounts were fixed for 10 minutes in 4% paraformaldehyde, after which they were washed twice in 2XPBS for 20 minutes. Finally, they were mounted on microscope slides using Mowiol mounting media.

Antibodies used for immunohistochemical staining included rabbit anti-collagen type IV (Biorad), biotinylated rabbit anti ERG 1,2,3 (Santa Cruz), goat anti-mouse IBA1 (AbCam), biotinylated isolectin B4 (Vectorlabs), FITC-conjugated isolectin B4 (Vectorlabs), rat PE anti-mouse Cd11b (BD Pharmingen), rabbit anti-mouse Cd11b (Novus Biologicals) and secondary Alexa-430, Alexa-488 and Alexa-647 antibodies (Life Technologies).

2.6.1 – EF5 Hypoxia Staining

EF5 staining was used to demonstrate tissue hypoxia in retinal wholemounted tissue. Mouse pups were injected intraperitoneally with 50µl of EF5 solution (10mM in normal saline) (Koch, 2002) using a 50µl microliter glass Hamilton syringe at P14, 2 hours before they were scheduled to be sacrificed. The EF5 nitromidazole forms a covalent bond to macromolecules in the cell after being reduced under hypoxic conditions. EF5 is then detected through the binding of a fluorescent anti EF5 antibody (ELK3-51 directly conjugated with Cy3, diluted 1:1 in retinal blocking buffer, purchased from University of Pennsylvania Department of Radiation Oncology) on fixed tissue. To ensure staining of EF5 in the retina, the retinal wholemounts were fixed with 4% PFA rather than methanol (West, Richardson and Fruttiger, 2005).

2.6.2 – BrDU Proliferation Staining

5-bromo-2'-deoxy-uridine (BrdU; Boehringer Manheim) was used to demonstrate proliferating cells in retinal wholemounted tissue. Mouse pups were injected intraperitoneally with 50µl of BrdU solution (10mg/ml BrdU in 1xPBS) using a 50µl glass Hamilton syringe at P14, 2 hours before they were scheduled to be sacrificed. Wholemounted retinas were fixed in cold methanol as previously described.

Prior to performing the BrdU staining protocol (as described in (West, Richardson and Fruttiger, 2005)) the retinal wholemounts were stained with Collagen IV to highlight the retinal vasculature, using the same immunohistochemical staining protocol described previously. However, after incubating in the secondary antibody solution and washing in wholemount block the retinas were then transferred to a 24 well plate and fixed in 4% PFA for 10 minutes. Following this the retinas were washed. This was followed by a 15 minute exposure to 70% ethanol and then a 30 minute exposure to 6M HCL containing 1% Triton-X-100. Retinas were then repeatedly washed in 2xPBS over 10 minutes prior to a longer wash in 2xPBS over 45 minutes. The pH of the 2xPBS was then tested to ensure neutrality had been reached after the HCl exposure. Once neutrality had been confirmed the tissue was blocked in wholemount blocking buffer for an hour prior to being stained with mouse anti-BrdU antibody (BrdU antibody (Abcam) solution of a 1:5 concentration in 1% Triton-X-100 in PBS) (Magaud *et al.*, 1989). The wholemount staining protocol then continued as previously described using an alexa -594 secondary antibody (Life Technologies).

Antibody	**Company**	**Cat. #**	**Dilution**
Retinal Vasculature			
Biotinylated GSL Isoectin B4 (ILB4)	Vector Laboratories, UK	B-1205	1:200
Fluorescein labelled GSL Isolectin B4 (ILB4)	Vector Laboratories, UK	FL-1201	1:200
Rabbit anti mouse Collagen IV (Col IV)	Biorad, UK	2150-1470	1:200
Rabbit Erg - 1,2,3	Santa Cruz Biotechnology, USA	Sc-354	1:200
Inflammatory Cells			
Goat anti mouse IBA1	AbCam, UK	Ab5076	1:500
Rat PE anti mouse Cd11b	BD Pharmingen, UK	557397	1:200
Rabbit anit-mouse Cd11b	Novus Biologicals	NB110-40766	1:200
Hypoxia			

Cy3 conjugated Anti-EF5 antibody (ELK3-51)	University of Pennsylvannia, USA		1:1
Proliferation			
Mouse anti BrdU	AbCam, UK	Ab8152	1:5
Secondary Antibodies			
Alexa-Flour® 350 donkey anti goat IgG	Life Technologies, UK	A21081	1:200
Alexa-Flour® 594 donkey anti mouse IgG	Life Technologies, UK	A11005	1:200
Alexa-Flour® 647 chicken anti rat IgG	Life Technologies, UK	A21472	1:200
Alexa-Flour® 647 donkey anti rabbit IgG	Life Technologies, UK	A31573	1:200
Streptavidin Alexa-Flour® 647	Life Technologies, UK	S32357	1:200

Table 2.2. List of antibodies, suppliers and dilutions used.

2.7 – Retinal Wholemount Imaging

Retinal wholemounts were imaged using an Olympus SZX16 dissection stereo microscope with an Olympus U-RFL-T fluorescent lamp, fitted with a Hamamatsu ORCA-100 C4742-95 digital camera and Simple PCI software v6.6 (Legacy). Images were taken at both 1.6 x and 5x magnification using the Olympus dissection microscope. For higher magnification the wholemounts were imaged using a 10x objective on a Zeiss widefield fluorescence imaging system, comprising of a Zeiss Axioskop 2 MOT microscope with a Prior Scientific Lumen 200 metal halide lamp, fitted with a Hamamatsu ORCA-ER digital camera and Simple PCI software v6.6 (Legacy, USA).

2.8 – Image J Retinal Wholemount Analysis

Digital images were analysed using Image J software version 1.47 (National Institutes of Health, USA). Images were randomised and analysis was performed blinded to prevent bias.

2.8.1 – Avascular Area Analysis

Using the split channel function on ImageJ, the avascular area was calculated using 1.6x magnified images of isolectin stained retina. The freehand selection tool was used to outline the vaso-obliterated region (**Figure 2.1B**). Once the avascular region had been highlighted the area in pixels squared could be calculated using the measurement function.

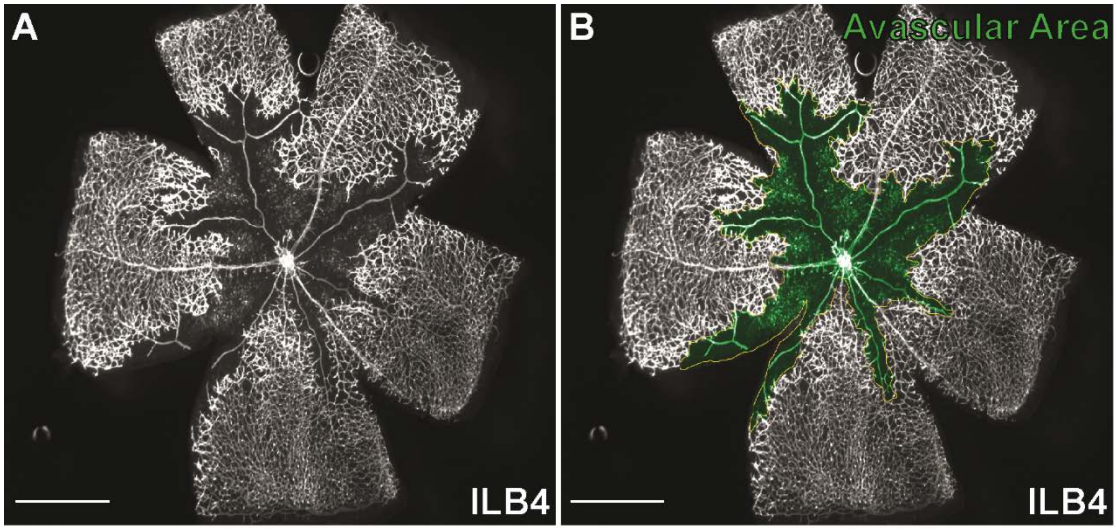

Figure 2.1 - Avascular Area Analysis. Retinal wholemounts from P14 mice having undergone OIR labelled with isolectin to demonstrate the retinal vasculature (A). The vaso-obliterated area has been selected (green) to allow analysis of the avascular area (B). Scale bars = 100µm.

2.8.2 – Vessel Tortuosity Analysis: Tortuosity Index and Integrated Curvature

Using the same 1.6x magnified images of the isolectin stained retinal wholemount, the retinal arteries were analysed using an ImageJ macro plugin designed to assess the tortuosity of the vessel (Scott, Powner and Fruttiger, 2014). Arteries were tracked using the straight, segmented line function. The vessels paths were traced from the retinal centre radiating out towards the periphery, to contain 10 segments ensuring that the segments remained within the width of the vessels (**Figure 2.2**). The resulting

zigzag path was then used as an approximation for the vessel to be analysed using the tortuosity macro. The macro calculates the overall line length divided by the distance between the first and the last point providing an approximation of the Tortuosity Index (a straight line has a TI of 1) (**Figure 2.2A**). In addition, the macro also calculates the sum of the angles between the segments divided by the distance between the first and last point and used as an approximation for the Integrated Curvature (a straight line has an IC value of 0) **(Figure 2.2B)**. 4 arteries in each wholemount were measured and 10 segments taken for each artery to ensure consistency between retinas. The tortuosity index and integrated curvatures for each vessel were calculated and then averaged for each retina.

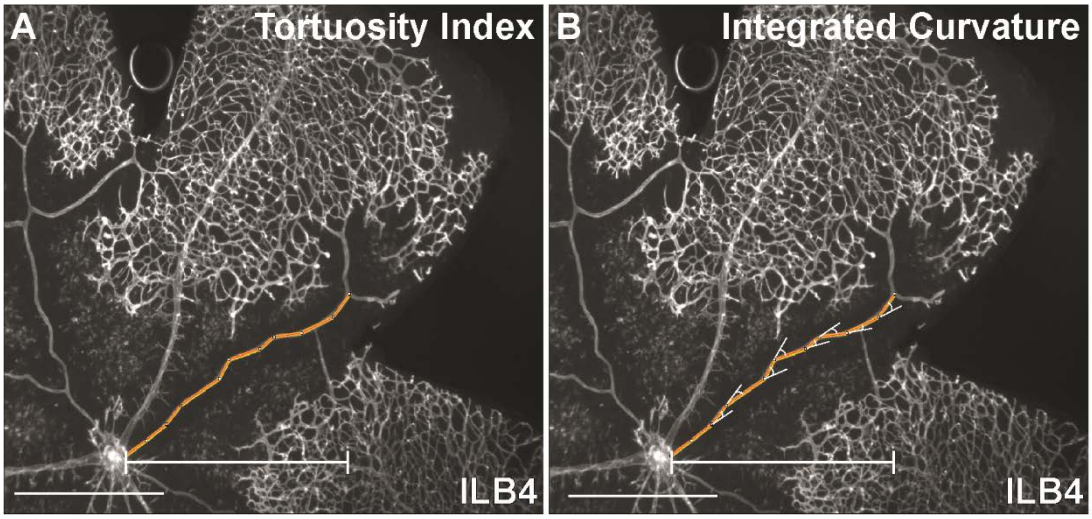

Figure 2.2 - Vessel Tortuosity Analysis: Tortuosity Index and Integrated Curvature. *Retinal wholemount from P14 mice having undergone OIR labelled with isolectin to demonstrate the retinal vasculature. The tortuosity index was calculated by dividing the length of the segmented line (yellow segmented line) by the distance between the start and finish points (white line) (A). The integrated curvature was calculated by dividing the sum of the angles between the line segments the distance between the start and finish points (B). Scale bars = 50µm.*

2.8.3 – Hypoxia Analysis: EF5 Hypoxic Area, Hypoxic Intensity and Hypoxic Density

Using the split channel function on ImageJ, the hypoxic area was calculated using 1.6x magnified images of EF5 stained retina. The freehand selection tool was used to outline the EF5 stained regions (**Figure 2.3B**). Once the hypoxic regions had been highlighted the area in pixels squared could be calculated using the measurement function. ImageJ also calculated the mean grey value of the EF5 stained area (hypoxic area intensity), which is the sum of the grey values of all the pixels in the selection divided by the number of pixels, and the integrated density of the EF5 stained area (hypoxic area density), which is the product of the area and the mean grey value.

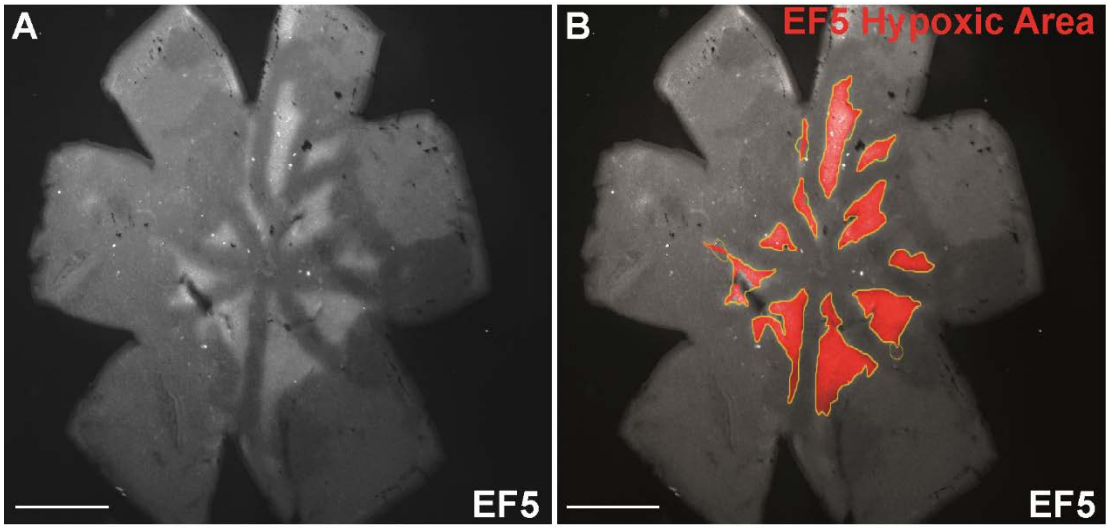

Figure 2.3 - Hypoxia Analysis: EF5 Hypoxic Area. *Retinal wholemount from P14 mice having undergone OIR labelled with EF5 antibody to demonstrate hypoxia (A). The area positive for EF5 staining has been highlighted (red) to allow analysis of the hypoxic area (B). Scale bars = 100μm.*

2.8.4 – Neovascular Area

In P17 retinas the neovascular area was calculated by analysing the neovascular tufts using 1.6x magnified images of collagen IV stained retina. The freehand selection tool was used to outline the neovascular tufts (**Figure 2.4B**). Once all the tufts had been

highlighted the area in pixels squared could be calculated using the measurement function.

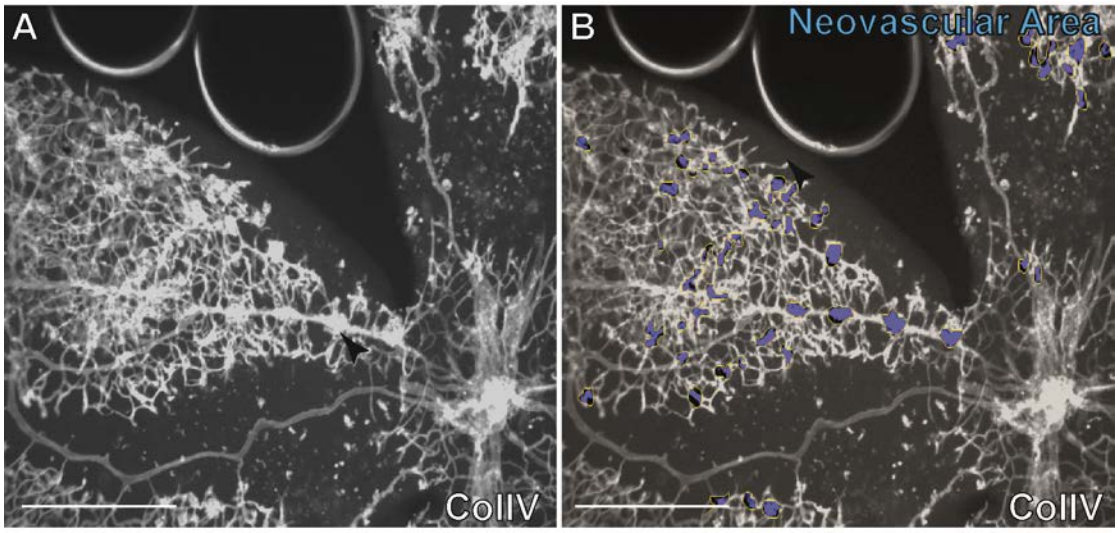

Figure 2.4 – Neovascular Area Analysis. *Retinal wholemount from P17 mice having undergone OIR labelled with Collagen IV antibody to demonstrate neovascular tufts growth towards the vitreous from the retinal vasculature (A). The total area of neovascular growth has been selected (blue) to allow analysis of the neovascular area (B). Scale bars = 50µm.*

2.8.5 – Cell Counting

To count cells, thresholding was performed to select the desired cell population and the resulting image turned into binary data. Image J particle analysis was then used to count number of cells.

2.8.6 – Statistical Analysis

Statistically analysis was performed using Statistical Package for the Social Sciences v.24 (SPSS, IBM Software, USA). The Shapiro-Wilk test was used to ensure the normality of the data to be analysed and a Levene's test was used to look for equal variance. Means were compared using a two tailed, independent *t*-test and a p-value less than 0.05 was deemed as significant. Bar charts were created using Microsoft Excel 2016 software 2016 (Redmond, USA).

2.9 – Flow Cytometry

2.9.1 – Mice

A litter of C57 mice were separated into three treatment groups at P7. The first group were to be age matched controls while the other two groups we placed in the OIR chamber to undergo the OIR protocol. At P12 on return to normoxia group 2 were injected with PBS intraperitoneally and group 3 were injected with LPS intraperitoneally. At P14 the mice were weighed to ensure sufficient weight gain and were euthanised so that the retinal tissue could be prepared for flow cytometry.

2.9.2 – Tissue Preparation

Samples and buffers were kept on ice throughout the preparation protocol. Mice were sacrificed and eyes were enucleated and dissected microsurgically in 100µl flow buffer to isolate the retina. Both retinas from each mouse pup were pooled prior to undergoing enzymatic cell dissociation with a solution containing 25 mg/ml DNAse 1 (Sigma-Aldrich Ltd., UK) and 10 mg/ml Collagenase D (Roche Diagnostics Ltd., UK) for 30 minutes at a temperature of 37°C. For homogenisation, the digested tissue was then titurated using a pipette before being passed through a 96-well 60µm cell strainer plate (Millipore UK Ltd., UK). The 96 well plate was then centrifuged (300g for 5 minutes) and the resulting supernatant was discarded.

2.9.3 – Flow Cytometry Staining

Technical Acknowledgements: Flow Cytometry was performed by Dr Sidath Liyanage, UCL Institute of Ophthalmology, London.

Following centrifugation, to produce a single cell suspension the cell pellet was re-suspended in flow buffer. Rat anti-mouse CD16/32 Fc block (1:100; clone 2.4G2; BD, UK) was added for 10 minutes at 4°C. The 96 well plates were then covered in foil and surface staining was performed for 20 minutes at 4°C in staining buffer. Between each incubation cells were washed with flow buffer. Between each step, the plate was centrifuged at 300g for 5 minutes. Immediately prior to flow cytometry a final suspension with the cell viability stain DRAQ7 in flow buffer was performed.

The following surface markers were used to create the myeloid specific panel for these experiments: CD11b clone M1/70 BV711 (1:80; Biolegend Ltd., UK); CD11b clone M1/70 BB515 (1:200; BD, UK); CD11b clone M1/70 PE-Cy7 (1:100; eBioscience Ltd., UK); CD11c clone N418 BV605 (1:100; Biolegend Ltd., UK); CD11c clone N418 FITC (1:400; eBioscience Ltd., UK); Ly6C clone HK1.4 BV510 (1:160; Biolegend Ltd., UK); Ly6G clone 1A8 BV421 (1:160; Biolegend Ltd., UK); Ly6G clone 1A8 APC (1:100; eBioscience Ltd., UK).

2.9.4 – Data Acquisition

For flow cytometry immunophenotyping experiments, cells were acquired on a Fortessa X-20 cytometer (BD Immunocytometry Systems, USA) equipped with 355 nm, 405 nm, 488 nm, 561 nm and 633 nm excitation lasers. Each sample was made up to a volume of 300µl and analysed at a 12µl/min flow rate over 3 minutes. Data was collected using BD FACS Diva software (BD Immunocytometry Systems, USA). The 'application settings' function was utilised in each experiment to ensure that any inter-experimental variation due to photomultiplier tube voltage variation was minimized. This feature calibrates the voltage settings to match those of the initial experiment, based on standardized calibration beads (CS&T beads; BD, UK). Reproducibility in the

voltage settings was confirmed through the use of 8-peak rainbow beads (Spherotec; BD, UK).

2.9.5 – Data Analysis

Analysis of the data was performed using FlowJo v.10.0.7 software (FlowJo LLC., USA). Compensation using single colour controls prepared from OneComp eBeads (eBiosciences Ltd., UK) and dead splenocytes (heated at 65°C for 1 minute) for live or dead discrimination was performed. Compensation matrices were calculated and applied using FlowJo. Fluorescence minus one (FMO) controls were used for gating analyses to distinguish positively from negatively staining cell populations.

Absolute cell counts were obtained through using unstained beads. 50000 AccuCount blank polystyrene beads (Spherotech Inc., USA) were diluted into 300µl of PBS and eight two-fold serial dilutions were made. These were acquired on the flow cytometer using the same settings and time as samples. Gating around the bead region resulted in an absolute count, allowing a standard curve to be constructed, using a linear regression constrained through zero (Prism 6; GraphPad Software, USA). This method was used to estimate the absolute number of cells in each flow cytometry experiment.

2.10 – RNA Sequencing

2.10.1 - Mice

Once again, litters of C57 mice were separated into three treatment groups at P7 (P14 age matched controls, OIR injected with intraperitoneal PBS and OIR injected with intraperitoneal LPS) and euthanised at P14.

2.10.1 – Retinal RNA and Wholemount Preparation

Prior to collected the tissue all bench surfaces were cleaned using with RNAse Zap® (Sigma Aldrich) decontaminating solution. Dissection instruments were cleaned by being soaked in 4% paraformaldehyde for 5 minutes followed by a 10 minute soak in 70% ethanol.

Mice were culled by decapitation and their eyes were enucleated using curved forceps. The left eye was placed into a petri dish of DEPC treated 1xPBS for RNA isolation and the right eye placed into a petri dish of 4% paraformaldehyde in for wholemount preparation. The eye for RNA isolation was dissected in DEPC treated 1x PBS using the RNA free instruments. Cornea, outer sclera, iris, lens and vitreous were all removed to leave the retina alone. A radial incision was made in the retinal cup up to the mid-periphery and then the dissecting scissors were turned 90^{o} to make a circumferential section, thereby separating the central and peripheral retina. The central retina contained the vaso-obliterated area while the peripheral retina contained the vascularised area. Both central and peripheral retinal samples were placed into RNA free Eppendorfs and snap frozen on dry ice prior to being stored at -80^{o}C. A retinal wholemount was then prepared from the right as previously described to ensure that the OIR and LPS injections had worked.

2.10.2 – RNA Extraction

Retinal tissue stored at -80^{o}C was defrosted straight into 1ml of Trizol and left to stand for 1 minute at room temperature. The solution was disaggregated to lyse the cells using a 25 gauge needle. 200µl of chloroform was then added to the sample and the sample repeatedly inverted. The sample was allowed to stand at room temperature for 2-3 minutes and then centrifuged for 15minutes at 12,000RCF while at 4^{o}C. On

removal from the centrifuge the sample had separated into three separate layers. The clear aqueous supernatant was carefully removed with a P200 Gilson pipette and placed into a fresh sterile Eppendorf. To precipitate the RNA from this aqueous phase, 500µl of isopropanol and 1µl of glycogen were added and left at room temperature for 10 minutes and then centrifuged for 10 minutes at 12,000RCF while at 4 ^{o}C. On removal from the centrifuge the supernatant was discarded to leave a pellet of RNA. The pellet was washed with 1ml of 70% Ethanol (RNAse free, DEPC treated) and centrifuged for 5 minutes at 7,400RCF while at 4^{o}C. The supernatant was again discarded and the pellet allowed to air dry. The pellet was then finally suspended in 30µl of RNAsecure (Ambion, UK) and heated to 50^{o}C for 10min on a heating block to ensure complete re-suspension. The RNA was then kept at -80 ^{o}C.

2.10.3 – RNA Sequencing

Technical acknowledgements: RNA sequencing was performed by Tony Brookes, UCL Genomics, Institute of Child Health, London.

The RNA sequencing protocol used was Illumina TruSeq RNA v2. The protocol begins with two rounds of Poly-A RNA selection using dT-beads. This RNA is then fragmented to ~200bp by metal hydrolysis and reverse transcribed to cDNA primed with random hexameric primers. The RNA template is then removed from the reaction and double stranded cDNA is created. Then the overhangs generated from the fragmentation are converted to blunt ends with an exonuclease and a polymerase. This cDNA is then end-repaired and dA-tailed to prevent self-ligation, allowing for ligation of the Illumina TruSeq indexed adapters. Finally, samples are amplified by 15 cycles of PCR enriching those DNA fragments that have adapter molecules on both ends before quality check, library quantification using qPCR (optimum cluster 79 densities across every lane of

every flow cell), normalisation to 10nM and equimolar pooling. Sequencing is then carried out in one lane of the Illumina HiSeq 2000, generating >180m 100bp paired end reads from the pool. The reads were then demultiplexed using Illumina CASAVA 1.8.2 software generating ~36m paired end reads per sample in FASTQ format.

Technical Acknowledgement: FASTQ files were then sent for alignment to Monte Radeke, a collaborator of our group at the Neuroscience Research Institute (NRI), University of California Santa Barbara (UCSB).

3. Results:

3.1 The effect of inflammation in ischaemic retinopathy on hypoxia and neovascularisation

3.1.1 The effect of systemic LPS injection on neovascularisation at P17 in OIR

It is still not fully understood why the angiogenesis that follows hypoxia results in pathological neovascularisation rather than healthy physiological regeneration. There is some evidence that has shown that retinal microglia in the form of both macrophages and monocytes are involved in the formation of new retinal blood vessels and that inhibiting them in rodent OIR can reduce the pathological sequelae associated with ischaemic retinopathy (S Yoshida *et al.*, 2003; Checchin *et al.*, 2006). Inflammatory cytokines such as IL-10 and TNFα have also shown to be pro-angiogenic and when inhibited in OIR can also reduce neovascularisation (Gardiner *et al.*, 2005; Kociok *et al.*, 2006; Dace *et al.*, 2008), further implying that inflammation in the context of ischaemia contributes to pathology. However, there is growing evidence that suggests macrophages undergo an angiogenic switch depending on their polarisation and therefore have the potential to be anti-angiogenic under the right conditions (Dace *et al.*, 2008; Wu *et al.*, 2010; Medina *et al.*, 2011)

Preliminary experiments, previously performed in the lab, explored the effect of local macrophage polarisation on neovascularisation by performing an intraocular injection of LPS into the left eyes of a P12 litter of C57B6 pups that had been exposed to 5 days of hyperoxia (75% O2) between P7-12. As per the traditional OIR model protocol the

pups were then returned to normoxic conditions and the pups were culled at P17 so that retinal wholemounts could be prepared and examined for neovascularisation. Based on the existing literature it was hypothesised that there would be an increase in the neovascular response. However, despite an intense inflammatory reaction characterised by a large influx of inflammatory cells into both the vitreous and the retina of the injected eye, a regenerated vasculature with no abnormal neovascularisation was noted (**Figure 3.1a**). In comparison, the contralateral non-injected eye showed a much milder inflammatory reaction with the influx of fewer inflammatory cells but also showed similar signs of suppressed neovascularisation and healthy regeneration (**Figure 3.1b**).

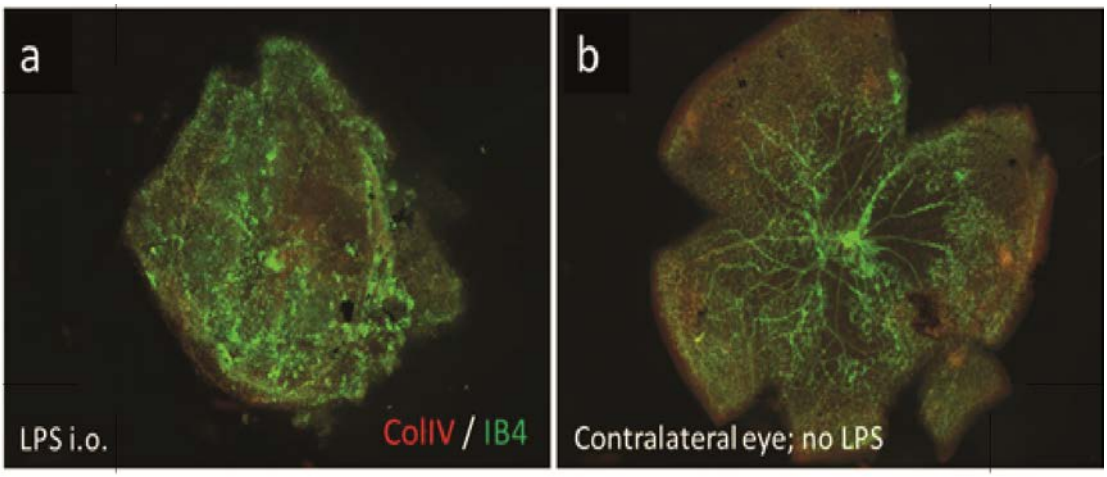

Figure 3.1 – Intraocular injection of LPS results in retinal inflammatory reaction and reduced pathological neovascularisation (Scott 2013 unpublished). *Retinal wholemounts from P17 C57BL6 mice after OIR stained with isolectin B4 (green) and collagen IV (red). Intraocular injection of LPS (a) results in aggressive inflammatory reaction characterised by thick vitreous and large influx of lectin positive inflammatory cells in both vitreous and retina. Through the vitreous a fully regenerated retinal vasculature is observed with no evidence of retinal neovascularisation. The contralateral eye demonstrates a much less severe influx of inflammatory cells but there is a noticeable reduction in the OIR neovascular phenotype as demonstrated by reduced vaso-obliterated area and reduced neovascular tufts.*

These results implied that in the injected eye LPS had a local anti-angiogenic effect resulting in reduction of neovascularisation, but in the contralateral eye the LPS injection must have had a systemic effect.

To test this hypothesis a litter of C57BL6 pups that had been exposed to 5 days of hyperoxia (75% O2) between P7-12 were divided into two groups at P12 on return to normoxia. The treatment group received an intraperitoneal injection of LPS and the control group received an intraperitoneal injection of PBS. Pups were culled at P17 and immunohistochemistry was performed on retinal wholemounts to examine neovascularisation (**Figure 3.2**).

Mouse pups in the control group injected with PBS intraperitoneally were found to demonstrate the typical neovascular phenotype associated with the OIR model at P17, characterised by tortuous retinal arteries **(Figure 3.2I**), central areas of vaso-obliteration (**Figure 3.2C**) which were positive for EF5 hypoxia staining (**Figure 3.2A**) and neovascular tuft formation **(Figure 3.2G**).

Whereas mouse pups in the treatment group injected with LPS intraperitoneally demonstrated a more suppressed neovascular phenotype with areas of healthy vascular regeneration, similar to that seen in the contralateral eyes of the mice injected with intraocular LPS. On examination of the retinal wholemounts, the retinal arteries appeared straight (**Figure 3.2D**) and the retinal vasculature appeared to have regenerated physiologically with few areas of vaso-obliteration (**Figure 3.2D**) and associated EF5 hypoxia stain **(Figure 3.2F**) resulting in less neovascular tufts (**Figure 3.2J**).

When compared with the control group, the avascular area derived from isolectin B4 staining was significantly smaller ($p<0.05$) as was the neovascular area ($p<0.05$) derived from collagen IV staining of the neovascular tufts. Retinal arteries were found to be significantly straighter, as calculated by both tortuosity index ($p<0.05$) and integrated curvature ($p<0.05$), in the LPS treatment group compared to the PBS control group.

Retinal hypoxia, as measured by area of EF5 hypoxia staining and intensity of EF5 hypoxia staining was reduced in the LPS treatment group but this did not reach statistical significance (**Table 3.1**).

Table 3.1: P17 OIR: PBS vs LPS groups

	TreatmentGroup	N	Mean	Std. Deviation	Std. Error Mean
AvascularArea	PBS	3	72808.3	8671.94213	5006.74812
	LPS	3	32044.7	22055.67139	12733.84781
VesselTortuosityIndex	PBS	3	1.1092	.01157	.00668
	LPS	3	1.0169	.00593	.00342
VesselIntegratedCurvature	PBS	3	1.8757	.04213	.02433
	LPS	3	.5687	.14013	.08091
EF5HypoxicArea	PBS	3	21747.3	12267.99292	7082.92902
	LPS	3	6693.67	4520.87838	2610.13035
EF5HypoxicIntensity	PBS	3	104.839	20.82681	12.02437
	LPS	3	95.0513	19.82237	11.44445
EF5HYpoxicDensity	PBS	3	2.44E+6	1810756.820	1045440.937
	LPS	3	578472	343072.8476	198073.2009
NeovascularArea	PBS	3	39657.3	8115.138	4685.277
	LPS	3	2462.00	882.551	509.541

	Levene's Test for Equality of Variances		t-test for Equality of Means						
								95% Confidence Interval of the Difference	
	F	Sig.	t	df	Sig. (2-tailed)	Mean Difference	Std. Error Difference	Lower	Upper
AvascularArea	1.434	.297	2.979	4	.041	40763.66667	13682.77775	2774.18536	78753.14797
VesselTortuosityIndex	1.393	.303	12.294	4	.000	.09225	.00750	.07142	.11308
VesselIntegratedCurvature	4.542	.100	15.470	4	.000	1.30700	.08448	1.07243	1.54157
EF5HypoxicArea	1.747	.257	1.994	4	.117	15053.66667	7548.55376	-5904.47848	36011.81181
EF5HypoxicIntensity	.010	.924	.590	4	.587	9.78800	16.60002	-36.30105	55.87705
EF5HYpoxicDensity	5.334	.082	1.752	4	.155	1864486.000	1064039.354	-1089760.86	4818732.856
NeovascularArea	9.323	.038	7.892	4	.001	37195.333	4712.903	24110.218	50280.449

Table 3.1 – Statistical Comparison of P17 OIR PBS vs LPS treatment groups

These results further demonstrate that LPS injection prior to the induction of OIR can be protective against the neovascular consequences of ischaemic retinopathy and can promote healthy regeneration of the retinal vasculature. They also support the hypothesis that systemic stimulation of the inflammatory system via intraperitoneal LPS injection has an effect on angiogenesis and neovascularisation in the retinal vasculature.

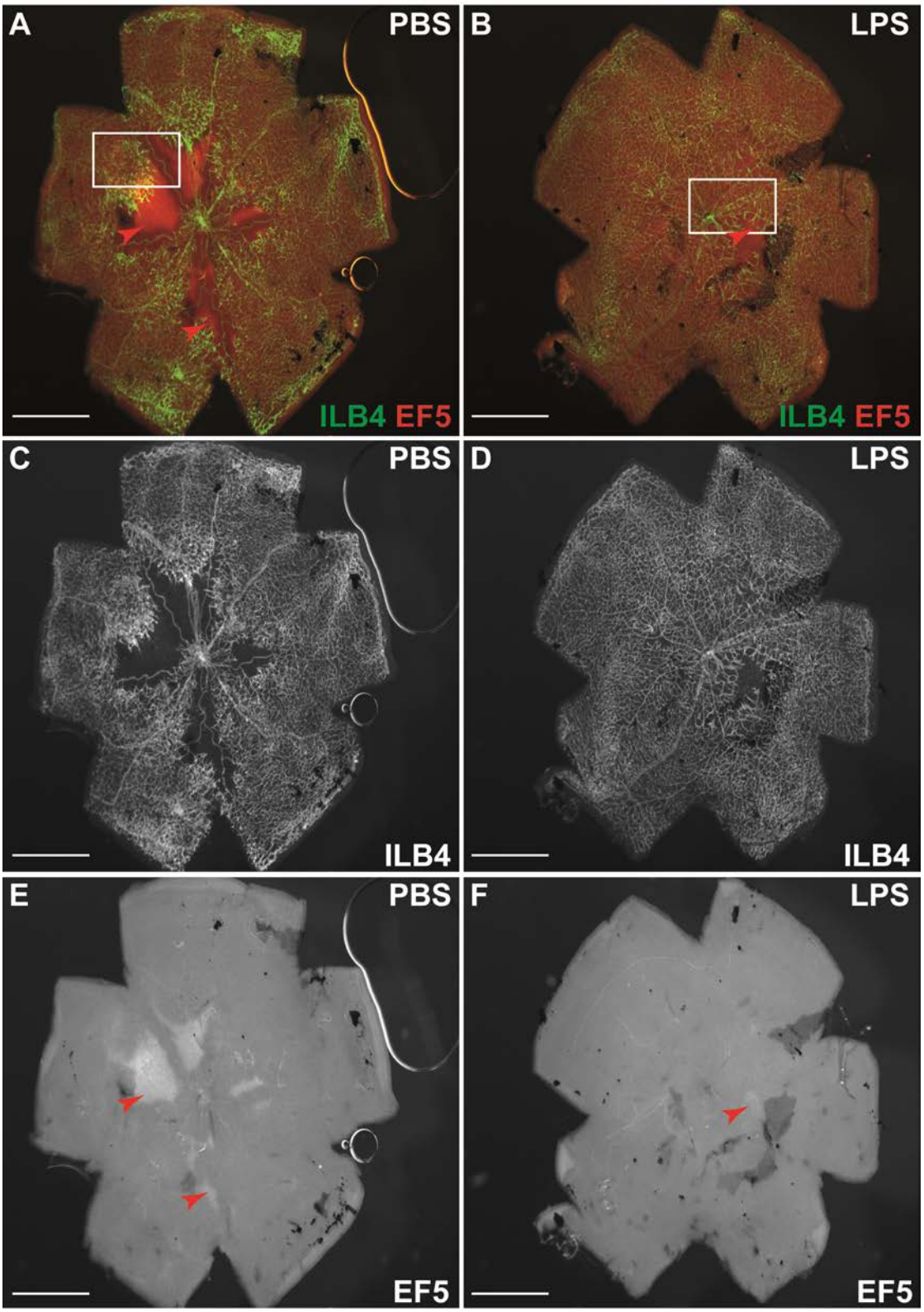

Figure 3.2(a) – Intraperitoneal injection of LPS at P12 after hyperoxia leads to reduced neovascular phenotype at P17 in OIR. Retinal wholemounts from P17 C57BL6 mice after OIR stained with isolectin B4, EF5 hypoxia stain and collagen IV (not shown). Mouse pups in the PBS control group demonstrate central areas of vaso-obliteration (C) which are positive for EF5 hypoxia staining (E) (red arrows) whereas mouse pups in the LPS treatment group demonstrated a retinal vasculature that has regenerated physiologically with few areas of vaso-obliteration (D) and little EF5 hypoxia staining(F). Scale bars = 100µm

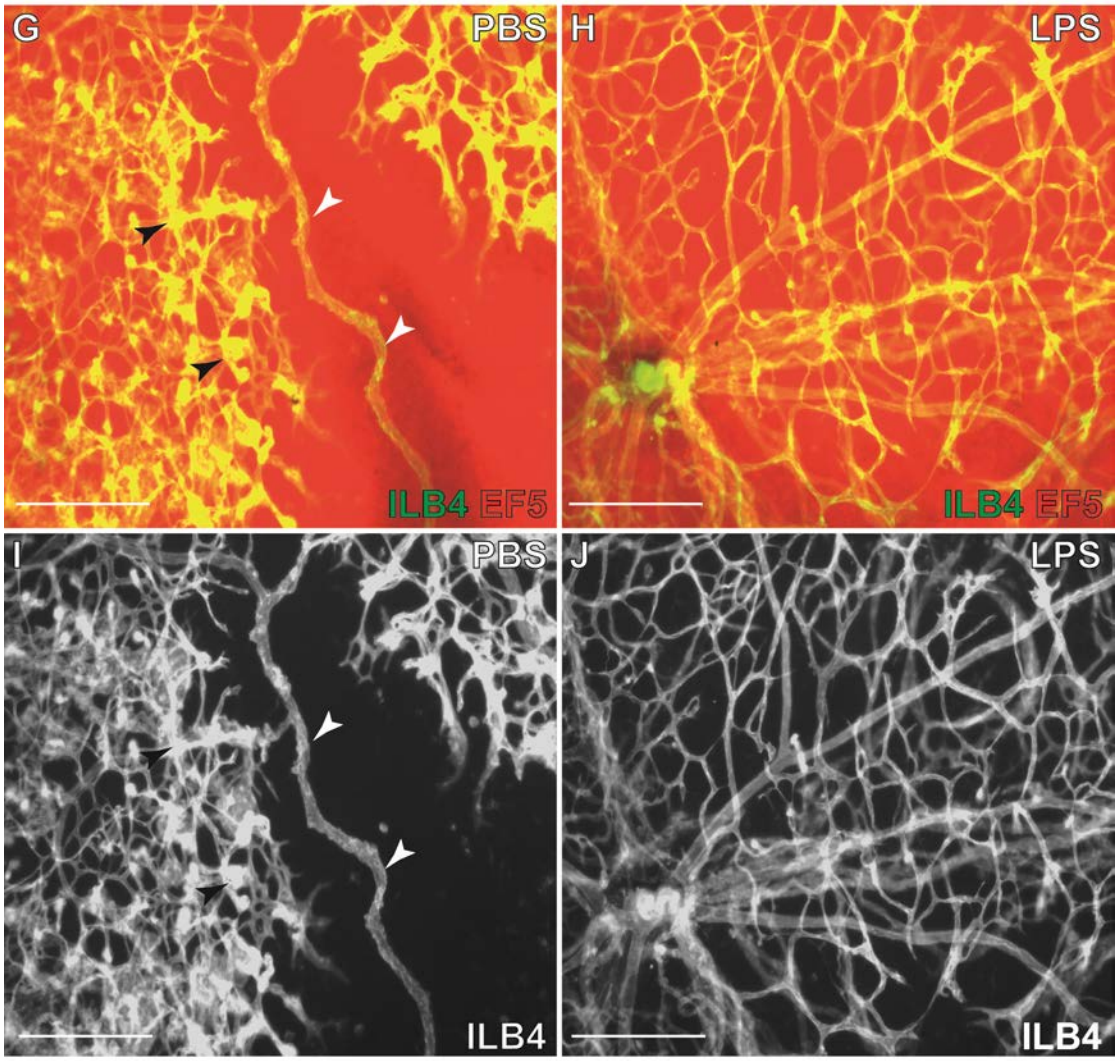

Figure 3.2(b) - Intraperitoneal injection of LPS at P12 after hyperoxia leads to reduced neovascular phenotype at P17 in OIR. *Higher magnification images demonstrate the classical tortuous retinal arteries (I) (white arrows) and neovascular tuft formation (I) (black arrows) associated with OIR at P17 seen in the PBS control group. Whereas in the LPS treated group the retinal arteries are significantly straighter and there is less neovascular growth (J). Scale bars = 50µm*

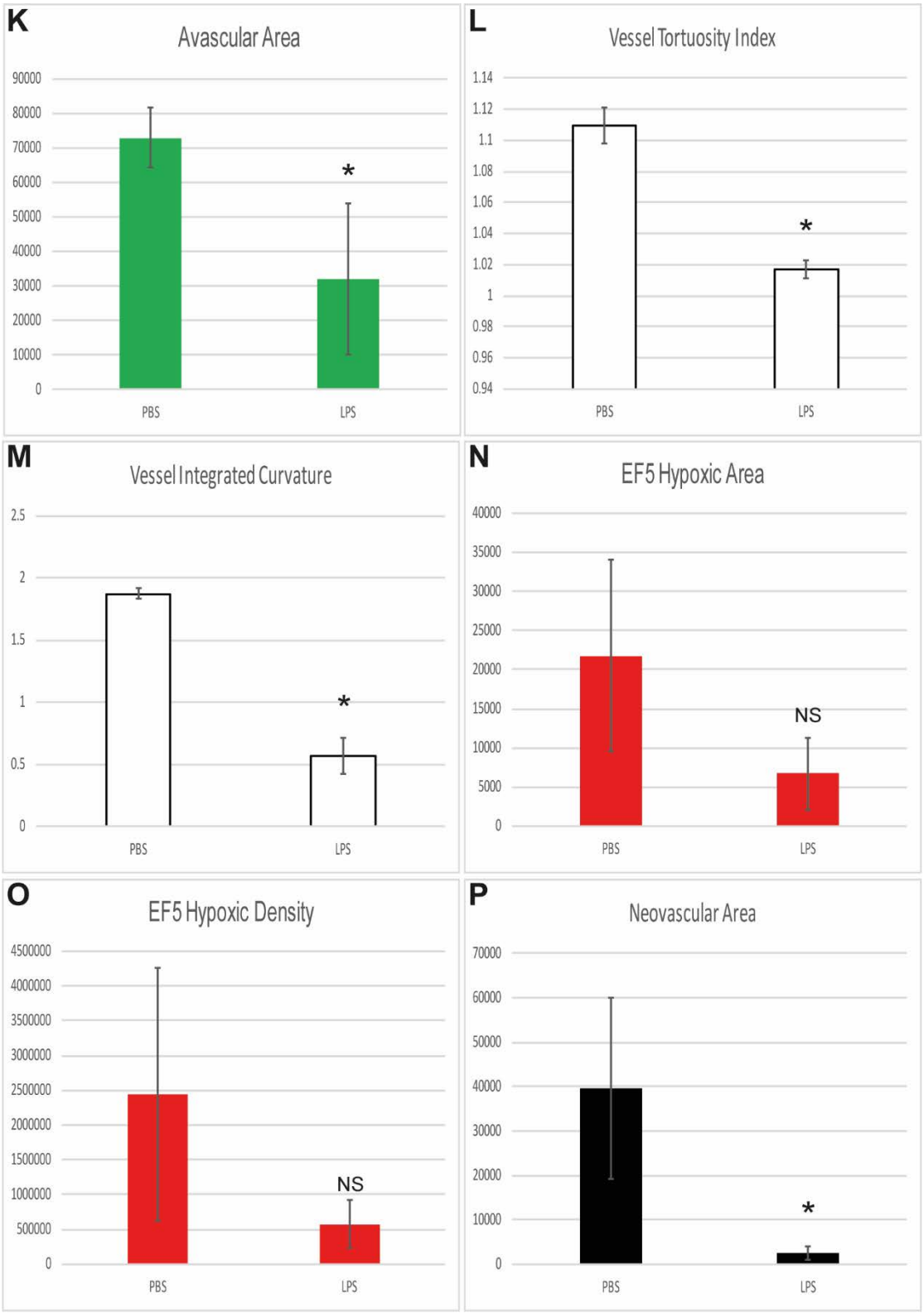

Figure 3.2(c) - Intraperitoneal injection of LPS at P12 after hyperoxia leads to reduced neovascular phenotype at P17 in OIR. *Avascular area (K), vessel tortuosity (both tortuosity index (L) and integrated curvature (M) and neovascular area (P) were all significantly reduced in the LPS treatment group. Hypoxic EF5 area (N) and intensity were both non-significantly reduced in the LPS group. (n= PBS 3 vs LPS 3; error bar = standard deviation; NS = non-significant, * = p<0.05)*

3.1.2 The effect of systemic LPS injection on hypoxia at P14 in OIR

In the OIR model, the pathological neovascularisation seen at P17 is the result of the retinal ischaemia that occurs when the mouse pups are returned to normoxia at P12. During the vaso-obliterative stage, where the pups are exposed to 75% oxygen from P7 until P12, retinal capillary growth is inhibited, resulting in central avascular areas. On return to normoxia, these avascular areas become hypoxic and trigger both normal vessel regrowth as well as pathological neovascularisation. Vascular regrowth occurs between P12 and P17, with neovessel formation occurring between P14 and P17 (Connor et al., 2009).

Given that the neovascularisation is a response to the retinal hypoxia induced by the model, the systemic LPS injections given at P12 when the mice are removed from hyperoxia may be protective against the initial hypoxia experienced on return to normoxic conditions between P12 and P14 and this may explain the reduced neovascular phenotype seen at P17.

To test this hypothesis a litter of C57BL6 pups that had been exposed to 5 days of hyperoxia (75% O2) between P7-12 were divided into two groups at P12 on return to normoxia. Once again, the treatment group received an intraperitoneal injection of LPS and the control group received an intraperitoneal injection of PBS. However, this time pups were culled at P14 and immunohistochemistry was performed on retinal wholemounts to examine hypoxia (**Figure 3.3**).

Mouse pups in the control group injected with PBS intraperitoneally, as expected, were found to demonstrate the typical hypoxic phenotype associated with the OIR model at P14 characterised by tortuous retinal arteries **(Figure 3.3I**), central areas of vaso-

obliteration (**Figure 3.3C**) which are positive for EF5 hypoxia staining (**Figure 3.3E**) (Scott, Powner and Fruttiger, 2014).

Mouse pups in the treatment group injected with LPS intraperitoneally demonstrated a similar picture of central areas of vaso-obliteration (Figure 3.3D), however within these avascular areas the retinal arteries appeared straight (Figure 3.3D) and the areas of EF5 hypoxia stain within them appeared smaller (Figure 3.3F). This is in keeping with reduced retinal hypoxia. Further examination of the avascular areas in the LPS group found that there was an influx of activated isolectin and Cd11b positive immune cells (Figure 3.3 J & L).

Comparison between the two groups showed no significant difference in the avascular areas suggesting that both groups underwent similar vaso-obliterative periods in the hyeproxic period with equal levels of vascular regeneration between P12 and P14.

The retinal arteries were less tortuous in the LPS group, however only the difference in mean integrated curvature was shown to be significant ($p<0.05$). The EF5 stained area was also significantly reduced ($p<0.05$) in the retinas of the LPS group suggesting that LPS treated mice experienced less hypoxia at P14. On analysis of the EF5 intensity it appears that bleed through from the Cd11b stained cells in the avascular area have increased the EF5 intensity measured and explains the speculated appearance of the EF5 stain (Figure 3.3L) and why the EF5 hypoxic intensity is significantly higher ($p<0.05$) in the LPS group. This has therefore also affected the EF5 hypoxic density result.

As hypothesised, these findings suggest that systemic LPS injection at P12, prior to the retinal ischaemia that occurs on return to normoxia, reduces the resulting hypoxia in the avascular retina. This reduced hypoxic angiogenic drive may explain the switch

away from pathological neovascularisation towards healthy vascular regeneration seen in P17 pups treated with LPS. The result would also suggest that it is possible to reduce hypoxia in the retina without altering the supply of oxygen as there was no difference in the vasculature between the two groups.

Table 3.2: P14 OIR: PBS vs LPS

	TreatmentGroup	N	Mean	Std. Deviation	Std. Error Mean
AvascularArea	PBS	4	276589	19036.11600	9518.05800
	LPS	6	307632	48397.89554	19758.35812
VesselTortuosityIndex	PBS	4	1.0641	.02696	.01348
	LPS	6	1.0312	.02847	.01162
VesselIntegratedCurvature	PBS	4	1.0590	.18151	.09075
	LPS	6	.4480	.10833	.04422
EF5HypoxicArea	PBS	4	90839.5	12468.21927	6234.10963
	LPS	6	53787.2	15399.73268	6286.91454
EF5HypoxicIntensity	PBS	4	112.365	13.20446	6.60223
	LPS	6	140.770	8.89971	3.63329
EF5HYpoxicDensity	PBS	4	1.03E+7	2198470.333	1099235.166
	LPS	6	7.53E+6	1978010.054	807519.2231

	Levene's Test for Equality of Variances		t-test for Equality of Means						
								95% Confidence Interval of the Difference	
	F	Sig.	t	df	Sig. (2-tailed)	Mean Difference	Std. Error Difference	Lower	Upper
AvascularArea	4.419	.069	-1.202	8	.264	-31043.33333	25818.78213	-90581.55168	28494.88502
VesselTortuosityIndex	.028	.872	1.826	8	.105	.03290	.01802	-.00865	.07445
VesselIntegratedCurvature	3.278	.108	6.746	8	.000	.61100	.09057	.40213	.81987
EF5HypoxicArea	.450	.521	3.994	8	.004	37052.33333	9276.22495	15661.32023	58443.34643
EF5HypoxicIntensity	.128	.730	-4.105	8	.003	-28.40483	6.91879	-44.35959	-12.45008
EF5HYpoxicDensity	.028	.871	2.065	8	.073	2750855.583	1331947.866	-320621.705	5822332.871

Table 3.2 – Statistical Comparison of P14 OIR PBS vs LPS treatment groups

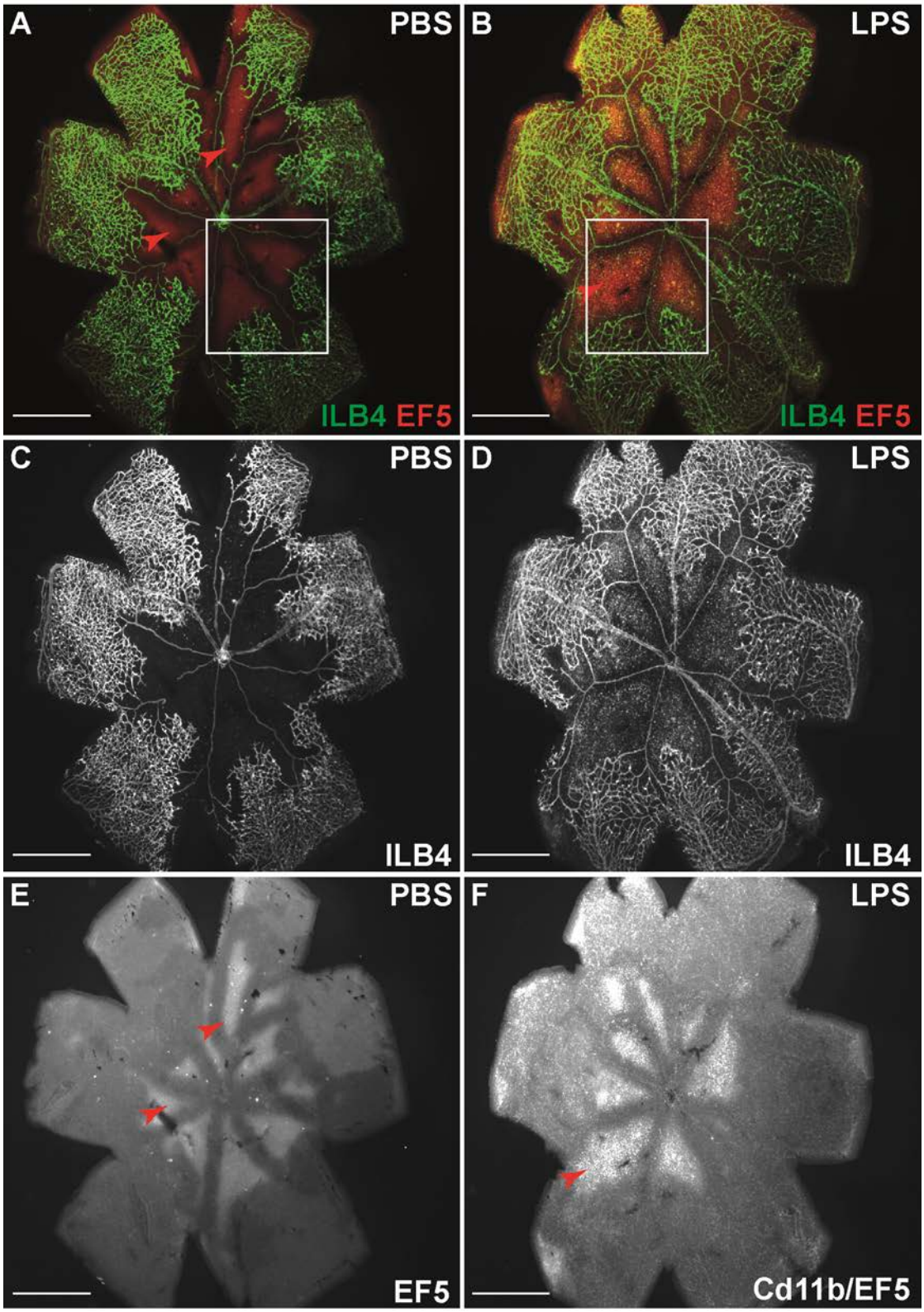

Figure 3.3(a) – Intraperitoneal injection of LPS at P12 after hyperoxia leads to reduced hypoxia at P14 in OIR. *Retinal wholemounts from P14 C57BL6 mice after OIR stained with isolectin B4 and EF5 hypoxia stain. Mouse pups in the PBS control group demonstrate central areas of vaso-obliteration (C) which are positive for EF5 hypoxia staining (E) (red arrows). No difference was seen in the avascular area between the two groups (C&D) whereas mouse pups in the LPS treatment group demonstrated reduced area of EF5 hypoxia staining (F). Scale bars = 100μm*

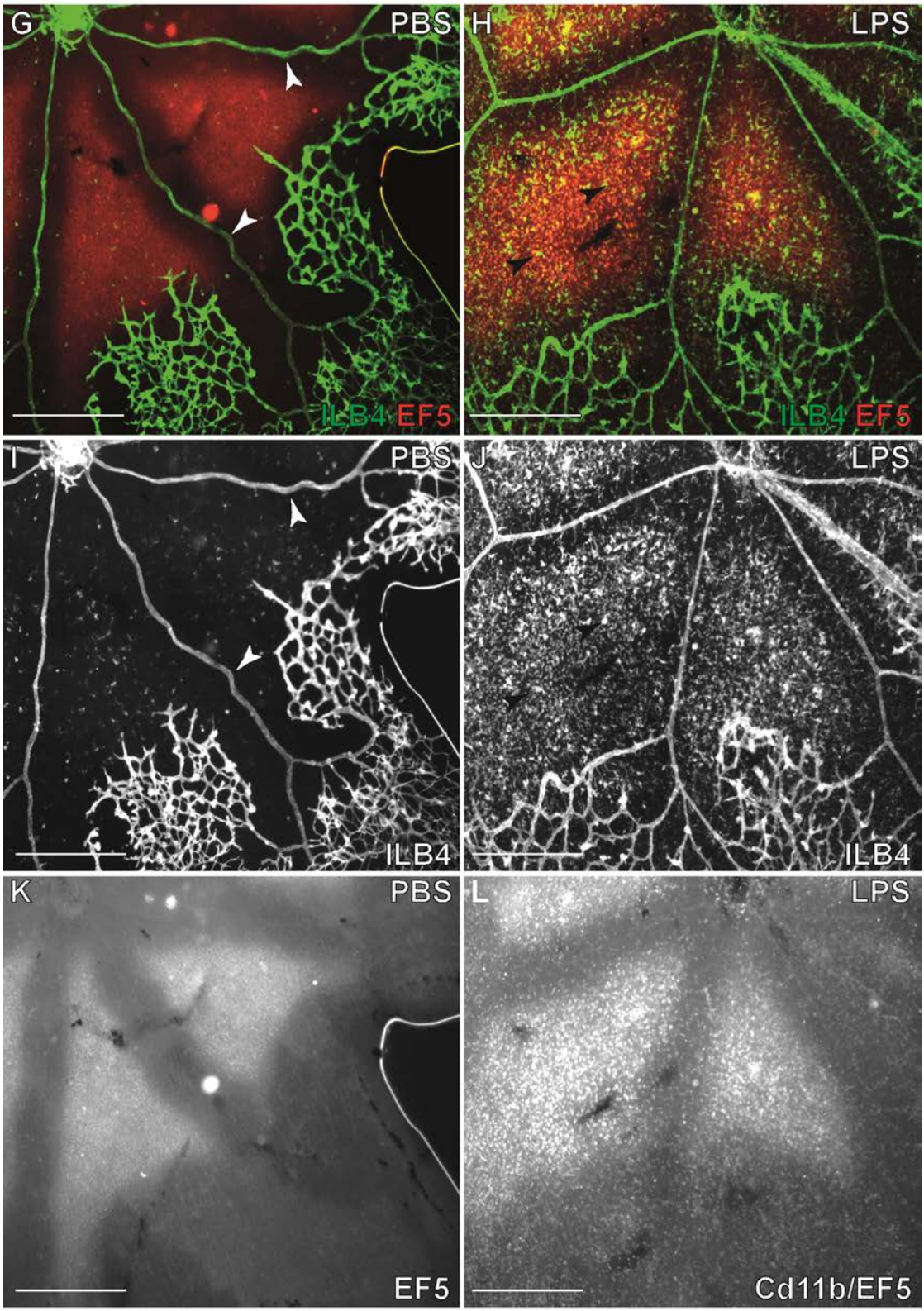

Figure 3.3(b) – Intraperitoneal injection of LPS at P12 after hyperoxia leads to reduced hypoxia at P14 in OIR. *Higher magnification images demonstrate the classical tortuous retinal arteries (I) (white arrows) associated with OIR at P14 seen in the PBS control group. Whereas in the LPS treated groups the retinal arteries are straighter (J). In the LPS group an influx of isolectin and Cd11b positive cells is seen in the avascular area (J&L) (black arrows). Scale bars = 50µm*

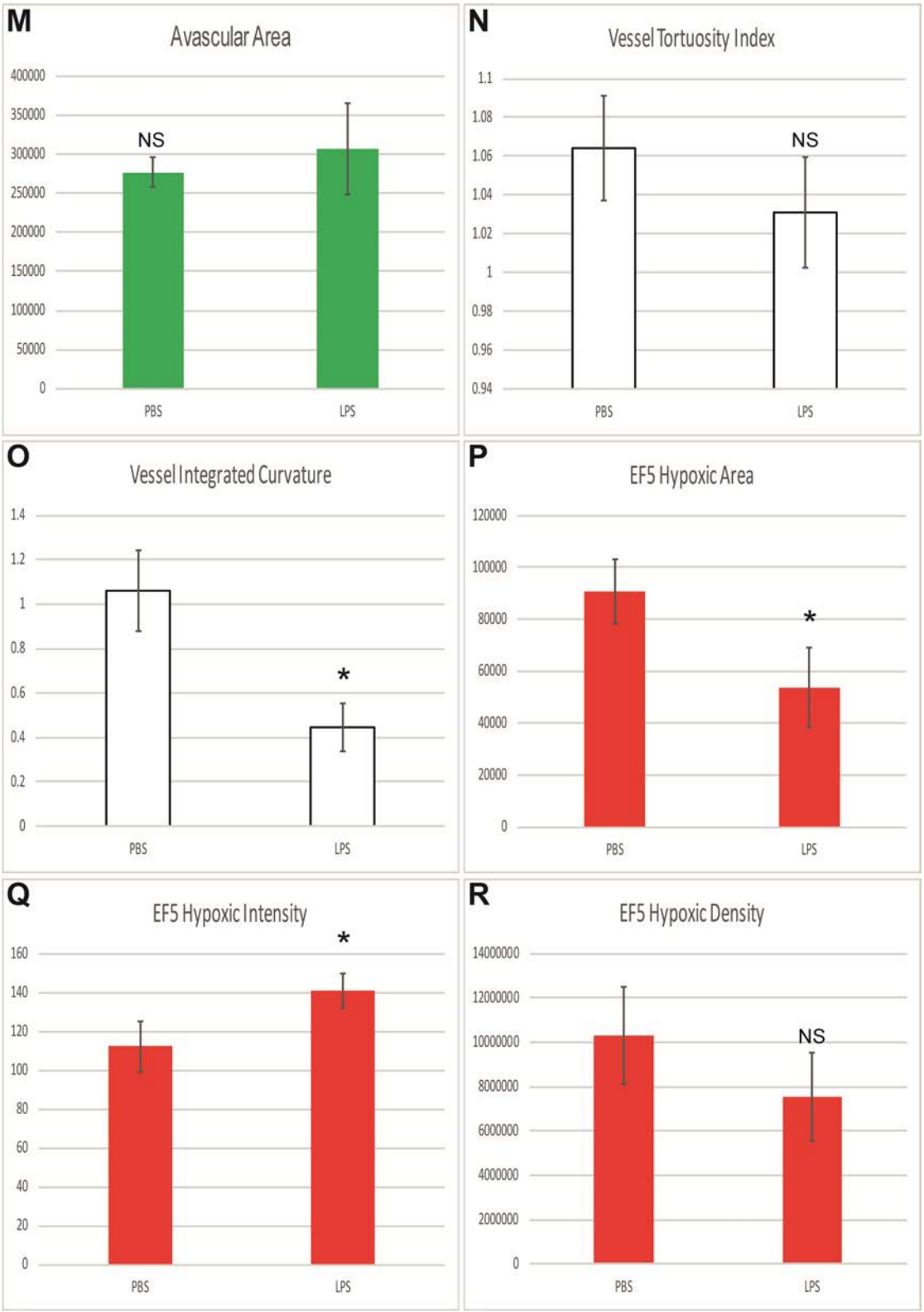

Figure 3.3(c) - Intraperitoneal injection of LPS at P12 after hyperoxia leads to reduced hypoxia at P14 in OIR. *No significant difference was seen in the avascular area between the two groups (M). The LPS group showed reduced vessel tortuosity but only integrated curvature (O) achieved significance. Hypoxic EF5 area (P) was significantly reduced in the LPS group, however EF5 hypoxic intensity was significantly higher (Q) due to bleed through from the Cd11b stain (L). (n= PBS 4 vs LPS 6; error bar = standard deviation; NS = non-significant, * = p<0.05)*

3.1.3 - Systemic LPS injection appears to reduce proliferation at P14 in OIR

The hypoxia seen in the OIR model is the result of an imbalance between the supply and demand of oxygen in the retina. In this model of systemic LPS injection, there was no change in the supply of oxygen to LPS treated retinas, as evidenced by similar avascular areas between the control and treated groups. This would imply that systemic LPS injection is able to reduce the oxygen demand of the retina, thereby reducing retinal hypoxia.

A possible explanation for this could be that systemic inflammation could reduce metabolic activity in the retina through down-regulation of proliferation in the immature, developing retinal vasculature.

To investigate this hypothesis a litter of C57BL6 pups underwent the same LPS vs PBS OIR protocol previously described, and mice were once again culled at P14. Immunohistochemistry was performed on retinal wholemounts to examine proliferation. To determine whether proliferation in the retinal vasculature was affected by LPS injection, BrdU staining alongside vascular specific, Collagen IV stain and endothelial cell marker, Erg 1,2,3 stain was used (**Figure 3.4**).

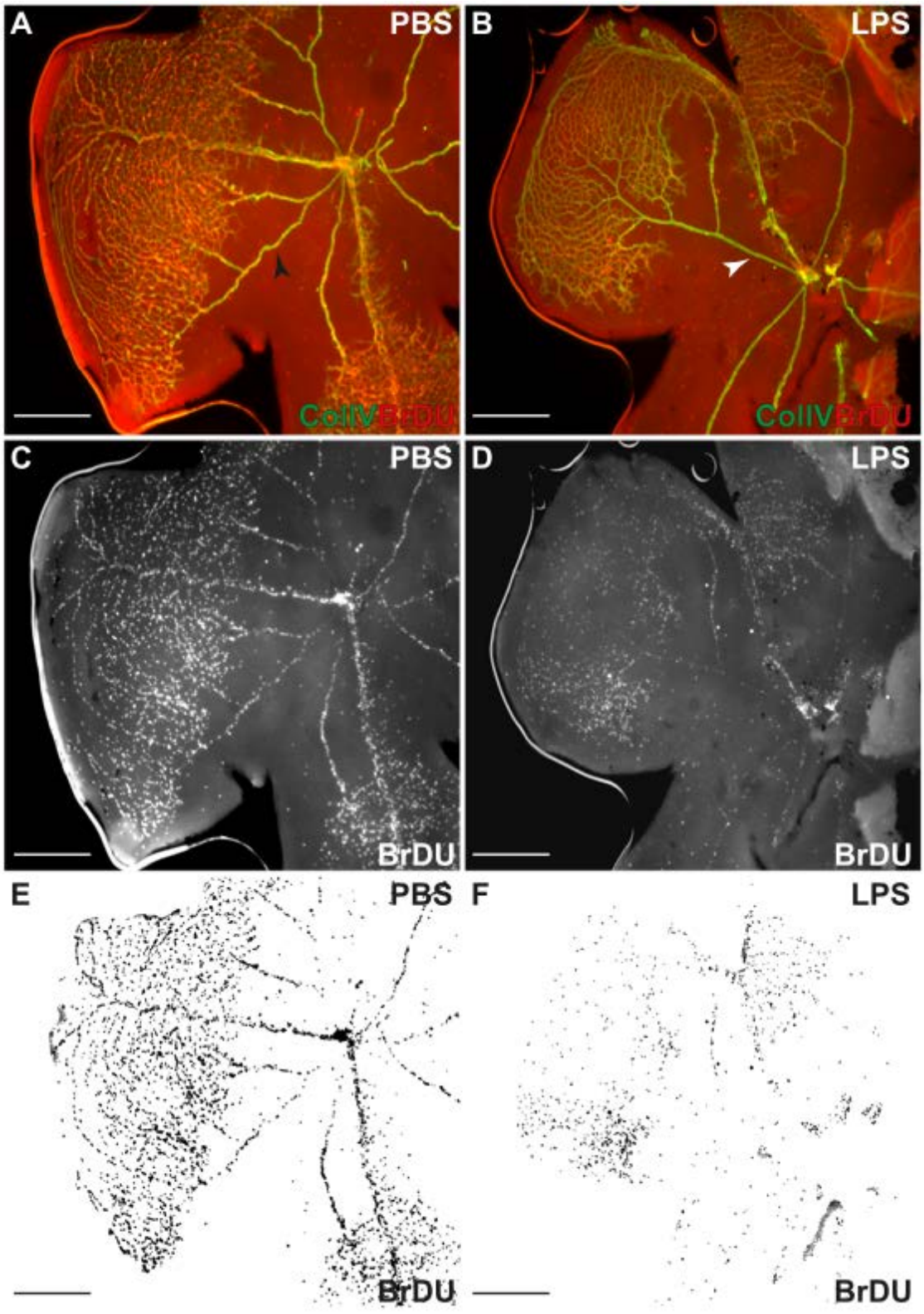

Figure 3.4(a) - Intraperitoneal injection of LPS at P12 after hyperoxia leads to reduced proliferation at P14 in OIR. *Retinal wholemounts from P14 C57BL6 mice after OIR stained with Collagen IV (green) to highlight the vasculature and BrdU (red) to indicate proliferating cells. Mouse pups in the control group (A,C,E) demonstrate mitotic activity restricted to the retinal vasculature (red arrows), in particular in the tortuous retinal arteries (black arrow). Similarly in pups in the LPS treatment group (B,D,F) mitotic activity was restricted to the retinal vasculature. Reduced proliferation was seen in the straight retinal arteries (white arrow) of the LPS group. Scale bars = 20µm in A, B, E, F; scale bars = 50µm in C, D.*

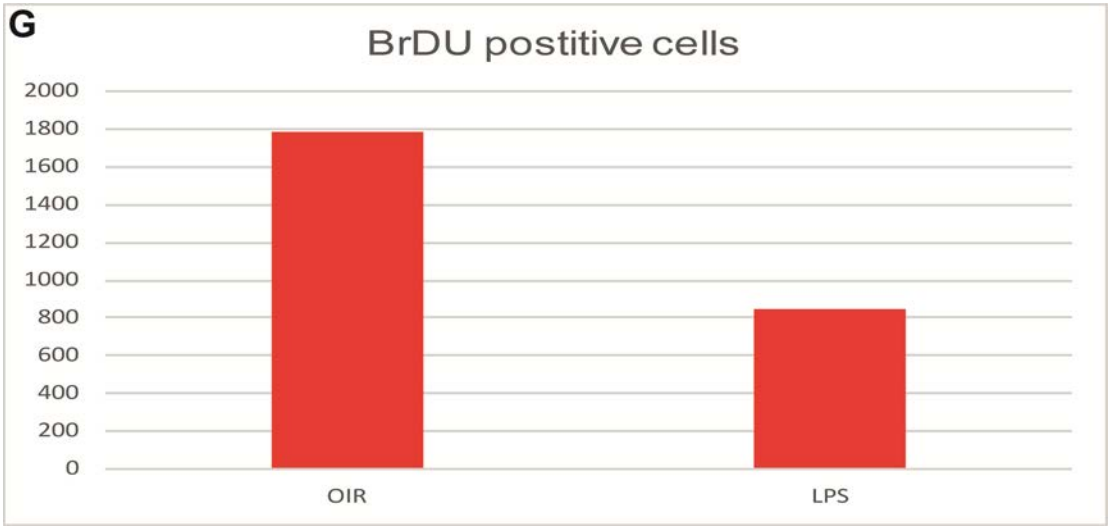

Figure 3.4(b) - Intraperitoneal injection of LPS at P12 after hyperoxia leads to reduced proliferation at P14 in OIR. *The number of cells proliferating, as demonstrated by particle analysis of BrdU positive cells was reduced by over 50% on the LPS treated group (G)* (n = OIR 1 vs LPS 1)

In both groups, the proliferating cells in the retinal flatmounts, as indicated by BrdU staining, were restricted to the retinal vasculature. The PBS control group (**Figure 3.4A,C&E**) demonstrated large numbers of proliferating cells in the tortuous retinal arteries and veins in the avascular area as well as in the capillaries in the periphery. In comparison the LPS treatment group (**Figure 3.4B,D,F**) showed much less mitotic activity, as evidenced by the straighter retinal arteries and the weaker BrdU staining. A particle analysis of BrdU positive cells suggested a greater than 50% reduction in proliferating cells of the retinal vasculature (**Figure 3.4G**).

The reduction in proliferating cells in the retinal arteries of LPS treated mice may explain why the arteries appear less tortuous than in their PBS control counterparts. A possible explanation for this could be that the reduction in hypoxia seen in the avascular area as a result of LPS treatment results in reduced VEGF production. A reduction in VEGF would lead to less proliferation amongst vascular endothelial cells and therefore less tortuosity. It is also possible that the LPS treatment directly down-regulates proliferation in order to reduce metabolic activity in the retina and therefore

relieve the hypoxia. To investigate whether the proliferating cells in the retinal vasculature were specific to the vascular endothelium a co-stain with an Erg 1,2,3 antibody was performed (**Figure 3.5**).

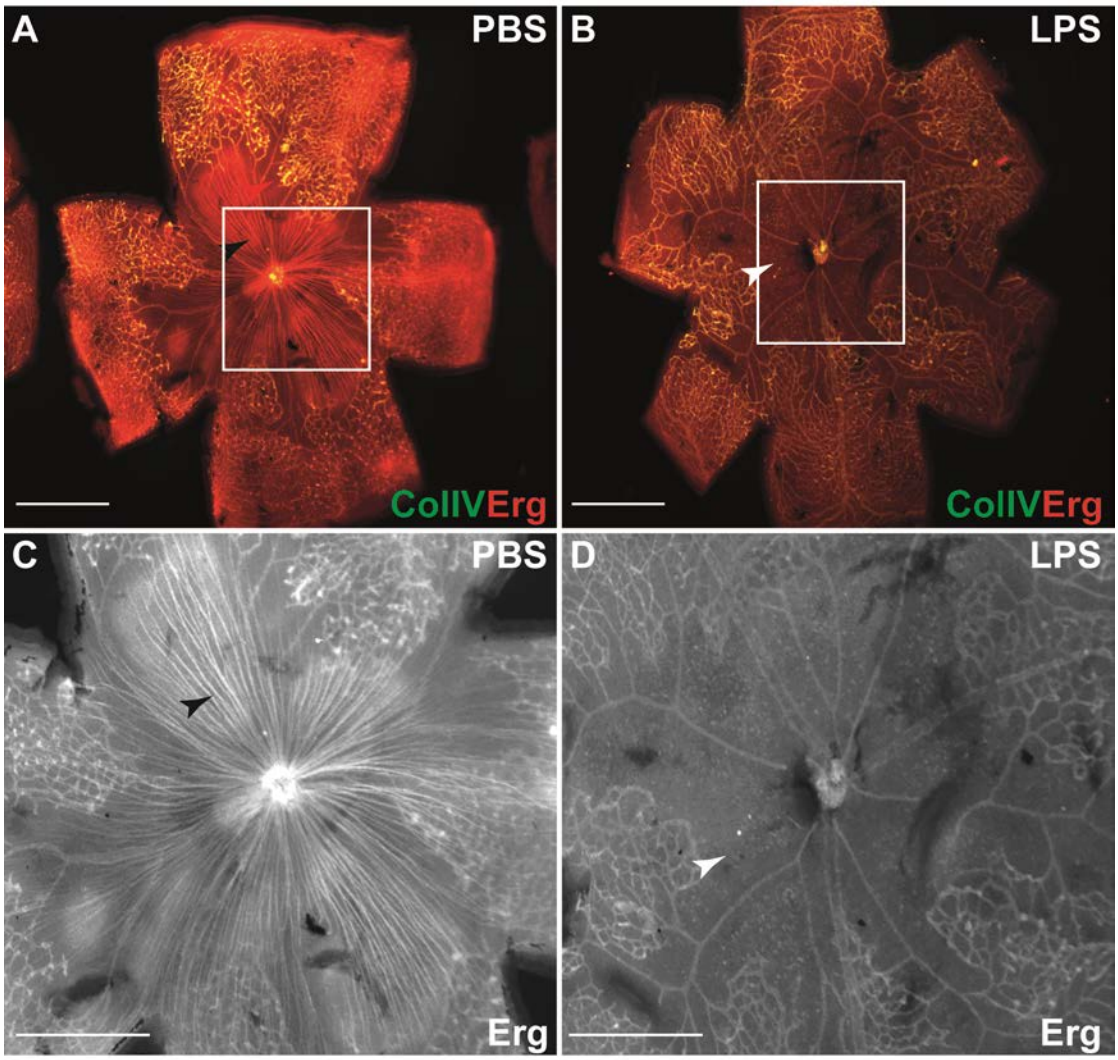

Figure 3.5(a) - Intraperitoneal injection of LPS at P12 after hyperoxia leads to Erg staining of the retinal ganglion cell axons in the avascular area at P14 in OIR *Retinal wholemounts from p14 C57BL6 mice after OIR stained Collagen IV (green) to highlight the vasculature and Erg 1,2,3 (red) to stain endothelial cells. Erg staining failed to stain the endothelial cell nuclei in both the PBS control group (A,C) and the LPS treatment group (B,D). However, in the PBS group, Erg was noted to stain retinal ganglion axons in a similar distribution to that of EF5 hypoxia staining (black arrows). The same effect was not seen in the LPS treated avascular area (white arrows). In both groups there appears to be bleed though of the collagen staining in the Erg staining image (C,D). Scale bar = 20µm in A&B, 50µm in C&D.*

The resulting immunohistochemistry produced an unexpected result. In both the PBS and the LPS treated group the Erg antibody failed to stain endothelial cell nuclei,

however in the PBS control group the Erg antibody appeared to stain the linear retinal ganglion cell axons in the avascular area. This staining was confined to the avascular area and gave a staining pattern very similar to that seen with EF5 hypoxia staining in the same control group. In both groups there appeared to be bleed through from the collagen stain in the Erg staining images.

This artefact may be related to the cold methanol fixation of the retinal tissue after dissection, as when tissue is fixed in paraformaldehyde the effect is less severe and the Erg staining works well. However, there is a pronounced difference in appearance between the two groups. These results would suggest that systemic LPS treatment causing a fundamental change to the hypoxic area seen in the OIR model at P12 which results in reduced proliferation and reduced metabolic demand.

Another possible explanation for the reduced proliferation and reduced metabolic demand seen in the retina would be that LPS triggers as systemic immune response that results in retinal cell death. To investigate this retinal cross sections were analysed to look for changes in retinal thickness between the PBS and LPS treated retinas (**Figure 3.5B**). No significant differences were seen between the average retinal thickness of both the PBS and LPS treated retinas **(Figure 3.5C)**.

Therefore, how LPS activation of inflammatory cells in the peritoneum can influence metabolic demand in the hypoxic retina is yet to be elucidated.

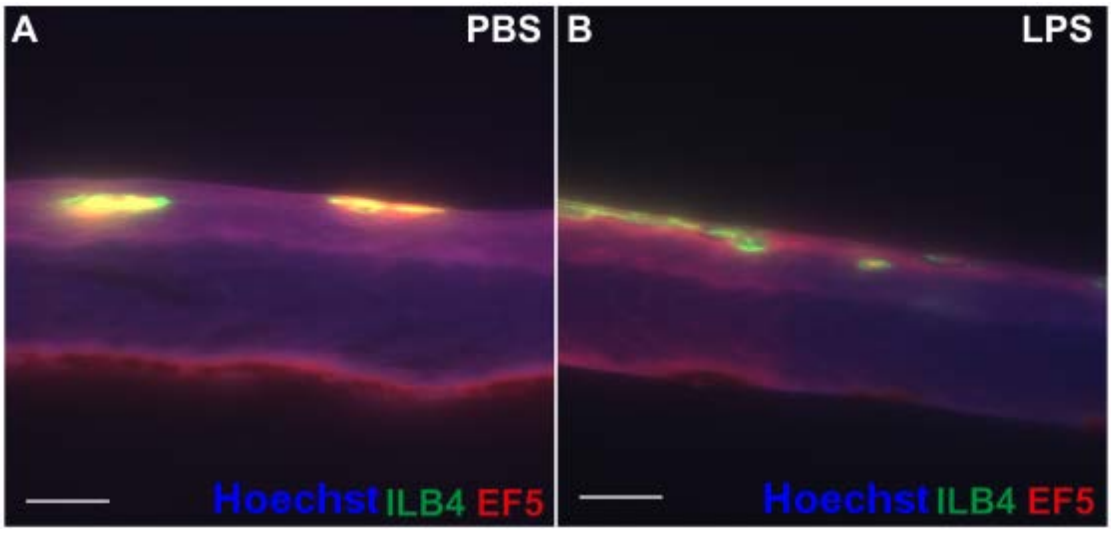

Figure 3.5(b) - Intraperitoneal injection of LPS at P12 after hyperoxia does not affect retinal thickness at P14 in OIR *Retinal crossections from p14 C57BL6 mice after OIR stained Collagen IV (green) to highlight the vasculature, EF5 for hypoxia (red) and hoescht to stain nuclei (blue). NO significant difference in retinal thickness was found between the PBS control group (A) and the LPS treatment group (B). Scale bar = 20µm*

Table 3.2.1: P14 OIR: PBS vs LPS Retinal Thickness Analysis

	TreatmentGroup	N	Mean	Std. Deviation	Std. Error Mean
Average_Retinal_Thickness	PBS	12	71.51367	10.406055	3.003969
	LPS	18	70.67656	7.698176	1.814477

	Levene's Test for Equality of Variances		t-test for Equality of Means						
								95% Confidence Interval of the Difference	
	F	Sig.	t	df	Sig. (2-tailed)	Mean Difference	Std. Error Difference	Lower	Upper
Average_Retinal_Thickness	3.033	.093	.253	28	.802	.837111	3.302385	-5.927518	7.601740
			.239	18.866	.814	.837111	3.509439	-6.511763	8.185985

Table 3.2.1 – Statistical Comparison of P14 OIR PBS vs LPS treatment groups

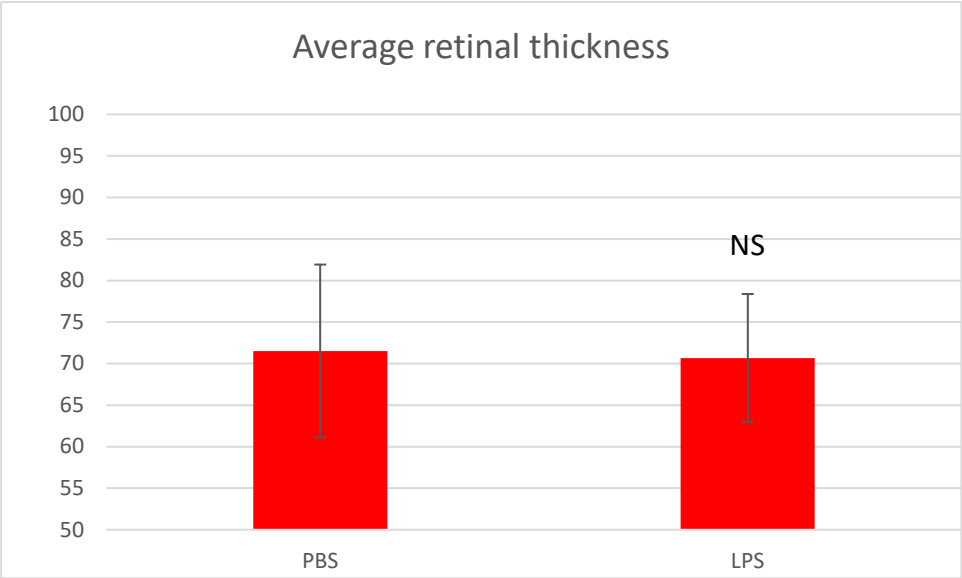

Figure 3.5(c) - Intraperitoneal injection of LPS at P12 after hyperoxia does not affect retinal thickness at P14 in OIR *No significant difference was seen retinal thickness between the two groups (n= PBS 4 vs LPS 6; error bar = standard deviation; NS = non-significant)*

3.1.4 – The effect of systemic LPS injection on hypoxia in TLR4 deficient mice at P14 in OIR

LPS polarises macrophages into a pro-inflammatory or M1 state (Benoit et al., 2008) by binding to the CD14/TLR4/MD2 receptor complex. TLR4 is expressed on many cell types including epithelial and endothelial cells but of particular note is expressed by inflammatory cells, such as monocytes, dendritic cells, B- and T-lymphocytes (O'Neill 2006; O'Neill 2008). LPS agonism of TLR4 in these cells promotes the release of pro-inflammatory cytokines such as TNFα, IL-6, IL-1β, eicosanoids and nitric oxide which can then trigger a systemic inflammatory response. In the mice that undergo OIR and are treated with LPS it is this systemic inflammatory response that is hypothesised to lead to the reduction in retinal oxygen demand and protect against neovascularisation.

To prove that LPS binding of the CD14/TLR4/MD2 complex causes the reduction in hypoxia a litter of P12 C3H/HeJOlaHsd-TLR4$^{Lps\text{-}d}$ pups underwent the same LPS vs PBS OIR protocol previously described and mice were once again culled at P14. Immunohistochemistry was performed on retinal wholemounts to examine hypoxia (**Figure 3.6**).

Mouse pups in the PBS control group (**Figure 3.6A**) failed to show the normal hypoxic OIR phenotype as there was only small areas of avascularity, no evidence of retinal artery tortuosity (**Figure 3.6I**) and only mild hypoxia, as demonstrated by EF5 staining (**Figure 3.6K**). Mouse pups in the LPS treatment group (**Figure 3.6B**) presented with a similar phenotype as the control group, with straight retinal arteries (**Figure 3.6J**) and mild EF5 staining (**Figure 3.6L**), although they appeared to have significantly larger avascular areas ($p<0.05$). In previous experiments where C57BL6 pups were injected with LPS IP an increased inflammatory response could be seen in the hypoxic area, as represented by an influx of lectin positive cells. In the TLR4 deficient mice this did not occur. This confirms that TLR4 is required for the influx of the pro-inflammatory cells into the hypoxic area after LPS injection.

However, it was hypothesised that the TLR4 deficient mice would show signs of hypoxia despite being treated with LPS. Interestingly the LPS group were found to have a significantly larger avascular area ($p<0.05$) than compared to the PBS control group. Given that no significant differences were seen when arterial tortuosity and EF5 hypoxic staining measures were compared between the two groups (**Table 3.3**), this would suggest that the lack of hypoxia was due to the C3H background of the mice.

Table 3.3: TLR4 Deficient Mice P14 OIR PBS vs LPS groups

	TreatmentGroup	N	Mean	Std. Deviation	Std. Error Mean
AvascularArea	PBS	3	165254	10144.69084	5857.03999
	LPS	3	195603	6767.56414	3907.25498
VesselTortuosityIndex	PBS	3	1.0133	.00507	.00293
	LPS	3	1.0160	.00628	.00363
VesselIntegratedCurvature	PBS	3	.2909	.04389	.02534
	LPS	3	.2943	.04601	.02657
EF5HypoxicArea	PBS	3	24850.0	9519.18016	5495.90123
	LPS	3	37157.3	24188.96340	13965.50453
EF5HypoxicIntensity	PBS	3	71.4917	6.27512	3.62294
	LPS	3	72.9717	6.60647	3.81425
EF5HypoxicDensity	PBS	3	1.74E+6	575517.2335	332275.0297
	LPS	3	2.74E+6	1933751.824	1116452.136

	Levene's Test for Equality of Variances		t-test for Equality of Means						
								95% Confidence Interval of the Difference	
	F	Sig.	t	df	Sig. (2-tailed)	Mean Difference	Std. Error Difference	Lower	Upper
AvascularArea	.378	.572	-4.311	4	.013	-30349.00000	7040.70727	-49897.13724	-10800.86276
			-4.311	3.486	.017	-30349.00000	7040.70727	-51088.50446	-9609.49555
VesselTortuosityIndex	.409	.557	-.590	4	.587	-.00275	.00466	-.01569	.01019
			-.590	3.831	.588	-.00275	.00466	-.01592	.01042
VesselIntegratedCurvatur e	.022	.890	-.091	4	.932	-.00333	.03671	-.10527	.09860
			-.091	3.991	.932	-.00333	.03671	-.10536	.09869
EF5HypoxicArea	1.547	.281	-.820	4	.458	-12307.33333	15008.00610	-53976.23841	29361.57174
			-.820	2.605	.480	-12307.33333	15008.00610	-64440.30756	39825.64090
EF5HypoxicIntensity	.077	.795	-.281	4	.792	-1.48000	5.26063	-16.08585	13.12585
			-.281	3.989	.792	-1.48000	5.26063	-16.10109	13.14109
EF5HypoxicDensity	3.552	.133	-.856	4	.440	-996645.333	1164848.517	-4230783.30	2237492.631
			-.856	2.352	.470	-996645.333	1164848.517	-5354809.97	3361519.303

Table 3.3 – Statistical Comparison of TLR4 deficient P14 OIR PBS vs LPS treatment groups

C3H mice are known to carry the Pde6b^{Rd1} mutation which manifests as degeneration of the photoreceptors in the retina with preservation of all other retinal cell types (Chang *et al.*, 2002). Degeneration of the photoreceptor layer results in thinning of the retina, reduced metabolic activity and therefore less oxygen demand. The thin retina of C3H/Hej mice have been shown not to become ischaemic during the OIR model and as a result do not develop neovascularisation (Scott et al., 2014). This would explain why in the C3H TLR4 deficient mice the typical hypoxic OIR presentation at P14 was not seen in either the control or treatment groups.

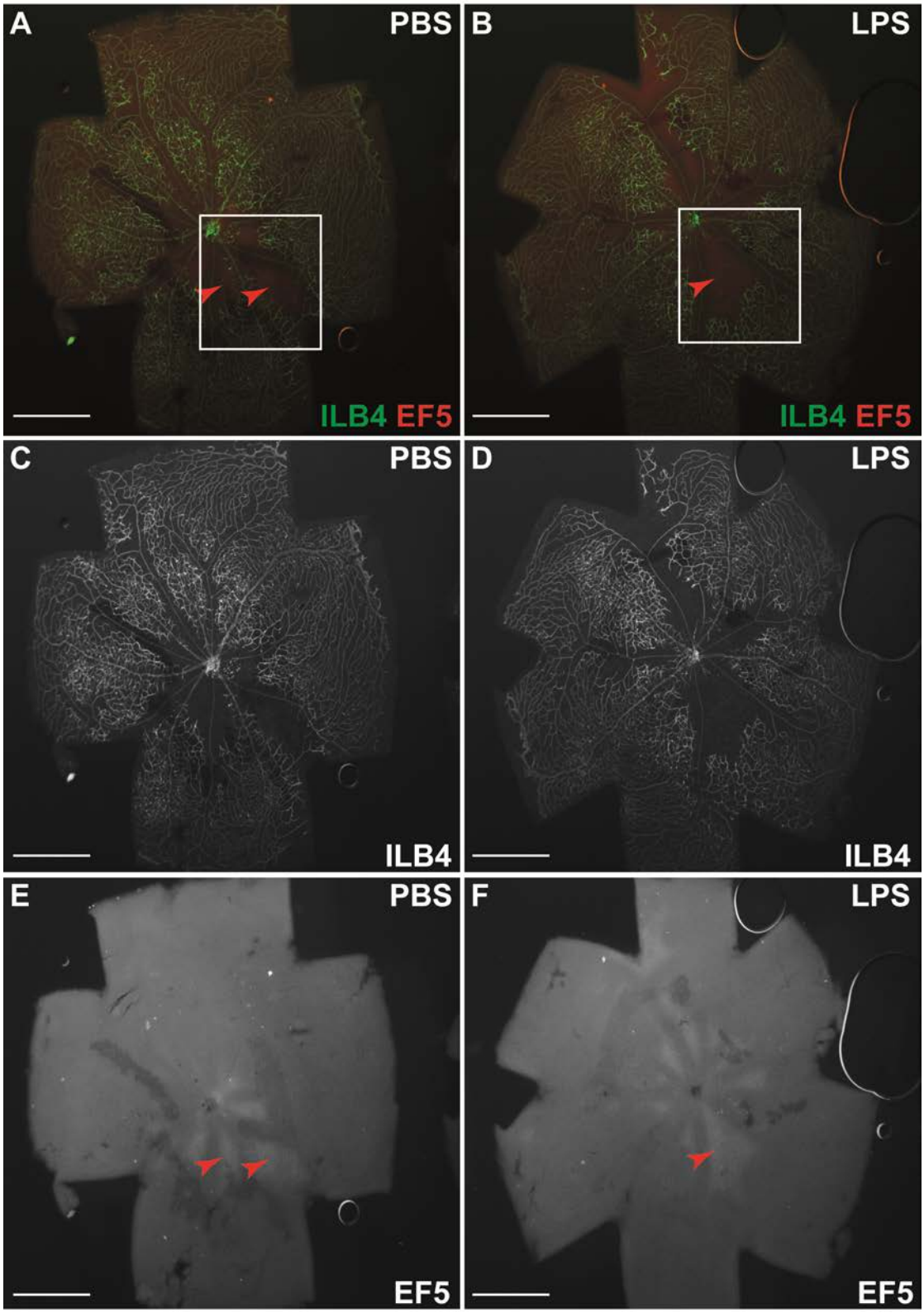

Figure 3.6(a) – Intraperitoneal injection of LPS at P12 in C3H TLR4 deficient mice after hyperoxia does not change hypoxia seen at P14 in OIR. *Retinal wholemounts from P14 C3H TLR4 deficient mice after OIR stained with isolectin B4 and EF5 hypoxia stain. Mouse pups in the PBS control group demonstrated mild signs of hypoxia associated with OIR at P14, small avascular area (C) and mild EF5 hypoxia staining (E) (red arrows). Mouse pups in the LPS treatment group demonstrated similarly mild EF5 hypoxia staining(F), however they appeared to have a larger avascular area(D). Scale bars = 100µm.*

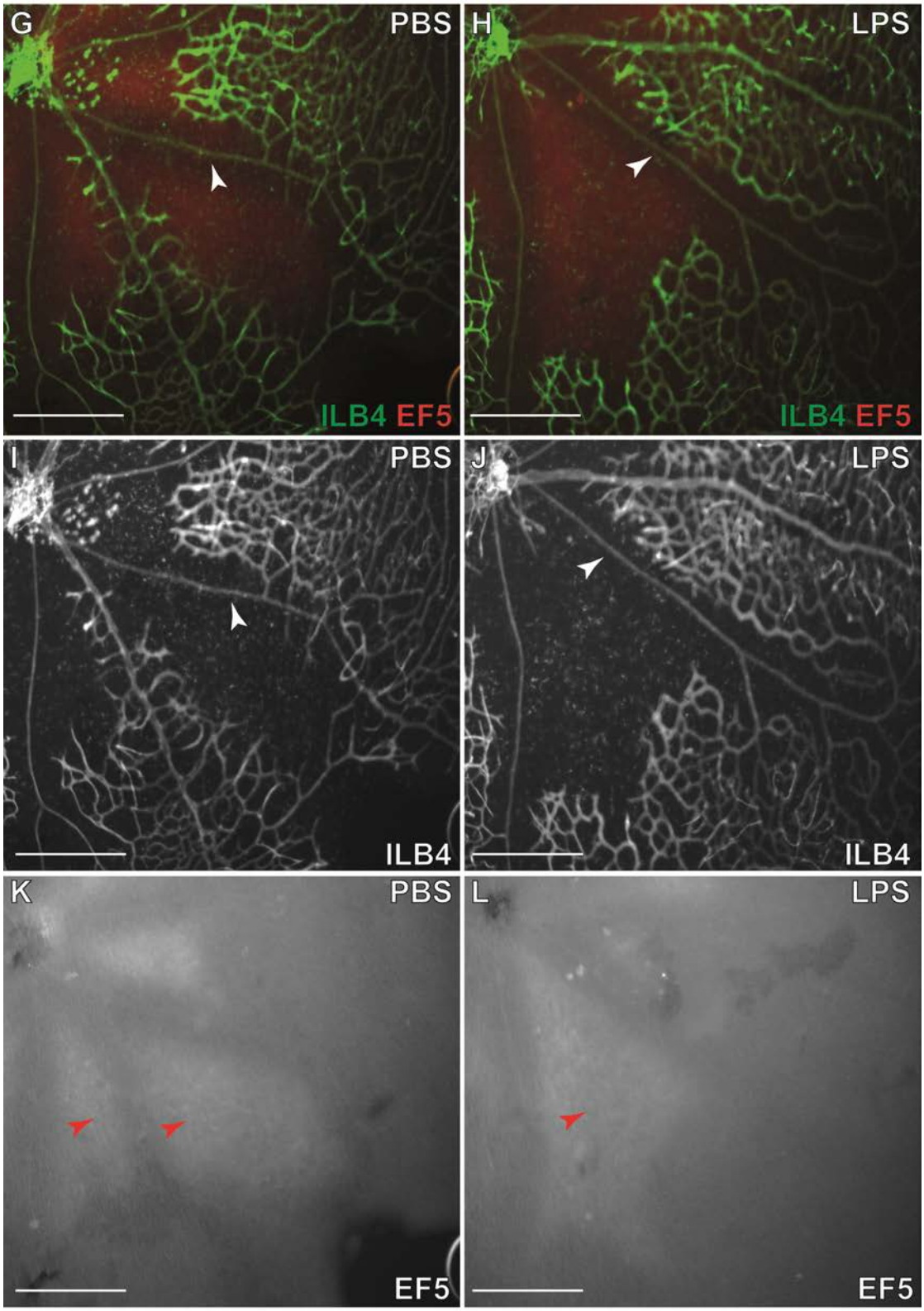

Figure 3.6(b) – Intraperitoneal injection of LPS at P12 in C3H TLR4 deficient mice after hyperoxia does not change hypoxia seen at P14 in OIR. *Higher magnification images demonstrate straight retinal arteries(I) (white arrows) which is not typically associated with OIR at P14 in the PBS control group. The LPS treated group have similarly straight retinal arteries (J). In the LPS there is no evidence of the influx of isolectin positive cells into the avascular area (red arrows) previously seen in experiments with C57BL6 mice (J). Scale bars = 50µm*

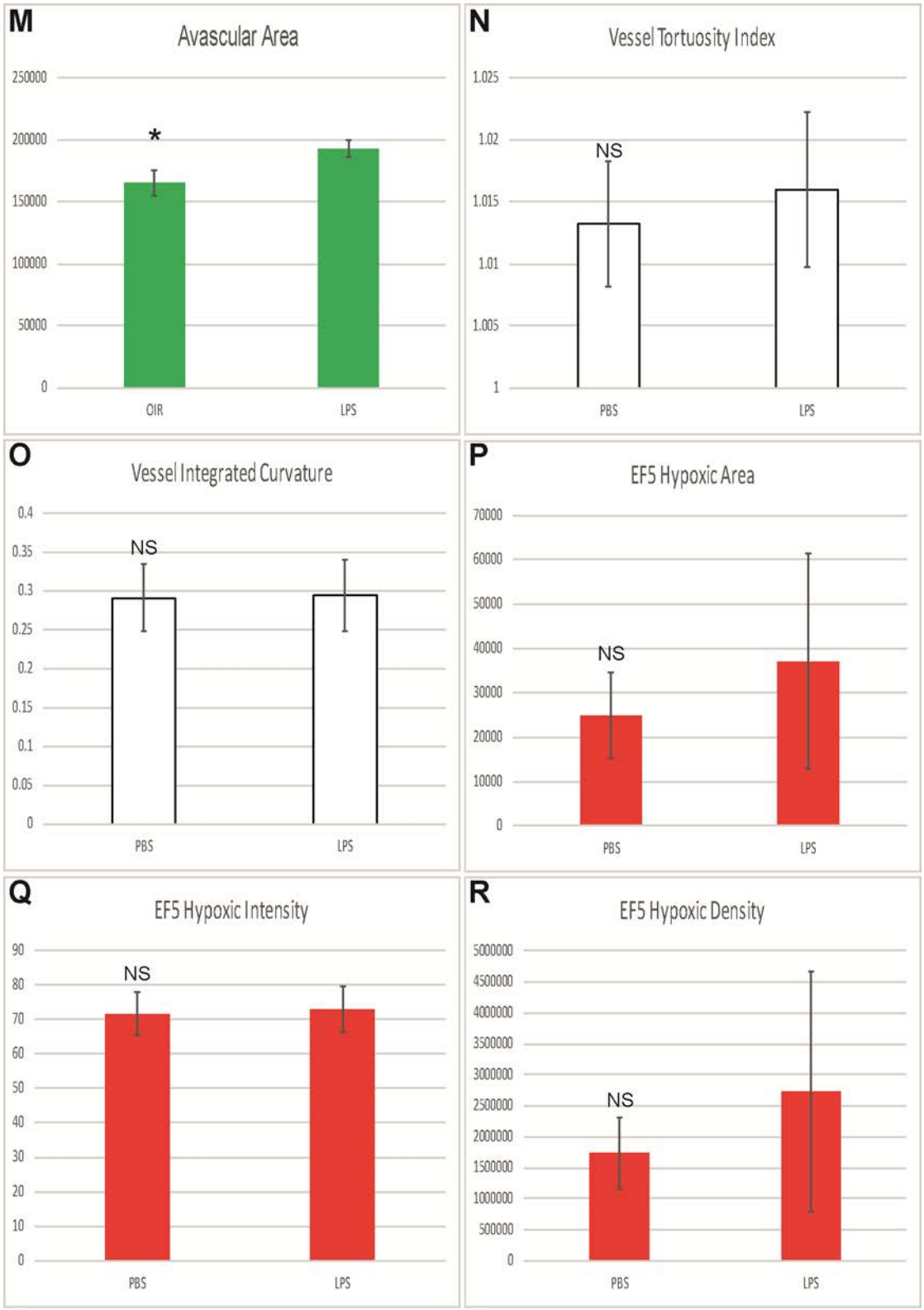

Figure 3.6(c) Intraperitoneal injection of LPS at P12 in C3H TLR4 deficient mice after hyperoxia does not change hypoxia seen at P14 in OIR. *The avascular area was found to be significantly larger in the LPS treated group (M). Otherwise no significant differences were noted in either vessel tortuosity measures (N&O), or EF5 hypoxia measures (P,Q,R). (n= PBS 3 vs LPS 3; error bar = standard deviation; NS = non-significant, * = p<0.05)*

In order to confirm that the reduced hypoxia seen in both groups was due to the $Pde6b^{Rd1}$ mutation a litter of C3H/HeNHsd mouse pups underwent the same LPS vs PBS OIR protocol previously described and mice were once again culled at P14. Immunohistochemistry was performed on retinal wholemounts to examine hypoxia (**Figure 3.7**).

Mouse pups in the PBS control group (**Figure 3.7A**) once again failed to show the normal OIR phenotype as there was no evidence of retinal artery tortuosity (**Figure 3.7I**) and only mild EF5 hypoxia staining EF5 staining (**Figure 3.7K**). Mouse pups in the LPS treatment group (**Figure 3.7B**) also presented with a similar phenotype to the control group, with straight retinal arteries (**Figure 3.7J**) and mild EF5 staining (**Figure 3.7L**) and with, yet again, the exception that they appeared to have larger avascular areas. This experiment appeared to yield exactly the same results as the experiment in TLR4 deficient mice, with the exception that an influx of lectin positive cells could be seen in the avascular areas of the LPS treatment group (**Figure 3.7J**).

Table 3.4: C3H Rd1 Mice P14 OIR PBS vs LPS groups

	TreatmentGroup	N	Mean	Std. Deviation	Std. Error Mean
AvascularArea	PBS	4	198955	28391.49382	14195.74691
	LPS	5	331497	71872.22575	32142.23649
VesselTortuosityIndex	PBS	4	1.0174	.00754	.00377
	LPS	5	1.0147	.00309	.00138
VesselIntegratedCurvature	PBS	4	.2759	.07073	.03536
	LPS	5	.3474	.07501	.03354
EF5HypoxicArea	PBS	4	44505.8	12996.09119	6498.04560
	LPS	5	49357.2	13090.19124	5854.11149
EF5HypoxicIntensity	PBS	4	111.926	20.26083	10.13041
	LPS	5	109.572	44.43008	19.86974
EF5HypoxicDensity	PBS	4	5.09E+6	1931509.316	965754.6578
	LPS	5	5.78E+6	3381887.616	1512426.120

	Levene's Test for Equality of Variances		t-test for Equality of Means						
								95% Confidence Interval of the Difference	
	F	Sig.	t	df	Sig. (2-tailed)	Mean Difference	Std. Error Difference	Lower	Upper
AvascularArea	1.558	.252	-3.441	7	.011	-132541.850	38519.59454	-223626.217	-41457.48259
			-3.772	5.437	.011	-132541.850	35137.48137	-220725.798	-44357.90170
VesselTortuosityIndex	1.943	.206	.747	7	.479	.00274	.00366	-.00592	.01140
			.682	3.808	.535	.00274	.00402	-.00863	.01411
VesselIntegratedCurvature	.007	.937	-1.455	7	.189	-.07146	.04911	-.18758	.04465
			-1.466	6.737	.188	-.07146	.04874	-.18764	.04471
EF5HypoxicArea	.034	.858	-.554	7	.597	-4851.45000	8754.16973	-25551.77204	15848.87204
			-.555	6.590	.597	-4851.45000	8746.15446	-25796.46255	16093.56255
EF5HypoxicIntensity	.773	.408	.097	7	.925	2.35395	24.22347	-54.92545	59.63335
			.106	5.825	.919	2.35395	22.30318	-52.61987	57.32777
EF5HypoxicDensity	.396	.549	-.362	7	.728	-691845.450	1913238.767	-5215936.24	3832245.337
			-.386	6.489	.712	-691845.450	1794467.840	-5003832.14	3620141.236

Table 3.4 – Statistical Comparison of C3H Rd1 mice P14 OIR PBS vs LPS treatment groups

These results would suggest that both LPS and TLR4 are required and that LPS binding of the CD14/TLR4/MD2 is responsible for the influx of the pro-inflammatory cells into the avascular area. Given that there was no statistically significant difference in arterial tortuosity measures or EF5 hypoxic measures between the two groups in both experiments (**Table 3.4**) this would suggest that the reduced hypoxia seen in both groups is secondary to the thin retinas and the low retinal metabolic demand of the C3H mice. Interestingly the LPS group were found to have a significantly larger avascular area than compared to the PBS control group ($p<0.05$) again, suggesting that intraperitoneal injection of PBS alone may have an effect on retinal angiogenesis out with the LPS/TLR4 signalling mechanism.

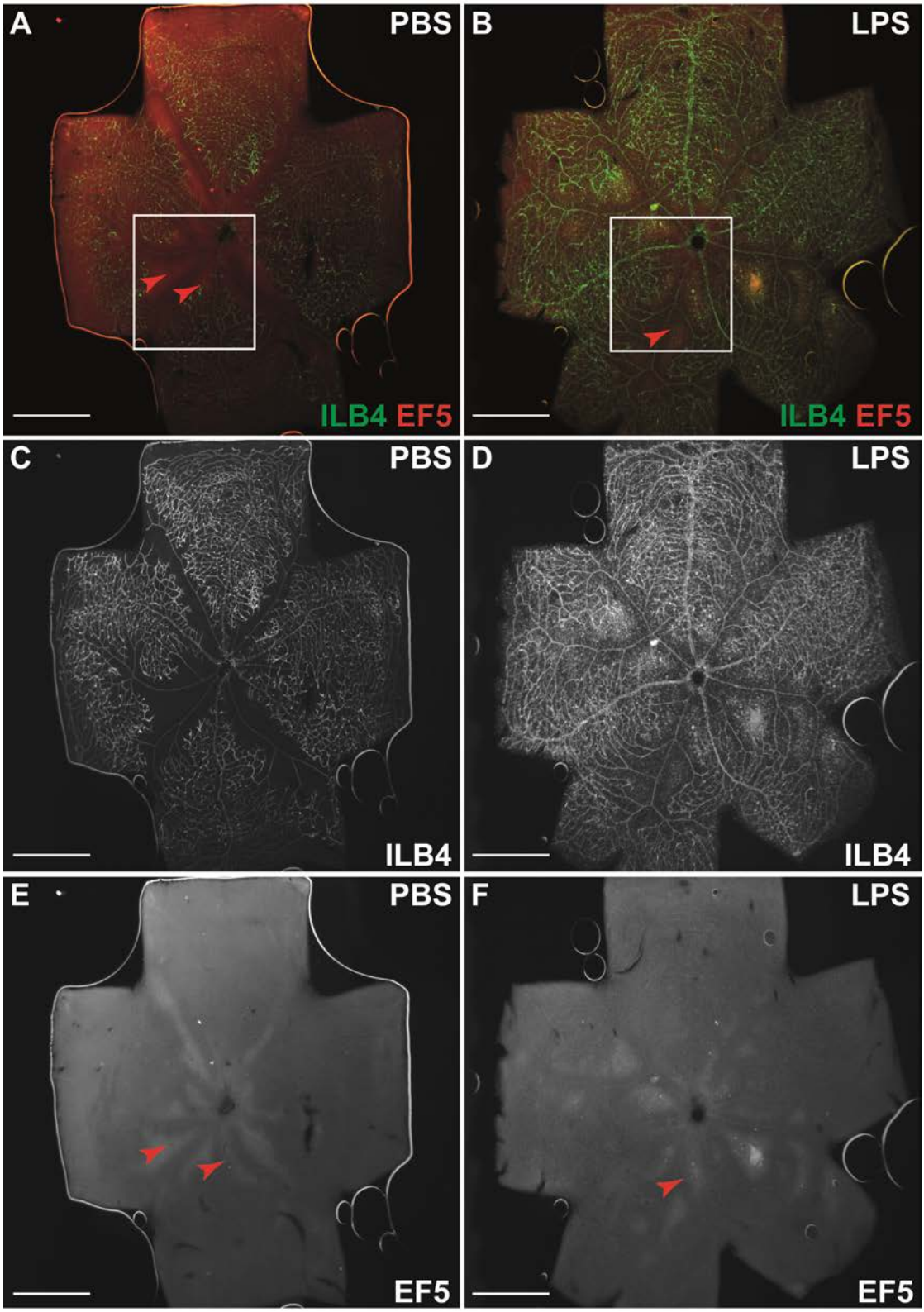

Figure 3.7(a) – Intraperitoneal injection of LPS at P12 in C3H mice after hyperoxia does not change hypoxia seen at P14 in OIR. *Retinal wholemounts from P14 C3H mice after OIR stained with isolectin B4 and EF5 hypoxia stain. Mouse pups in the PBS control group demonstrated mild signs of hypoxia associated with OIR at P14, small avascular area (C) and mild EF5 hypoxia staining. (E) (red arrows). Mouse pups in the LPS treatment group demonstrated similarly mild EF5 hypoxia staining(F), however they appeared to have a larger avascular area(D). Scale bars = 100µm.*

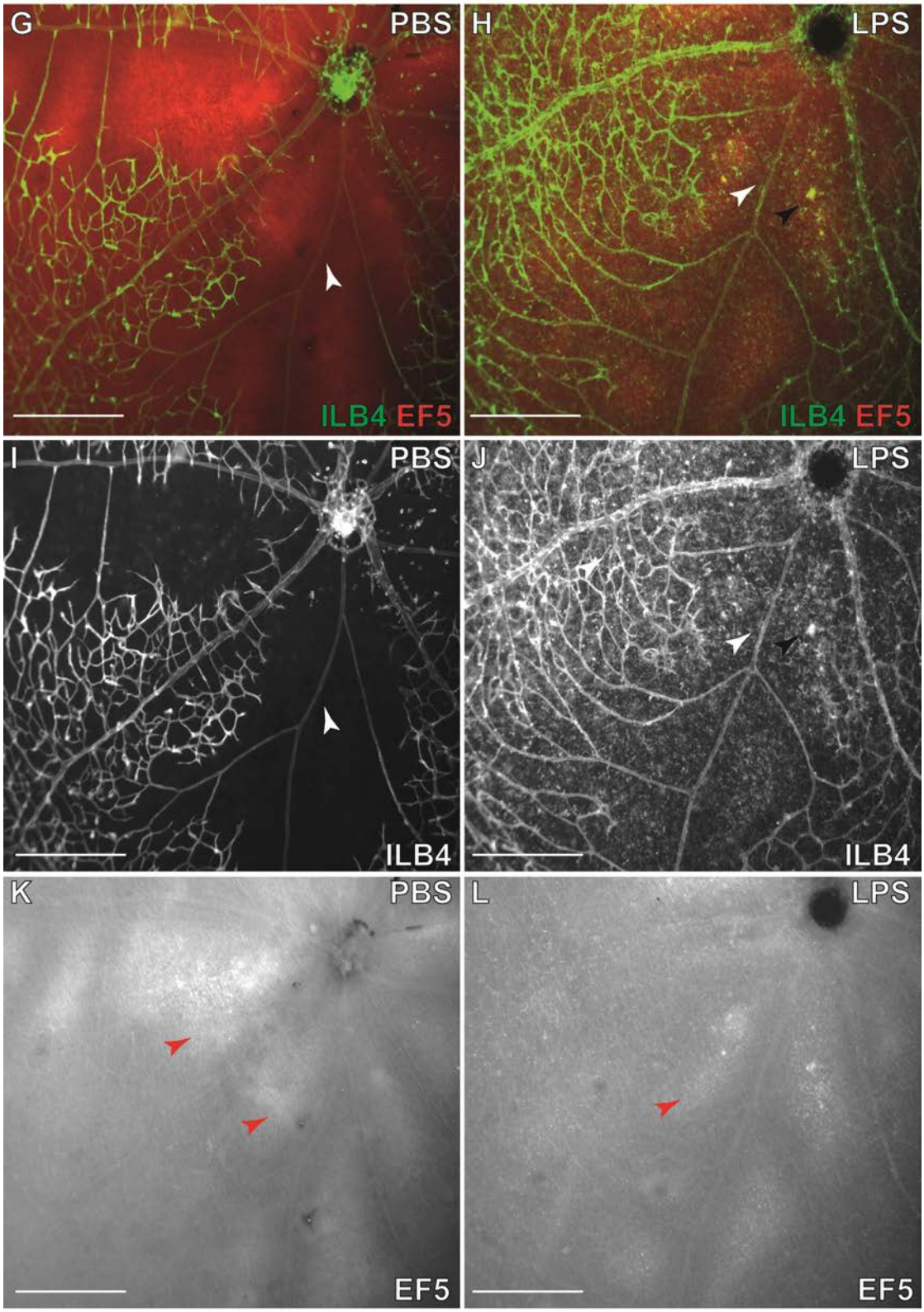

Figure 3.7(b) – Intraperitoneal injection of LPS at P12 in C3H mice after hyperoxia does not change hypoxia seen at P14 in OIR. *Higher magnification images demonstrate straight retinal arteries(I) (white arrows) which are not typically associated with OIR at P14 in the PBS control group. The LPS treated group have similarly straight retinal arteries (J). In the LPS group the presence of isolectin positive cells (black arrow) in the avascular area (red arrows) is seen (J). Scale bars = 50µm*

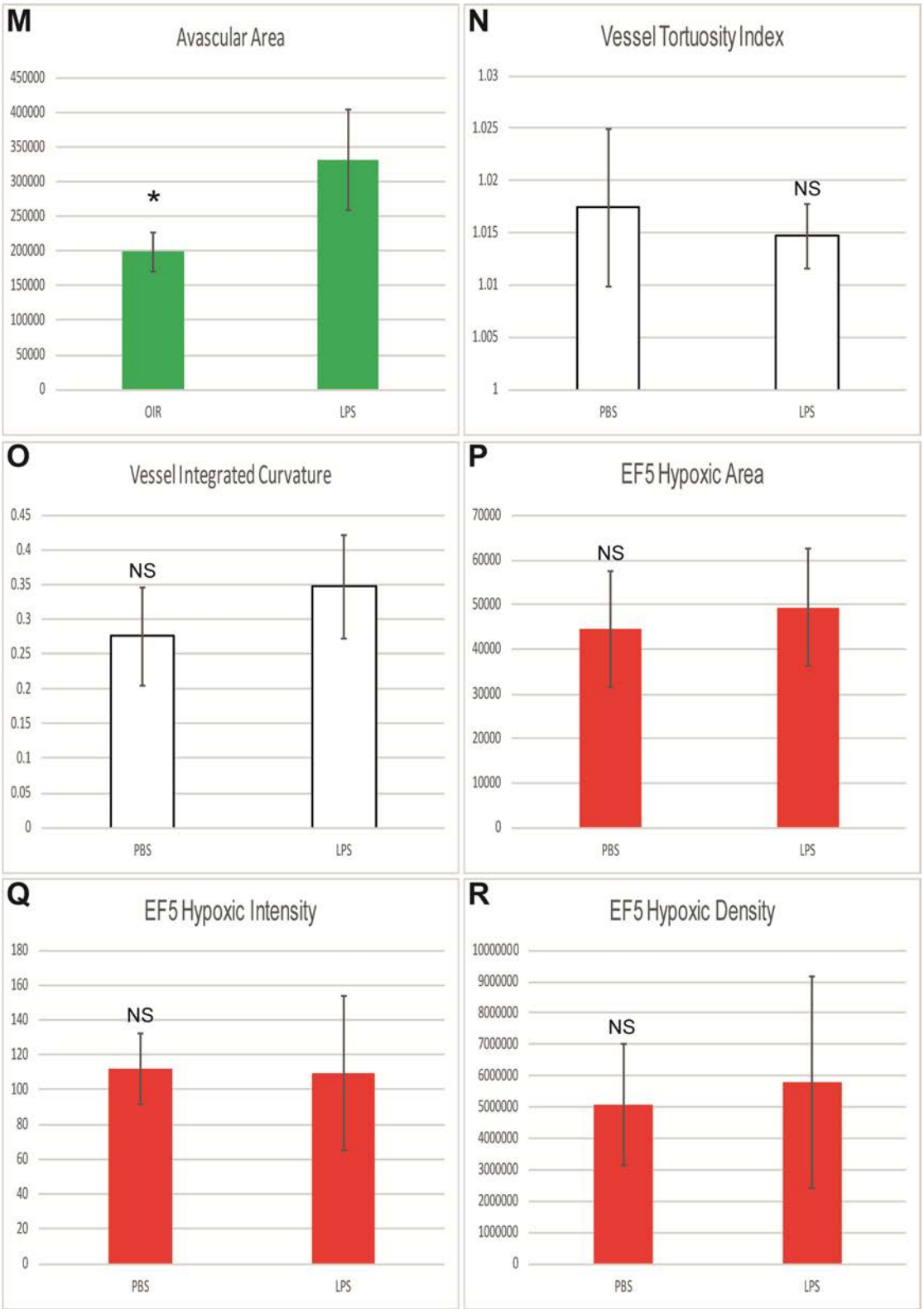

Figure 3.7(c) Intraperitoneal injection of LPS at P12 in C3H mice after hyperoxia does not change hypoxia seen at P14 in OIR. *The avascular area was found to be significantly larger in the LPS treated group (M). Otherwise no significant differences were noted in either vessel tortuosity measures (N&O), or EF5 hypoxia measures (P,Q,R). (n= PBS 4 vs LPS 5; error bar = standard deviation; NS = non-significant, * = p<0.05)*

3.2 Systemic Inflammation induces an invasion of inflammatory cells into hypoxic areas of ischaemic retina

3.2.1 Inflammatory cells which invade into hypoxic retinas of mice treated systemically with LPS are of myeloid origin

In previous experiments where C57B6 pups were injected with intraperitoneal LPS an increased inflammatory response was seen in the hypoxic area, as represented by an influx of lectin positive cells. As the LPS was injected into the peritoneum, it would appear that LPS induced polarisation of inflammatory cells occurs in the periphery and then these cells travel via the blood stream to the retinal vasculature where they are then able to invade the hypoxic retina.

The mouse M lysosome gene is exclusively expressed in myeloid cells of the haemopoietic system and is progressively turned on upon cell differentiation (Möllers *et al.*, 1992). The LysMCre mouse is a mouse line that specifically expresses Cre under control of the LysM gene in peripheral monocytes/macrophages and neutrophils (B. E. Clausen *et al.*, 1999).

To investigate whether the invading population of cells seen in the hypoxic area of LPS treated mice are invading myeloid cells a LysMCre Reporter strain was used to see if the cells in the hypoxic area were labelled by the reporter.

To establish that there were no labelled myeloid cells in the retina prior to the vaso-obliterative, hyperoxia stage or prior to LPS injection at P12, LysMCre reporter mouse pups were culled at various stages; P6, P10 after 3 days exposure to hyperoxia (75%

O2) between P7-10 and P12 after 5 days exposure to hyperoxia (75% O2) between P7-12 (**Figure 3.8**).

At P6, when the primary plexus of the retinal vasculature is radiating out towards the periphery, which is known to be hypoxic, cells expressing GFP are seen at the vascular front and in the avascular area. These cells have an ameboid appearance unlike the round appearance of the lectin positive cells seen invading the hypoxic area of LPS treated mice retinas. They also stain for IBA1 which would also suggest that these GFP expressing cells are resident microglia rather than invading myeloid cells. Similar cells are seen to express GFP in the avascular area and periphery of retina of mice undergoing vaso-obliteration between P7-12.

Having established that there was an absence of the round lectin positive cells previously seen to invade the hypoxic area of C57B6 mice treated with LPS prior to LPS injection at P12, the reporter strain was used to test whether the same invading population would express GFP, and therefore be of the myeloid lineage. A litter of LysMCre reporter pups underwent the same LPS vs PBS OIR protocol previously described and mice were once again culled at P14. Immunohistochemistry was performed on retinal wholemounts to examine hypoxia (**Figure 3.9**).

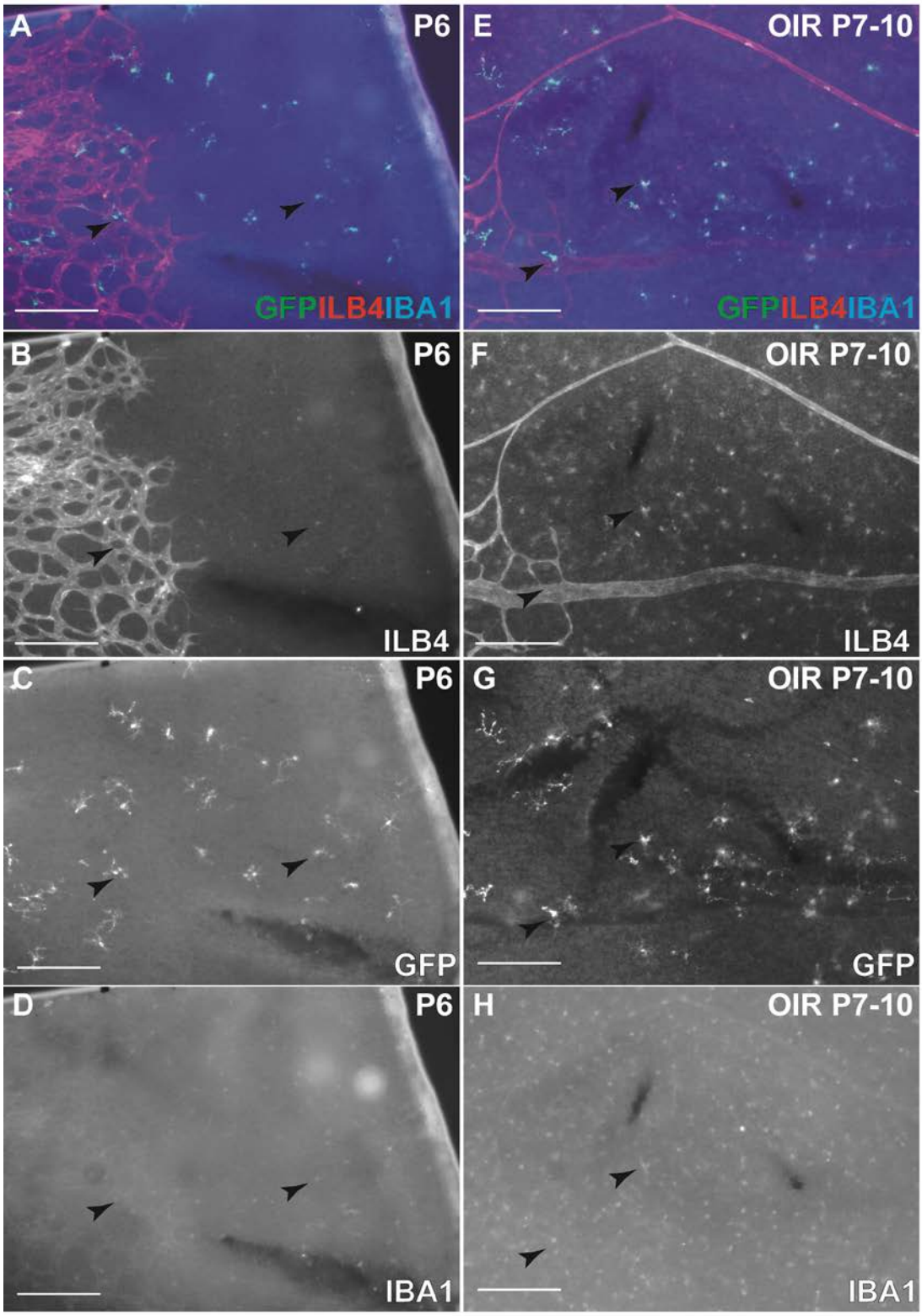

Figure 3.8(a) – GFP expression in LysMCre Reporter Mice at P6 and during the vaso-obliterative stage of the OIR model at P10 *Retinal wholemounts from LysMCre reporter mice at P6 (A-D), P10 after hyperoxia (75%) between P7-10 (E-H) stained with isolectin B4 and IBA1 to stain resident microglia. At each time point the presence of GFP expressing cells (black arrows) could be seen in avascular areas of the retina. These cells have a ramified appearance and stain for IBA1 suggesting that they are resident microglia rather than invading myeloid cells. Scale bar = 20μm*

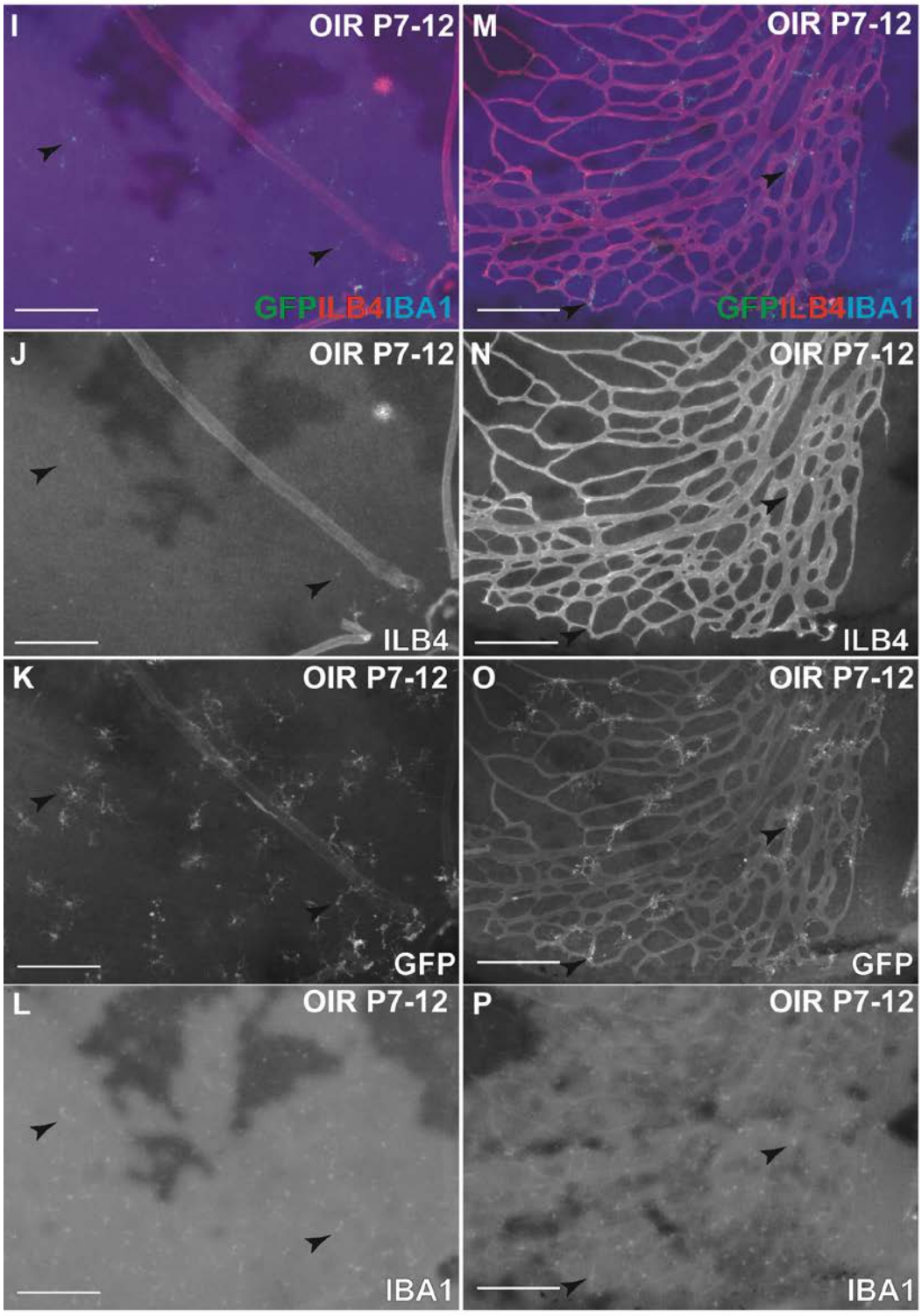

Figure 3.8(b) – GFP expression in LysMCre Reporter Mice at P12 following vasobliteration. *Retinal wholemounts from LysMCre reporter mice at P12 after hyperoxia (75%) between P7-12 stained with isolectin B4 and IBA1. The presence of GFP expressing cells (black arrows) could be seen in both central avascular (I-L) and peripheral vascularised areas (M-P) of the retina. Again, these cells have a ramified appearance and stain for IBA1 suggesting that they are resident microglia rather than invading myeloid cells. Scale bar = 20µm*

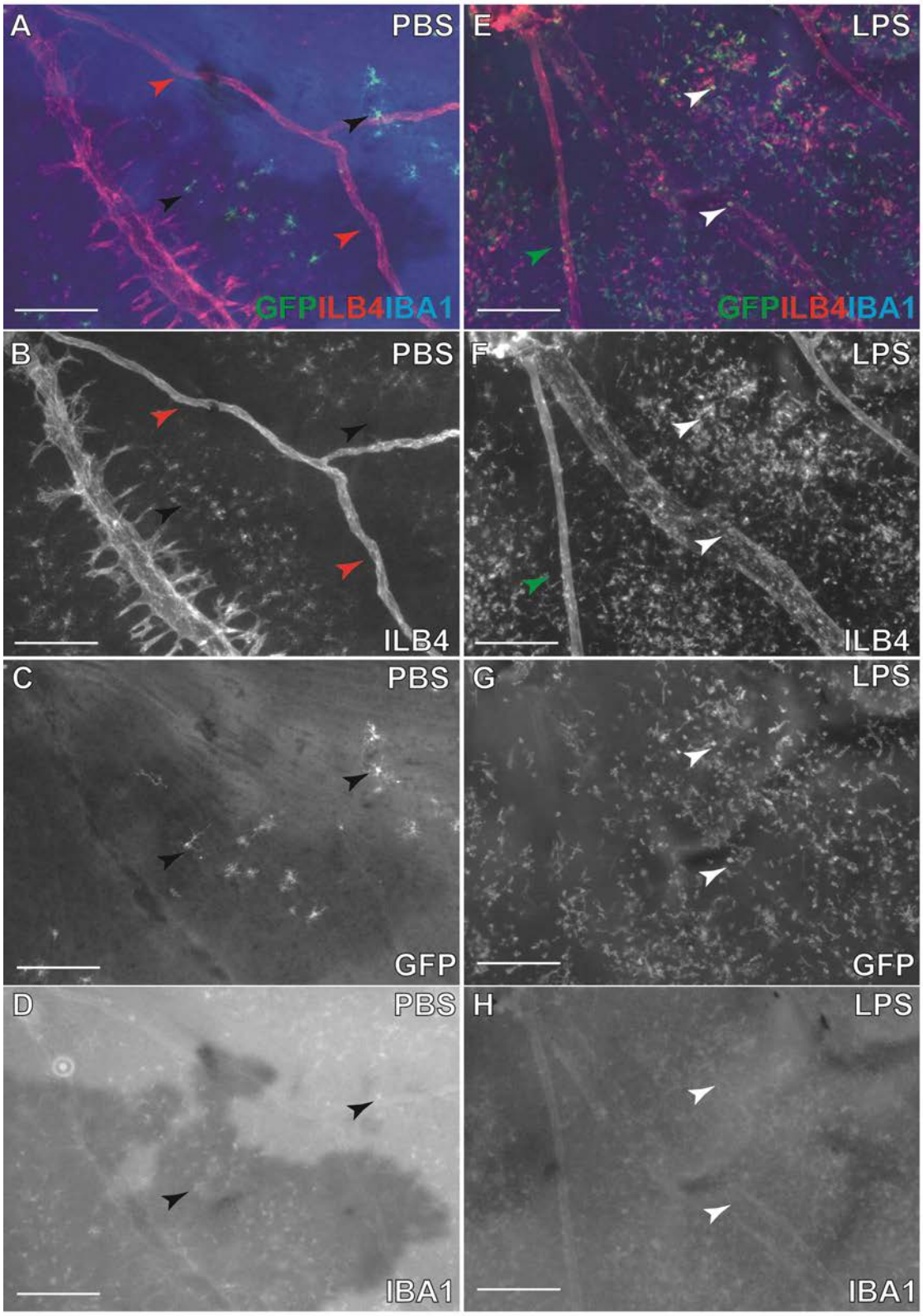

Figure 3.9(a) - Intraperitoneal injection of LPS at P12 after hyperoxia leads to influx of GFP expressing peripheral myeloid cells in LysMCre reporter mice retina at P14 in OIR *Retinal wholemounts of P14 LysMCre reporter pups after OIR were stained with isolectin B4 and IBA1. Mouse pups in the PBS control group (A- D) demonstrated ramified, GFP and IBA1 expressing resident microglia in the central avascular area (black arrows). Mouse pups in the LPS treated group (E-H) demonstrated an influx of round lectin and GFP positive cells in the central avascular area (white arrows). Given both their appearance and that they express GFP in the model would suggest that they*

are peripheral monocytes/macrophages or neutrophils. This is associated with straightening of the retinal arteries (red arrows vs green arrow). Scale bar = 20µm

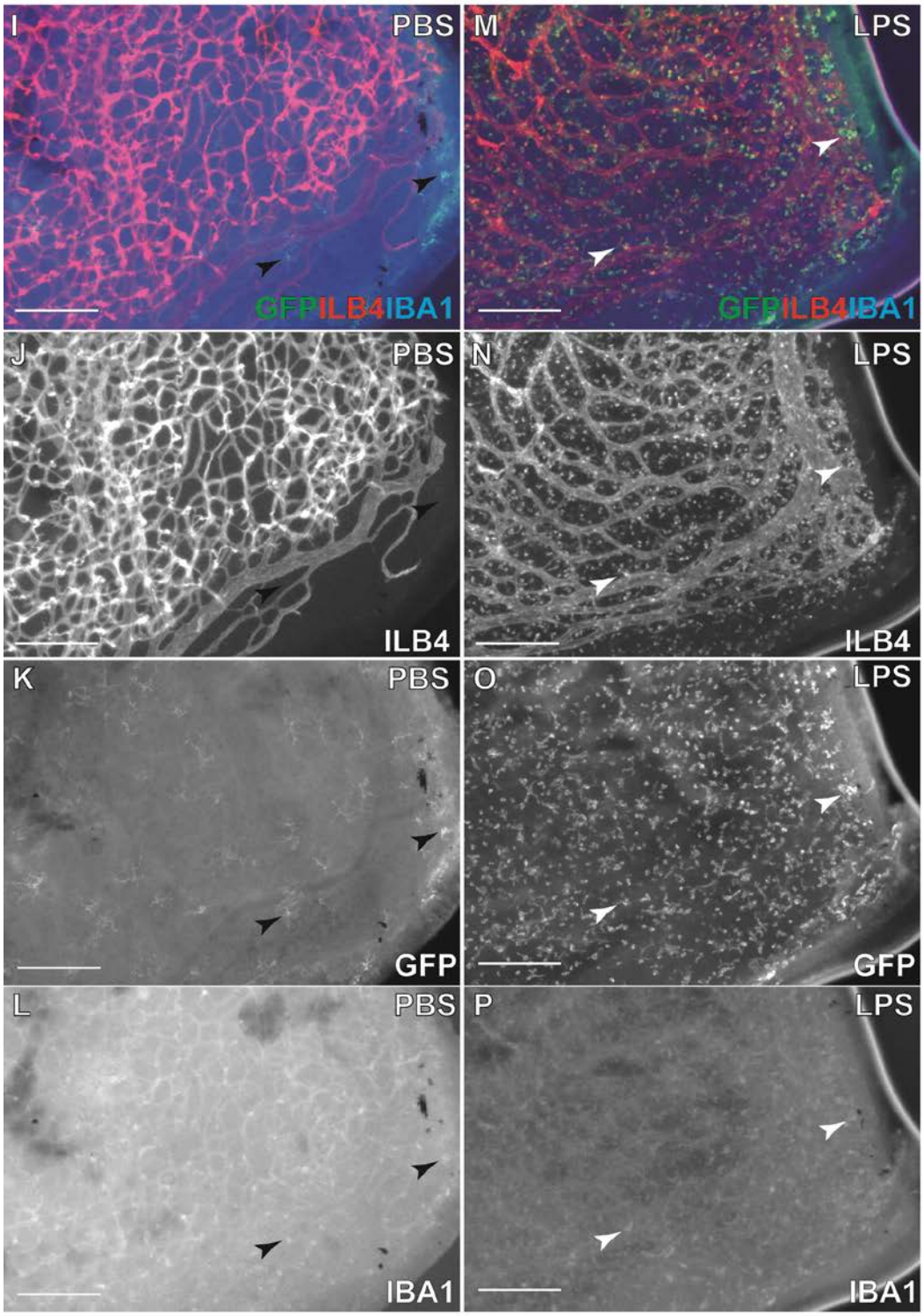

Figure 3.9(b) - Intraperitoneal injection of LPS at P12 after hyperoxia leads to influx of GFP expressing peripheral myeloid cells in LysMCre reporter mice retina at P14 in OIR *Retinal wholemounts of P14 LysMCre reporter pups after OIR were stained with isolectin B4 and IBA1. Mouse pups in the PBS control group (A- E) demonstrated the same population of resident microglia (black arrows) in the peripheral vascularised area. Mouse pups in the LPS treated group demonstrated an influx of the same peripheral myeloid cells (white arrows) in the peripheral vascularised area. Scale bar = 20µm*

Mouse pups in the PBS control group showed the typical tortuous retinal arteries associated with OIR and mouse pups in the LPS treatment group demonstrated straightening of the retinal arteries, as was seen in previous experiments with C57Bl6 strains. The control pups demonstrated GFP expression in ameboid cells in both the avascular area and periphery, which co-stained with IBA1 suggesting that this is the same resident microglial population seen prior to the hypoxic stage. In pups treated with LPS there was an influx of round lectin positive cells in both hypoxic areas and retinal periphery, as was seen in C57Bl6 mice treated with LPS. This incoming population expressed GFP suggesting that they are peripheral monocytes, macrophages or neutrophils activated in the blood stream which invade the hypoxic retina.

To further characterise this population of invading myeloid cells a litter of C57BL6 pups underwent the same LPS vs PBS OIR protocol previously described and mice were once again culled at P14. To determine the nature and number of this cell population staining was performed for isolectin B4, (known to stain immunocompetent cells) (**Figure 3.10B,E**), IBA1 (known to stain resident microglia) (**Figure 3.10C,F**) and Cd11b (known to be expressed on leukocytes, including monocytes, macrophages and granulocytes) (**Figure 3.11**).

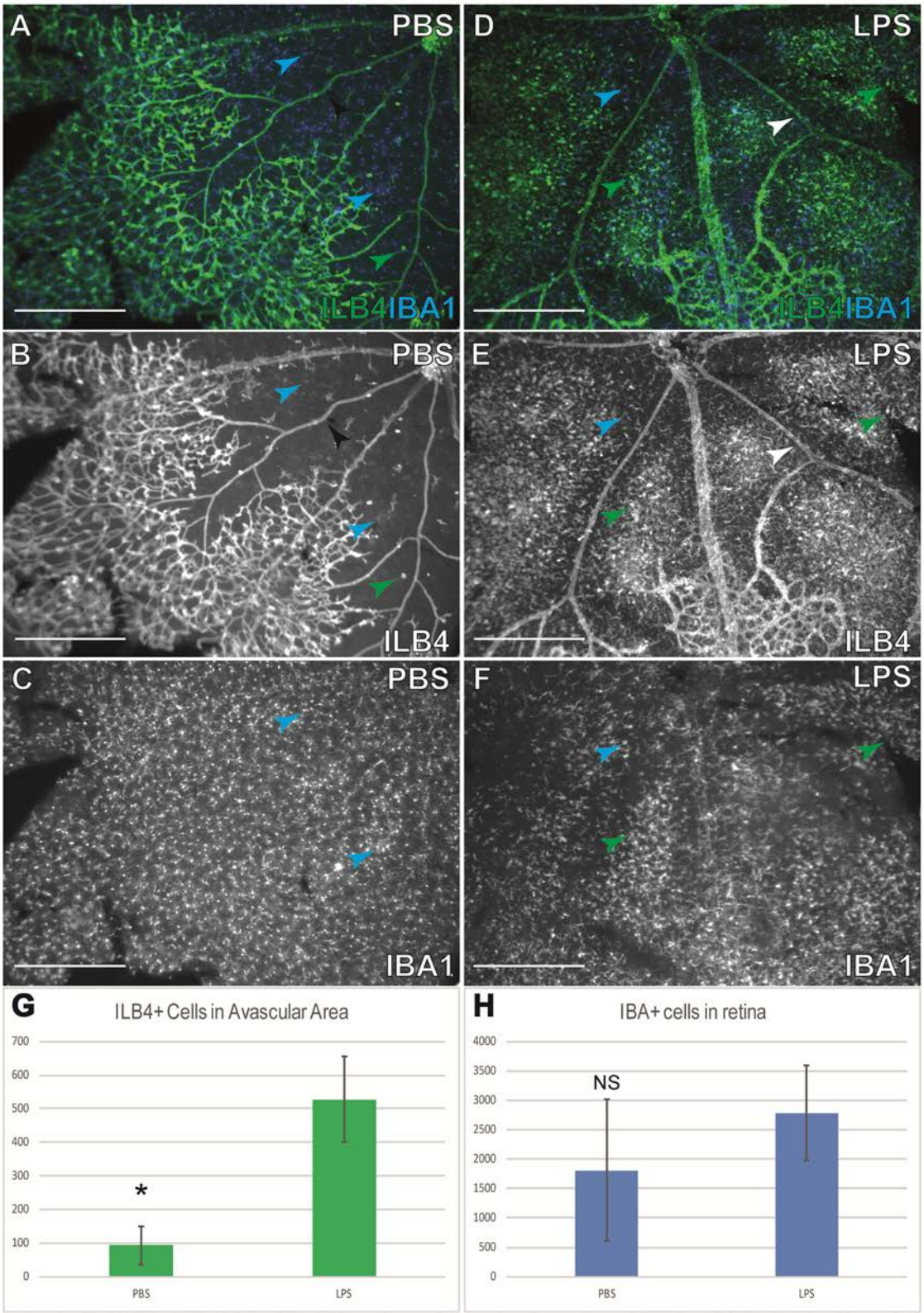

Figure 3.10 - Intraperitoneal injection of LPS at P12 after hyperoxia leads to influx of lectin positive, IBA1 negative cells in the avascular area at P14 in OIR *Retinal wholemounts from P14 C57BL6 mice after OIR stained with isolectin B4 and IBA1. Mouse pups in the control (A-C) showed positive lectin and IBA1 staining of resident microglia (blue arrows) in the avascular area. Pups in the LPS treated group (D-F) showed positive lectin and IBA1 stained cells (green arrows) in the avascular area but in greater numbers. This is associated with straightening of the retinal arteries*

*(black arrows vs white arrows). There was no significant difference in IBA1 positive cells between the two groups (H), whereas there was significant increase in round-bodied lectin stained cells into the avascular area (G). (ILB4 - n= PBS 4 vs LPS 6; IBA1 – n= PBS 5 vs LPS 4; error bar = standard deviation; NS = non-significant, * = <0.05) scale bar = 20um*

Table 3.5: P14 OIR: PBS vs LPS Inflammatory Cell Analysis

	TreatmentGroup	N	Mean	Std. Deviation	Std. Error Mean
ILB4cells	PBS	4	93.2500	55.90692	27.95346
	LPS	6	528.333	128.20556	52.33970
IBA1cells	PBS	5	1811.80	742.24740	331.94313
	LPS	4	2788.75	802.99621	401.49811
Cd11bcells	PBS	2	43.0000	1.41421	1.00000
	LPS	2	1291.00	142.83557	101.00000

	Levene's Test for Equality of Variances		t-test for Equality of Means						
								95% Confidence Interval of the Difference	
	F	Sig.	t	df	Sig. (2-tailed)	Mean Difference	Std. Error Difference	Lower	Upper
ILB4cells	2.490	.153	-6.300	8	.000	-435.08333	69.05617	-594.32714	-275.83952
			-7.332	7.273	.000	-435.08333	59.33667	-574.33177	-295.83490
IBA1cells	.002	.962	-1.894	7	.100	-976.95000	515.77405	-2196.56183	242.66183
			-1.875	6.296	.108	-976.95000	520.94814	-2237.25488	283.35488
Cd11bcells	.	.	-12.356	2	.006	-1248.00000	101.00495	-1682.58923	-813.41077
			-12.356	1.000	.051	-1248.00000	101.00495	-2530.79524	34.79524

Table 3.5 Statistical comparison of inflammatory cell populations at P14 OIR in PBS vs LPS treatment groups

In the PBS control group ramified cells positive for isolectin and IBA1 staining were seen in the central avascular area. IBA1 staining of these cells could be seen throughout the retina and would suggest that this is the resident microglial population. A similar population is seen in pups in the LPS treatment group. When comparing the number of IBA1 positive cells in retinal wholemounts there was a non-significant increase seen in the pups injected with LPS (**Figure 3.10H**). In the pups injected with LPS there was a significant increase in lectin positive cells into the avascular area ($p<0.05$) (**Figure 3.10G**). The round-bodied cells do not co-stain with ILB4 which would indicate that they are not resident microglia. They do however stain for Cd11b (**Figure 3.11G**) and Cd11b staining in the avascular area is significantly increased with LPS IP injection ($p<0.05$) (**Figure 3.11I**).

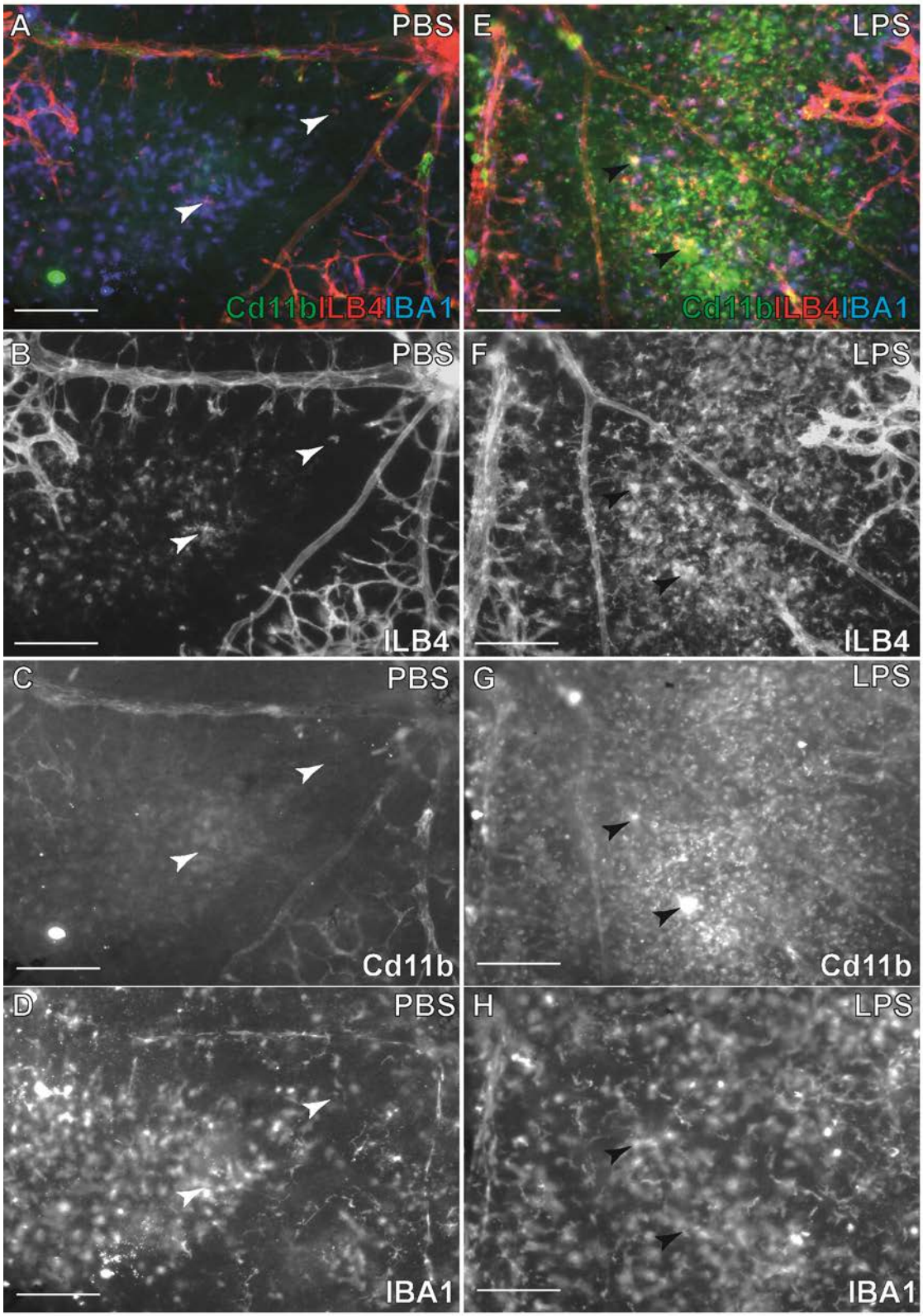

Figure 3.11(a) - Intraperitoneal injection of LPS at P12 after hyperoxia leads to influx of Cd11b, lectin positive, IBA1 negative cells in the avascular area at P14 in OIR *Retinal wholemounts from P14 C57BL6 mice after OIR stained with isolectin B4, IBA1 and Cd11b. Mouse pups in the PBS control group demonstrate resident microglia in the avascular area (white arrows). The invading lectin positive cells seen in the avascular area of the LPS treated mouse pups are positive for Cd11b (black arrows). Scale bar = 20μm*

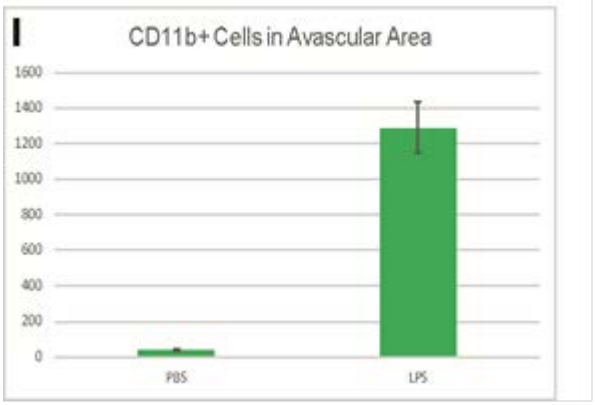

Figure 3.11(b) - Intraperitoneal injection of LPS at P12 after hyperoxia leads to influx of Cd11b, lectin positive, IBA1 negative cells in the avascular area at P14 in OIR *Pups in the LPS treated group showed a significant increase in Cd11b positive cells in the avascular retina. (n= PBS 2 vs LPS 2; error bar = standard deviation;*=<0.005)*

These results indicate that the round-bodied population that are seen in increasing number in P14 retina after LPS IP injection at P12 are of myeloid lineage, e.g. macrophages, monocytes or neutrophils and are non-resident to the retina.

3.2.2 Myeloid cells which invade into hypoxic retinas of mice treated systemically with LPS are predominantly neutrophils

Both LysM and Cd11b are known to be expressed by monocytes, macrophages and neutrophils. Although they all stem from the myeloid lineage, these cell populations can be separated by their expression of other cell surface markers such as F4/80, Ly6C and Ly6G. Macrophages and monocytes are known to express F4/80 and can then be separated into classical/inflammatory or non-classical/resident by their expression of Ly6C (Rose, Misharin and Perlman, 2012). Ly6G is known to be expressed in neutrophils.

To further classify the incoming population of LysM, Cd11b positive cells that invade the retinas of the LPS treated mice, flow cytometry was performed in C57BL6 mouse

pups. Pups were separated into 3 groups for comparison: a control group of P14 age matched controls, a group with PBS injected intraperitoneally at P12 after being exposed to 5 days of hyperoxia (75% O2) between P7-12 and a group with LPS injected intraperitoneally at P12 after being exposed to 5 days of hyperoxia (75% O2) between P7-12. A myeloid panel of Cd11b, Cd11c, F4/80, Ly6C and Ly6G was used to immunophenotype the myeloid population seen in the retinas of the mouse pups. The myeloid panel was able to identify four different populations; Cd11b+ Cd11c+ dendritic cells, Cd11b+ $Ly6G^{hi}$ neutrophils, Cd11b+ F4/80+ $Ly6C^{lo}$ resident monocyte/macrophages and Cd11b+ F4/80+ $Ly6C^{hi}$ inflammatory monocyte macrophages (Rose, Misharin and Perlman, 2012). Frequencies of cells in each sub-gate were then counted (**Figure 3.12**).

The most predominant myeloid cell seen in the retinas of both the P14 age matched controls and the PBS injected OIR mice were Cd11b+ F4/80+ $Ly6C^{lo}$ resident monocyte/macrophages. In the PBS injected OIR group there were no Cd11b+ F4/80+ $Ly6C^{hi}$ inflammatory monocyte macrophages. When compared to the P14 age matched controls there was a small increase in the number of Cd11b+ $Ly6G^{hi}$ neutrophils in the PBS OIR group. However, in the LPS treatment group there was a huge increase in the number of Cd11b+ $Ly6G^{hi}$ neutrophils seen in the retina and they made up 70% of the Cd11b+ cells seen in the retina. An increase in Cd11b+ F4/80+ $Ly6C^{hi}$ inflammatory monocyte macrophages was also seen in LPS treated mice pups but this was much less than the increase seen in the neutrophil population. In terms of cell counts the number of Cd11b+ F4/80+ $Ly6C^{lo}$ resident monocyte/macrophages showed little change between the three groups.

These results indicate that the Cd11b, Lectin positive cells seen in the avascular and retinal periphery of LPS treated OIR retinas are predominantly neutrophilic in nature.

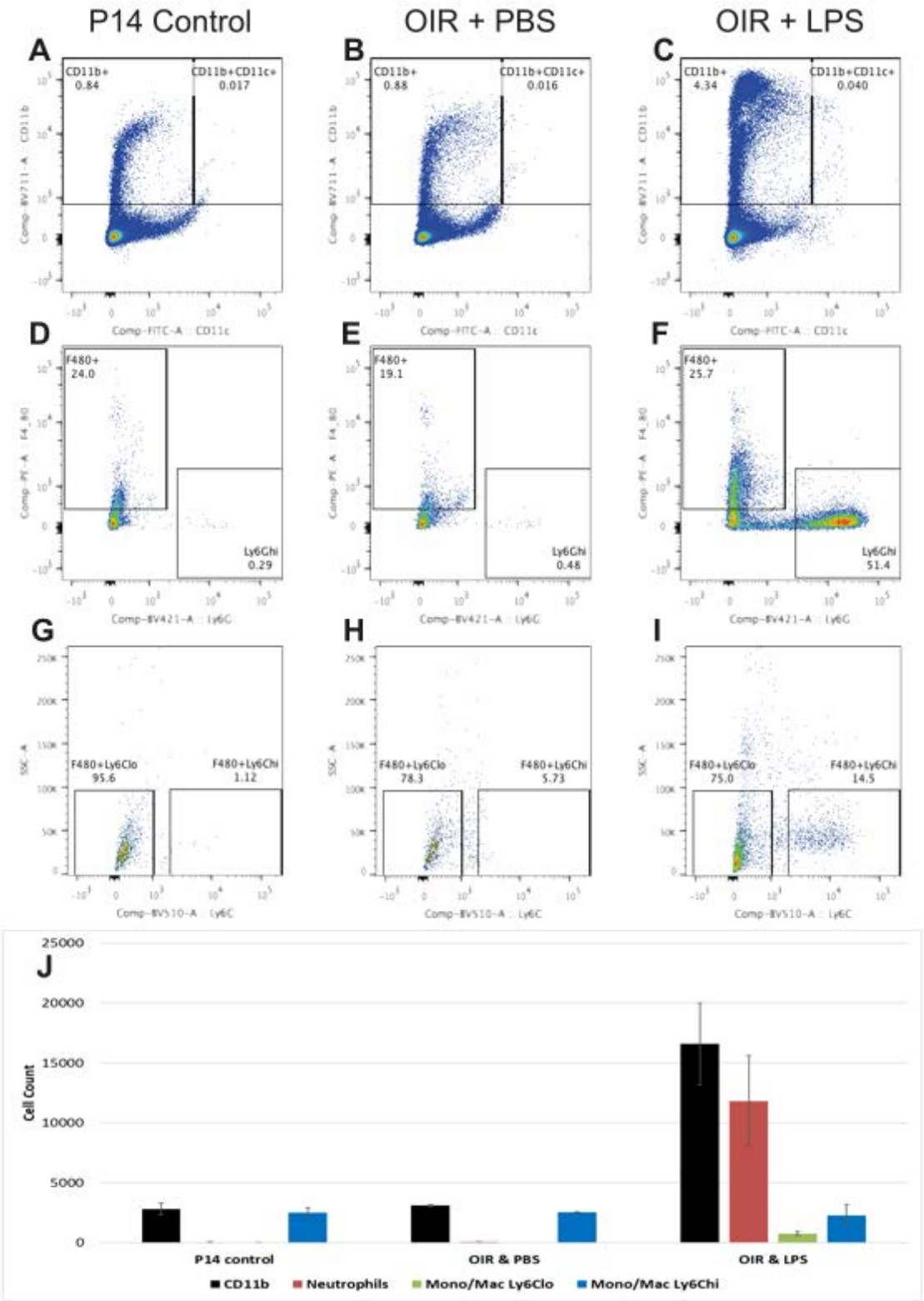

Figure 3.12 – Flow cytometry using a myeloid panel of cell surface markers highlights a large increase in neutrophils in the retina of OIR mice at P14 in the LPS group. *C57BL6 mouse pups were separated into 3 groups for comparison; P14 age controls (A,D,G), PBS control group (B,E,H) and LPS treatment group (C,F,I). The myeloid panel was able to differentiate between 4 subtypes of myeloid cell: dendritic cells (Cd11b+Cd11c+), neutrophils (Cd11b+ Ly6G^{hi}) (red bar), resident monocyte/macrophages (Cd11b+ F4/80+ Ly6C^{lo}) (green bar) and inflammatory monocyte/macrophages (Cd11b+ F4/80+ Ly6C^{hi}) (blue bar). In the LPS treatment group there is a large increase in Cd11b+ cells (black bar) in the retina with the biggest subset of myeloid cells being neutrophils (F, J). (n= P14 control 3 vs OIR+PBS 3 vs OIR+LPS 3)*

3.3 The role of invading myeloid population on hypoxia in ischaemic retina

3.3.1 The effect of depleting invading myeloid population seen in LPS treated OIR retinas on hypoxia in LysmCreDTA mice

As demonstrated previously, systemic LPS injection in the OIR model results in the invasion of large number of immune cells of myeloid lineage into the retina. An association is seen between the reduction in hypoxia seen in LPS treated mouse pups undergoing OIR and the influx of these neutrophils into the retina. Therefore, it is possible that the invading neutrophils and monocyte/macrophages may be causally linked to the reduction in hypoxia and subsequent healthy regeneration of retinal vasculature observed in this model. On examination of the retinal flatmounts it appears that their role is not related to revascularisation as there is little difference between the size of the avascular area at P14 between the PBS control and LPS treatment groups. A possible hypothesis is that their invasion into the avascular area is followed by the release of cytokines which alter the metabolism of the hypoxic retina, reducing its oxygen demand and therefore alleviating the hypoxia, thereby promoting healthy vascular regeneration to occur.

Having previously identified that the LysMCre strain successfully targets the same invading population, this allows the incoming neutrophils to be manipulated to assess their role in reducing the hypoxia seen at P14 in the LPS treatment group. The LysMCre strain was crossed with a conditional ROSA-DTA strain (Ivanova *et al.*, 2005) in an attempt to deplete the incoming neutrophil and monocyte/macrophage populations. By depleting the number of cells entering the avascular area it is possible to see if LPS

activation of TLR4 in the OIR model is still able to prevent the hypoxia seen at P14, therefore determining if these incoming myeloid cells are responsible for the reduction in oxygen demand in the retina. To investigate whether in the absence of these cells LPS still reduced the hypoxia seen in the OIR model a litter of LysMCreDTA mouse pups underwent the same LPS vs PBS OIR protocol previously described and mice were once again culled at P14. Immunohistochemistry was performed on retinal wholemounts to examine hypoxia.

In mice from the LysMCreDTA WT group treated with LPS, the typical influx of round neutrophilic myeloid cells is seen in both the central avascular area (**Figure 3.13B**) and the retinal periphery (**Figure 3.13C**). Whereas in mice from the LysMCreDTA Tg group treated with LPS, these cells appeared almost absent with the exception of a few cells, as demonstrated by a reduction in lectin stained cells in both the central avascular (**Figure 3.13E**) and peripheral areas (**Figure 3.13F**). The remaining lectin and IBA1 positive cells appear to be the resident microglial population.

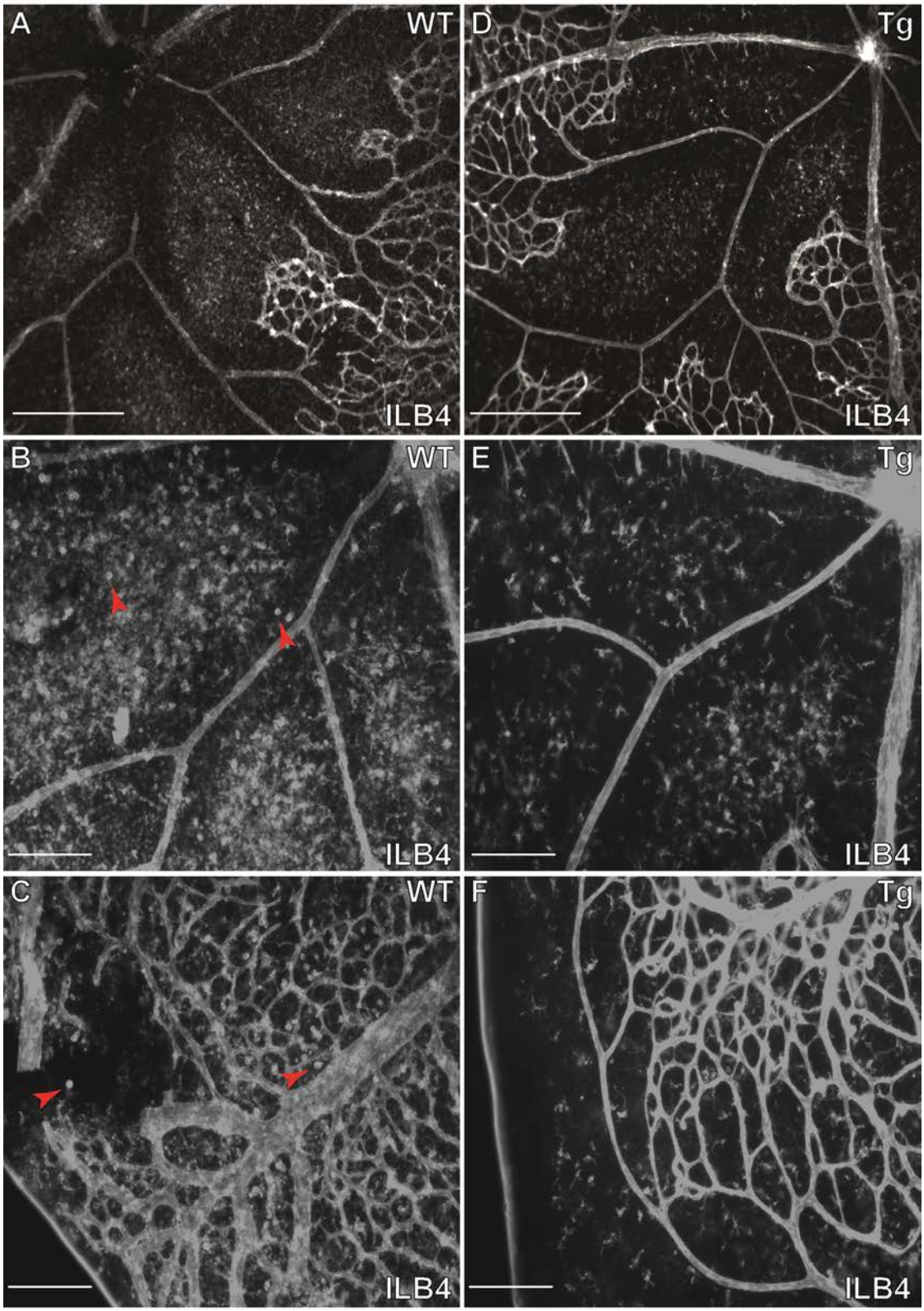

Figure 3.13 – LysMCreDTA mice demonstrate a reduction in lectin stained cells in both the central avascular and peripheral areas in the LPS treatment group. *Retinal wholemounts from P14 LysMCreDTA mice after OIR in the LPS treatment group stained with isolectin B4. In the WT group (A-C) an influx of round boded lectin positive cells (red arrows) is seen in the avascular area (B) and the periphery (C). In the Tg group (D-F) this population is almost completely absent in both the central avascular area (E) and the periphery (F). Scale bar = 50um in A&D, scale bar = 20µm in B,C,E,F.*

Having determined that the peripheral myeloid population had been reduced, the effect of the depletion on the LPS treatment group was studied **(Figure 3.14**). Mice in both the wildtype and transgenic groups when treated with LPS demonstrated straightening on the retinal arteries (**Figure 3.14I,J**) and central areas of vaso-obliteration which were positive for EF5 hypoxia staining (**Figure 3.14E,F**), suggesting a similar level of hypoxia in the two groups. When compared against each other, no significant differences could be found between the two groups in terms of avascular area, vessel tortuosity measures or EF5 hypoxia measures (**Table 3.6**).

Table 3.6: LysMCreDTA P14 OIR LPS: WT vs Tg

	Genotype	N	Mean	Std. Deviation	Std. Error Mean
AvascularArea	WT	6	253325	42139.24794	17203.27593
	TG	4	218266	19808.68238	9904.34119
VesselTortuosityIndex	WT	6	1.0303	.01476	.00603
	TG	4	1.0345	.01151	.00575
VesselIntegratedCurvature	WT	6	.7292	.27811	.11354
	TG	4	.8163	.22817	.11408
EF5HypoxicArea	WT	6	84946.3	16054.65284	6554.28458
	TG	4	79286.5	12974.63460	6487.31730
EF5HypoxicIntensity	WT	6	167.750	30.06067	12.27222
	TG	4	148.781	11.03062	5.51531
EF5HypoxicDensity	WT	6	1.41E+7	2697762.968	1101357.120
	TG	4	1.19E+7	2647169.434	1323584.717

	Levene's Test for Equality of Variances		t-test for Equality of Means						
								95% Confidence Interval of the Difference	
	F	Sig.	t	df	Sig. (2-tailed)	Mean Difference	Std. Error Difference	Lower	Upper
AvascularArea	1.253	.295	1.532	8	.164	35059.08333	22885.28090	-17714.46907	87832.63573
			1.766	7.492	.118	35059.08333	19850.65936	-11262.49455	81380.66121
VesselTortuosityIndex	.838	.387	-.483	8	.642	-.00425	.00880	-.02454	.01604
			-.510	7.661	.624	-.00425	.00833	-.02361	.01511
VesselIntegratedCurvature	.946	.359	-.518	8	.619	-.08704	.16815	-.47481	.30072
			-.541	7.482	.604	-.08704	.16095	-.46272	.28864
EF5HypoxicArea	.097	.763	.586	8	.574	5659.83333	9665.72235	-16629.36236	27949.02903
			.614	7.538	.557	5659.83333	9221.92670	-15835.03500	27154.70167
EF5HypoxicIntensity	6.301	.036	1.189	8	.268	18.96850	15.94790	-17.80743	55.74443
			1.410	6.764	.203	18.96850	13.45459	-13.07313	51.01013
EF5HypoxicDensity	.058	.816	1.285	8	.235	2221322.917	1729224.043	-1766274.88	6208920.710
			1.290	6.673	.240	2221322.917	1721878.047	-1891056.45	6333702.285

Table 3.6 – Statistical Comparison of P14 LysMCreDTA P14 OIR & LPS WT vs Tg groups

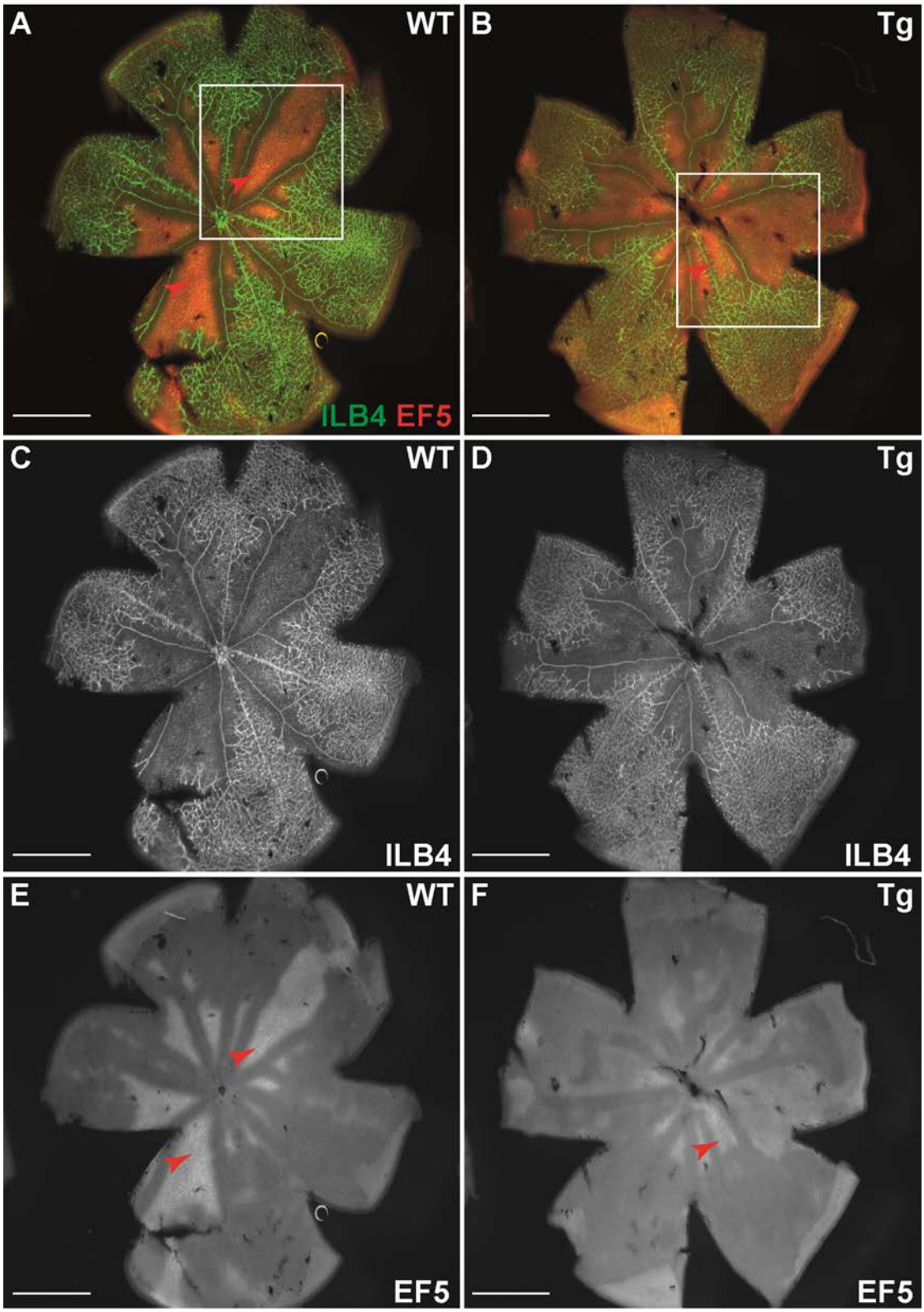

Figure 3.14(a) – No difference in hypoxia is seen at P14 between LysMCreDTA WT and Tg mouse pups injected with LPS at P12. *Retinal wholemounts from P14 LysMCreDTA mice after OIR stained with isolectin B4 and EF5 hypoxia stain. Mouse pups in both the WT group (A,C,E) and the Tg group (B,D,F) had similar avascular areas (C,D) that were positive for EF5 hypoxia stain (red arrows) (E,F). Scale bar = 100µm.*

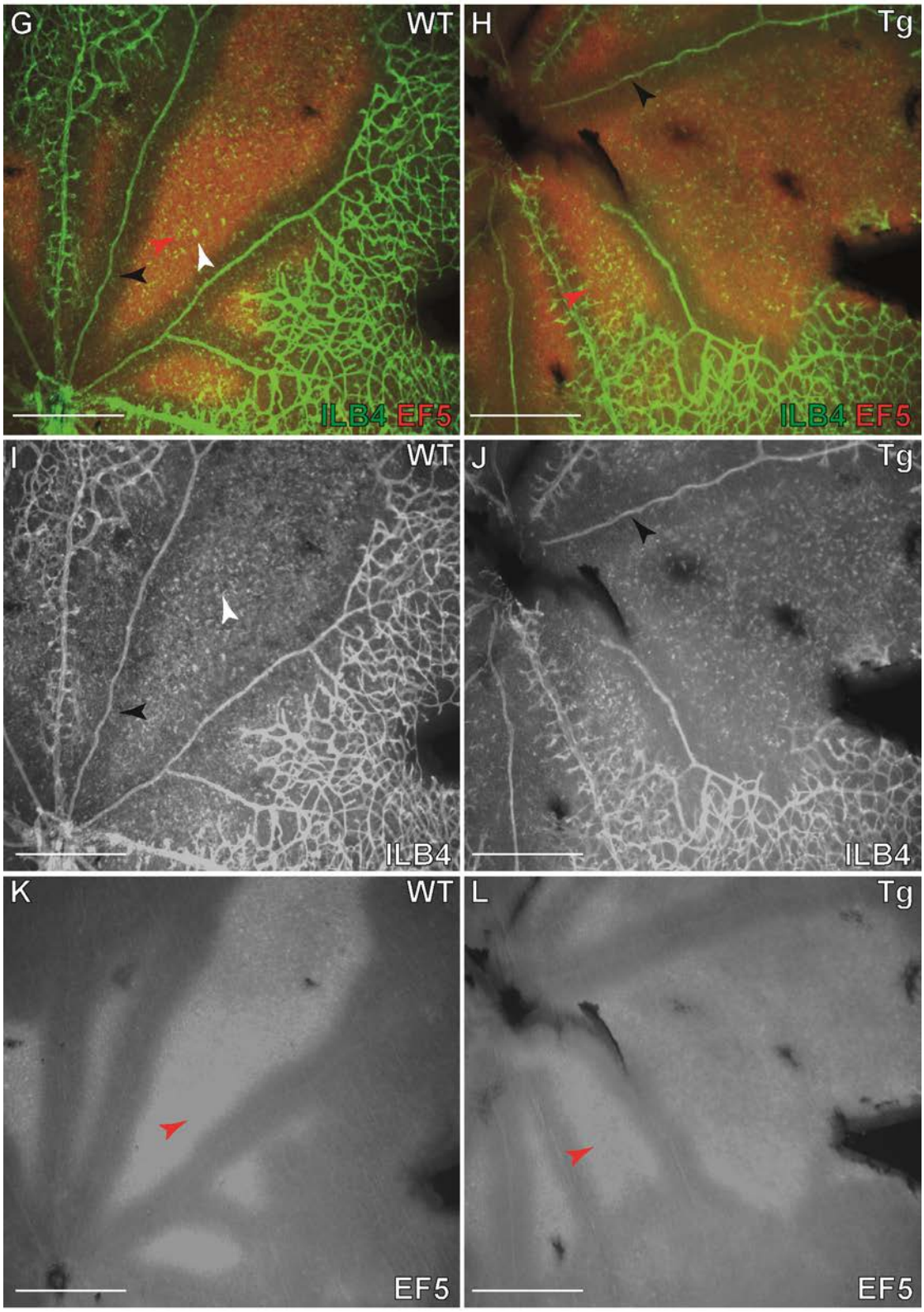

Figure 3.14(b) – No difference in hypoxia is seen at P14 between LysMCreDTA WT and Tg mouse pups injected with LPS at P12. *Higher magnification images demonstrate similar retinal artery tortuosity in both the WT (I) and Tg (J) groups (black arrows). The WT group demonstrated an increased number of round lectin positive cells (white arrows) in the avascular, hypoxic area (red arrows) than the Tg group. Scale bar = 50µm.*

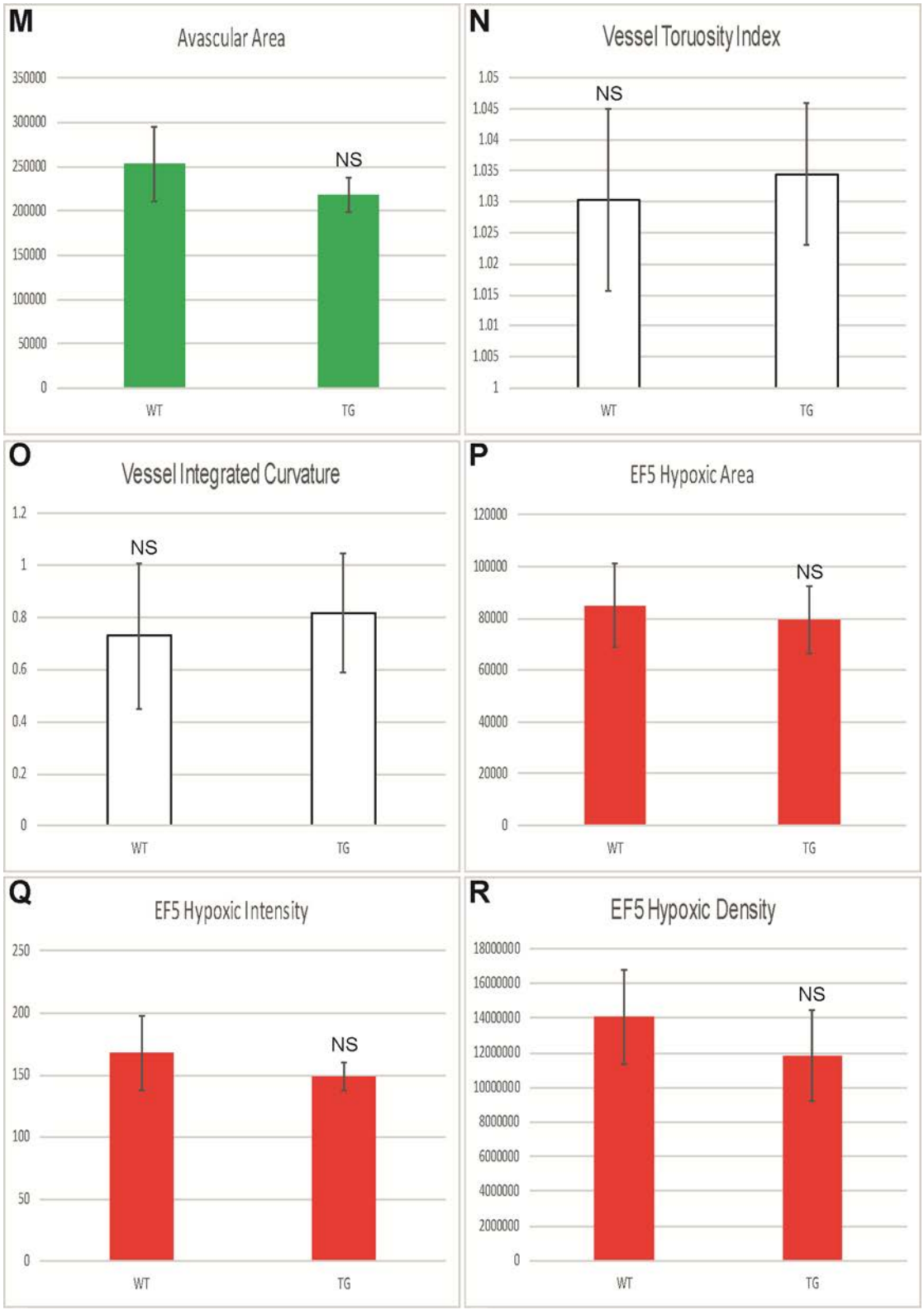

Figure 3.14(c) – No difference in hypoxia is seen at P14 between LysMCreDTA WT and Tg mouse pups injected with LPS at P12. *No significant differences were seen in avascular area, arterial vessel tortuosity or EF5 hypoxia measures between the two groups. (n= WT 6 vs TG 4; error bar = standard deviation; NS = nonsignificant)*

To confirm that the LysM population were not responsible for the reduction in hypoxia previously seen in the LPS treated group of C57BL6 mice, PBS control groups and LPS treatment groups were compared in LysMCreDTA Tg mice (**Figure 3.15**).

Mouse pups in the PBS control group demonstrated a similar hypoxic phenotype to that seen in PBS control groups in previous experiments using C57BL6 mice, characterised by tortuous retinal arteries (**Figure 3.15I**) and central avascular areas (**Figure 3.15C**) which were positive for EF5 hypoxia staining (**Figure 3.15E**). As described previously, mouse pups in the LPS treatment group responded in a similar way to the LPS treatment group of C57BL6 mice. When compared retinal arteries were found to be significantly straighter in the LPS treatment group, as calculated by both tortuosity index and integrated curvature ($p<0.05$) (**Figure 3.15N,O**). The LPS treatment group was found to have a greater avascular area with reduced EF5 hypoxia measures, however these differences did not reach statistical significance (**Table 3.7**).

Table 3.7: LysMCreDTA P14 OIR Tg: PBS vs LPS

	TreatmentGroup	N	Mean	Std. Deviation	Std. Error Mean
AvascularArea	PBS	4	188949	15965.07556	7982.53778
	LPS	4	218266	19808.68238	9904.34119
VesselTortuosityIndex	PBS	4	1.0793	.00814	.00407
	LPS	4	1.0345	.01151	.00575
VesselIntegratedCurvature	PBS	4	1.5894	.16369	.08184
	LPS	4	.8163	.22817	.11408
EF5HypoxicArea	PBS	4	85289.0	10433.08625	5216.54312
	LPS	4	79286.5	12974.63460	6487.31730
EF5HypoxicIntensity	PBS	4	170.156	17.39526	8.69763
	LPS	4	148.781	11.03062	5.51531
EF5HypoxicDensity	PBS	4	1.45E+7	2424668.954	1212334.477
	LPS	4	1.19E+7	2647169.434	1323584.717

	Levene's Test for Equality of Variances		t-test for Equality of Means						
								95% Confidence Interval of the Difference	
	F	Sig.	t	df	Sig. (2-tailed)	Mean Difference	Std. Error Difference	Lower	Upper
AvascularArea	.294	.607	-2.305	6	.061	-29317.75000	12720.72654	-60444.24654	1808.74654
VesselTortuosityIndex	.262	.627	6.358	6	.001	.04481	.00705	.02757	.06206
VesselIntegratedCurvature	.179	.687	5.506	6	.002	.77313	.14040	.42957	1.11668
EF5HypoxicArea	.189	.679	.721	6	.498	6002.50000	8324.51848	-14366.86292	26371.86292
EF5HypoxicIntensity	.650	.451	2.075	6	.083	21.37525	10.29890	-3.82526	46.57576
EF5HypoxicDensity	.016	.905	1.481	6	.189	2657419.750	1794890.355	-1734518.73	7049358.231

Table 3.7 – Statistical Comparisons of P14 LysMCreDTA Tg OIR PBS vs LPS treatment groups

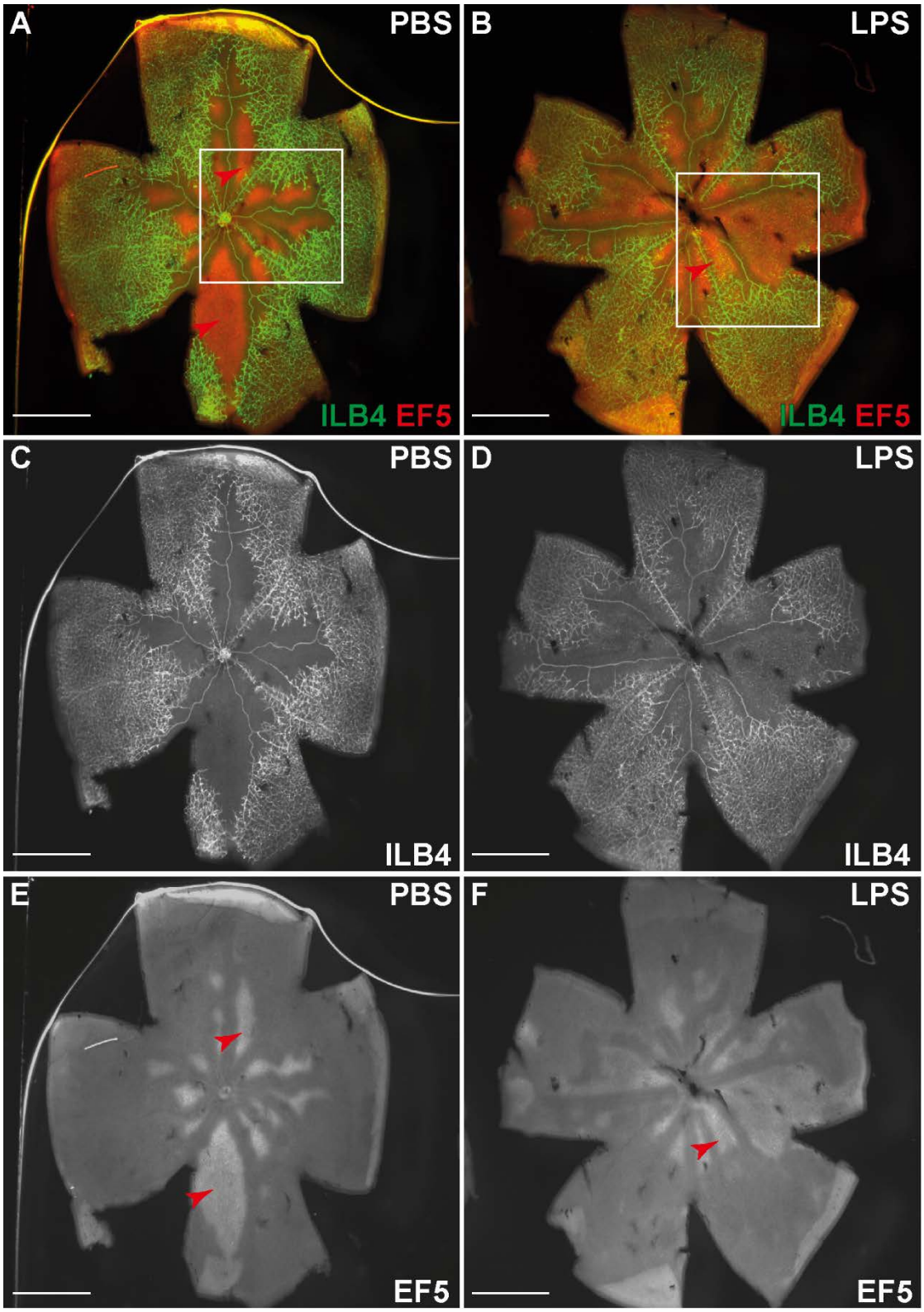

Figure 3.15(a) – Intraperitoneal injection of LPS at P12 after hyperoxia leads to reduced vessel tortuosity in LysMCreDTA Tg mouse pups at P14 in OIR *Retinal wholemounts from P14 LysMCreDTA Tg mice after OIR stained with isolectin B4 and EF5 hypoxia stain. Mouse pups in the PBS group (A,C,E) demonstrated central avascular areas which were positive for EF5 hypoxia stain (red arrows.) Mouse pups in the LPS treatment group (B,D,F) appeared to similar areas of EF5 hypoxia staining with similiar intensity of stain (F). Scale bar = 100µm*

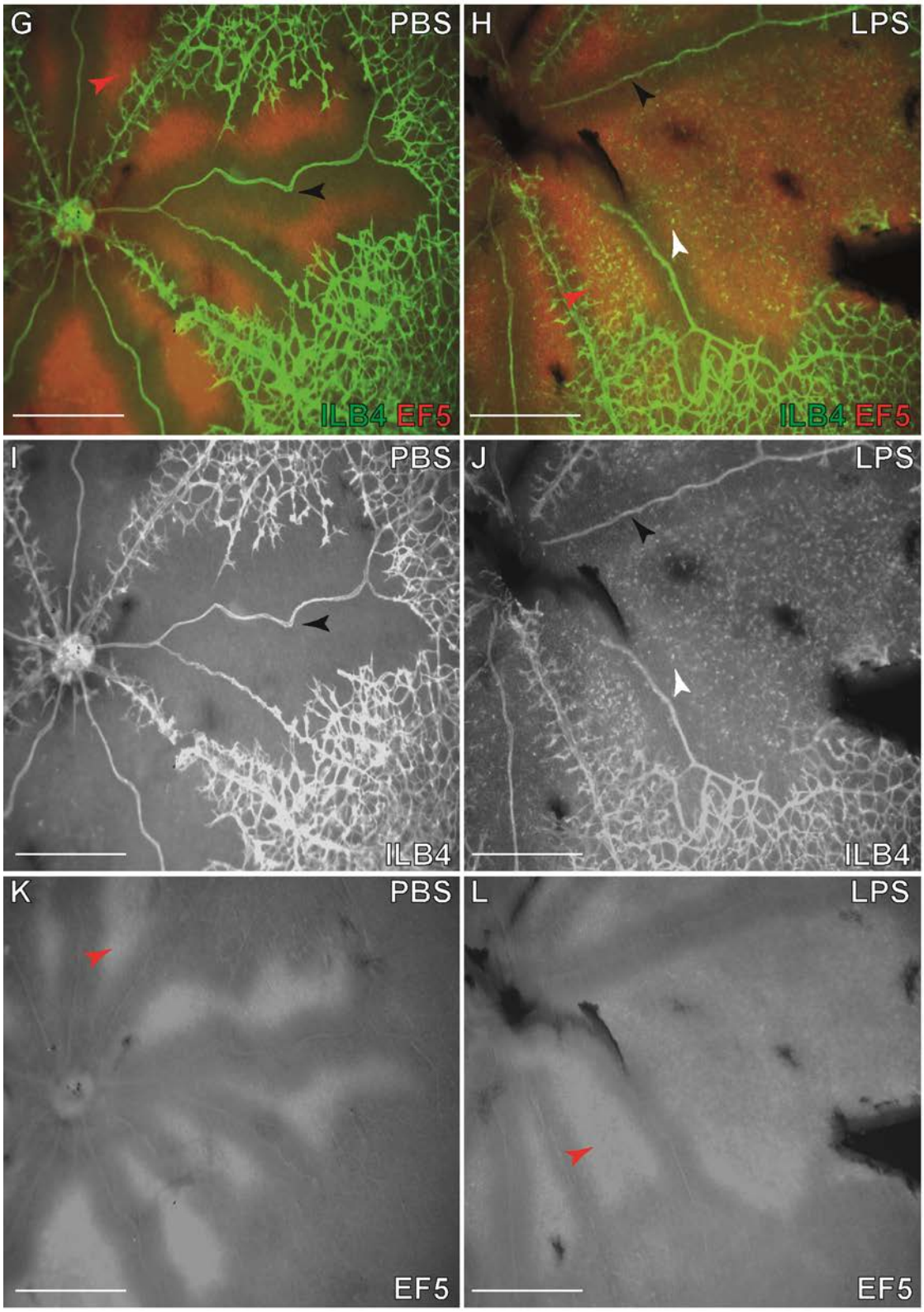

Figure 3.15(b) – Intraperitoneal injection of LPS at P12 after hyperoxia leads to reduced vessel tortuosity in LysMCreDTA Tg mouse pups at P14 in OIR *Higher magnification images demonstrate increased retinal artery tortuosity (black arrows) in the PBS control group (I) compared to the LPS treatment group (J). In the LPS treatment group there are still some round lectin positive cells (white arrows) seen in the hypoxic avascular area (J). Scale bar = 50µm.*

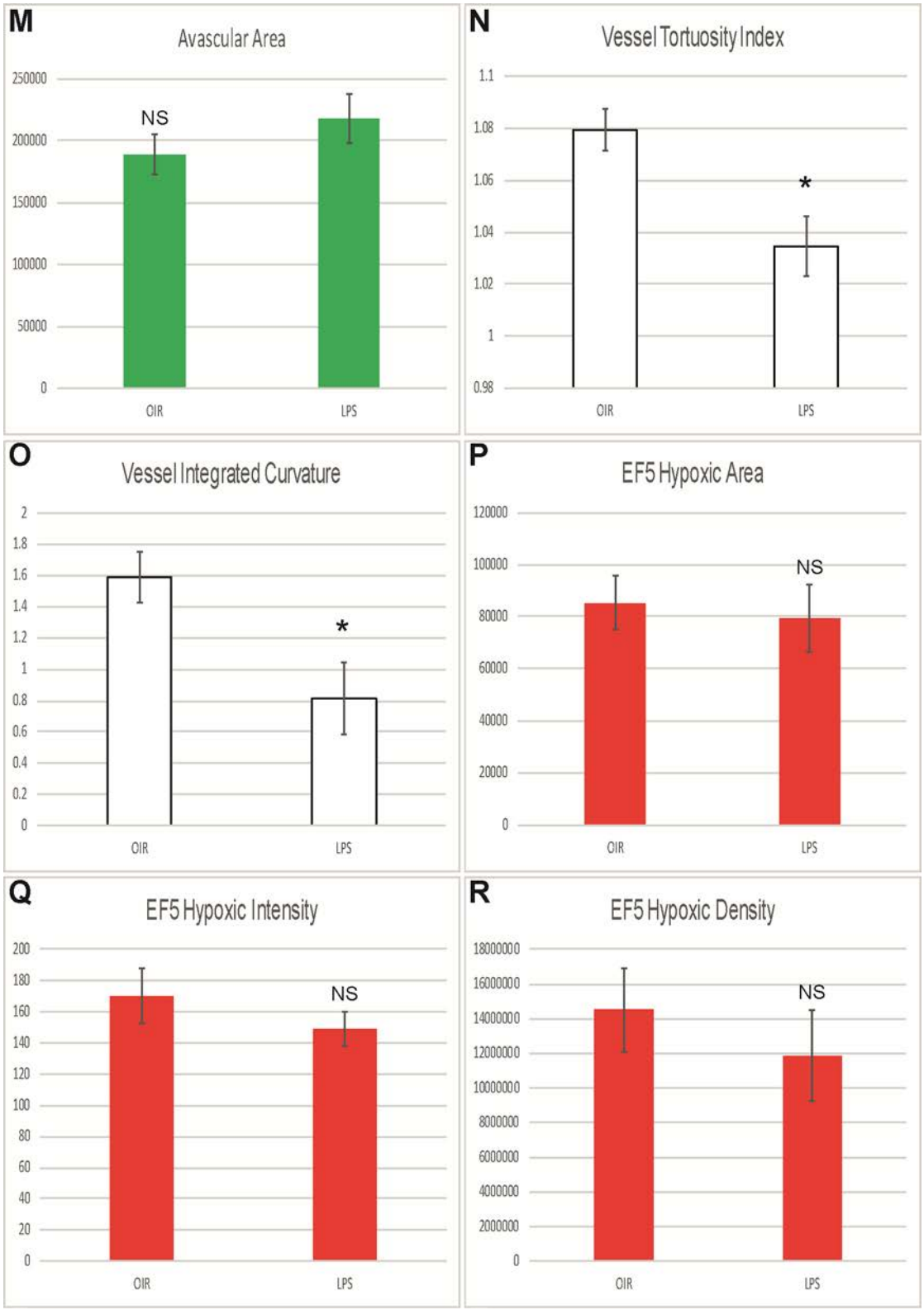

Figure 3.15(c) – Intraperitoneal injection of LPS at P12 after hyperoxia leads to reduced vessel tortuosity in LysMCreDTA Tg mouse pups at P14 in OIR *Pups in the LPS treatment group demonstrated a significant reduction in arterial tortuosity, as calculated by vessel tortuosity and integrated tortuosity (N,O). A non-significant reduction in EF5 hypoxic area measures was seen (P-R). (n= PBS 4 vs LPS 4; error bar = standard deviation; NS=non-significant, * = <0.05)*

These results indicate that reducing the number of invading LysMcre cells does not affect the reduced vessel tortuosity LPS treatment group phenotype. However no significant difference was seen in the EF5 hypoxic area between the two groups. These experiments were not able to completely eradicate the LysMCre population as the occasional round bodied lectin positive cell was still visible. A possible explanation for these findings could be that only a few of these cells are needed to enter the avascular area and cause LPS treatment phenotype.

3.3.2 The effect of depletion of the invading immune cell population seen in LPS treated OIR retinas on hypoxia in CCL2 and CRR2 knockout mice

Given that Cre-induced DTA depletion of the LySM population wasn't able to completely eradicate the invasion of neurophils and monocyte/macrophages into the retina of LPS treated mice, it was decided that a genetic knockout approach may be more successful. CCR2 knockout mice and CCL2 knockout mice have both been shown to demonstrate impaired monocyte and macrophage recruitment (Lu *et al.*, 1998; Saederup *et al.*, 2010) and were thought to be an appropriate model to test whether the invading immune cell population is responsible for the reduction in hypoxia seen in the LPS treatment group.

To investigate whether in the absence of these cells LPS still reduced the hypoxia seen in the OIR model litters of $CCR2^{-/-}$ and $CCL2^{-/-}$ mouse pups underwent the same LPS vs PBS OIR protocol previously described and mice were once again culled at P14. Immunohistochemistry was performed on retinal wholemounts to examine hypoxia.

In CCR$^{-/-}$ mice treated with LPS, the typical influx of lectin positive cells in the avascular area typically seen in C57BL6 mice (**Figure 3.16A**), appeared almost absent with the exception of a few cells. This was demonstrated by a reduction in lectin stained cells in the central avascular area (**Figure 3.16B**).

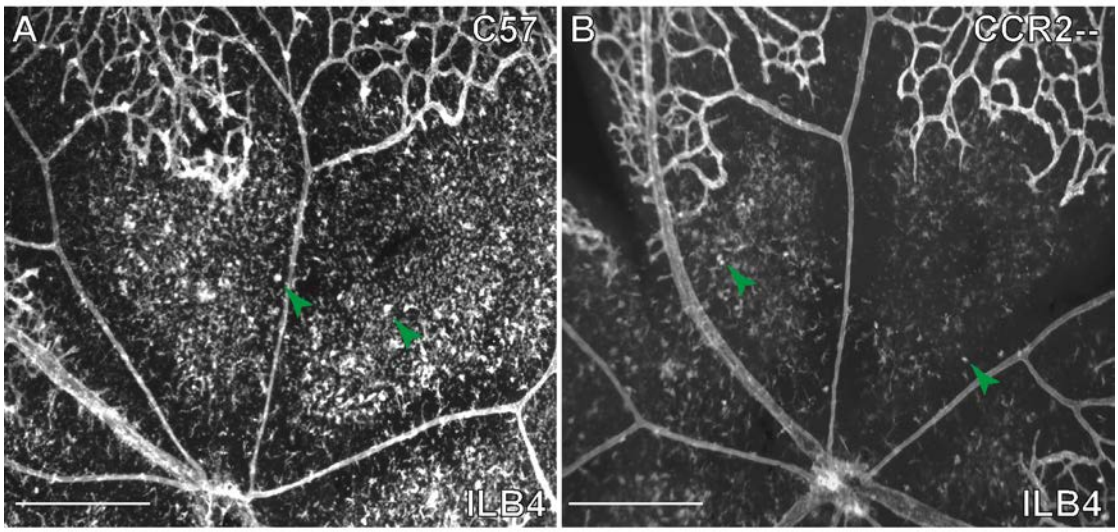

Figure 3.16 – CCR2-/- mice demonstrate a reduction in lectin stained cells in the central avascular area in the LPS treatment group. *Retinal wholemounts from P14 CCR2$^{-/-}$ mice after OIR in the LPS treatment group stained with isolectin B4. In C57 mice (A) an influx of round boded lectin positive cells (green arrows) is seen in the avascular area. In CCR2$^{-/-}$ mice (B) this population is almost completely absent in the central avascular area. Scale bar = 50µm*

Having determined that the moncocyte/macrophage recruitment had been reduced, the effect of CCR2$^{-/-}$ depletion on both PBS control and LPS treatment groups was studied **(Figure 3.17**).

Mouse pups in the PBS control group demonstrated a similar hypoxic phenotype to that seen in PBS control groups in previous experiments using C57BL6 and LysMCreDTA mice, characterised by tortuous retinal arteries (**Figure 3.17I**) and central avascular areas (**Figure 3.17C**) which were positive for EF5 hypoxia staining (**Figure 3.17E**). Mouse pups in the LPS treatment group responded in a similar way to the LPS treatment groups of C57BL6 and LysMCreDTA mice with straightening of the

retinal arteries **(Figure 3.17D**) and smaller, less intense EF5 hypoxia staining (**Figure 3.17F**). When compared retinal arteries were found to be significantly straighter in the LPS treatment group, as calculated by both tortuosity index and integrated curvature ($p<0.05$) (**Figure 3.17N,O**). The LPS treatment group was found to have a greater avascular area with reduced EF5 hypoxia measures, however only the EF5 hypoxic intensity measure was found to be statistically significant ($p<0.05$). (**Table 3.8**).

Table 3.8: CCR2-/- P14 OIR PBS vs LPS

	TreatmentGroup	N	Mean	Std. Deviation	Std. Error Mean
AvascularArea	PBS	3	242220	46191.44	26668.64
	LPS	4	280338	24137.45	12068.73
VesselTortuosityIndex	PBS	3	1.0698	.02	.01
	LPS	4	1.0214	.01	.00
VesselIntegratedCurvature	PBS	3	1.0712	.09	.05
	LPS	4	.3271	.06	.03
EF5HypoxicArea	PBS	3	75105.3	33604.53	19401.59
	LPS	4	59030.0	20513.94	10256.97
EF5HypoxicIntensity	PBS	3	195.030	14.77	8.53
	LPS	4	144.578	8.86	4.43
EF5HypoxicDensity	PBS	3	1.44E+7	5725406.29	3305564.87
	LPS	4	8.49E+6	2837232.64	1418616.32

	Levene's Test for Equality of Variances		t-test for Equality of Means						
								95% Confidence Interval of the Difference	
	F	Sig.	t	df	Sig. (2-tailed)	Mean Difference	Std. Error Difference	Lower	Upper
AvascularArea	2.64	.17	-1.44	5.00	.21	-38117.42	26490.89	-106214.42	29979.59
VesselTortuosityIndex	4.74	.08	4.04	5.00	.01	.05	.01	.02	.08
VesselIntegratedCurvature	.58	.48	12.81	5.00	.00	.74	.06	.59	.89
EF5HypoxicArea	.44	.54	.79	5.00	.46	16075.33	20267.77	-36024.64	68175.31
EF5HypoxicIntensity	1.36	.30	5.70	5.00	.00	50.45	8.85	27.69	73.21
EF5HypoxicDensity	2.23	.20	1.83	5.00	.13	5932328.67	3235149.54	-2383887.97	14248545.30

Table 3.8 – Statistical Comparisons of P14 CCR2$^{-/-}$ OIR PBS vs LPS treatment groups

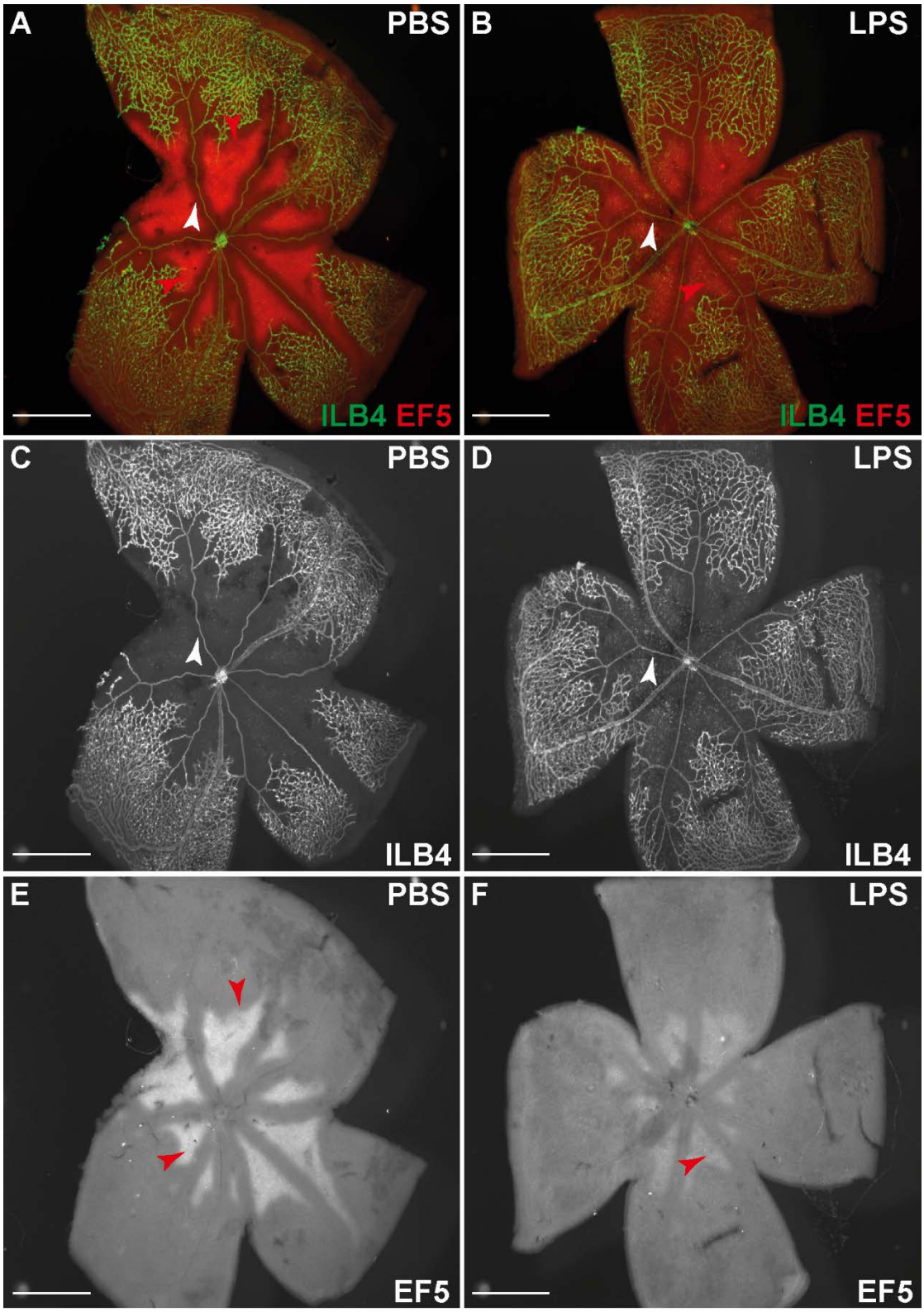

Figure 3.17(a) – Intraperitoneal injection of LPS at P12 after hyperoxia leads to reduced vessel tortuosity in CCR2-/- mouse pups at P14 in OIR *Retinal wholemounts from P14 CCR2$^{-/-}$ mice after OIR stained with isolectin B4 and EF5 hypoxia stain. Mouse pups in the PBS group (A,C,E) demonstrated central avascular areas which were positive for EF5 hypoxia stain (red arrows). Mouse pups in the LPS treatment group (B,D,F) appeared to similiar areas of EF5 hypoxia staining with reduced intensity of stain (F) and straighter retinal arteries (white arrows) (F). Scale bar = 100µm*

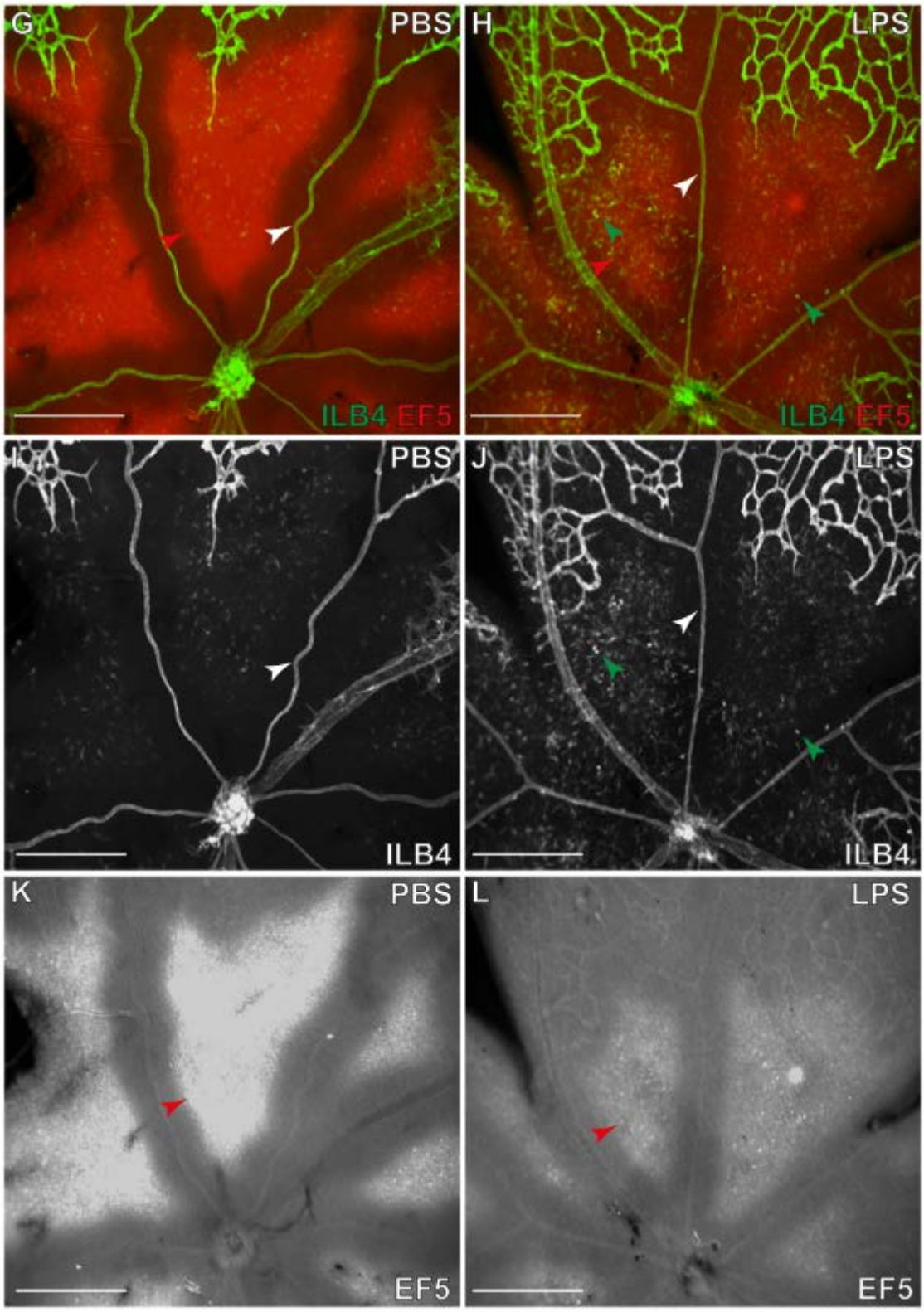

Figure 3.17(b) – Intraperitoneal injection of LPS at P12 after hyperoxia leads to reduced vessel tortuosity in CCR2$^{-/-}$ mouse pups at P14 in OIR *Higher magnification images demonstrate increased retinal artery tortuosity (white arrows) in the PBS control group (I) compared to the LPS treatment group (J). In the LPS treatment group the occasional round bodied lectin positive cell (green arrows) is seen in the avascular area (J). Scale bar = 50µm.*

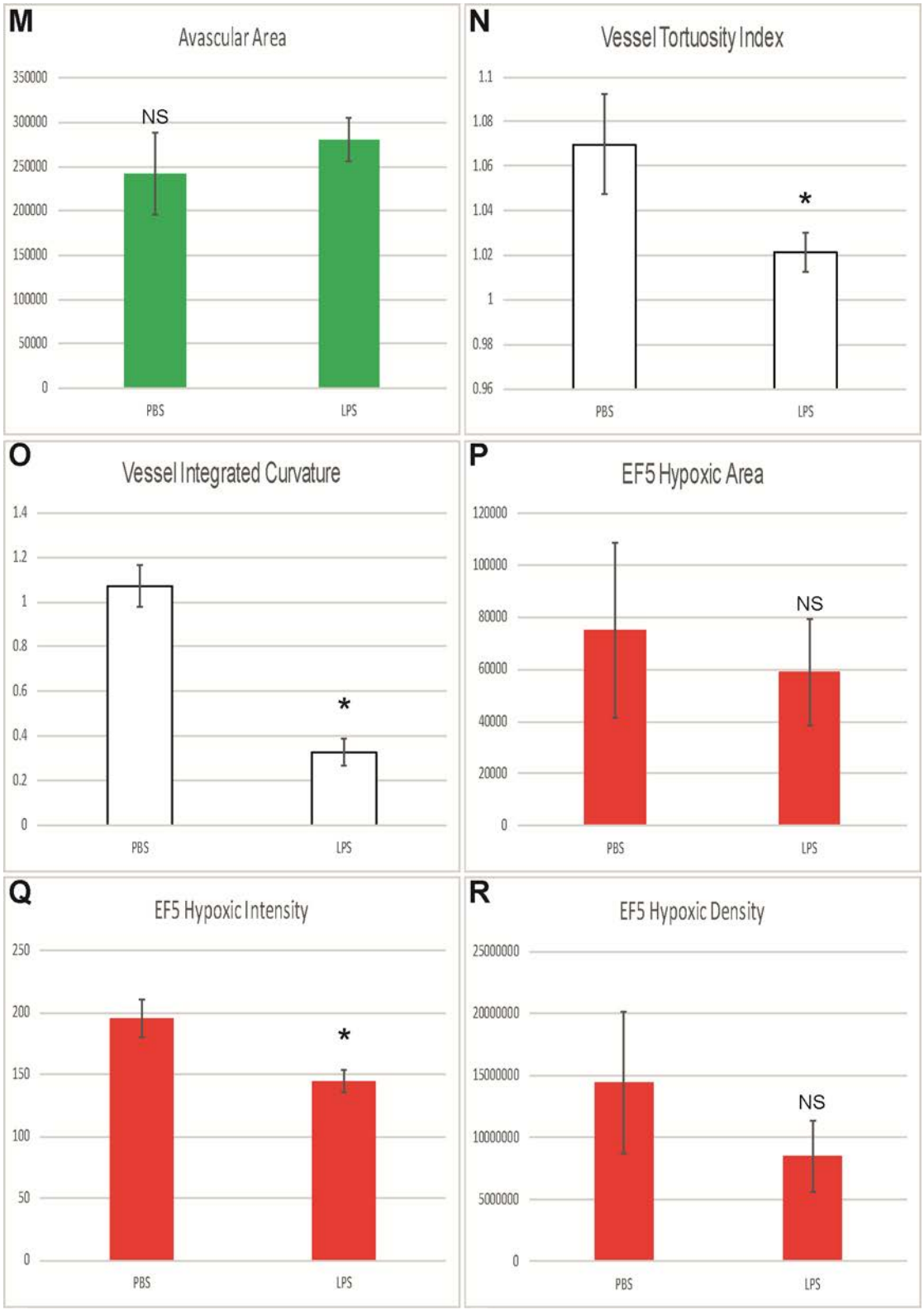

Figure 3.17(c) – Intraperitoneal injection of LPS at P12 after hyperoxia leads to reduced vessel tortuosity in CCR2-/- mouse pups at P14 in OIR *Pups in the LPS treatment group demonstrated a significant reduction in arterial tortuosity, as calculated by vessel tortuosity and integrated tortuosity (N,O). A significant reduction in EF5 hypoxic intensity was also seen in the LPS group(Q). Differences in avascular area and EF5 hypoxic area were not shown to be statistically significant (M,P,R).(n= PBS 3 vs LPS 4; error bar = standard deviation; NS=non-significant, * = <0.05)*

In CCL2$^{+/-}$ mice treated with LPS, the typical influx of lectin positive cells in the avascular area typically seen in C57BL6 mice (**Figure 3.18A**), appeared reduced. This was demonstrated by a reduction in lectin stained cells in the central avascular area (**Figure 3.18B**). In CCL2$^{-/-}$ mice treated with LPS, this population is almost absent with the exception of a few cells **(Figure 3.18C)**.

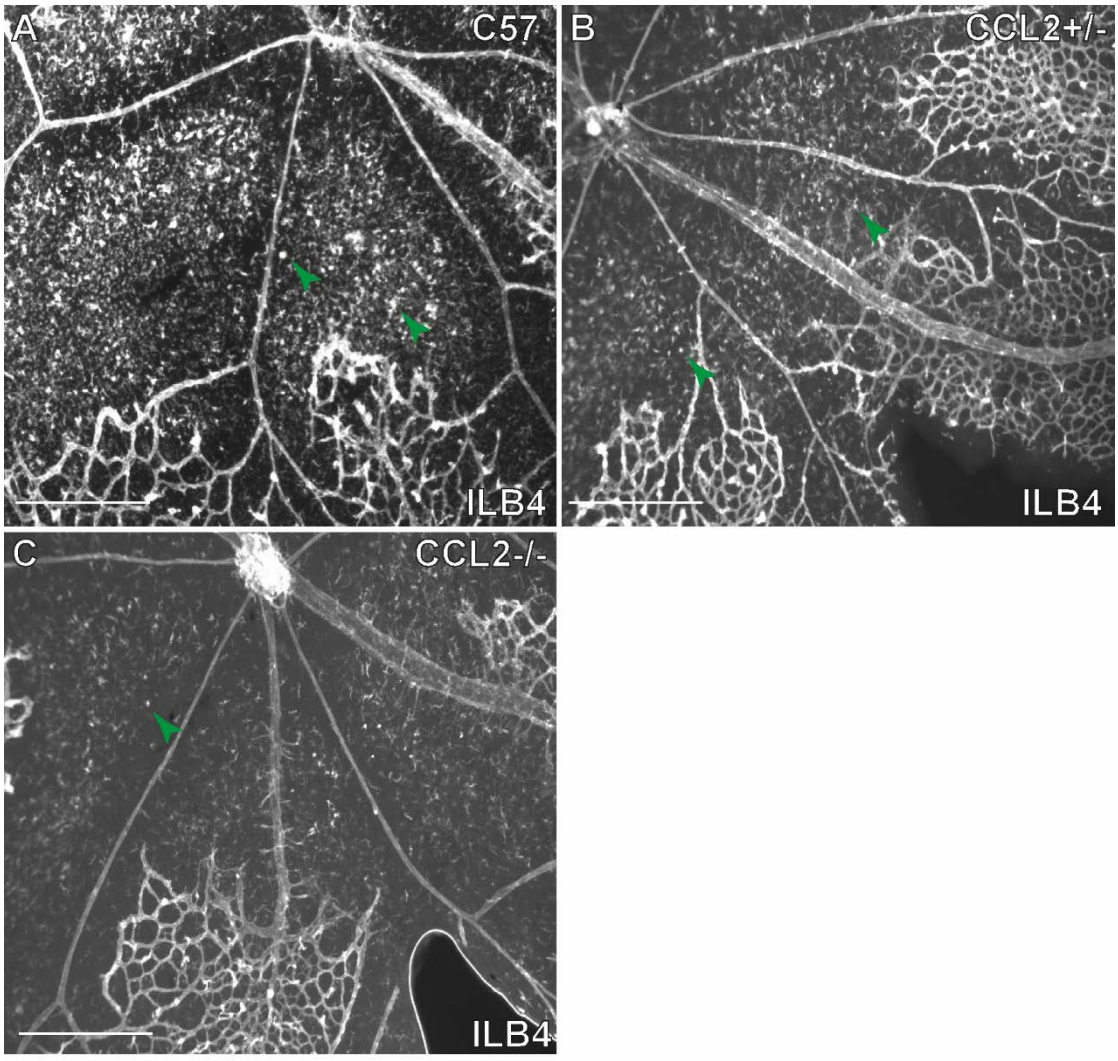

Figure 3.18 – CCL2-/- mice demonstrate a reduction in lectin stained cells in the central avascular area in the LPS treatment group. *Retinal wholemounts from P14 CCRL$^{-/-}$ mice after OIR in the LPS treatment group stained with isolectin B4. In C57 mice (A) an influx of round boded lectin positive cells (green arrows) is seen in the avascular area. In CCL2$^{+/-}$ mice (B) this population is reduced and in CCL2$^{-/-}$ mice (C) is almost completely absent in the central avascular area. Scale bar = 50µm*

Having determined that the moncocyte/macrophage recruitment had been reduced, the effect of $CCL^{-/-}$ depletion on both PBS control and LPS treatment groups was studied **(Figure 3.19**).

Mouse pups in the PBS control group demonstrated a similar hypoxic phenotype to that seen in PBS control groups in previous experiments using C57BL6 and $CCR2^{-/-}$ mice, characterised by tortuous retinal arteries (**Figure 3.19I**) and central avascular areas (**Figure 3.19C**) which were positive for EF5 hypoxia staining (**Figure 3.19E**). Mouse pups in the LPS treatment group responded in a similar way to the LPS treatment groups of C57BL6 and $CCR2^{-/-}$ mice with straightening of the retinal arteries **(Figure 3.19D**) and smaller, less intense EF5 hypoxia staining (**Figure 3.19F**). When compared retinal arteries were found to be significantly straighter in the LPS treatment group, as calculated by both tortuosity index and integrated curvature ($p<0.05$) (**Figure 3.19N,O**). The LPS treatment group was again found to have a greater avascular area with reduced EF5 hypoxia measures, however these differences were not statistically significant. (**Table 3.9**).

Table 3.9: CCL2-/- P14 OIR PBS vs LPS

	TreatmentGroup	N	Mean	Std. Deviation	Std. Error Mean
AvascularArea	PBS	3	196525	12799.51	7389.80
	LPS	2	203268	11136.93	7875.00
VesselTortuosityIndex	PBS	3	1.05	.00	.00
	LPS	2	1.02	.00	.00
VesselIntegratedCurvature	PBS	3	1.19	.17	.10
	LPS	2	.53	.01	.01
EF5HypoxicArea	PBS	3	56497.3	9818.62	5668.78
	LPS	2	43024.5	18436.40	13036.50
EF5HypoxicIntensity	PBS	3	146.66	16.75	9.67
	LPS	2	129.08	2.63	1.86
EF5HypoxicDensity	PBS	3	8.19E+6	878879.71	507421.43
	LPS	2	5.58E+6	2492970.01	1762796.00

	Levene's Test for Equality of Variances		t-test for Equality of Means						
								95% Confidence Interval of the Difference	
	F	Sig.	t	df	Sig. (2-tailed)	Mean Difference	Std. Error Difference	Lower	Upper
AvascularArea	.294	.625	-.602	3	.590	-6742.66667	11201.26405	-42390.08805	28904.75472
VesselTortuosityIndex	2.098	.243	8.089	3	.004	.03054	.00378	.01853	.04256
VesselIntegratedCurvature	4.114	.136	5.096	3	.015	.65892	.12929	.24744	1.07039
EF5HypoxicArea	4.846	.115	1.108	3	.349	13472.83333	12164.51325	-25240.07691	52185.74357
EF5HypoxicIntensity	2.144	.239	1.400	3	.256	17.58533	12.55959	-22.38489	57.55556
EF5HypoxicDensity	13.724	.034	1.780	3	.173	2613933.000	1468158.195	-2058401.62	7286267.623
			1.425	1.169	.364	2613933.000	1834373.531	-14074366.3	19302232.28

Table 3.9 – Statistical Comparisons of P14 CCL2$^{-/-}$ OIR PBS vs LPS treatment groups

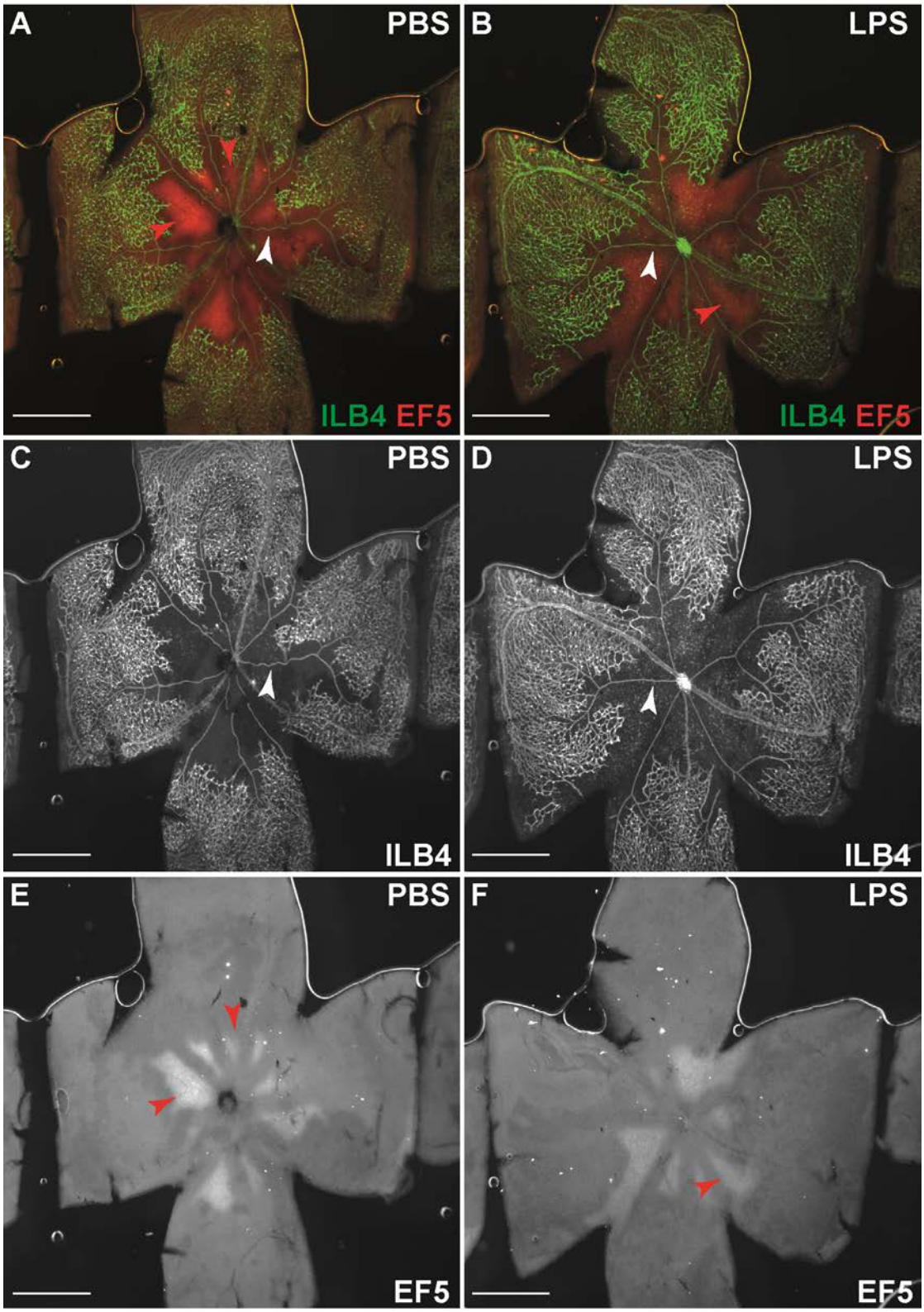

Figure 3.19(a) – Intraperitoneal injection of LPS at P12 after hyperoxia leads to reduced hypoxia in CCL2-/- mouse pups at P14 in OIR *Retinal wholemounts from P14 CCL2$^{-/-}$ mice after OIR stained with isolectin B4 and EF5 hypoxia stain. Mouse pups in the PBS group (A,C,E) demonstrated central avascular areas which were positive for EF5 hypoxia stain (red arrows). Mouse pups in the LPS treatment group (B,D,F) appeared to have smaller areas of EF5 hypoxia staining with reduced intensity of stain (F) and* straighter retinal arteries (white arrows) (D). *Scale bar = 100µm*

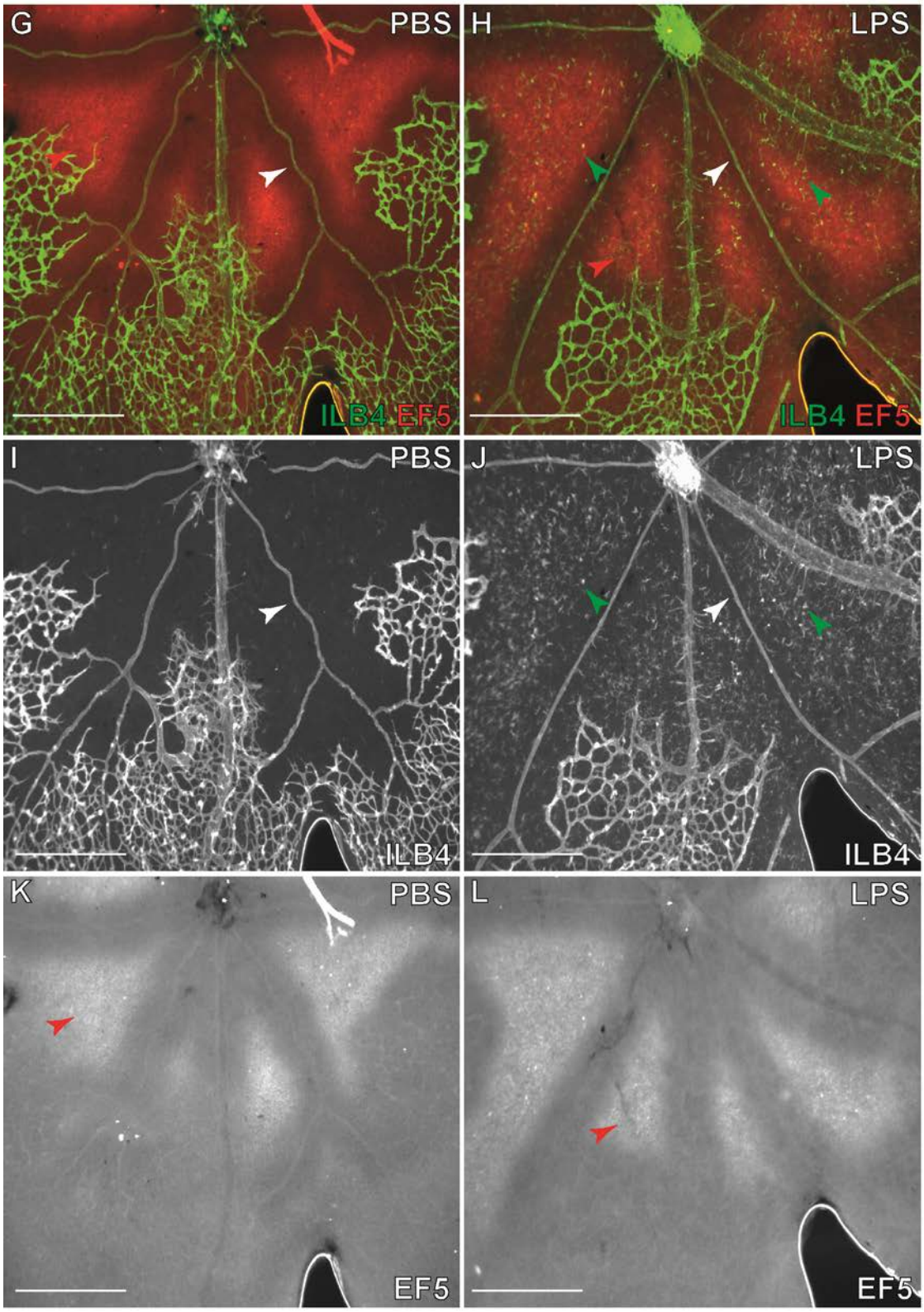

Figure 3.19(b) – Intraperitoneal injection of LPS at P12 after hyperoxia leads to reduced hypoxia in CCL2-/- mouse pups at P14 in OIR *Higher magnification images demonstrate increased retinal artery tortuosity (white arrows) in the PBS control group (I) compared to the LPS treatment group (J) In the LPS treatment group there are still some round bodied lectin positive cells (green arrows) seen in the hypoxic avascular area (red arrows) (J). Scale bar = 50µm.*

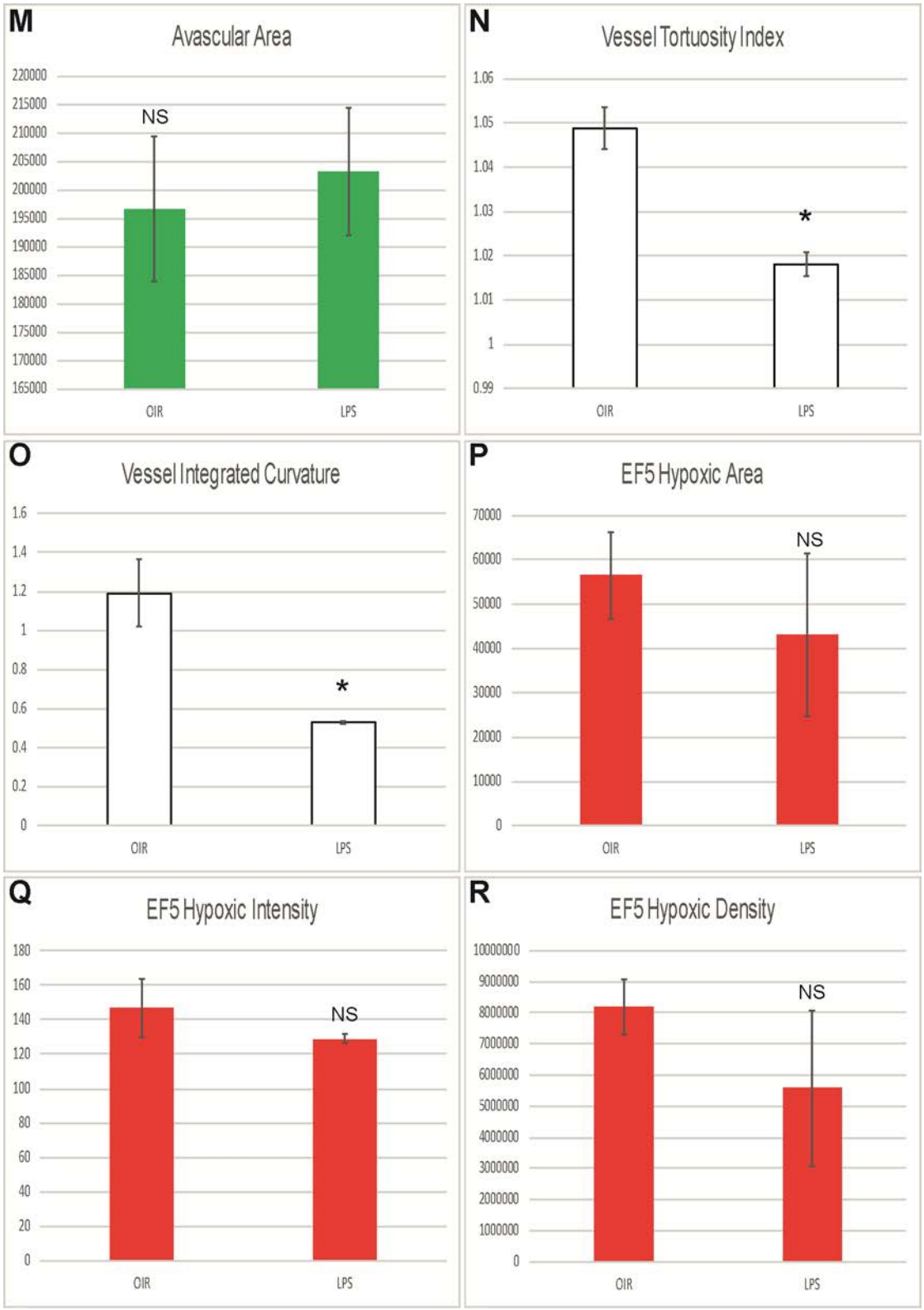

Figure 3.19(c) – Intraperitoneal injection of LPS at P12 after hyperoxia leads to reduced hypoxia in CCL2-/- mouse pups at P14 in OIR *Pups in the LPS treatment group demonstrated a significant reduction in arterial tortuosity, as calculated by vessel tortuosity and integrated tortuosity (N,O). EF5 hypoxia staining measures were lower in the LPS treated group but these differences were not statistically significant. (n= PBS 3 vs LPS 2; error bar = standard deviation; NS=non-significant, * = <0.05)*

These results are similar to the findings from the LysMCreDTA mice experiments and indicate that reducing the number of invading CCL2 positive cells does not affect the reduced vessel tortuosity LPS treatment group phenotype. However once again no significant difference was seen in the EF5 hypoxic area between the two groups. Even though the depletion appeared more successful than in the LysMCreDTa experiments, these experiments were not able to completely eradicate the invading immune cell population, as the occasional round bodied lectin positive cell was still visible.

3.3.3 The effect of depletion of invading CCR2+ cells seen in LPS treated OIR retinas on hypoxia in anti-CRR2 treated mice

As genetic manipulation of the invading neutrophils and monocyte/macrophage population hadn't resulted in complete deletion of the targeted populations or a change in the LPS treatment group phenotype, a therapeutic approach with the use of the MC21 anti CCR2 antibody was attempted.

A litter of C57BL6 mouse pups underwent the same LPS vs PBS OIR protocol previously described and mice were treated with repeated injections of either the MC21 antibody or the IgG2b negative control prior to being culled at P14. Immunohistochemistry was performed on retinal wholemounts to examine hypoxia.

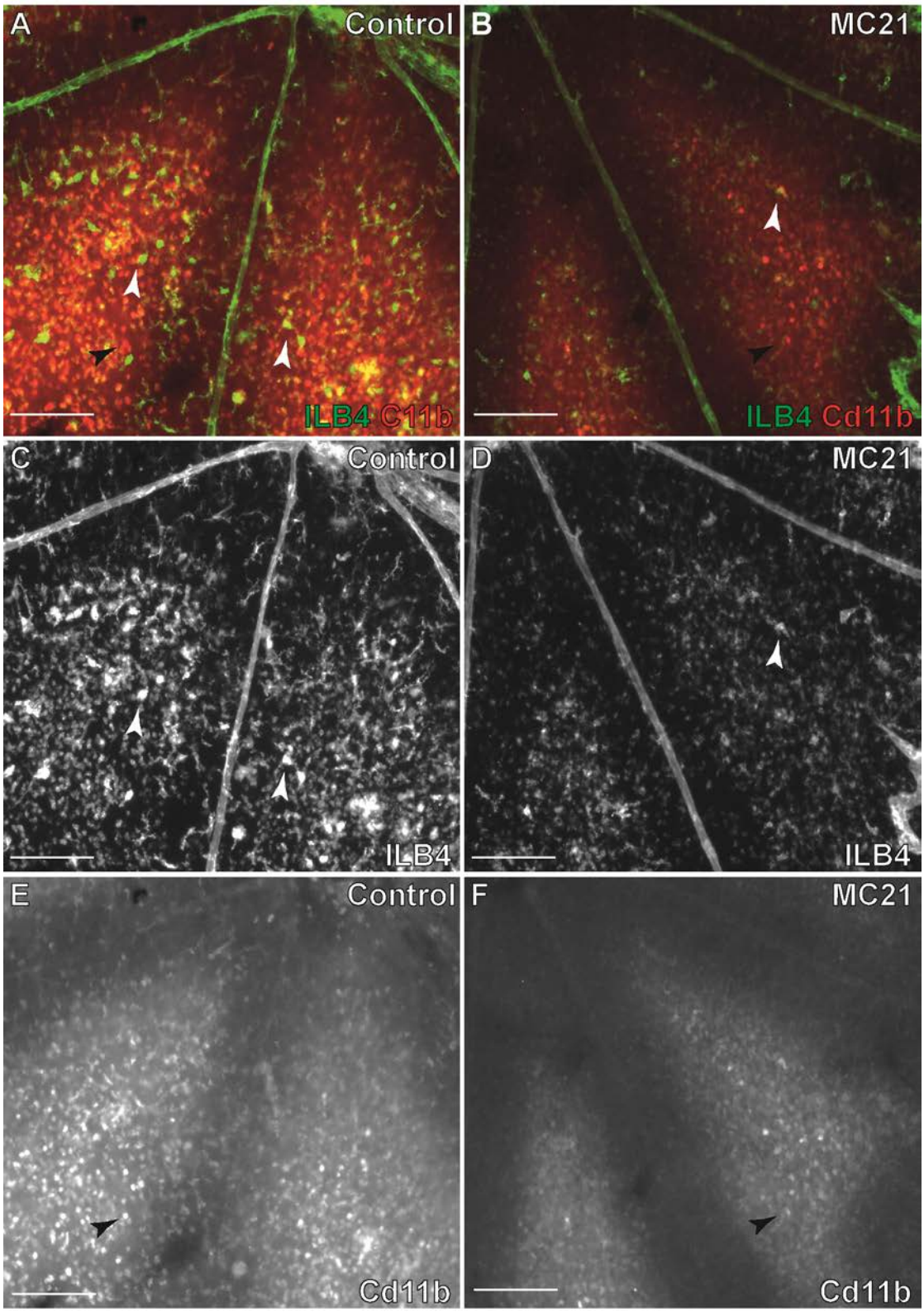

Figure 3.20 – MC21 treated mice demonstrate a reduction in lectin stained cells in the central avascular in the LPS treatment group. *Retinal wholemounts from P14 C57BL6 mice after OIR in the LPS treatment group stained with isolectin B4 and Cd11b. In the control treated group (A,C,E) an influx of round boded lectin positive cells (C) (white arrows) and Cd11b positive cells (E) (black arrows) is seen in the avascular area. In the MC21 treated group (B,D,F) these populations are reduced in the central avascular area (D,F) . Scale bar = 50µm*

In mice from the IgG2b control treated group treated with LPS, the typical influx of round neutrophilic myeloid cells is seen in the central avascular area (**Figure 3.20A**). Whereas in mice from the MC21 treated group treated with LPS, these cells appeared reduced (**Figure 3.20B**), as demonstrated by a reduction in lectin and Cd11b stained cells in the central avascular area (**Figure 3.20D,F**). On examination it would appear that the reduction is not greater than that seen in both the $CCR2^{-/-}$ and $CCL2^{-/-}$ experiments.

Having determined that the CCR2 population had been reduced, the effect of the depletion on the LPS treatment group was studied **(Figure 3.21**). Mice in both the negative control and MC21 treated groups when treated with LPS demonstrated straightening on the retinal arteries (**Figure 3.21I,J**) and central areas of vaso-obliteration which were positive for EF5 hypoxia staining (**Figure 3.21E,F**), suggesting a similar level of hypoxia in the two groups. However, when compared against each other, the MC21 treated group appeared to have significantly larger avascular and EF5 hypoxic areas ($p<0.05$) (**Figure 3.21M,P**), which would suggest that more hypoxia was experienced by the MC21 group. However, the vessel tortuosity was seen to be reduced in the MC21 treated group with integrated curvature reaching statistical significance ($p<0.05$) (**Figure 3.21O**) which would suggest that more hypoxia was experienced by the control group. The other measures of EF5 hypoxia showed no significant difference between the two groups but this may be due to bleed through from the Cd11b stained cells (**Figure 3.21K,L**).

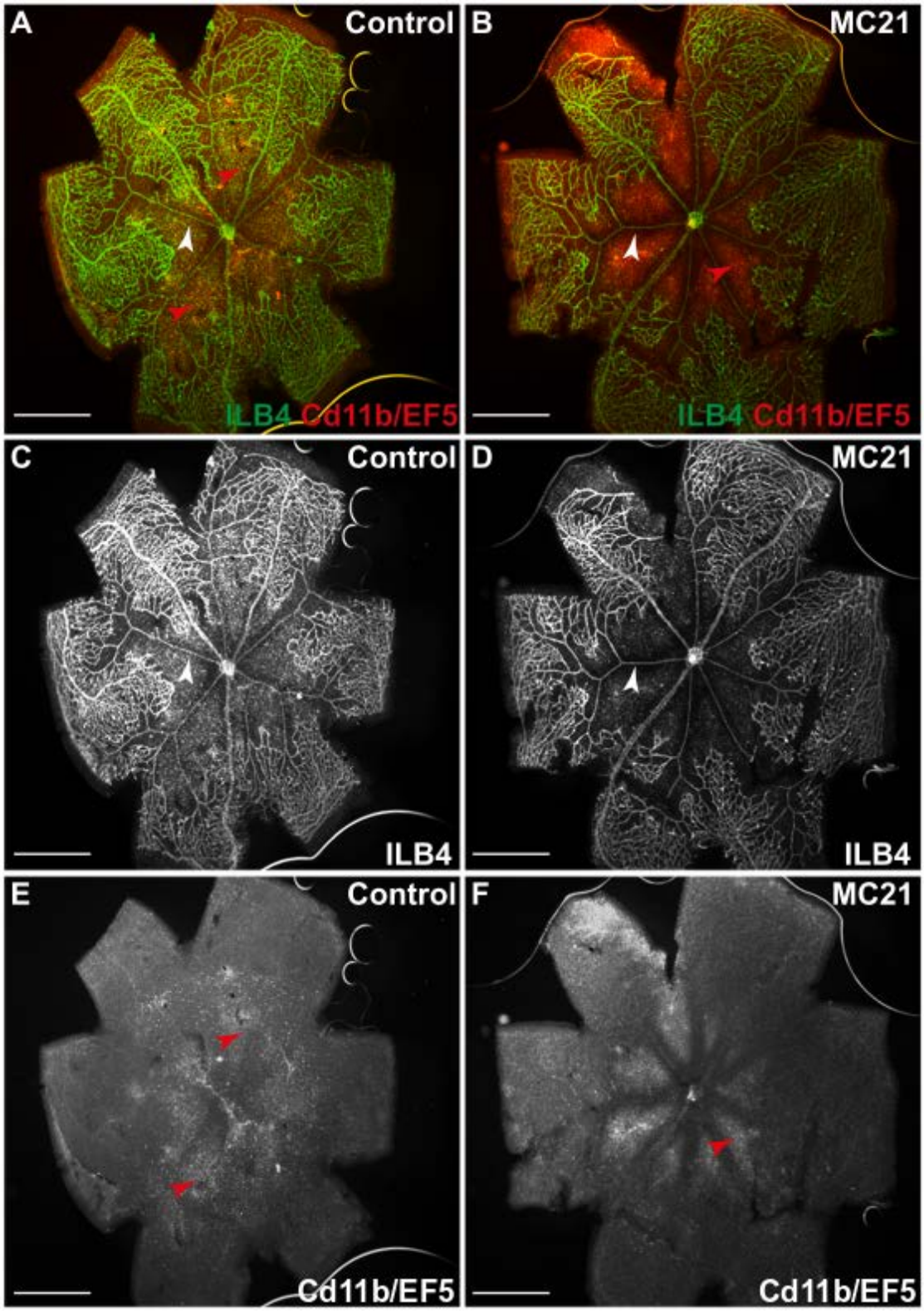

Figure 3.21(a) – Differences in hypoxia are seen at P14 between control and MC21 treated groups injected with LPS at P12. *Retinal wholemounts from P14 C57BL6 mice after OIR stained with isolectin B4, Cd11b and EF5 hypoxia stain. Mouse pups in the both the control treated group (A,C,E) and the MC21 treated group (B,D,F) had similar avascular areas (C,D) that were positive for EF5 hypoxia stain (red arrows) (E,F).Retinal arteries appeared similar in both groups (white arrows). Scale bar = 100µm.*

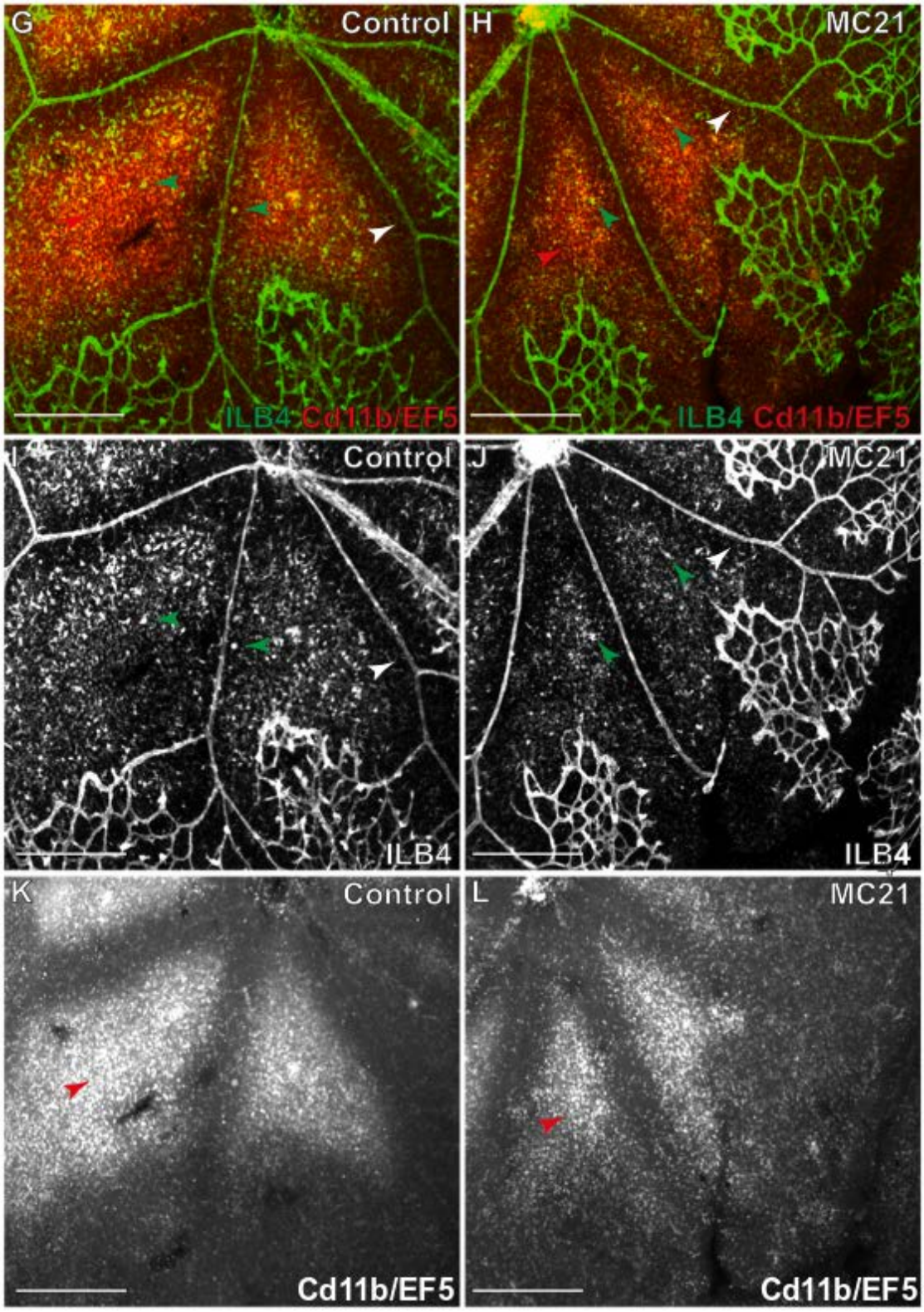

Figure 3.21(b) – Differences in hypoxia are seen at P14 between control and MC21 treated groups injected with LPS at P12. *Higher magnification images demonstrate similar retinal artery tortuosity in both the control treated (I) and MC21 treated (J) groups (white arrows). The control treated group demonstrated an increased number of round lectin positive cells (green arrows) in the avascular area (red arrows) than the MC21 treated group. Scale bar = 50µm.*

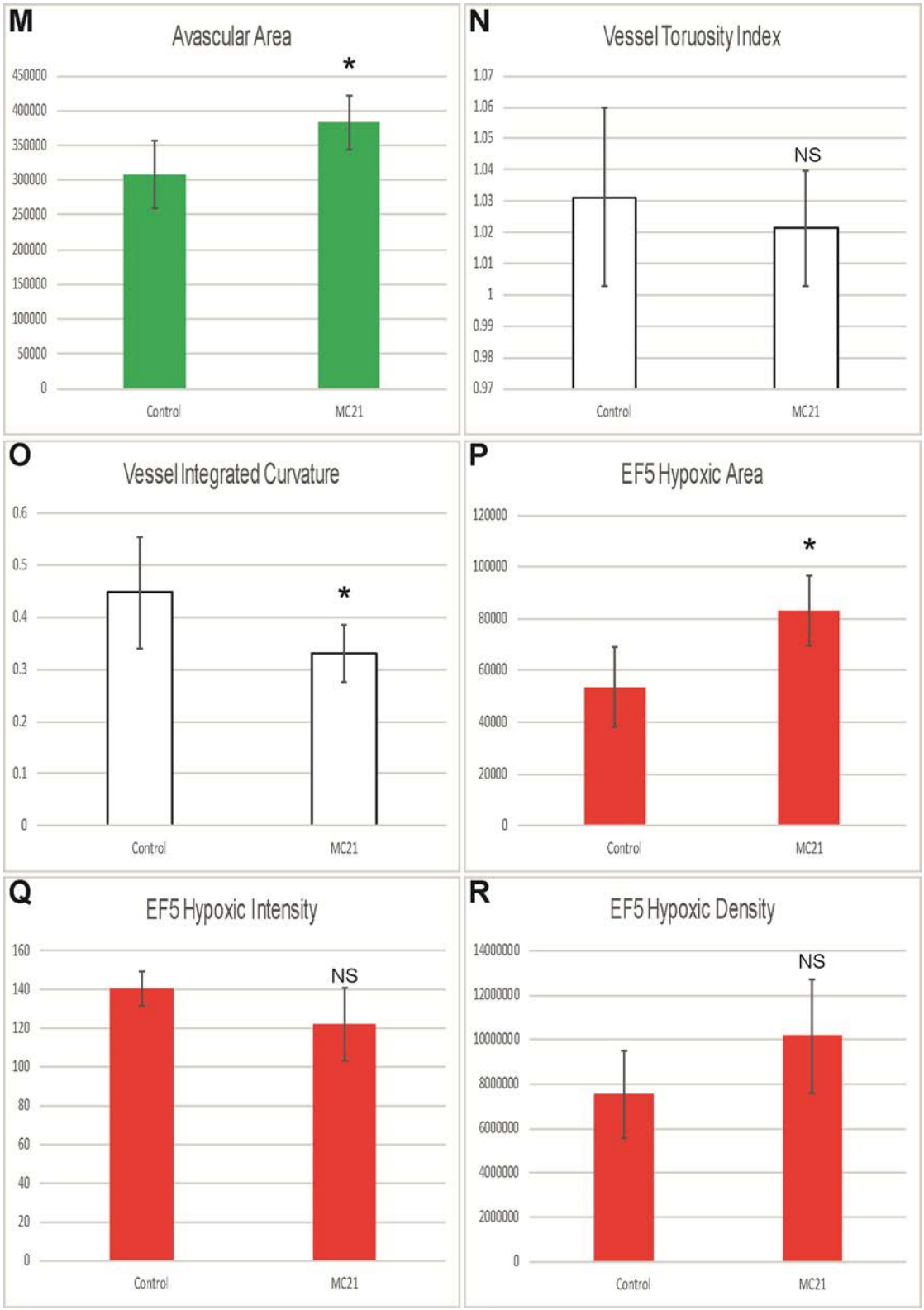

Figure 3.21(c) – Differences in hypoxia are seen at P14 between control and MC21 treated groups injected with LPS at P12. *On comparison the MC21 treated group demonstrated significantly larger avascular (M) and EF5 hypoxic areas (P) while retinal arteries appeared straighter with the difference in integrated curvature being statistically significant. Differences in EF5 hypoxic intensity and density were found to be non-significant. (n= control 6 vs MC21 6; error bar = standard deviation; NS=nonsignificant, *=p<0.05)*

Table 3.10: P14 OIR & LPS: Control vs MC21

	TreatmentGroup	N	Mean	Std. Deviation	Std. Error Mean
AvascularArea	Control	6	307632	48397.90	19758.36
	MC21	6	382644	38098.78	15553.76
VesselTortuosityIndex	Control	6	1.03	.03	.01
	MC21	6	1.02	.02	.01
VesselIntegratedCurvature	Control	6	.45	.11	.04
	MC21	6	.33	.05	.02
EF5HypoxicArea	Control	6	53787.2	15399.73	6286.91
	MC21	6	83097.5	13535.64	5525.90
EF5HypoxicIntensity	Control	6	140.77	8.90	3.63
	MC21	6	121.94	18.82	7.69
EF5HypoxicDensity	Control	6	7.53E+6	1978010.05	807519.22
	MC21	6	1.02E+7	2552591.35	1042091.05

	Levene's Test for Equality of Variances		t-test for Equality of Means						
								95% Confidence Interval of the Difference	
	F	Sig.	t	df	Sig. (2-tailed)	Mean Difference	Std. Error Difference	Lower	Upper
AvascularArea	.849	.378	-2.983	10.000	.014	-75011.67	25145.82	-131040.04	-18983.29
VesselTortuosityIndex	1.313	.279	.714	10.000	.492	.01	.01	-.02	.04
VesselIntegratedCurvature	1.132	.312	2.384	10.000	.038	.12	.05	.01	.23
EF5HypoxicArea	.012	.914	-3.502	10.000	.006	-29310.33	8370.24	-47960.39	-10660.28
EF5HypoxicIntensity	1.521	.246	2.216	10.000	.051	18.83	8.50	-.11	37.78
EF5HypoxicDensity	.278	.609	-1.998	10.000	.074	-2633680.33	1318347.85	-5571142.40	303781.74

Table 3.10 – Statistical Comparisons of P14 OIR & LPS Control vs MC21 treatment groups

Given the mixed results of this experiment, to confirm that the CCR2 population were not responsible for the reduction in hypoxia previously seen in the LPS treated group of C57BL6 mice, PBS control groups and LPS treatment groups were compared in mice treated with MC21 (**Figure 3.22**).

Mouse pups in the control group demonstrated a similar hypoxic phenotype to that seen in PBS control groups in previous experiments using $CCL2^{-/-}$ and $CCR2^{-/-}$ mice, characterised by tortuous retinal arteries (**Figure 3.22I**) and central avascular areas (**Figure 3.22C**) which were positive for EF5 hypoxia staining (**Figure 3.22E**). As described previously, mouse pups in the MC21 treatment group also responded in a similar way to the LPS treatment groups of $CCL2^{-/-}$ and $CCR2^{-/-}$ mice. When compared retinal arteries were found to be significantly straighter in the LPS treatment group, as calculated by both tortuosity index and integrated curvature ($p<0.05$) (**Figure**

3.22N,O). The LPS treatment group was found to have a significantly greater avascular area ($p<0.05$) with reduced EF5 hypoxic intensity and density, however these differences did not reach statistical significance (**Table 3.11**).

Table 3.11: P14 OIR MC21: PBS vs LPS

	TreatmentGroup	N	Mean	Std. Deviation	Std. Error Mean
AvascularArea	PBS	6	327391	25848.23	10552.49
	LPS	6	382644	38098.78	15553.76
VesselTortuosityIndex	PBS	6	1.07	.03	.01
	LPS	6	1.02	.02	.01
VesselIntegratedCurvature	PBS	6	1.02	.19	.08
	LPS	6	.33	.05	.02
EF5HypoxicArea	PBS	6	96267.2	11127.69	4542.86
	LPS	6	83097.5	13535.64	5525.90
EF5HypoxicIntensity	PBS	6	127.59	19.53	7.97
	LPS	6	121.94	18.82	7.69
EF5HypoxicDensity	PBS	6	1.22E+7	1551895.59	633558.72
	LPS	6	1.02E+7	2552591.35	1042091.05

	Levene's Test for Equality of Variances		t-test for Equality of Means						
								95% Confidence Interval of the Difference	
	F	Sig.	t	df	Sig. (2-tailed)	Mean Difference	Std. Error Difference	Lower	Upper
AvascularArea	.350	.567	-2.940	10.000	.015	-55252.17	18795.60	-97131.38	-13372.96
VesselTortuosityIndex	.510	.491	3.469	10.000	.006	.04	.01	.02	.07
VesselIntegratedCurvature	2.202	.169	8.624	10.000	.000	.69	.08	.51	.87
EF5HypoxicArea	.562	.471	1.841	10.000	.095	13169.67	7153.54	-2769.42	29108.75
EF5HypoxicIntensity	.015	.904	.511	10.000	.621	5.65	11.07	-19.02	30.32
EF5HypoxicDensity	.912	.362	1.663	10.000	.127	2028503.33	1219569.77	-688867.45	4745874.11

Table 3.11 – Statistical Comparisons of P14 OIR & MC21 PBS vs LPS treatment groups

These results are similar to the findings from previous experiments aimed at repressing the invading neutrophil and monocyte/macrophage populations. In summary, they all indicate that reducing the number of these invading cells does not affect the reduced vessel tortuosity LPS treatment group phenotype. However there was no significant difference seen in the EF5 hypoxic area between the PBS and LPS treated groups. As the LPS phenotype seen in these experiments is not identical to that seen in C57Bl6 mice it would suggest that the influx of invading cells alone isn't responsible for the reduced hypoxia seen in LPS treated mice. LPS may exert its hypoxia reducing effects

via another mechanism other than neutrophil and monocyte/macrophage invasion into the hypoxic retina. However, despite multiple attempts complete depletion could not be achieved.

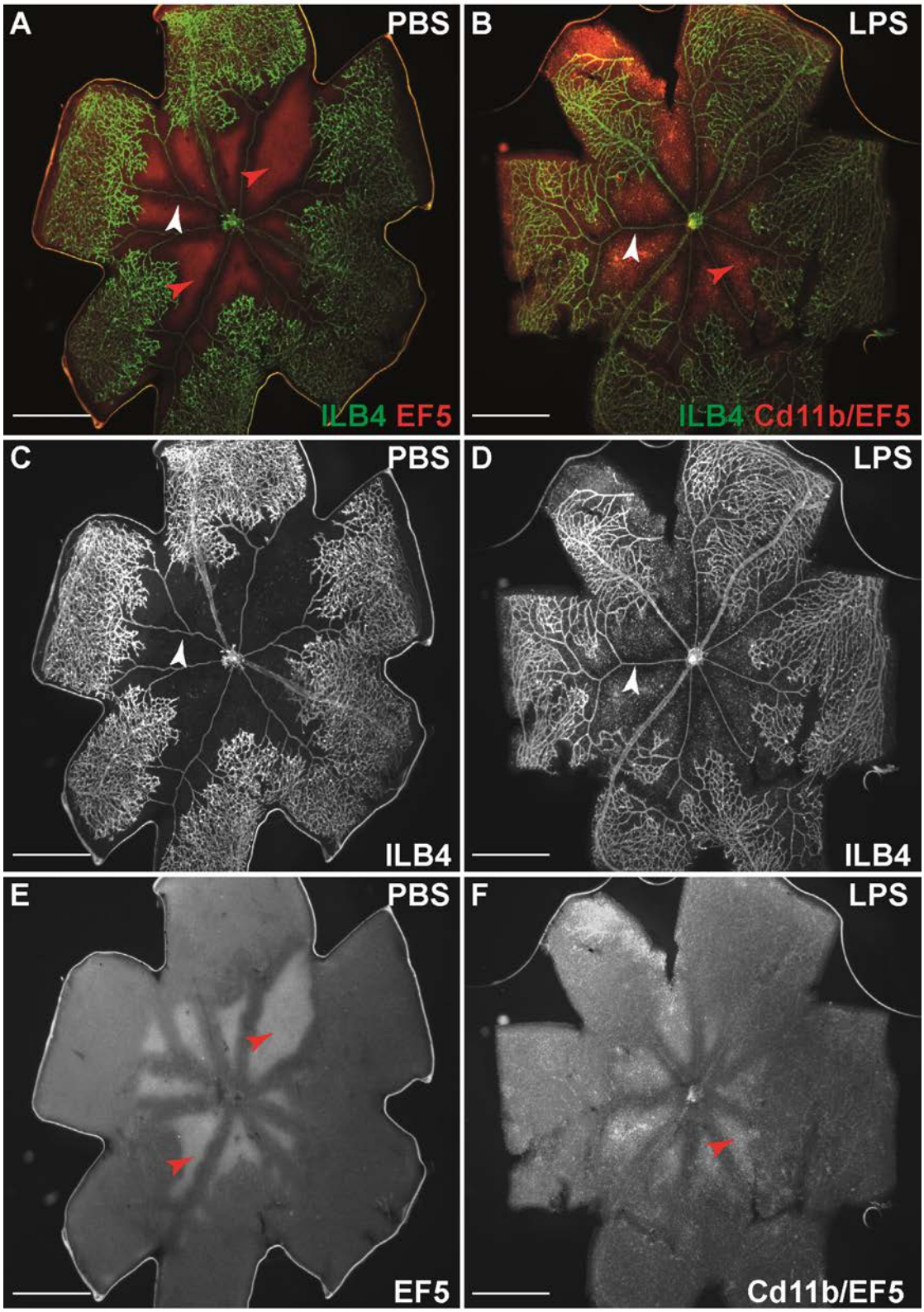

Figure 3.22(a) – Intraperitoneal injection of LPS at P12 after hyperoxia leads to reduced vessel tortuosity in MC21 treated mouse pups at P14 in OIR *Retinal wholemounts from P14 C57BL6 mice after OIR stained with isolectin B4, Cd11b and EF5 hypoxia stain. Mouse pups in the PBS control group (A,C,E) demonstrated central avascular areas which were positive for EF5 hypoxia stain (red arrows.) Mouse pups in the LPS treatment group (B,D,F) appeared to have similar areas of EF5 hypoxia staining with similair intensity of stain (F). Retinal arteries (white arrows) appear straighter in the LPS treatment group (D). Scale bar = 100µm*

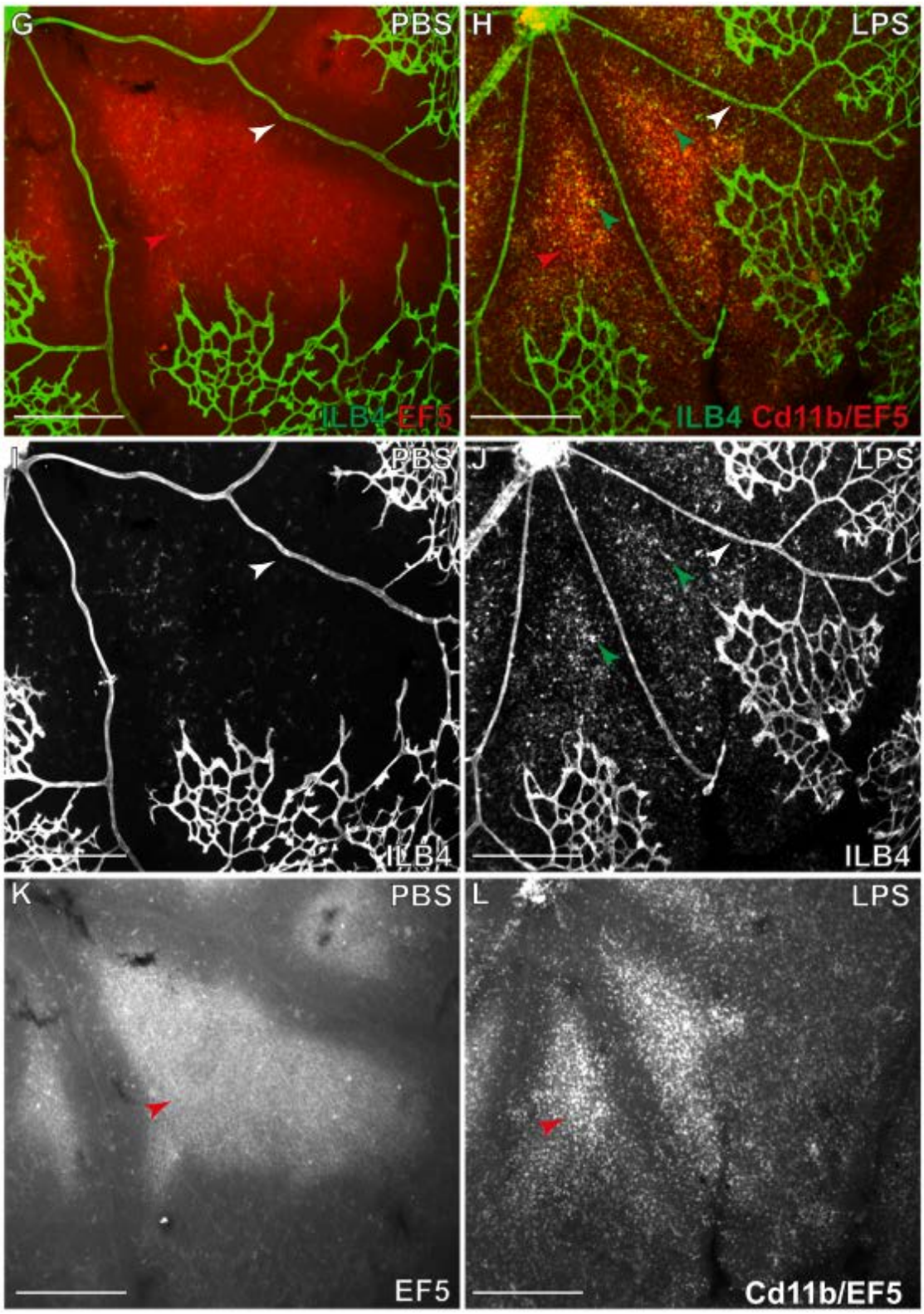

Figure 3.22(b) – Intraperitoneal injection of LPS at P12 after hyperoxia leads to reduced vessel tortuosity in MC21 treated mouse pups at P14 in OIR *Higher magnification images demonstrate increased retinal artery tortuosity (white arrows) in the PBS control group (I) compared to the LPS treatment group (J) In the LPS treatment group there are still some round bodied lectin positive cells (green arrows) seen in the hypoxic avascular area (red arrows) (J). Scale bar = 50µm*

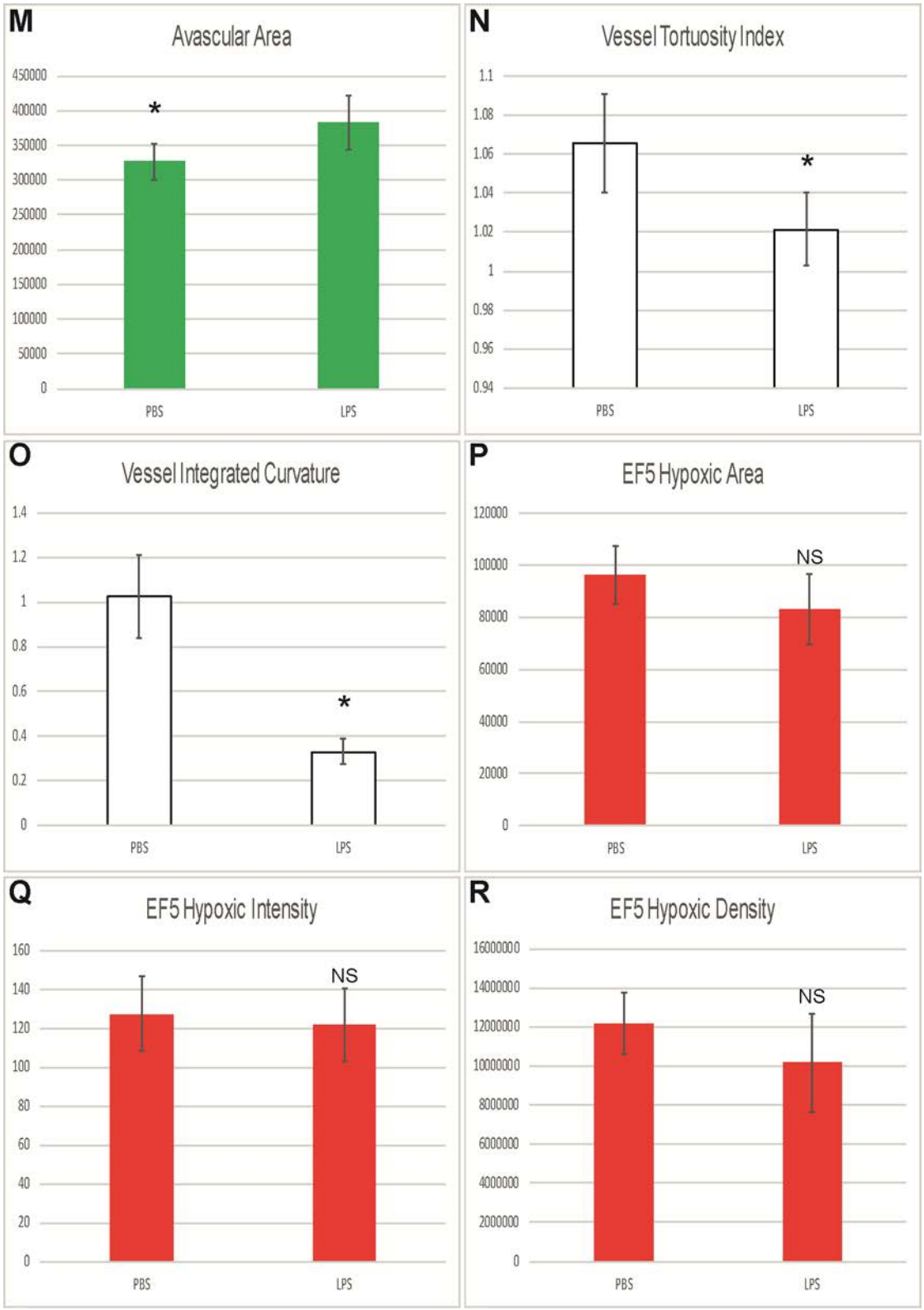

Figure 3.22(c) – Intraperitoneal injection of LPS at P12 after hyperoxia leads to reduced hypoxia in MC21 treated mouse pups at P14 in OIR *Pups in the LPS treatment group demonstrated a significant reduction in arterial tortuosity, as calculated by vessel tortuosity and integrated tortuosity (N,O). EF5 hypoxia staining measures were lower in the LPS treated group but these differences were not statistically significant. Avascular area was found to be significantly larger in the LPS treated group. (n= PBS 6 vs LPS 6; error bar = standard deviation; NS=non-significant, * = <0.05)*

3.4 Systemic LPS injection modulates retinal hypoxia and metabolism through cytokine signalling

As a reduction in the invading myeloid population did not result in a change in the retinal vessel tortuosity it is possible that cytokines released into the retina as a result of LPS stimulation of TLR4 are responsible for the change in retinal oxygen metabolism.

The exact mechanisms of metabolic control in the retina are very complex and involve many different factors, systems and pathways. Previous work using qPCR to measure levels of mRNA of individual genes can only reveal isolated information. To try and understand the effect LPS is having on the retinas in mouse pups undergoing OIR the retina needed to be looked at a whole.

By using RNA sequencing to compare the differences in gene expression between the PBS control and LPS treatment groups it was possible to find particular genes or pathways that were up- or down-regulated and may have been responsible for the reduction in hypoxia. The sequencing could also highlight certain cytokines or signals that were upregulated as a result of TLR4 stimulation by LPS. Suitable candidates could then be injected into pups at P12 to see if a similar reduction in hypoxia is possible.

C57BL6 mouse pups were separated into 3 groups for comparison; a control group of P14 age matched controls, a group with PBS injected intraperitoneally at P12 after being exposed to 5 days of hyperoxia (75% O2) between P7-12 and a group with LPS injected intraperitoneally at P12 after being exposed to 5 days of hyperoxia (75% O2) between P7-12. Pups were culled at P14 and retinas were dissected into central and peripheral sections for comparison. RNA was then isolated from the digested retinas and sent for sequencing.

3.4.1 Systemic LPS injection as a modulator of retinal hypoxia.

In earlier experiments the LPS treatment group demonstrated signs in keeping with reduced hypoxia at P14 after OIR, such as reduced EF5 hypoxia staining and straight retinal arteries. It was hypothesised that this reduction in hypoxia was the result of a decrease in oxygen demand caused by the LPS injection.

Genes known to be up or down-regulated in hypoxia were examined to see if there were any differences in the expression between central and peripheral retina and between groups (**Figure 3.23**).

All hypoxic markers examined, with the exception of Hif1a, were up-regulated in both retinas undergoing OIR when compared to the P14 age match control. In both OIR retinas upregulation of hypoxic markers was seen in the central retina when compared to the peripheral retina and this correlates to the phenotype that is seen on immunohistochemical staining. LPS treatment appeared to reduce the expression of most hypoxia genes (Adm, Angpt2, VegfA, VegfB, Cdkna1, Igfbp3, Bnip3) in the central retina with the exception of Hif1a, Mt1 and Hmox1 which were all increased. However, when these differences are analysed as fold changes, with the exception of Angpt2 and Igfbp3 (whose expression is reduced by 52-56%), they are relatively small changes. Surprisingly there was only a 5% difference in VEGFA expression in the central retina of the LPS injected mouse compared with the PBS injected.

These findings suggest that LPS treatment at P12 leads to a small reduction in the expression of hypoxia genes in the retina of mice undergoing OIR.

	Hypoxia Related Genes	P14c Central	P14c Peripheral	LPS Central	LPS Peripheral	OIR Central	OIR Peripheral	P14c total	LPS total	OIR total	LPS central/ OIR central
Adm	adrenomedullin	14.6	24.1	198.0	105.5	309.3	85.3	38.7	303.5	394.6	0.64
Angpt2	angiopoietin 2	161.8	192.2	170.2	235.6	301.4	275.1	354.0	405.8	576.5	0.56
Vegfa	vascular endothelial growth factor A	5582.6	4651.0	11535.7	8369.5	12090.9	8411.9	10233.7	19905.2	20502.9	0.95
Vegfb	vascular endothelial growth factor B	653.8	671.1	667.3	699.0	754.9	654.4	1324.9	1366.3	1409.3	0.88
Hif1a	hypoxia inducible factor 1, alpha subunit	18549.3	19283.9	18351.6	18218.8	16972.2	17410.1	37833.2	36570.4	34382.3	1.08
Cdkn1a	p21 protein (Cdc42/Rac)-activated kinase	128.1	172.6	239.8	168.0	313.0	220.0	300.7	407.8	533.0	0.77
Igfbp3	insulin-like growth factor binding protei	127.6	177.1	451.8	384.3	861.7	329.6	304.8	836.1	1191.3	0.52
Mt1	metallothionein 1	562.7	472.5	2906.2	2174.8	1683.9	830.4	1035.2	5081.1	2514.3	1.73
Hmox1	heme oxygenase 1	58.1	42.0	237.8	157.7	213.6	171.6	100.1	395.5	385.2	1.11
Bnip3	BCL2/adenovirus E1B interacting protein	2414.6	2420.3	4229.4	3047.4	5738.8	2963.2	4834.9	7276.8	8702.0	0.74
	Metabolism Related Genes										
Pfkfb1	6-phosphofructo-2-kinase/fructose-2,6-b	43.9	24.0	34.7	30.4	38.1	51.7	67.9	65.0	89.8	0.91
Pfkfb3	6-phosphofructo-2-kinase/fructose-2,6-bi	987.1	937.0	1478.8	1303.2	1303.3	1077.2	1924.0	2782.0	2380.5	1.13
Pkm	pyruvate kinase, muscle	53491.6	50358.4	60077.5	55164.9	68316.6	53396.2	103850.0	115242.4	121712.8	0.88
Hk1	Hexokinase1	16043.8	17056.9	22492.3	18715.1	19489.1	16591.0	33100.7	41207.3	36080.0	1.15
Gpi1	glucose phosphate isomerase 1	20625.9	20125.5	26195.7	23304.5	29388.9	22139.9	40751.4	49500.2	51528.8	0.89
Pfkp	phosphofructokinase, platelet	8699.5	7653.9	15648.5	11586.3	15904.3	10669.9	16353.3	27234.8	26574.2	0.98
Tpi1	triosephosphate isomerase 1	11463.8	11603.5	15886.3	12778.5	18786.5	11801.3	23067.3	28664.9	30587.8	0.85
Pgam1	phosphoglycerate mutase 1	14253.4	13745.1	16346.7	14907.1	20057.1	14154.0	27998.5	31253.9	34211.1	0.82
Pgk1	phosphoglycerate kinase 1	10955.4	10420.6	13137.0	11294.8	15858.0	10860.6	21376.0	24431.8	26718.7	0.83
Hk2	hexokinase2	2901.1	1842.7	4162.4	2613.7	4150.1	2121.1	4743.7	6776.0	6271.2	1.00
Pdk1	pyruvate dehydrogenase kinase, isoenzy	1397.7	1376.1	2086.0	1892.2	2460.8	1618.4	2773.8	3978.2	4079.1	0.85
	Inflammation & Cytokine Related Genes										
Ccl6	chemokine (C-C motif) ligand 6	8.9	7.0	66.1	71.9	14.0	4.6	15.9	138.0	18.6	4.72
Ccl5	chemokine (C-C motif) ligand 5	1.1	3.0	114.2	137.1	8.9	1.1	4.1	251.3	10.0	12.89
Il1b	interleukin 1 beta	2.2	2.0	91.2	103.5	1.3	2.3	4.2	194.7	3.6	72.06
Cx3cr1	chemokine (C-X3-C motif) receptor 1	167.9	202.8	318.8	454.8	241.3	202.4	370.8	773.6	443.8	1.32
Cd14	CD14 antigen	9.0	6.0	38.8	30.3	22.8	12.6	15.0	69.1	35.4	1.70
Aif1	(Iba1) allograft inflammatory factor 1	15.7	23.0	57.6	88.6	22.8	17.2	38.7	146.2	40.0	2.53
Csf2rb2	colony stimulating factor 2 receptor, beta	59.6	51.9	183.4	153.9	60.3	94.7	111.5	337.3	155.0	3.04
Itgam	integrin alpha M (CD11b)	89.5	112.0	570.0	519.1	135.7	130.4	201.5	1089.1	266.1	4.20
Csf3r	colony stimulating factor 3 receptor (grar	177.7	154.1	1454.4	1632.8	163.6	209.5	331.8	3087.1	373.1	8.89
Ccr2	chemokine (C-C motif) receptor 2	9.3	10.9	122.3	99.5	9.7	11.5	20.2	221.8	21.2	12.58
Ptprc	(CD45) protein tyrosine phosphatase, rec	24.6	27.0	353.9	328.9	46.9	26.4	51.6	682.8	73.3	7.54
Ccr1	chemokine (C-C motif) receptor 1	2.2	5.0	119.6	115.5	7.6	5.7	7.2	235.1	13.3	15.74
Tlr4	toll-like receptor 4	8.9	6.0	44.0	39.3	16.5	24.1	14.9	83.3	40.6	2.67

Figure 3.23 – A selection of the RNA sequencing data to show the differences in gene expression between central and peripheral retina in a P14 control, PBS control and LPS treated mouse. *Analysis of genes involved in hypoxia, metabolic pathways and inflammation/cytokine signalling were analysed to look for differences between groups and between the central and peripheral retina. Differences in expression between the groups are demonstrated as heat maps for each gene with red indicating high expression and green indicating low expression.*

3.4.2 Systemic LPS Injection as a modulator of retinal metabolism.

The hypoxia seen in the OIR model is the result of an imbalance between the supply and demand of oxygen in the retina. In this model of systemic LPS injection, there was no change in the supply of oxygen to LPS treated retinas, as evidenced by similar avascular areas between the control and treated groups. This implies that in the LPS treated mice the oxygen demand of the retina is reduced. A possible hypothesis for this could be that systemic inflammation reduces oxygen demand by causing the retina to switch from oxidative metabolism towards glycolysis. This switch to a non-oxidative process would require less oxygen in the retina and would therefore reduce levels of hypoxia.

Genes known to be up- or down-regulated in metabolic pathways were examined to see if there were any differences in the expression between the central and peripheral retina of the different groups (**Figure 3.23**).

All metabolic markers examined, with the exception of Pfkfb1, were upregulated in both retina undergoing OIR when compared to the P14 age match control group. In both OIR tissues upregulation of metabolic markers was seen in the central retina when compared to the periphery. LPS treatment appeared to reduce the expression of Pkm1, Pfkp, Tpi1, Pgam1, Pgk1 and Pdk1 in the central retina and increase the expression of Pfkb3, Hk1 and Hk2 when compared to the central retina of the PBS control. However, when these differences are analysed as fold changes they are relatively small changes (82-115%).

These findings failed to show that LPS treatment at P12 leads to dramatic changes in the expression of genes involved in the metabolic pathways of the retina when compared to the PBS control.

3.4.3 Systemic LPS Injection as a modulator of cytokine expression in the retina.

In experiments with C57Bl6 mice, LPS treatment was shown to induce an influx of peripheral neutrophils and monocyte/macrophages into the avascular area of the central retina in mice undergoing OIR. It was hypothesised that this influx of neutrophils resulted in the reduction in vessel tortuosity and hypoxic area staining seen in this model. However on reducing this invading population LPS treatment still resulted in reduced vessel tortuosity but not a reduced hypoxic area. A possible explanation for this was that LPS treatment results in a change in cytokine expression in this area and it is this change in cytokine expression which mediates the change in both vessel tortuosity and hypoxic area, as well as attracting the neutrophils and monocyte/macrophages to the retina.

Genes known to be involved in inflammation and cytokine signalling were examined to see if there were any differences in their expression between the central and peripheral retina of the different groups (**Figure 3.23**).

As expected all inflammatory and cytokine markers were upregulated in the LPS treated tissue when compared to the PBS and age matched controls, confirming that the LPS treatment had worked. Expression of inflammatory genes was also upregulated in the PBS control tissue when compared to the P14 age matched control. When comparing the difference between the central and peripheral retina samples in

the LPS treated retina there was no difference. The most apparent changes in cytokine gene expression as a result of LPS treatment compared to the PBS control in the central retina were Il1β (72 fold increase), CCR1 (16 fold increase), CCL5 (13 fold increase) and CCR2 (13 fold increase). Some cytokine receptor genes known to be upregulated in inflammation such as Tnf, Il10 and Il8 were not found.

These findings confirm that LPS treatment at P12 leads to dramatic changes in expression of genes involved in inflammation and cytokine expression of the retina when compared to PBS control mice also undergoing OIR.

3.5 The effect of IL1β in ischaemic retinopathy on hypoxia and neovascularisation

3.5.1 The effect of intraocular injections of IL1β, CCL5 and vehicle on hypoxia at P14 in OIR

The RNA sequencing data showed that both Il1β and CCL5 expression underwent large fold changes in the hypoxic areas of LPS treated. It is possible that LPS injection through TLR4 signalling leads to an upregulation of these cytokines and they in turn are able to modulate oxygen demand in the hypoxic retina. The invading neutrophil and monocyte/macrophage population that are seen to invade the avascular area are likely to be secondary to this cytokine signalling.

To test this hypothesis a litter of C57BL6 pups that had been exposed to 5 days of hyperoxia (75% O2) between P7-12 were divided into three groups at P12 on return to normoxia. The first group received an intraocular injection of CCL5 to the left eye, the second group received an intraocular injection of Il1β to the left eye and the third

group received an intraocular injection of vehicle to the left eye. In each group the right non-injected eye was used as a control for comparison. Pups were culled at P14 and immunohistochemistry was performed on retinal wholemounts to examine hypoxia.

Non-injected eyes of mouse pups in the CCL5 injected group were found to demonstrate the typical hypoxic phenotype associated with the OIR model at P14, characterised by tortuous retinal arteries **(Figure 3.24I**), central areas of vaso-obliteration (**Figure 3.24C**) which were positive for EF5 hypoxia staining (**Figure 3.24E**). Injected eyes of mouse pups in the CCL5 injected group demonstrated a similiar hypoxic phenotype. On examination of the retinal wholemounts, the retinal arteries still appeared tortuous (**Figure 3.24J**) and the avascular areas appeared a similar size with areas of vaso-obliteration (**Figure 3.24D**) associated with less intense EF5 hypoxia stain **(Figure 3.24F**).

However, when CCL5 injected and non-injected eyes were compared no significant differences were seen between avascular area, retinal artery tortuosity or EF5 hypoxia staining (**Table 3.12**).

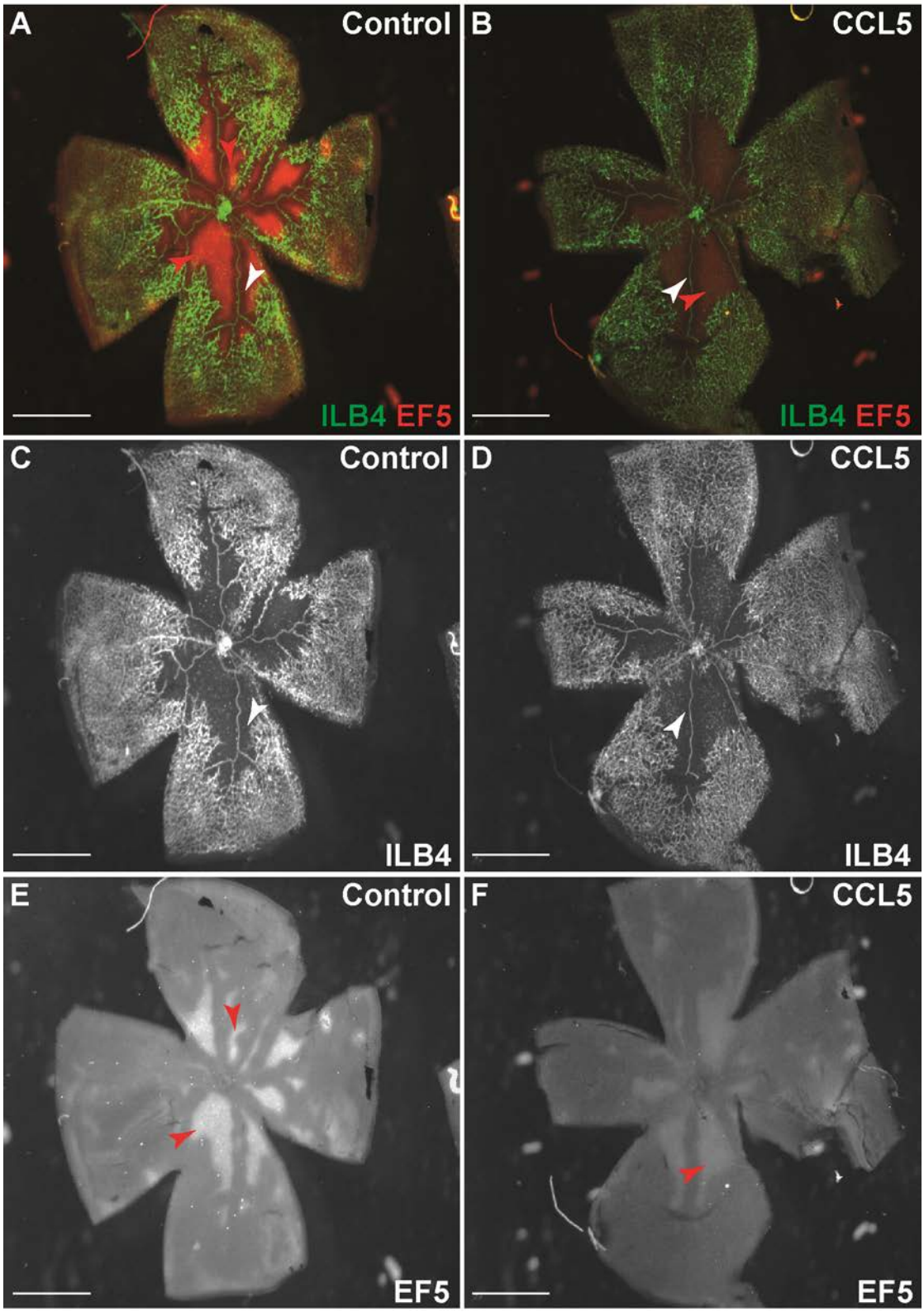

Figure 3.24(a) – Intraocular injection of CCL5 at P12 after hyperoxia does not change hypoxia at P14 in OIR. *Retinal wholemounts from P14 C57BL6 mice after OIR stained with isolectin B4 and EF5 hypoxia stain. Mouse pups in the non-injected control group demonstrate central areas of vaso-obliteration (C) which are positive for EF5 hypoxia staining (E) (red arrows). No difference was seen in the avascular area between the two groups (C&D). CCL5 injected eyes appeared to demonstrate reduced intensity of EF5 hypoxia staining (F). Retinal arteries (white arrows) appear tortuous in both groups. Scale bars = 100µm*

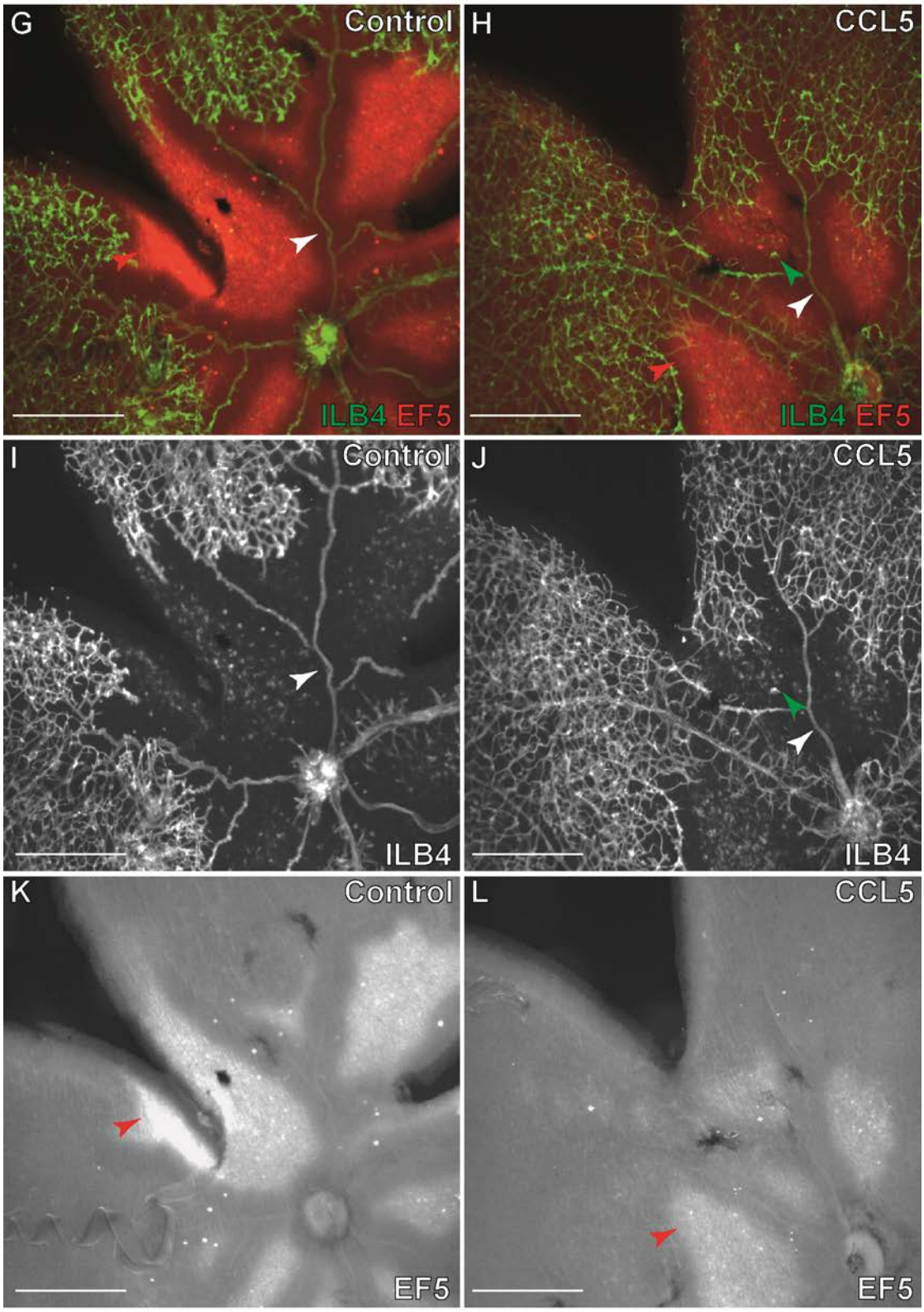

Figure 3.24(b) – Intraocular injection of CCL5 at P12 after hyperoxia does not change hypoxia at P14 in OIR. *Higher magnification images demonstrate the classical tortuous retinal arteries (I) (white arrows) associated with OIR at P14 seen in the non-injected control group. In the CCL5 injected group the retinal arteries still appear tortuous (J). In the CCL5 injected eyes some isolectin positive cells (green arrows) are seen in the avascular area (red arrows) (J). Scale bars = 50μm*

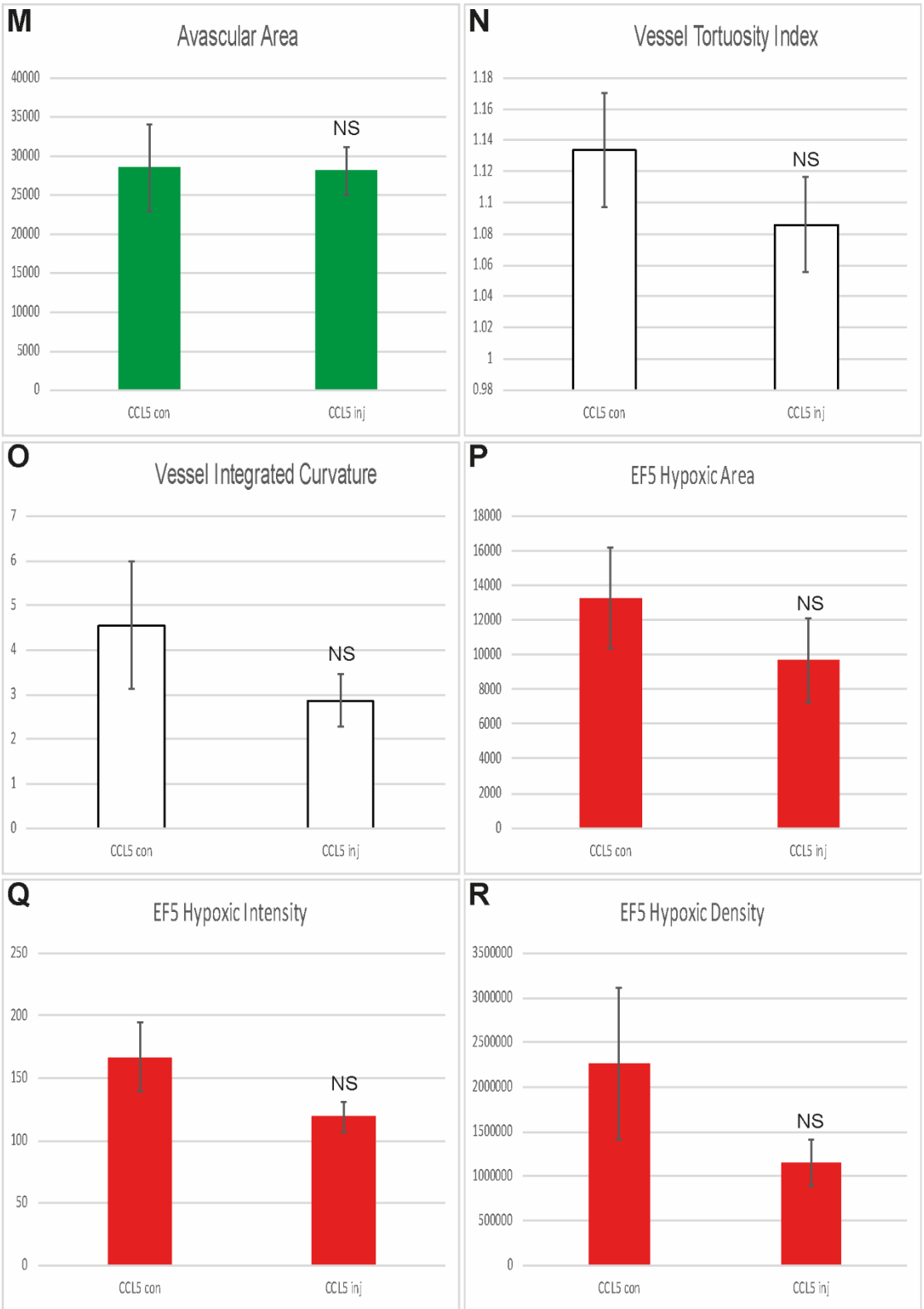

Figure 3.24(c) - Intraocular injection of CCL5 at P12 after hyperoxia does not change hypoxia at P14 in OIR. *No significant differences were seen in the avascular area(M), retinal artery tortuosity measures (N,O) or EF5 hypoxia measures (P-R). (n= control 3 vs CCL5 injected 3; error bar = standard deviation; NS = non-significant)*

Table 3.12: P14 OIR CCL5: Control vs Injected groups

	TreatmentGroup	N	Mean	Std. Deviation	Std. Error Mean
AvascularArea	Control	3	28450.0	5563.23	3211.93
	CCL5	3	28108.0	3087.01	1782.29
VesselTortuosityIndex	Control	3	1.13	.04	.02
	CCL5	3	1.09	.03	.02
VesselIntegratedCurvature	Control	3	4.55	1.44	.83
	CCL5	3	2.86	.60	.34
EF5HypoxicArea	Control	3	13269.7	2870.84	1657.48
	CCL5	3	9683.33	2434.50	1405.56
EF5HypoxicIntensity	Control	3	166.40	27.75	16.02
	CCL5	3	118.95	11.79	6.81
EF5HypoxicDensity	Control	3	2.26E+6	845280.09	488022.69
	CCL5	3	1.14E+6	265065.34	153035.54

	Levene's Test for Equality of Variances		t-test for Equality of Means						
								95% Confidence Interval of the Difference	
	F	Sig.	t	df	Sig. (2-tailed)	Mean Difference	Std. Error Difference	Lower	Upper
AvascularArea	.921	.392	.093	4	.930	342.00	3673.29	-9856.69	10540.69
VesselTortuosityIndex	.187	.688	1.738	4	.157	.05	.03	-.03	.12
VesselIntegratedCurvature	3.31	.143	1.869	4	.135	1.68	.90	-.82	4.18
EF5HypoxicArea	.067	.808	1.650	4	.174	3586.33	2173.21	-2447.46	9620.13
EF5HypoxicIntensity	1.56	.279	2.725	4	.053	47.44	17.41	-.89	95.78
EF5HypoxicDensity	2.20	.213	2.180	4	.095	1115214.67	511454.81	-304811.53	2535240.86

Table 3.12– Statistical Comparisons of P14 CCL5 control vs injected treatment groups

Non-injected eyes of mouse pups in the Il1β injected group were found to demonstrate the typical hypoxic phenotype associated with the OIR model at P14 previously described. (**Figure 3.25A,C,E,G,I,K**). Injected eyes of mouse pups in the Il1β injected group demonstrated a suppressed hypoxic phenotype. On examination of the retinal wholemounts, the retinal arteries appeared straight (**Figure 3.25J**) and the avascular areas appeared smaller with areas of vaso-obliteration (**Figure 3.25D**) associated with smaller but similar intensity of EF5 hypoxia stain **(Figure 3.25F**).

When IL1β injected and non-injected eyes were compared a significant difference was seen between the avascular areas of both groups ($p<0.05$). Retinal arteries were shown to be significantly straighter as measured my both tortuosity index and integrated curvature ($p<0.05$). Measures of EF5 hypoxic area and density were found to be

significantly reduced in the injected eyes ($p<0.05$). EF5 hypoxic intensity did not reach statistical significance. (**Table 3.13**).

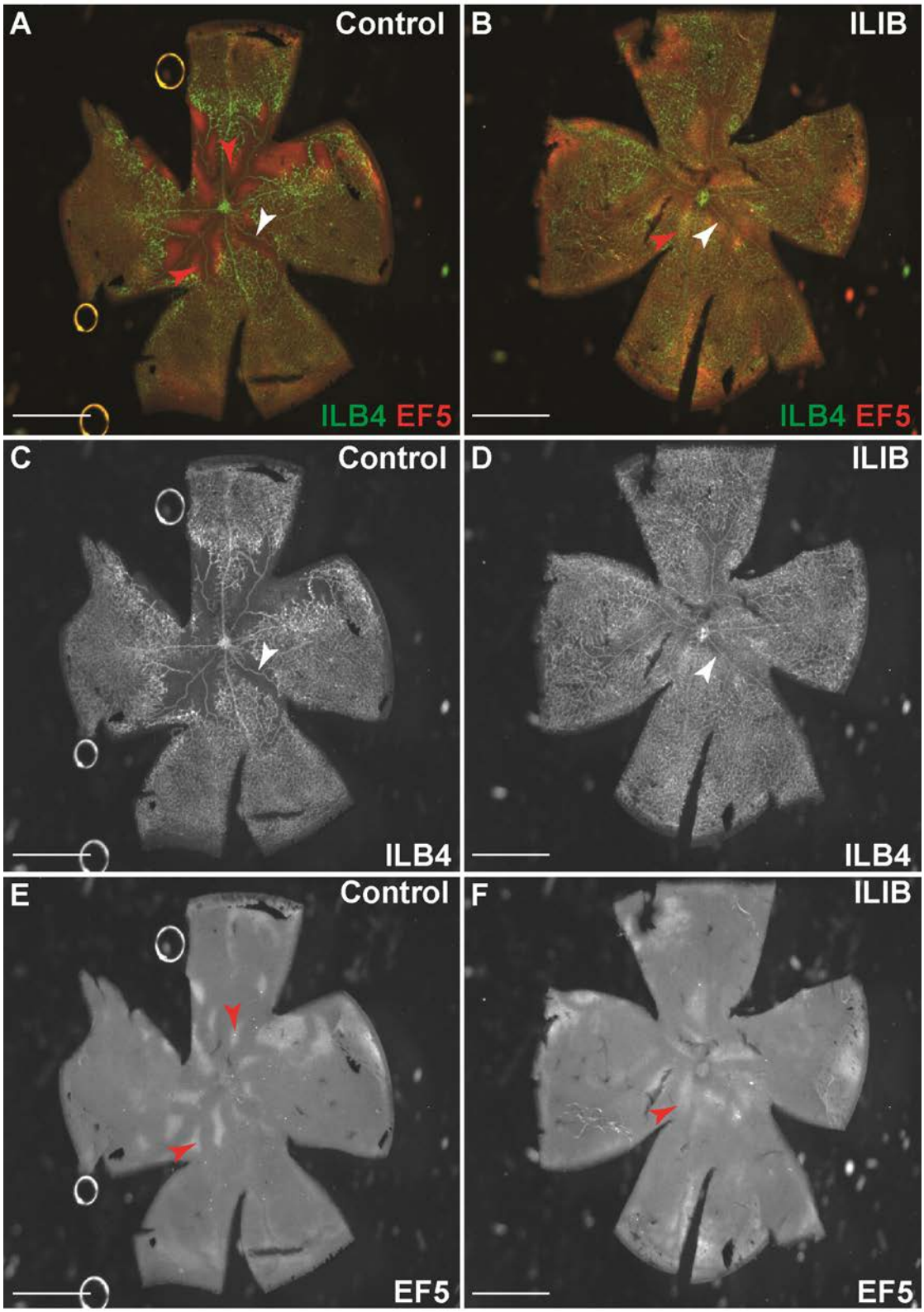

Figure 3.25(a) – Intraocular injection of IL1β at P12 after hyperoxia reduces hypoxia at P14 in OIR. *Retinal wholemounts from P14 C57BL6 mice after OIR stained with isolectin B4 and EF5 hypoxia stain. Mouse pups in the non-injected control group demonstrate central areas of vaso-obliteration (C) which are positive for EF5 hypoxia staining (E) (red arrows). IL1β injected eyes appeared to demonstrate reduced avascular area (D) and a reduction in area and of EF5 hypoxia staining (F). Retinal arteries (white arrows) appear straighter in the IL1β injected group (D). Scale bars = 100μm*

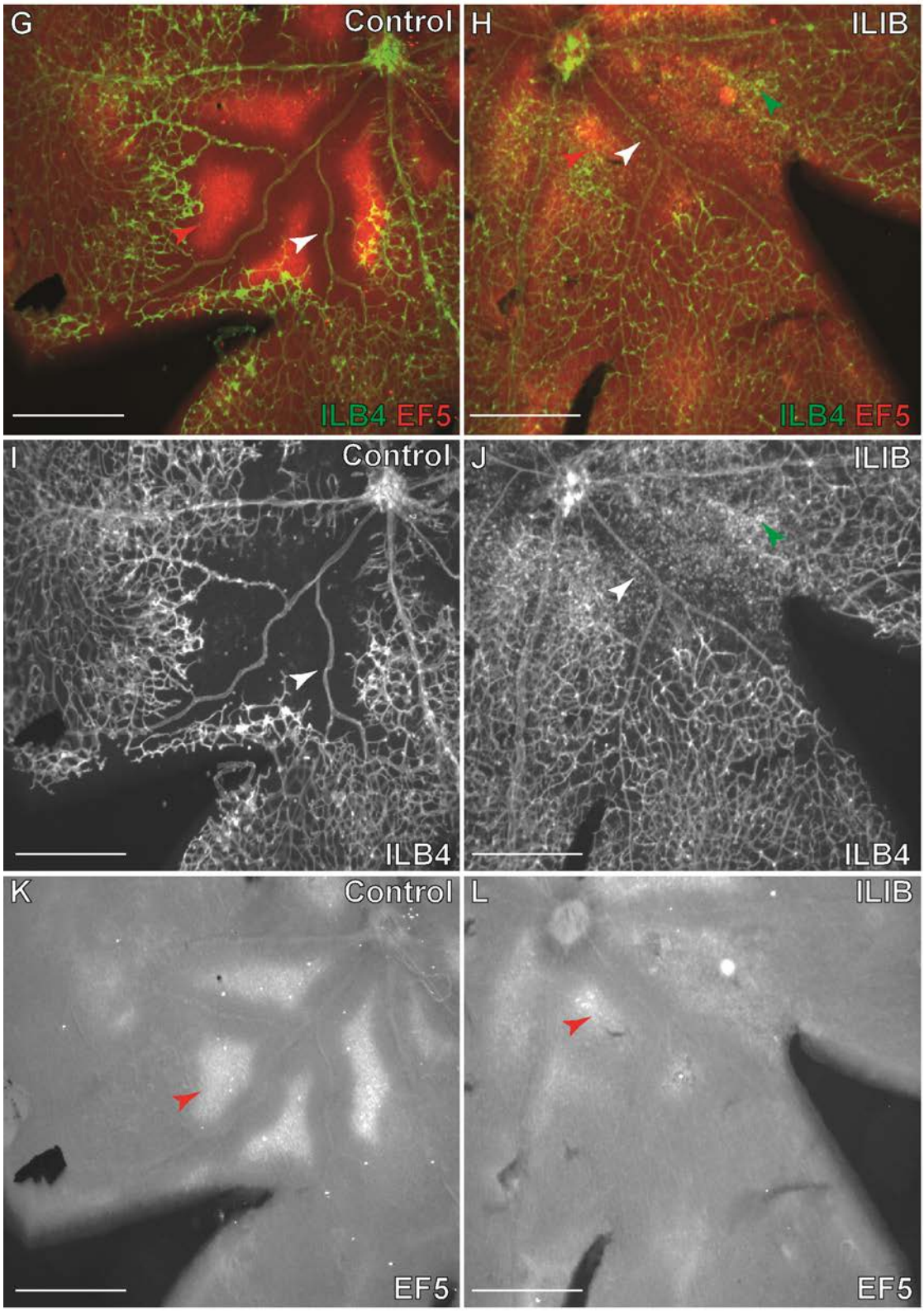

Figure 3.25(b) – Intraocular injection of IL1β at P12 after hyperoxia reduces hypoxia at P14 in OIR. *Higher magnification images demonstrate the classical tortuous retinal arteries (I) (white arrows) associated with OIR at P14 seen in the non-injected control group. In the IL1β injected group the retinal arteries appear straight (J). In the IL1β injected eyes isolectin positive cells (green arrows) are seen in the avascular area (red arrows) (J). Scale bars = 50µm*

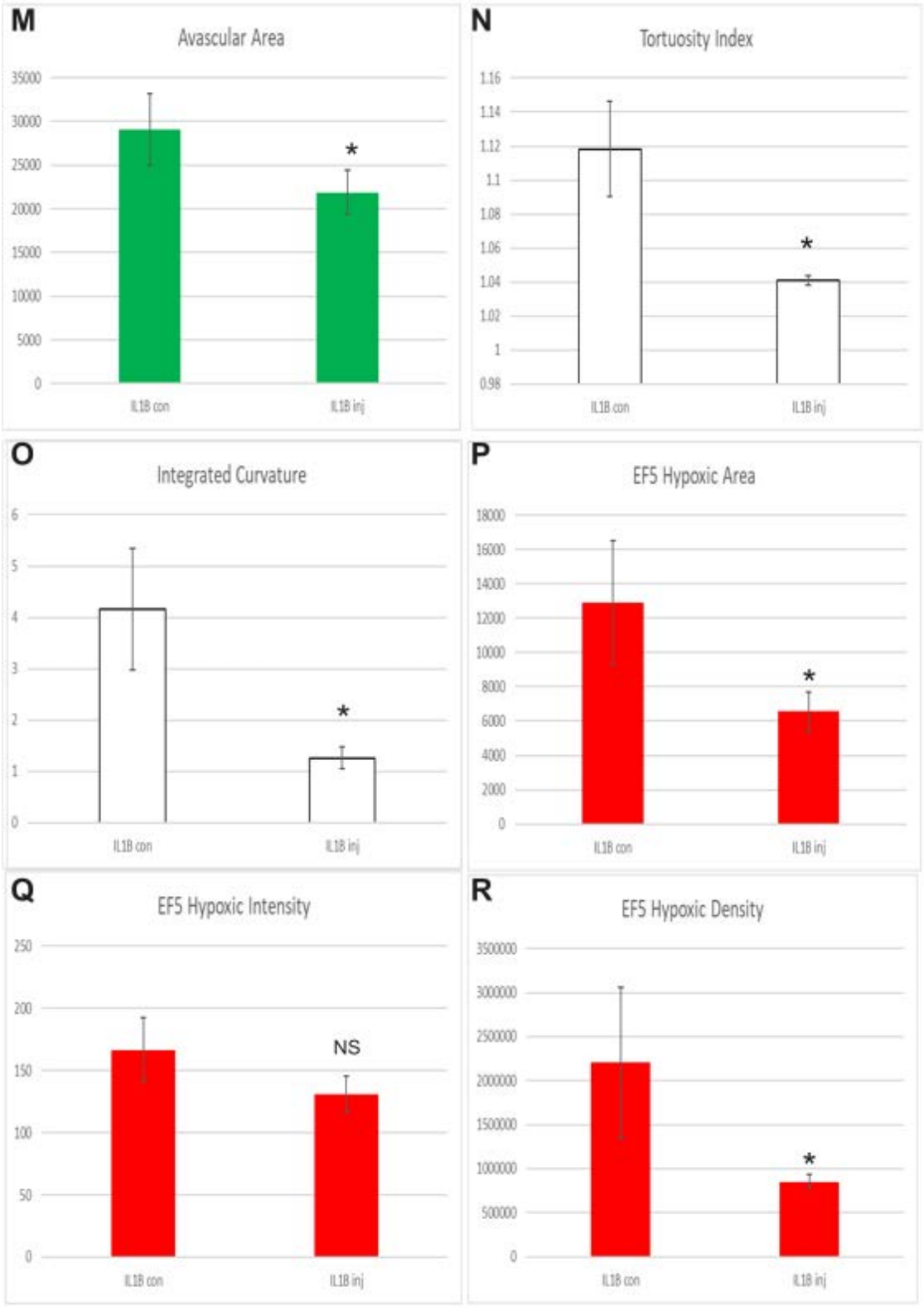

Figure 3.25(c) - Intraocular injection of IL1β at P12 after hyperoxia reduces hypoxia at P14 in OIR. *A significant difference was seen in the avascular area between the two groups (M). Retinal artery tortuosity measures were significantly reduced in IL1β injected eyes (N,O). EF5 hypoxia area and density were significantly reduced in IL1β injected eyes (P-R). ((n= control 9 vs IL1β injected 3; error bar = standard deviation; NS=non-significant, *=p<0.05)*

Table: 3.13: P14: OIR IL1B: COntrol vs injected groups

	TreatmentGroup	N	Mean	Std. Deviation	Std. Error Mean
AvascularArea	Control	9	29038.8889	4092.37671	1364.12557
	IL1B	3	21883.0000	2497.49855	1441.93146
VesselTortuosityIndex	Control	9	1.1183	.02780	.00927
	IL1B	3	1.0410	.00288	.00166
VesselIntegratedCurvature	Control	9	4.1587	1.18926	.39642
	IL1B	3	1.2612	.21029	.12141
EF5HypoxicArea	Control	9	12886.2222	3605.05599	1201.68533
	IL1B	3	6577.3333	1137.35761	656.65372
EF5HypoxicIntensity	Control	9	166.3124	26.02324	8.67441
	IL1B	3	131.2333	14.57812	8.41668
EF5HypoxicDensity	Control	9	2203200.222	859078.8421	286359.6140
	IL1B	3	853018.6667	76888.03979	44391.33047

	Levene's Test for Equality of Variances		t-test for Equality of Means						
								95% Confidence Interval of the Difference	
	F	Sig.	t	df	Sig. (2-tailed)	Mean Difference	Std. Error Difference	Lower	Upper
AvascularArea	.760	.404	2.805	10	.019	7155.88889	2551.29923	1471.23995	12840.53783
			3.605	5.984	.011	7155.88889	1984.94456	2295.70223	12016.07554
VesselTortuosityIndex	10.361	.009	4.658	10	.001	.07731	.01660	.04032	.11429
			8.212	8.489	.000	.07731	.00941	.05581	.09880
VesselIntegratedCurvature	3.008	.113	4.070	10	.002	2.89756	.71190	1.31134	4.48377
			6.989	9.246	.000	2.89756	.41460	1.96346	3.83165
EF5HypoxicArea	2.748	.128	2.899	10	.016	6308.88889	2176.22093	1459.96649	11157.81129
			4.607	9.944	.001	6308.88889	1369.39466	3255.36864	9362.40914
EF5HypoxicIntensity	1.593	.236	2.177	10	.055	35.07911	16.11447	-.82617	70.98440
			2.902	6.634	.024	35.07911	12.08660	6.17607	63.98215
EF5HypoxicDensity	8.786	.014	2.633	10	.025	1350181.556	512768.3123	207662.5569	2492700.554
			4.659	8.370	.001	1350181.556	289779.9489	687051.9658	2013311.145

Table 3.13 – Statistical Comparisons of P14 IL1β control vs injected treatment groups

Non-injected eyes of mouse pups in the vehicle injected group were found to demonstrate the typical hypoxic phenotype associated with the OIR model at P14 previously described. (**Figure 3.26A,C,E,G,I,K**). Injected eyes of mouse pups in the vehicle group unexpectedly demonstrated a suppressed hypoxic phenotype similar to that seen in the IL1β injected group. On examination of the retinal wholemounts, the retinal arteries had a mixed appearance with some being straight and some tortuous appeared straight (**Figure 3.25J**) and the avascular areas appeared smaller with areas of vaso-obliteration (**Figure 3.25D**) associated with smaller and less intense EF5 hypoxia stain **(Figure 3.25F**).

When vehicle injected and non-injected eyes were compared no significant difference was seen between the avascular areas of both groups. However, retinal arteries were shown to be significantly straighter as measured my both tortuosity index and integrated curvature ($p<0.05$). Measures of EF5 hypoxic staining were also found to be significantly reduced in the injected eyes as measured by EF5 hypoxic area, intensity and density ($p<0.05$) (**Table 3.14**).

Table 3.14: P14 OIR Vehicle: Control vs Injected groups

	TreatmentGroup	N	Mean	Std. Deviation	Std. Error Mean
AvascularArea	Control	3	29421.7	2460.38	1420.50
	Vehicle	3	22759.3	4458.15	2573.91
VesselTortuosityIndex	Control	3	1.12	.03	.02
	Vehicle	3	1.05	.02	.01
VesselIntegratedCurvature	Control	3	4.64	1.34	.77
	Vehicle	3	1.81	.57	.33
EF5HypoxicArea	Control	3	12917.0	2494.53	1440.22
	Vehicle	3	5254.00	1524.56	880.21
EF5HypoxicIntensity	Control	3	180.99	24.87	14.36
	Vehicle	3	123.17	12.61	7.28
EF5HypoxicDensity	Control	3	2.36E+6	627016.44	362008.11
	Vehicle	3	655965	240728.73	138984.80

	Levene's Test for Equality of Variances		t-test for Equality of Means						
								95% Confidence Interval of the Difference	
	F	Sig.	t	df	Sig. (2-tailed)	Mean Difference	Std. Error Difference	Lower	Upper
AvascularArea	.928	.390	2.266	4	.086	6662.33	2939.87	-1500.06	14824.72
VesselTortuosityIndex	.371	.575	3.009	4	.040	.07	.02	.01	.13
VesselIntegratedCurvature	4.061	.114	3.375	4	.028	2.84	.84	.50	5.17
EF5HypoxicArea	.512	.514	4.540	4	.010	7663.00	1687.90	2976.65	12349.35
EF5HypoxicIntensity	1.164	.341	3.591	4	.023	57.82	16.10	13.11	102.52
EF5HypoxicDensity	4.949	.090	4.385	4	.012	1700536.67	387771.38	623910.71	2777162.63
			4.385	2.577	.030	1700536.67	387771.38	343598.83	3057474.51

Table 3.14 – Statistical Comparisons of P14 vehicle control vs injected treatment groups

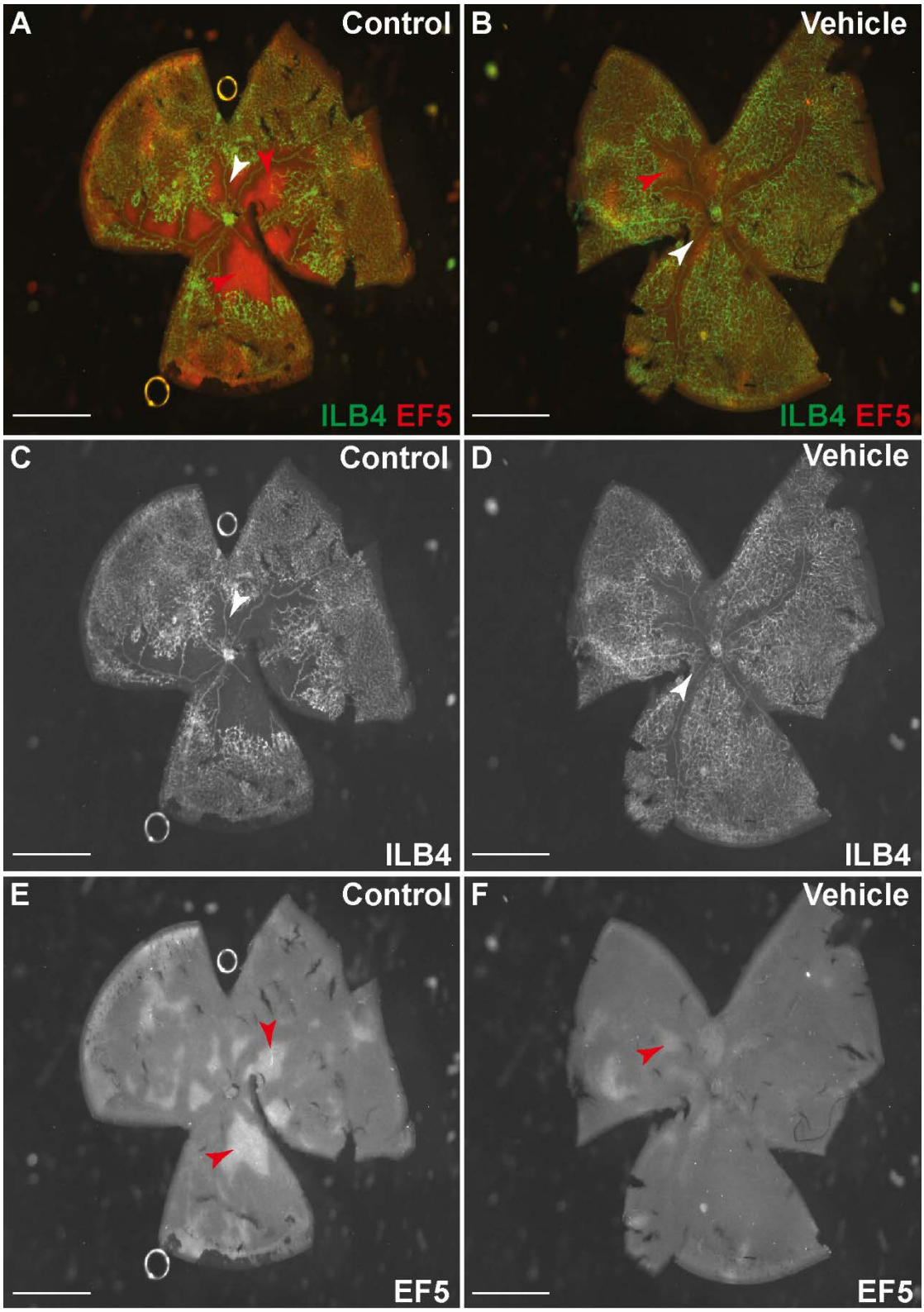

Figure 3.26(a) – Intraocular injection of vehicle at P12 after hyperoxia reduces hypoxia at P14 in OIR. *Retinal wholemounts from P14 C57BL6 mice after OIR stained with isolectin B4 and EF5 hypoxia stain. Mouse pups in the non-injected control group demonstrate central areas of vaso-obliteration (C) which are positive for EF5 hypoxia staining (E) (red arrows). Vehicle injected eyes appeared to demonstrate reduced avascular area (D) and a reduction in area and intensity of EF5 hypoxia staining (F). Retinal arteries (white arrows) appear straighter in the vehicle injected eyes (D). Scale bars = 100µm*

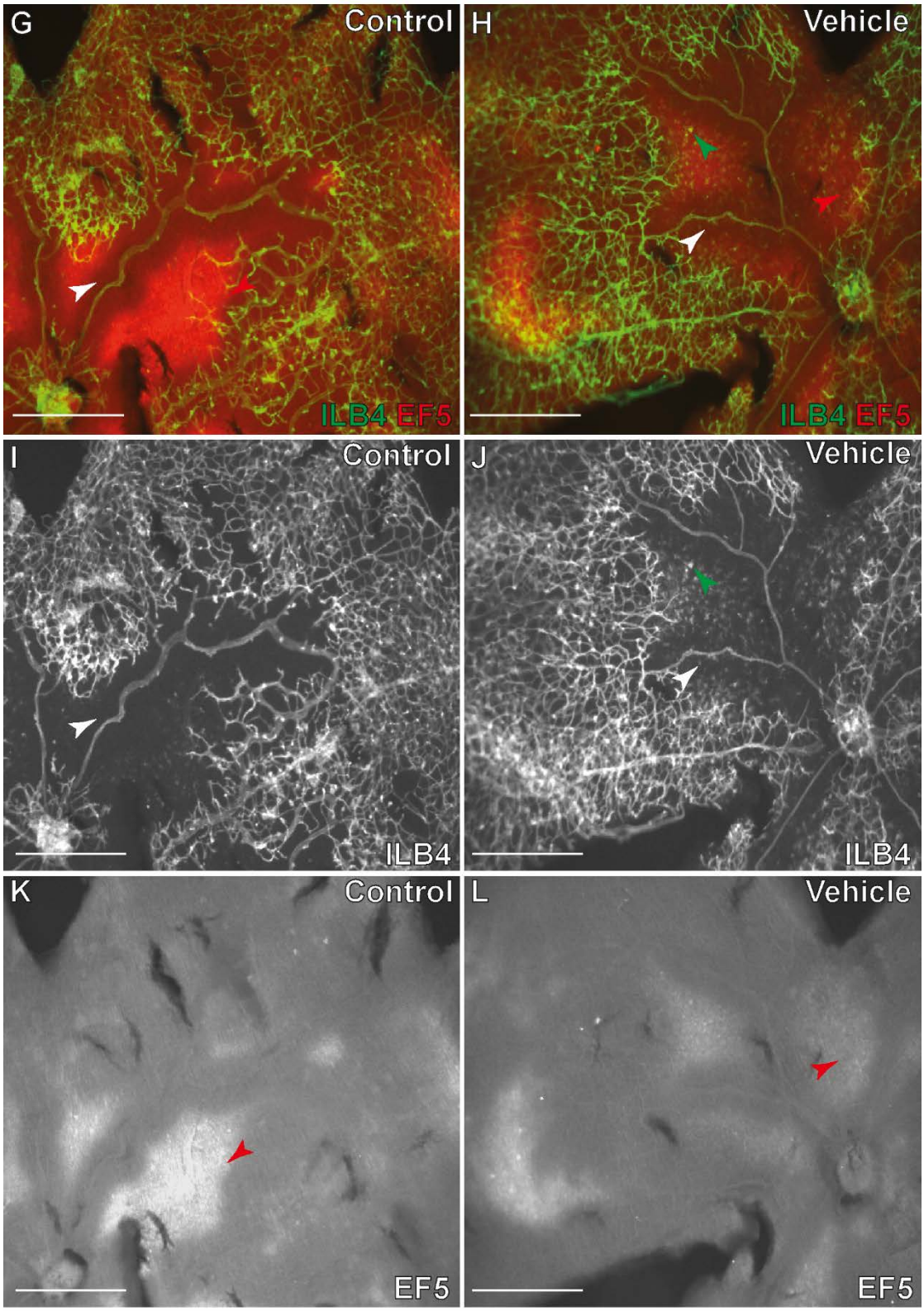

Figure 3.26(b) – Intraocular injection of vehicle at P12 after hyperoxia reduces hypoxia at P14 in OIR. *Higher magnification images demonstrate the classical tortuous retinal arteries (I) (white arrows) associated with OIR at P14 seen in the non-injected control group. In the vehicle injected group some of the retinal arteries appear straight while others remain tortuous (J). In the vehicle injected group the occasional isolectin positive cell (green arrows) is seen in the avascular area (red arrows) (J). Scale bars = 50µm*

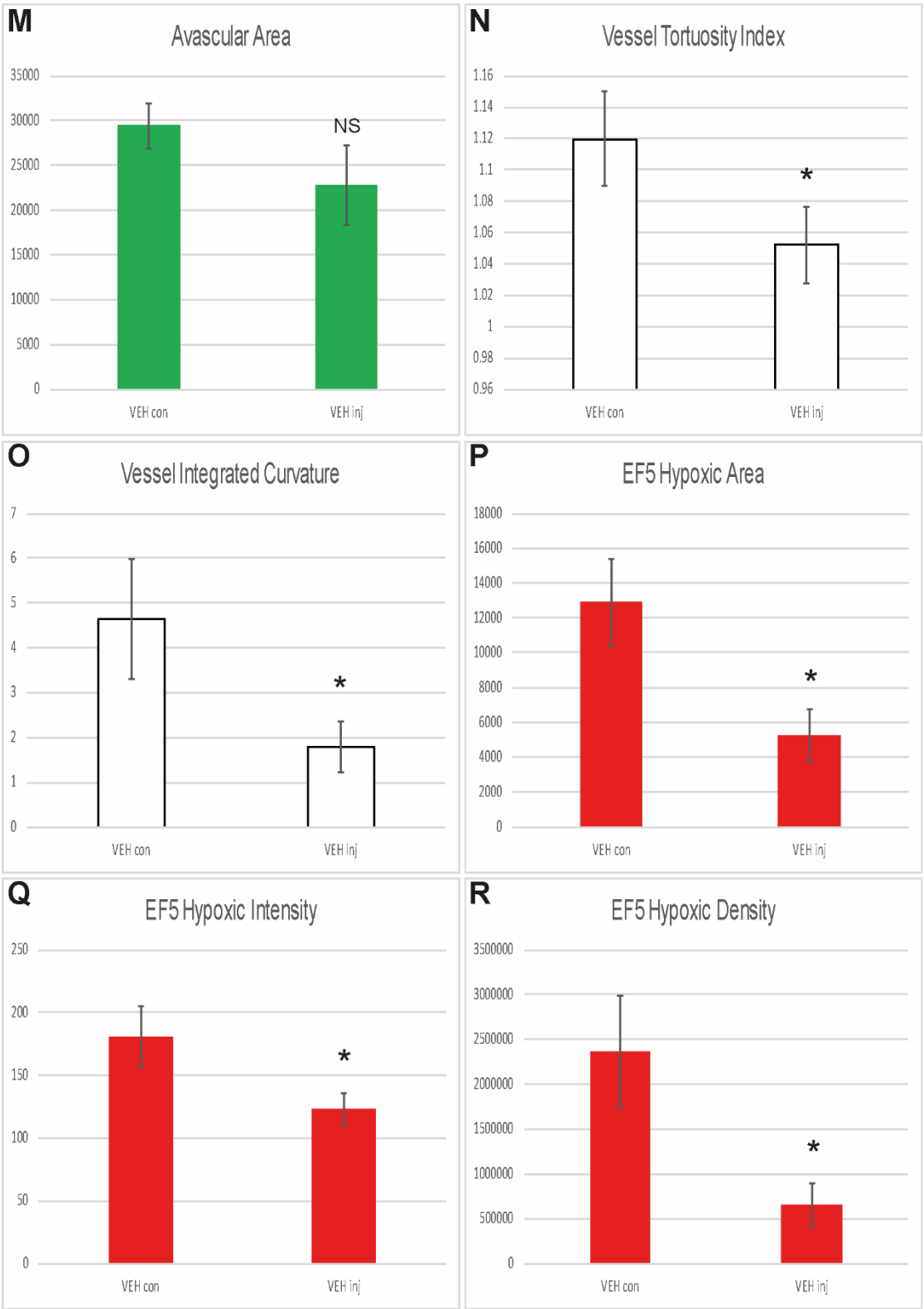

Figure 3.26(c) - Intraocular injection of vehicle at P12 after hyperoxia reduces hypoxia at P14 in OIR. *No significant differences were seen in the avascular area between the two groups (M). Retinal artery tortuosity measures were significantly reduced in vehicle injected eyes (N,O) as were EF5 hypoxia measures (P-R). (control 3 vs vehicle injected 3; error bar = standard deviation; NS=non-significant, *=p<0.05)*

These results show that IL1β intraocular injection is able to recreate the hypoxia reducing effects seen in the LPS treatment groups of previous experiments. IL1β also appears to attract the same population of neutrophils and monocyte/macrophages into the avascular areas. CCL5 although found to be upregulated in the RNA sequencing data was not able to create the same hypoxia reducing effect as IL1β although some invading inflammatory cells were noted in the avascular areas of these retina.

Interestingly, just injecting vehicle alone appears to reduce the hypoxic phenotype seen in OIR at P14 to a similar degree as IL1β injection but without the same level of invading inflammatory cells.

In all three groups the contralateral non-injected eye showed no change in the typical hypoxic phenotype seen at P14 after OIR. This would suggest that the effects of the intraocular injections were only local to the injected eye and did not reach the systemic circulation, unlike the initial LPS intraocular injection experiment described previously.

3.5.2 Intraocular injections of IL1β and vehicle reduce neovascularisation at P17 in OIR

In trying to understand why LPS intraocular injection led to a reduction in neovascularisation seen at P17 after OIR it was hypothesised that the LPS reduced hypoxia in order to prevent consequent neovascularisation occurring.

To investigate whether the reduced hypoxia seen at P14 with intraocular injections of vehicle and IL1β led to reduced neovascularisation at P17 a litter of C57BL6 pups underwent OIR and either the IL1β or vehicle intraocular injection protocol previously described. Pups were culled at P17 and immunohistochemistry was performed on retinal wholemounts to examine neovascularisation.

Non-injected eyes of mouse pups in the IL1β injected group were found to demonstrate the typical neovascular phenotype associated with the OIR model at P17, characterised by tortuous retinal arteries **(Figure 3.27I**), central areas of vaso-obliteration (**Figure 3.27C**) which were positive for EF5 hypoxia staining (**Figure 3.27E**) and neovascular tuft formation (**Figure 3.27I**). Injected eyes of mouse pups in the IL1β injected group demonstrated a small avascular phenotype. On examination of the retinal wholemounts, there were areas of healthy vascular regeneration with fewer areas of vaso-obliteration (**Figure 3.27D**). The retinal arteries appeared straight (**Figure 3.27J**), areas of EF5 hypoxia stain appeared reduced in area and intensity **(Figure 3.27F**) and less neovascular tufts were seen (**Figure 3.27J**).

However, when IL1β injected and non-injected eyes were compared despite the large apparent differences in the two groups, as a result of the small n–number, a significant difference was only seen between avascular area and retinal artery tortuosity index ($P<0.05$). EF5 hypoxia staining measures and neovascular area did not reach statistical significance. (**Table 3.15**).

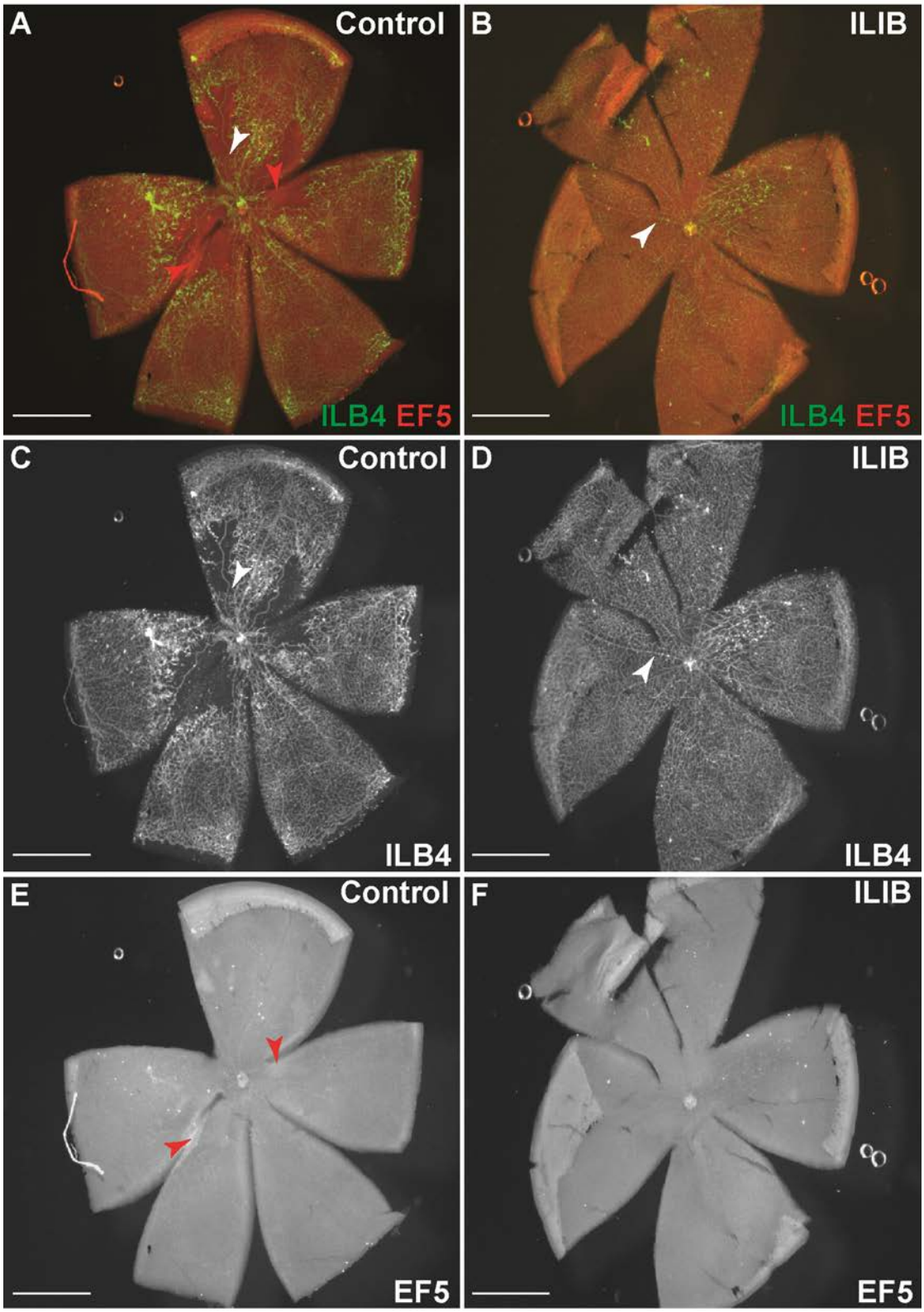

Figure 3.27(a) – Intraocular injection of IL1β at P12 after hyperoxia leads to reduced avascular area at P17 in OIR. Retinal wholemounts from P17 C57BL6 mice after OIR stained with isolectin B4, EF5 hypoxia stain and collagen IV (not shown). Non-injected control eyes demonstrated central areas of vaso-obliteration (C) which are positive for EF5 hypoxia staining (E) (red arrows) whereas IL1β injected eyes demonstrated a retinal vasculature that has regenerated physiologically with straight retinal arteries (white arrows), few areas of vaso-obliteration (D) and little EF5 hypoxia staining(F). Scale bars = 100µm

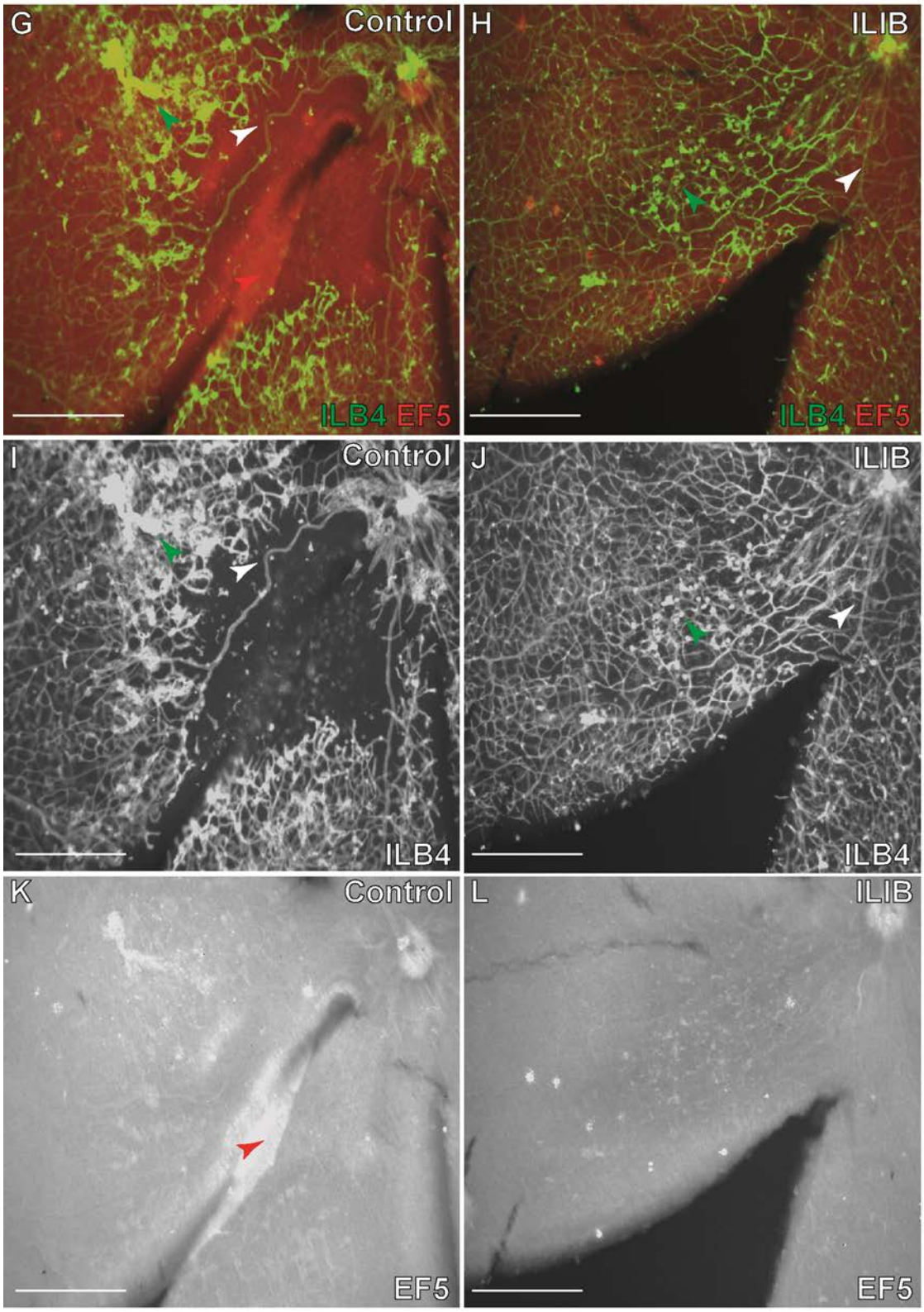

Figure 3.27(b) – Intraocular injection of IL1β at P12 after hyperoxia leads to reduced avascular area at P17 in OIR. *Higher magnification images demonstrate the classical tortuous retinal arteries (I) (white arrows) and neovascular tuft formation (I) (green arrows) associated with OIR at P17 seen in the non-injected control eyes. Whereas in the IL1β injected eyes the retinal arteries appear straighter with similiar neovascular growth (J). There was no significant difference in EF5 hypoxia staining (red arrows) between the two groups. Scale bars = 50μm*

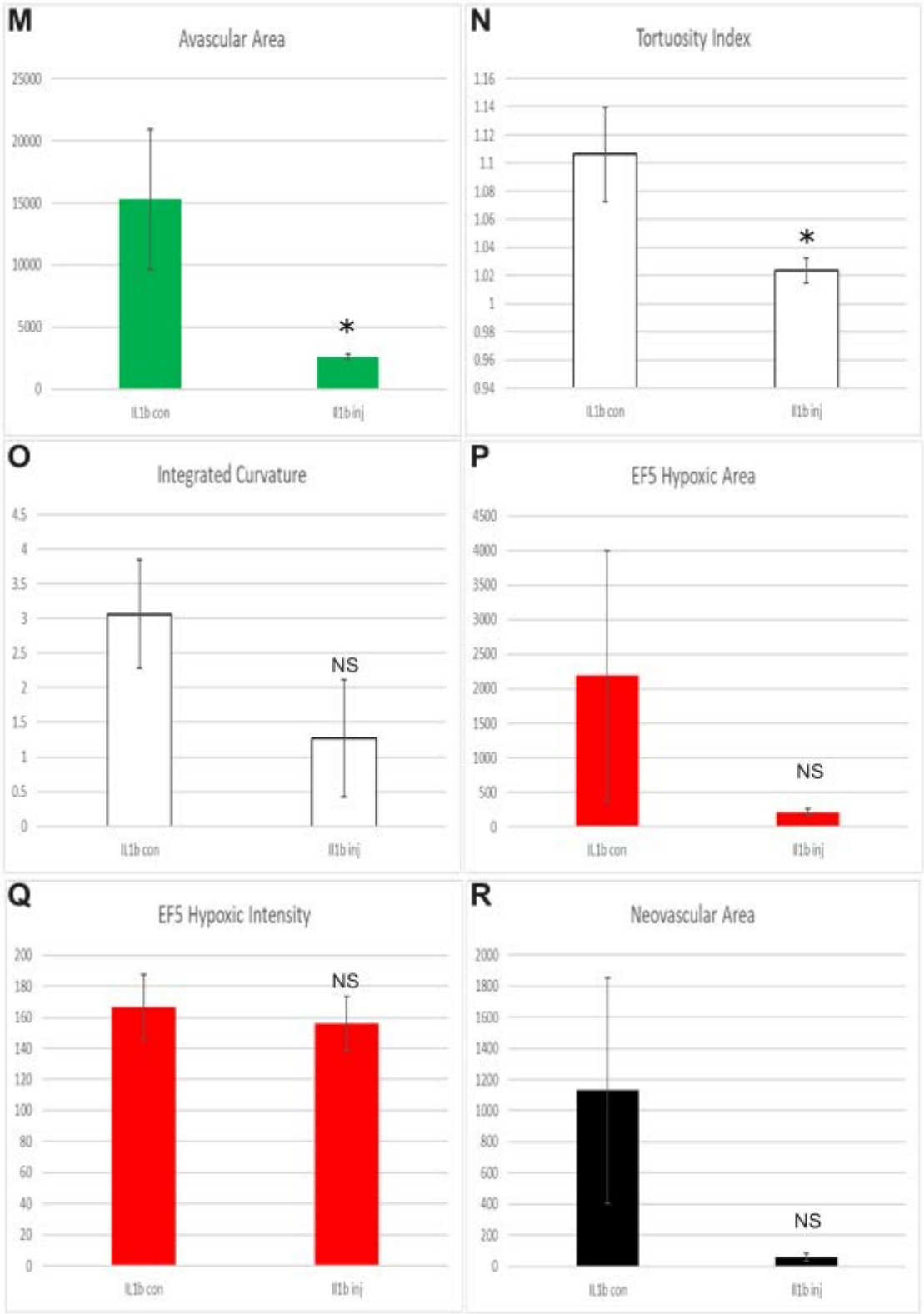

Figure 3.27(c) – Intraocular injection of IL1β at P12 after hyperoxia leads to reduced avascular area at P17 in OIR. *Avascular area (M), vessel tortuosity (N,O), EF5 hypoxic measures (P,Q) and neovascular area (R) where all reduced in the IL1β injected eyes. Only avascular area and tortuosity index were found to be statistically significant. (n= control 4 vs IL1β injected 2; error bar = standard deviation; NS = non-significant, *= p<0.05)*

Table 3.15: P17 OIR: IL1B control vs injected groups

	TreatmentGroup	N	Mean	Std. Deviation	Std. Error Mean
AvascularArea	Control	4	15279.5000	5687.66628	2843.83314
	IL1B	2	2607.0000	192.33304	136.00000
VesselTortuosityIndex	Control	4	1.1062	.03342	.01671
	IL1B	2	1.0235	.00884	.00625
VesselIntegratedCurvature	Control	4	3.0662	.78807	.39403
	IL1B	2	1.2673	.84641	.59850
EF5HypoxicArea	Control	4	2186.2500	1811.90864	905.95432
	IL1B	2	212.5000	48.79037	34.50000
EF5HypoxicIntensity	Control	4	166.5998	21.15228	10.57614
	IL1B	2	156.0555	17.00097	12.02150
EF5HypoxicDensity	Control	4	390733.0000	352913.7273	176456.8637
	IL1B	2	33576.5000	11226.73436	7938.50000
NeovascalarArea	Control	4	1129.2500	724.94017	362.47008
	IL1B	2	58.0000	25.45584	18.00000

	Levene's Test for Equality of Variances		t-test for Equality of Means						
								95% Confidence Interval of the Difference	
	F	Sig.	t	df	Sig. (2-tailed)	Mean Difference	Std. Error Difference	Lower	Upper
AvascularArea	7.899	.048	2.970	4	.041	12672.50000	4266.56262	826.62311	24518.37689
			4.451	3.014	.021	12672.50000	2847.08323	3635.05150	21709.94850
VesselTortuosityIndex	6.464	.064	3.261	4	.031	.08269	.02535	.01230	.15308
			4.635	3.682	.012	.08269	.01784	.03143	.13395
VesselIntegratedCurvature	.029	.872	2.587	4	.061	1.79900	.69546	-.13191	3.72991
			2.511	1.934	.133	1.79900	.71656	-1.38772	4.98572
EF5HypoxicArea	3.686	.127	1.452	4	.220	1973.75000	1359.09570	-1799.70459	5747.20459
			2.177	3.009	.117	1973.75000	906.61099	-906.78292	4854.28292
EF5HypoxicIntensity	.276	.627	.603	4	.579	10.54425	17.48905	-38.01314	59.10164
			.659	2.623	.563	10.54425	16.01160	-44.81318	65.90168
EF5HypoxicDensity	3.445	.137	1.349	4	.249	357156.5000	264729.9342	-377851.630	1092164.630
			2.022	3.012	.136	357156.5000	176635.3433	-203698.675	918011.6755
NeovascalarArea	2.828	.168	1.970	4	.120	1071.25000	543.81685	-438.62763	2581.12763
			2.952	3.015	.060	1071.25000	362.91674	-80.52081	2223.02081

Table 3.15 – Statistical Comparisons of P17 IL1β control vs injected treatment groups

Non-injected eyes of mouse pups in the vehicle injected group were found to demonstrate the typical neovascular phenotype associated with the OIR model at P17, previously described **(Figure 3.28A,G**). Injected eyes of mouse pups in the vehicle injected group also demonstrated a suppressed neovascular phenotype, similar to that seen IL1β injected eyes. On examination of the retinal wholemounts, avascular area (**Figure 3.28D**), retinal artery tortuosity (**Figure 3.28J**), EF5 hypoxia staining **(Figure 3.28F**) and neovascular tuft formation (**Figure 3.28J**) were all reduced.

When vehicle injected and non-injected eyes were compared despite the large apparent differences in the two groups, as a result of the small n–number, only measures of vessel tortuosity were found to be statistically significant ($p<0.05$) (**Table 3.16**).

Table 3.16: P17 OIR Vehicle: control vs injected groups

	TreatmentGroup	N	Mean	Std. Deviation	Std. Error Mean
AvascularArea	Control	2	17089.0	6146.17	4346.00
	Vehicle	2	1421.00	38.18	27.00
VesselTortuosityIndex	Control	2	1.10	.03	.02
	Vehicle	2	1.02	.01	.00
VesselIntegratedCurvature	Control	2	2.91	.63	.44
	Vehicle	2	.67	.13	.09
EF5HypoxicArea	Control	2	1814.00	923.48	653.00
	Vehicle	2	195.00	41.01	29.00
EF5HypoxicIntensity	Control	2	169.48	10.87	7.68
	Vehicle	2	175.93	.52	.36
EF5HypoxicDensity	Control	2	312453	176221.62	124607.50
	Vehicle	2	34317.0	7315.73	5173.00
NeovascularArea	Control	2	820.00	517.60	366.00
	Vehicle	2	58.00	25.46	18.00

	t-test for Equality of Means						
						95% Confidence Interval of the Difference	
	t	df	Sig. (2-tailed)	Mean Difference	Std. Error Difference	Lower	Upper
AvascularArea	3.605	2	.069	15668.00	4346.08	-3031.69	34367.69
VesselTortuosityIndex	4.661	2	.043	.09	.02	.01	.16
VesselIntegratedCurvature	4.962	2	.038	2.24	.45	.30	4.19
EF5HypoxicArea	2.477	2	.132	1619.00	653.64	-1193.40	4431.40
EF5HypoxicIntensity	-.839	2	.490	-6.45	7.69	-39.55	26.65
EF5HypoxicDensity	2.230	2	.155	278135.50	124714.83	-258469.11	814740.11
NeovascularArea	2.079	2	.173	762.00	366.44	-814.67	2338.67

Table 3.16 – Statistical Comparisons of P17 vehicle control vs injected treatment groups

These results would suggest that the initial reduction in hypoxia seen in eyes injected with either IL1β or vehicle is sustained and leads to a reduction in neovascularisation at P17 and allows for healthy vascular regeneration of the retinal vasculature. However, when compared to the initial intraocular LPS injection experiments the inflammatory response in these retinas is not as severe, despite the reduction in neovascularisation being similar. These results are more similar to the results seen in P17 mice when LPS was injected intraperitoneally at P12.

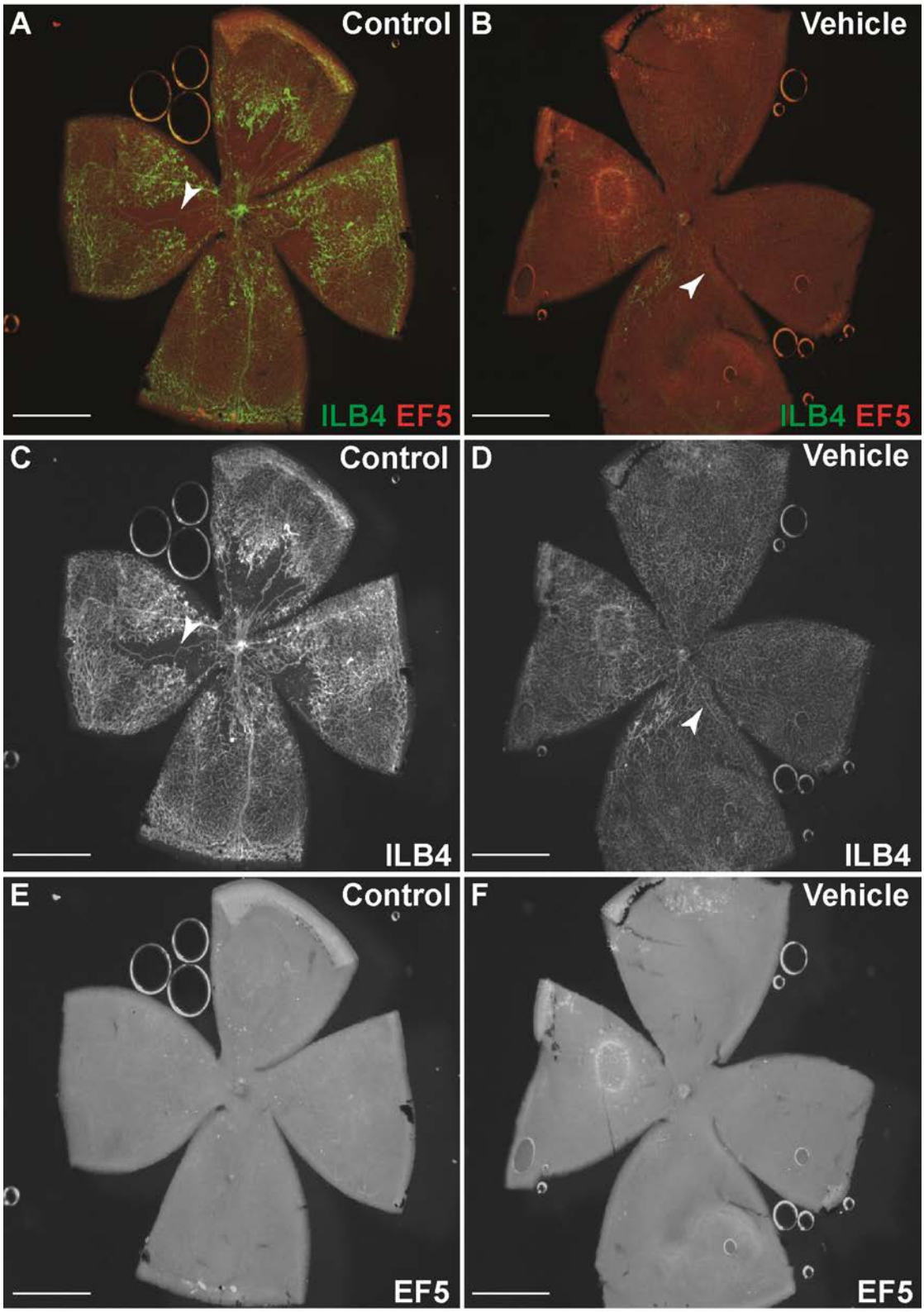

Figure 3.28(a) – Intraocular injection of vehicle at P12 after hyperoxia leads to reduced neovascular phenotype at P17 in OIR. Retinal wholemounts from P17 C57BL6 mice after OIR stained with isolectin B4, EF5 hypoxia stain and collagen IV (not shown). Non-injected control eyes demonstrated central areas of vaso-obliteration (C) which are weakly positive for EF5 hypoxia staining (E) whereas vehicle injected eyes demonstrated a retinal vasculature that has regenerated physiologically with straight retinal arteries (white arrows) (D), few areas of vaso-obliteration (D) and little EF5 hypoxia staining(F). Scale bars = 100µm

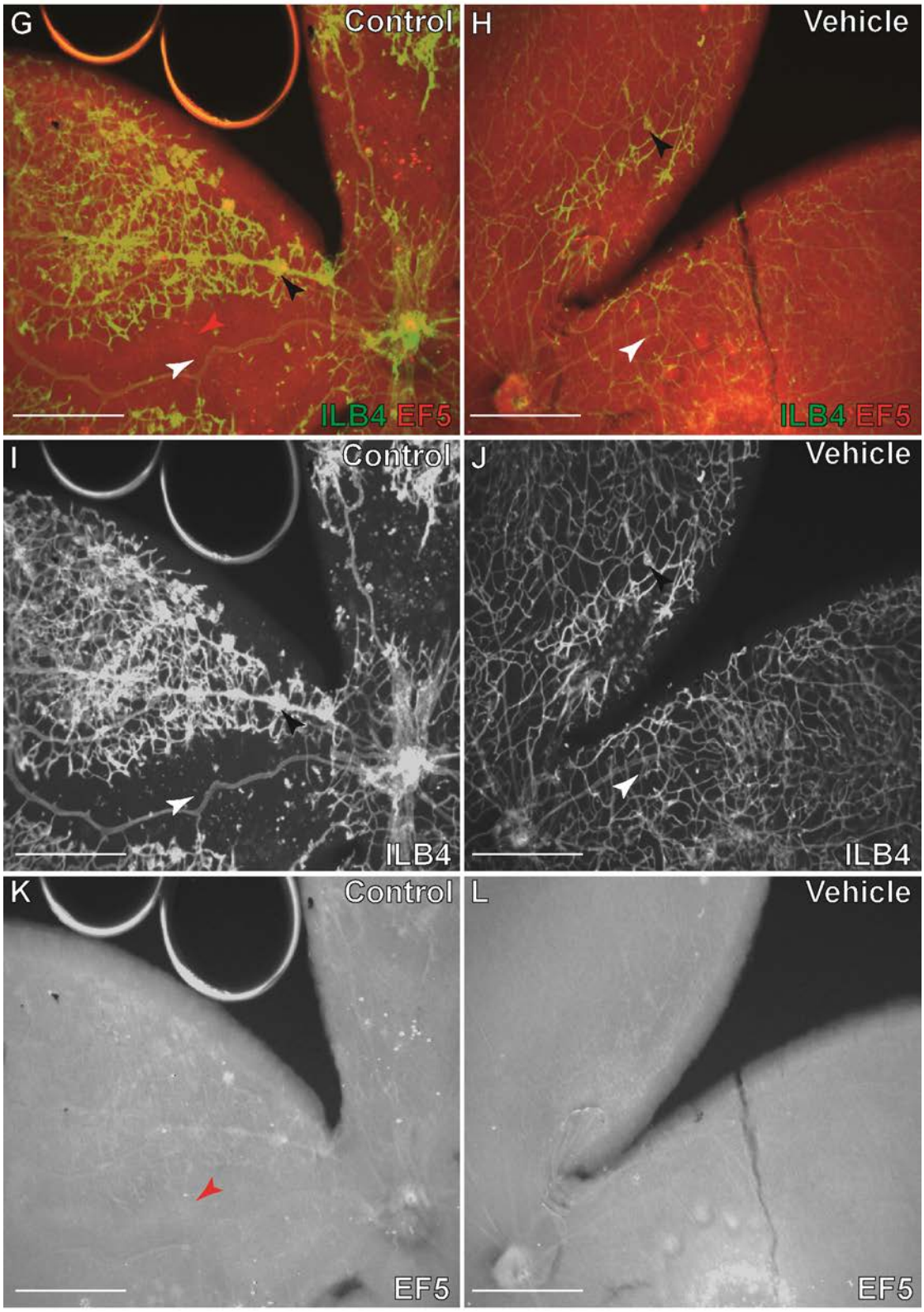

Figure 3.28(b) – Intraocular injection of vehicle at P12 after hyperoxia leads to reduced neovascular phenotype at P17 in OIR. *Higher magnification images demonstrate the classical tortuous retinal arteries (I) (white arrows), neovascular tuft formation (I) (black arrows) and* central areas of vaso-obliteration (K) which are weakly positive for EF5 hypoxia staining (red arrow) *associated with OIR at P17 seen in the non-injected control eyes. Whereas in the vehicle injected eyes the retinal arteries are significantly straighter and there is less neovascular growth (J). Scale bars = 50µm*

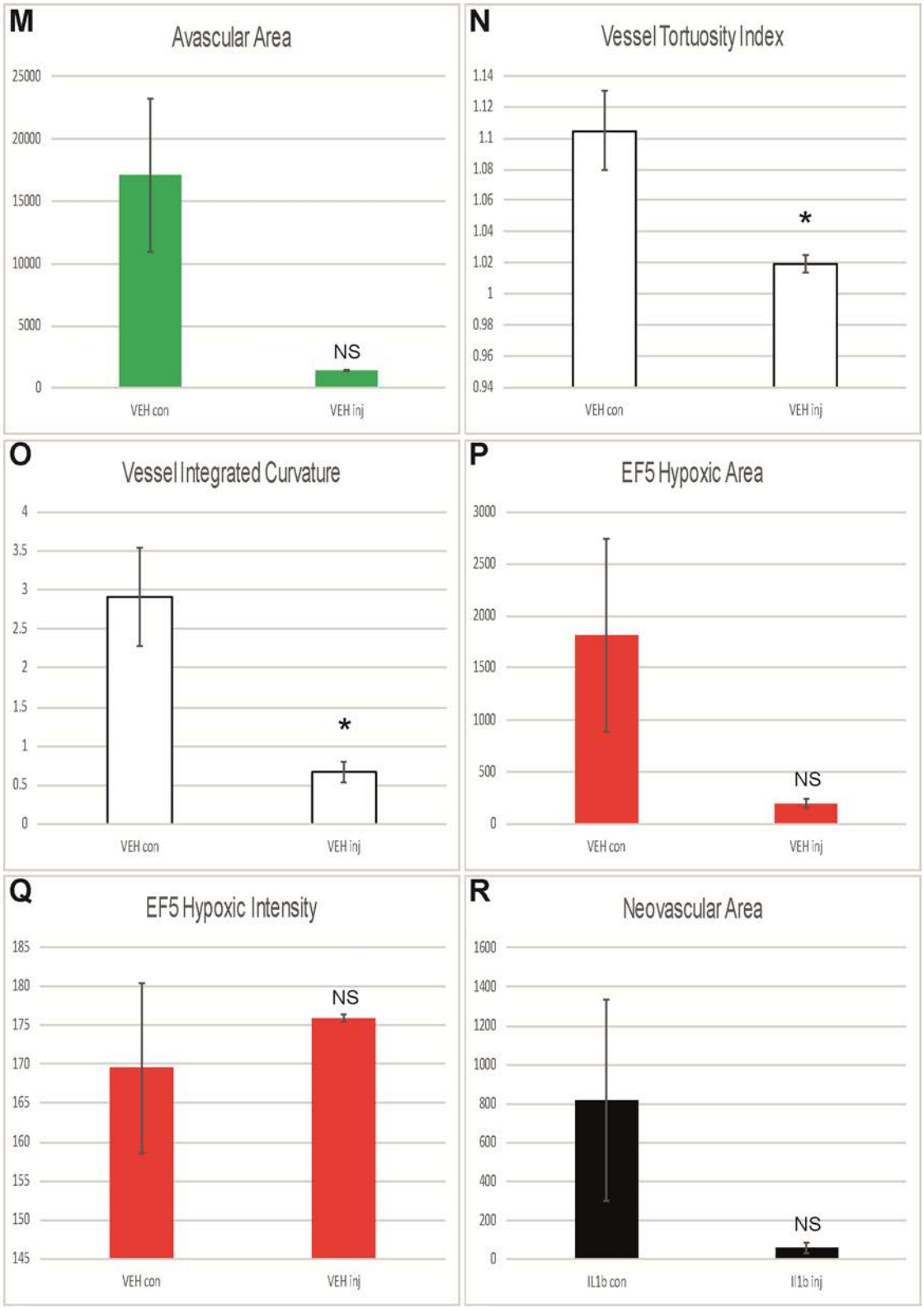

Figure 3.28(c) – Intraocular injection of vehicle at P12 after hyperoxia leads to reduced neovascular phenotype at P17 in OIR. *Avascular area (M), vessel tortuosity (N,O), EF5 hypoxic area (P) and neovascular area (R) where all reduced in the vehicle injected eyes. However, only retinal artery tortuosity as measured by tortuosity index (N) and integrated curvature (O) were statistically significant. (n= control 2 vs vehicle injected 2; error bar = standard deviation; NS=non-significant, NS = non-significant, *=p<0.05)*

3.5.3 Systemic injection of IL1β reduces hypoxia at P14 in OIR

As intraocular injections of IL1β and vehicle lead to a similar reduction in hypoxia and neovascularisation as intraperitoneal injections of LPS, it was hypothesised that systemic LPS upregulates ILβ1 expression in the retina which is then responsible for the reduction in hypoxia. This was corroborated by the RNA sequencing data. This however assumes that LPS exerts a local effect on the retina.

To investigate whether systemic IL1β or vehicle could cause the same phenotype seen in systemic LPS treated OIR mice, a litter of C57BL6 mouse pups underwent the same OIR protocol previously described but pups received either an intraperitoneal injection of IL1β or vehicle at P12. Pups were culled at P17 and immunohistochemistry was performed on retinal wholemounts to examine hypoxia (**Figure 3.29**).

Mouse pups in the vehicle injected group, were found to demonstrate the typical hypoxic phenotype associated with the OIR model at P14 characterised by tortuous retinal arteries **(Figure 3.29I**), central areas of vaso-obliteration (**Figure 3.29C**) which were positive for EF5 hypoxia staining (**Figure 3.29E**) and did not recreate the picture seen when vehicle was injected intraocularly.

Mouse pups in the IL1β treatment group demonstrated a similar picture of central areas of vaso-obliteration (**Figure 3.29D**), however within these avascular areas the retinal arteries appeared straight (**Figure 3.29D**) and the areas of EF5 hypoxia stain within them appeared smaller (**Figure 3.29F**) suggesting reduced retinal hypoxia. Further examination of the avascular areas revealed an influx of activated isolectin positive immune cells in the IL1β treated group but not in the vehicle treated group (**Figure 3.29I,J**).

Comparison between the two groups showed no significant difference in the avascular areas suggesting that both groups underwent similar vaso-obliterative periods in the hyperoxic period with equal levels of vascular regeneration between P12 and P14. The retinal arteries were significantly less tortuous in the IL1β treated group, as measured by tortuosity index and integrated curvature ($p<0.05$). The Il1β treated group also demonstrated significantly less hypoxia, as measured by EF5 stain area, intensity and density ($p<0.05$) (**Table 3.17**).

Table 3.17: P14 OIR: vehicle vs IL1B

	TreatmentGroup	N	Mean	Std. Deviation	Std. Error Mean
AvascularArea	Vehicle	10	40418.4	3994.63	1263.21
	IL1B	10	35456.0	9384.13	2967.52
VesselTortuosityIndex	Vehicle	10	1.07	.03	.01
	IL1B	10	1.03	.01	.00
VesselIntegratedCurvature	Vehicle	10	2.48	.57	.18
	IL1B	10	.96	.29	.09
EF5HypoxicArea	Vehicle	10	10297.6	1597.29	505.11
	IL1B	10	4677.80	2209.01	698.55
EF5HypoxicIntensity	Vehicle	10	113.39	22.80	7.21
	IL1B	10	96.65	7.08	2.24
EF5HypoxicDensity	Vehicle	10	1.15E+6	196749.06	62217.52
	IL1B	10	453451	220761.16	69810.81

	Levene's Test for Equality of Variances		t-test for Equality of Means						
								95% Confidence Interval of the Difference	
	F	Sig.	t	df	Sig. (2-tailed)	Mean Difference	Std. Error Difference	Lower	Upper
AvascularArea	5.389	.032	1.539	18	.141	4962.40	3225.20	-1813.49	11738.29
			1.539	12.158	.150	4962.40	3225.20	-2054.59	11979.39
VesselTortuosityIndex	8.962	.008	5.320	18	.000	.04	.01	.03	.06
			5.320	10.928	.000	.04	.01	.03	.06
VesselIntegratedCurvature	4.751	.043	7.568	18	.000	1.52	.20	1.10	1.95
			7.568	13.263	.000	1.52	.20	1.09	1.96
EF5HypoxicArea	2.305	.146	6.519	18	.000	5619.80	862.04	3808.73	7430.87
			6.519	16.391	.000	5619.80	862.04	3795.90	7443.70
EF5HypoxicIntensity	6.033	.024	2.218	18	.040	16.74	7.55	.89	32.60
			2.218	10.721	.049	16.74	7.55	.08	33.41
EF5HypoxicDensity	.358	.557	7.482	18	.000	699645.10	93512.40	503182.85	896107.35
			7.482	17.766	.000	699645.10	93512.40	502997.59	896292.61

Table 3.17 – Statistical Comparisons of P14 vehicle vs IL1β treatment groups

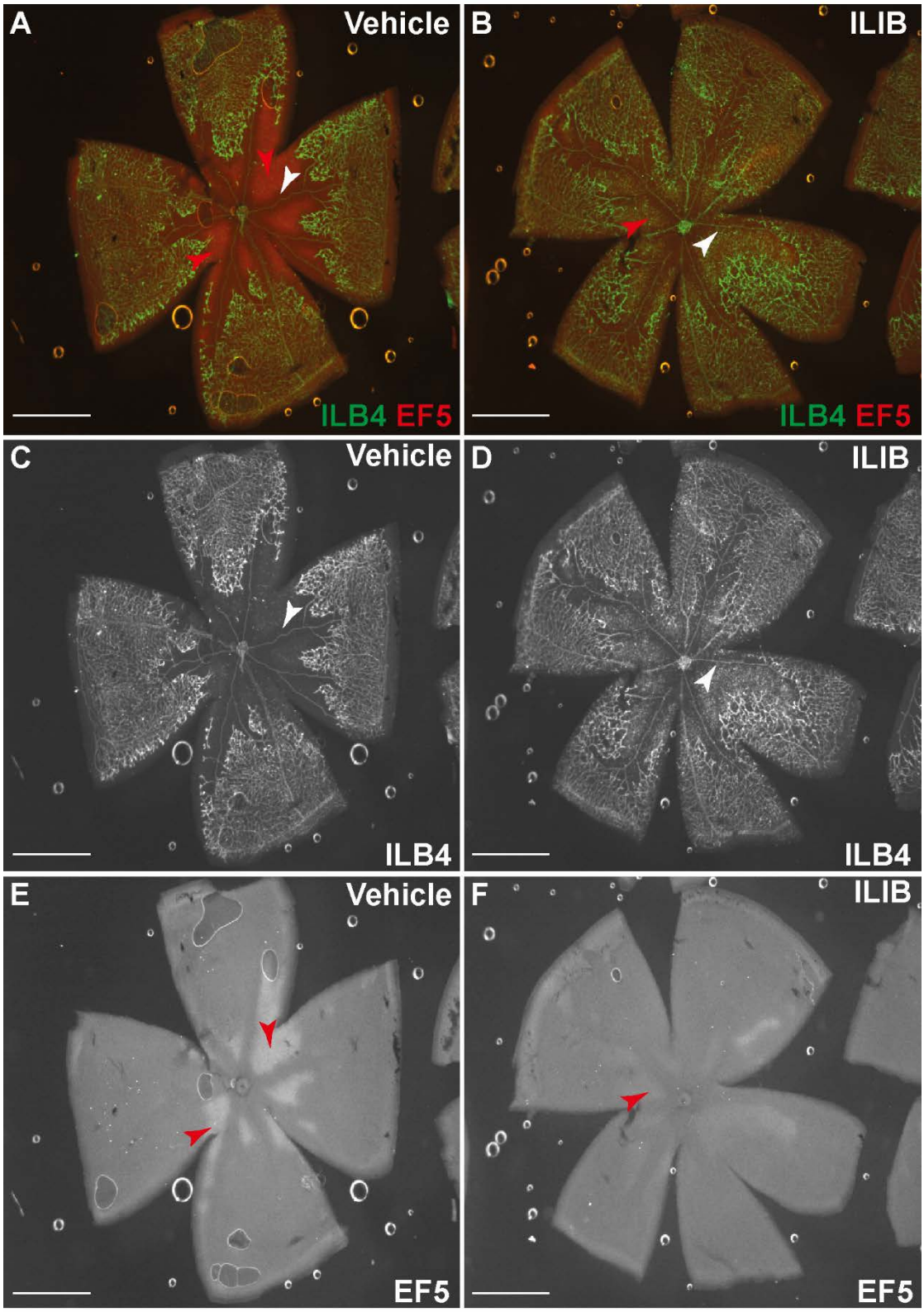

Figure 3.29(a) – Intraperitoneal injection of IL1β at P12 after hyperoxia reduces hypoxia at P14 in OIR. *Retinal wholemounts from P14 C57BL6 mice after OIR stained with isolectin B4 and EF5 hypoxia stain. Mouse pups in the vehicle injected control group demonstrate central areas of vaso-obliteration (C) which are positive for EF5 hypoxia staining (E) (red arrows). IL1β injected eyes appeared to demonstrate a reduction in area and intensity of EF5 hypoxia staining (F) Retinal arteries (white arrows) appear straighter in IL1β injected eyes (D). Scale bars = 100μm*

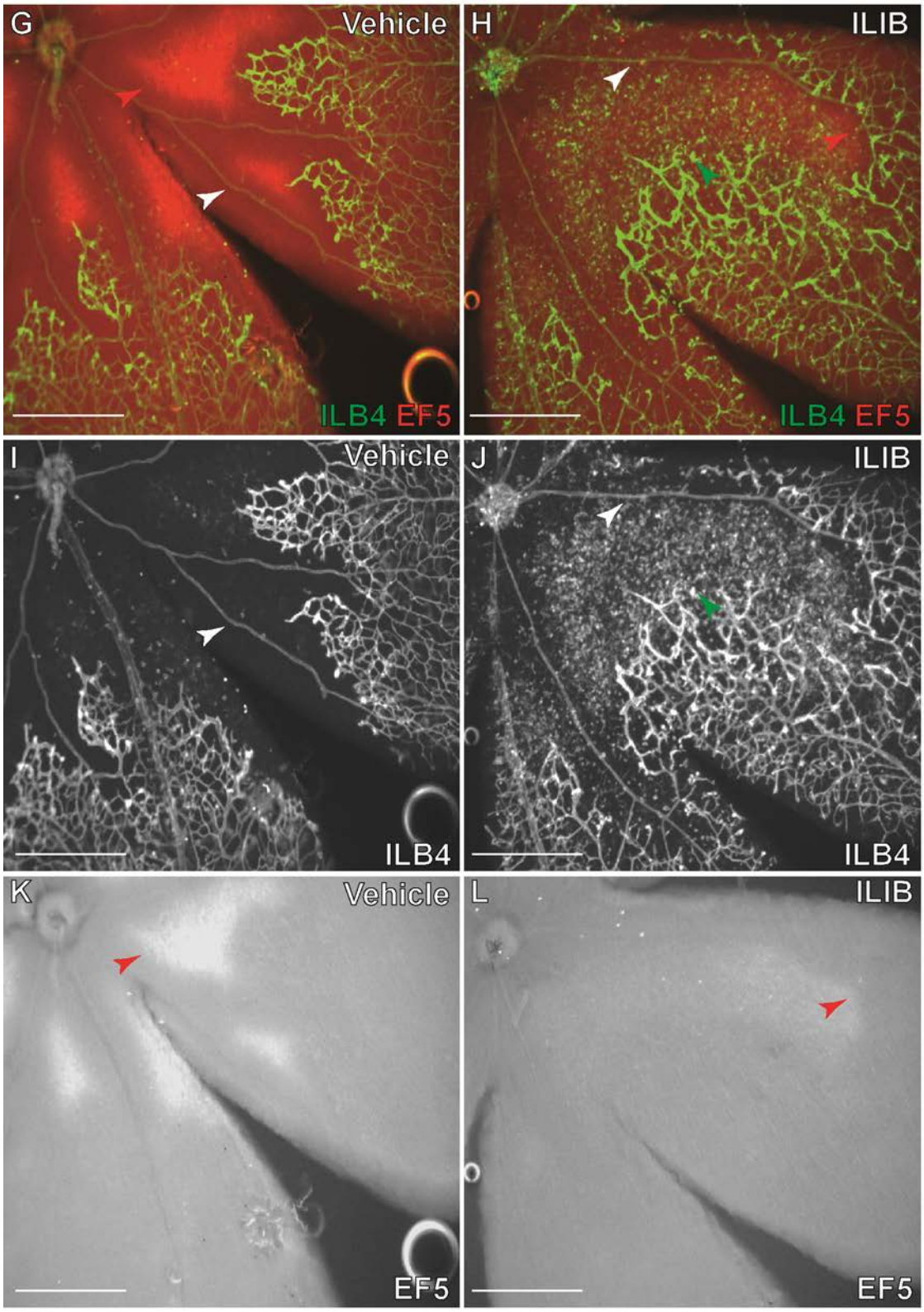

Figure 3.29(b) – Intraperitoneal injection of IL1β at P12 after hyperoxia reduces hypoxia at P14 in OIR. *Higher magnification images demonstrate the classical tortuous retinal arteries (I) (white arrows) associated with OIR at P14 seen in the vehicle injected group. In the IL1β injected group the retinal arteries appear straight (J). In the IL1β injected group a large influx of isolectin positive cells (green arrows) is seen in the avascular area (red arrows) (J). Scale bars = 50µm*

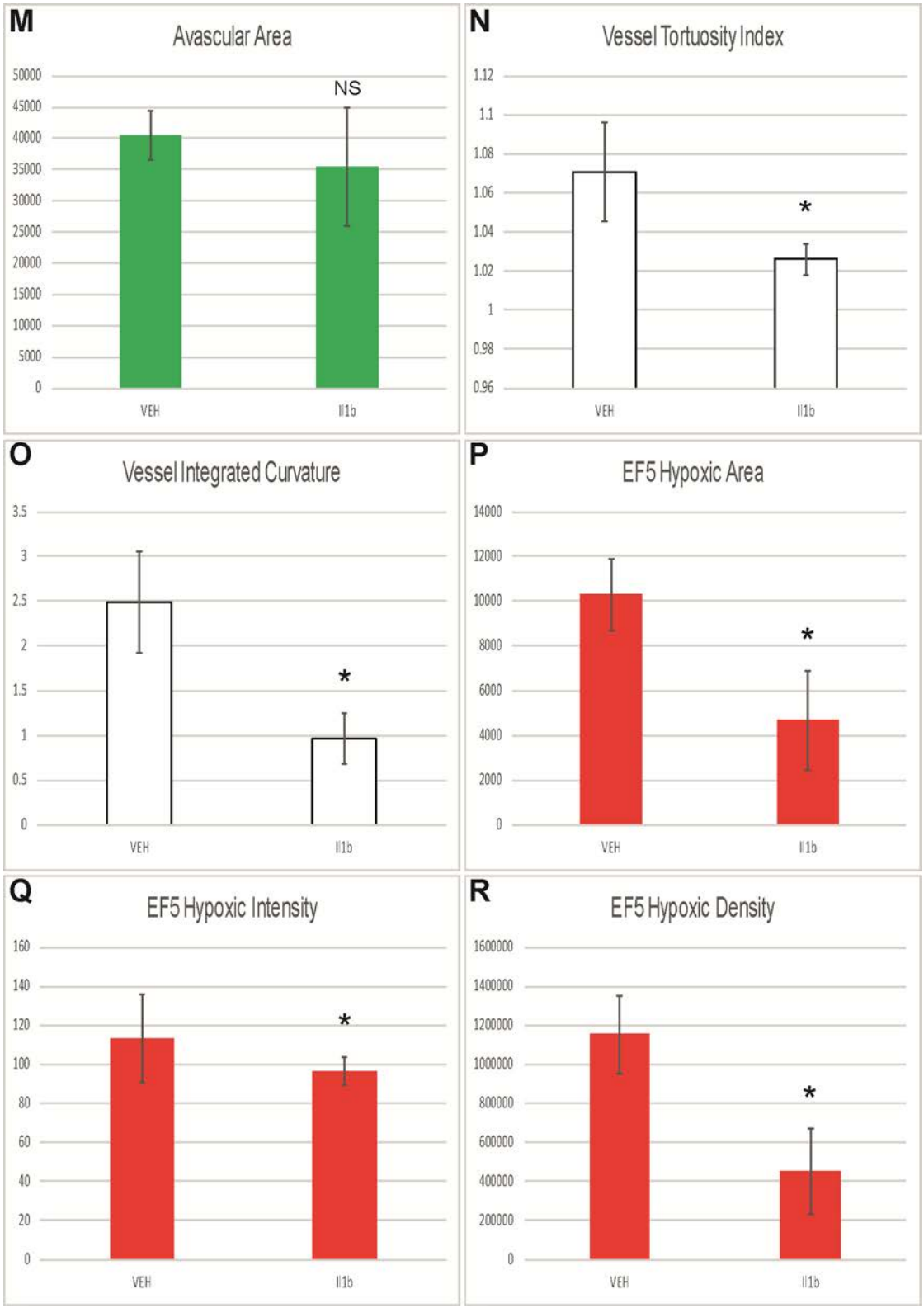

Figure 3.29(c) – Intraperitoneal injection of IL1β at P12 after hyperoxia reduces hypoxia at P14 in OIR. *No significant differences were seen in the avascular area between the two groups (M). Retinal artery tortuosity measures were significantly reduced in IL1β injected eyes (N,O) as were EF5 hypoxia measures (P-R). (n= vehicle 10 vs IL1β 10; error bar = standard deviation; NS=non-significant, *=p<0.05)*

These results demonstrate that systemic IL1β injection replicates the effects of systemic LPS injection at P12 in mice undergoing. Not only does the intraperitoneal injection of IL1β reduce the hypoxic phenotype seen at P14 but it also causes the same influx of lectin positive inflammatory neutrophils and monocyte/macrophages into the avascular area. Intraperitoneal injection of vehicle in comparison did not have the same effect that intraocular injections of vehicle had on retinal hypoxia.

4. Discussion:

4.1 Inflammation in ischaemic retinopathy reduces hypoxia and neovascularisation

Ischaemia is a key component in several retinal diseases and is usually caused by a deficient retinal vasculature. This may occur as a result of either inadequate vascularisation during development, as is seen in retinopathy of prematurity (ROP), or vascular degeneration and vessel occlusion, as is seen in diabetic retinopathy. In an attempt to restore oxygen delivery to the retina, angiogenic stimuli can result in pathological neovascularisation.

Using the OIR model it is possible to model the neovascular aspects of retinal ischaemia in mice. It is still not fully understood why the hypoxia-induced angiogenesis results in pathological neovascularisation rather than physiological normal vascular regeneration. Experiments in which mice are exposed to longterm hyperoxia show that eventually the retinal vasculature will develop as normal (Gu et al. 2002; Zhang et al. 2011). This would suggest that the neovascularisation seen in OIR mice is secondary to the pronounced hypoxia that arises in the retina when they are returned to normoxia rather than the exposure to hyperoxia.

The findings from this thesis demonstrate that systemic activation of inflammation can suppress the retinal neovascularisation seen in the OIR model and allow for healthy regeneration of the retinal vasculature. These results are similar to those seen in preliminary investigations where inflammation was activated locally via intravitreal injection of LPS into the left eye of a P12 litter of C57B6 pups that had been exposed to 5 days of hyperoxia (75% O2) between P7-12. Both these and the preliminary

findings demonstrated that LPS injection resulted in reduced avascular area and reduced formation of neovascular tufts.

This is a novel and somewhat unexpected finding. Activation of inflammation in the eye has traditionally been seen as unfavourable. Previous studies that have involved injection of LPS in mouse pups with developing retinal vasculature have all been noted to result in abnormal vascular development (Chu *et al.*, 2013; Tremblay *et al.*, 2013; Hong *et al.*, 2014). Clinically, postnatal infection and systemic inflammation have been proposed as possible contributing factors to ROP pathogenesis (Dammann, 2010; Lee and Dammann, 2012). There is some evidence that has shown that retinal microglia in the form of both macrophages and monocytes are involved in the formation of new retinal blood vessels and that inhibiting them in rodent OIR can reduce the pathological sequelae associated with ischaemic retinopathy (S Yoshida *et al.*, 2003; Checchin *et al.*, 2006). Inflammatory cytokines such as IL-10 and TNFα have also shown to be pro-angiogenic, and when inhibited in OIR can also reduce neovascularisation (Gardiner *et al.*, 2005; Kociok *et al.*, 2006; Dace *et al.*, 2008), further implying that inflammation in the context of ischaemia contributes to pathology.

However, there is growing evidence that suggests macrophages undergo an angiogenic switch depending on their polarisation and therefore have the potential to be anti-angiogenic under the right conditions (Dace *et al.*, 2008; Wu *et al.*, 2010; Medina *et al.*, 2011)

In this model it appears that in conditions where ischaemia is present, LPS via TLR4 can modulate hypoxia between P12 and P14 as demonstrated by the reduced EF5 staining at P14 in mouse pups injected with LPS IP at P12 in the OIR model.

The nitroimidazole EF5 was used to assess hypoxia in this study. EF5 is biochemically reduced to a product that can bind covalently to protein thiols. This redox-dependent process is progressively inhibited at increasing oxygen tensions and involves the cell-specific action of cellular nitroreductases such as cytochrome P-450 and cytochrome P-450 reductase. The Cy3 conjugated ELK3-51 specific monoclonal antibody recognises macromolecular adducts of EF5 and allows for their detection and localization. Hence, EF5 staining is an indirect measure of tissue hypoxia and provides information on the relative oxygenation of a tissue at a cellular resolution and is commonly used as a readout of tissue hypoxia in rodent models. Given that EF5 staining is not a direct measure of hypoxia, some caution needs to be used in the interpretation of the data derived from it, and hence why three measures of area, intensity and density were calculated. Of the hypoxia measures used, hypoxic area appeared to be the most valid read out and was less likely to be affected by bleed through or interference from other immunohistochemical stains. Vascular tortuosity was also used alongside EF5 hypoxia staining as a read out of hypoxia.

Vascular tortuosity was also found to be reduced at P14 in mouse pups injected with LPS IP at P12 in the OIR model. In the OIR mouse model vascular tortuosity is not commonly used as a readout of hypoxia at P14 (Scott et al. 2014) but has previously been used at P17 as a measure of neovascularisation (Lange *et al.*, 2009; Higgins *et al.*, 1999). Clinically, vessel tortuosity is a diagnostic sign of hypoxia and quantification of vessel tortuosity has been used to grade ROP (Wilson *et al.*, 2008).

As vascular regrowth occurs between P12 and P17 in the model, with neovessel formation occurring between P14 and P17, the reduction in hypoxia at P14 could explain the reduced neovascularisation seen in the same LPS IP treated mice at P17.

The hypoxia seen in the OIR model is the result of an imbalance between the supply and demand of oxygen in the retina. In this model of systemic LPS injection, there was no change in the supply of oxygen to LPS treated retinas, as evidenced by similar avascular areas between the control and treated groups. Therefore it is possible that in the LPS treated mice the oxygen demand of the retina was reduced. Most research into ischaemic retinopathy has been concerned with improving oxygen supply to the hypoxic retina, however this approach demonstrates that it would be possible to reduce hypoxia by reducing oxygen demand.

Laser photocoagulation and previously cryotherapy have been the treatment of choice for high risk ROP because they reduce the oxygen demand of the hypoxic retina by ablating tissue. Therefore, it should be considered that a potential mechanism by which LPS reduces oxygen demand in the retina is through cell death. However, no significant differences were seen in retinal thickness at P14 in cross sectioned retinal tissue taken from mouse pups treated with LPS or PBS at P12 after 5 days of hyperoxia exposure between P7-P12.

With the increasing use of anti-VEGF therapies for the treatment of neovascularisation associated with age related macular degeneration and diabetic retinopathy, anti-VEGF injections are now being considered in the treatment of proliferative ROP (although definitive data are not yet available). Another possible explanation for the reduction in metabolic activity in the retina could be that systemic inflammation down-regulates VEGF expression and the proliferation normally seen in the immature, developing retinal vasculature at P12. BrDU staining showed that proliferation in the retinal flatmounts of both LPS and PBS injected P12 C57B6 pups that had been exposed to 5 days of hyperoxia (75% O2) between P7-12 was restricted to the retinal vasculature at

P14. Notably, the number of proliferating vascular cells was considerably reduced in the LPS treated group. The reduction in proliferating cells in the retinal arteries of LPS treated mice may explain why the arteries appear less tortuous than in their PBS treated control counterparts. A possible explanation for this could be that the reduction in hypoxia seen in the avascular area as a result of LPS treatment results in reduced Hif1a, which is a known transcriptional activator of VEGF (Semenza, 2001) and has been shown to affect vascular development (Trollmann and Gassmann, 2009). A reduction in VEGF would lead to less proliferation amongst vascular endothelial cells and therefore less tortuosity.

The proliferation profile experiment was only successfully carried out in one litter and so statistical significance could not be applied to the reduction in proliferating cells seen in the vasculature of LPS treated mice. Further studies with the use of new proliferation assays such as EdU staining are required to confirm this finding.

In an attempt to do this and to examine whether the proliferating cells in the retinal vasculature were endothelial specific, an experiment with an Erg 1,2,3 antibody co-stain was performed. In both the PBS and the LPS treated group the Erg 1,2,3 antibody failed to stain endothelial cells, however in the PBS control group the Erg antibody appeared to stain the linear retinal ganglion cell axons in the avascular area. This staining was confined to the avascular area and gave a staining pattern very similar to that seen with EF5 hypoxia staining in the same control group.

ERG, a member of the ETS family of transcription factors, is a highly specific endothelial marker (Kim *et al.*, 2013). ERG was originally recognized for its role as a proto-oncogene in the development of several types of human cancers, especially in prostate cancer (Tomlins *et al.*, 2005), but has since been shown to have a critical role in the

regulation of several vascular-specific genes, including Tie1, Tie2, VEGFR1, VEGFR2, von Willebrand factor (vWF) and endothelial nitric oxide. With regards to the axonal distribution of the staining in the PBS group, it has been shown that LPS induced TLR4 signalling 48hours prior to retinal ischaemia prevented ischaemic cell damage in retinal cells. In particular, there was complete rescue of ganglion cells and this was thought to be associated with LPS induced activation and migration of retinal microglia (Halder *et al.*, 2013). Given that the staining correlates with the hypoxic area seen with EF5 staining this may be a stress response to hypoxia in the avascular area that is protected for by the LPS induction of TLR4.

LPS agonism of TLR4 in inflammatory, epithelial and endothelial cells is known to promote the release of pro-inflammatory cytokines such as TNFα. IL-6, IL-1β, eicosanoids and nitric oxide and causes a systemic inflammatory response. In the mice that undergo OIR and are treated with LPS it is this systemic inflammatory response that is thought to result in a reduction in oxygen demand in the retina. Experiments performed in TLR4 deficient mice showed that the usual inflammatory response seen in the retinas of LPS treated mice (represented by an influx of lectin positive cells) was not seen, confirming that TLR4 induced cytokine signalling and inflammatory cell activation had not occurred. However, surprisingly the usual hypoxic picture of prominent EF5 staining and tortuous retinal arteries was not seen. This could be explained by the fact that the TLR4 deficient mice were bred on the background of C3H mice. C3H mice are known to carry the $Pde6b^{Rd1}$ mutation, which manifests as degeneration of the photoreceptors and preservation of other retinal cell types (Chang *et al.*, 2002). Degeneration of the photoreceptor layer results in thinning of the retina, reduced metabolic activity and therefore less oxygen demand. These thinner C3H/Hej

retinas do not become ischaemic during the OIR model and do not develop neovascularisation (Scott et al, 2014). Further experiments using TLR4 non-deficient C3H mice showed little evidence of hypoxia. In the LPS treated TLR4 no-deficient mice an increased inflammatory response could be seen in the avascular area, as represented by an influx of lectin positive cells, confirming that both LPS and TLR4 are required for the influx of the pro-inflammatory cells into the avascular area.

In these mice, although the degree of hypoxia was reduced in the OIR model, due to reduced oxygen demand of the thinner retinas, there still appeared to be mild areas of hypoxia staining with EF5. To definitively prove that LPS binding the CD14/TLR4/MD2 complex causes the reduction in hypoxia seen, the TLR4 deficient gene would need to be crossed out of the C3H background. Also, to prove that it is the hypoxia that is driving the influx of the inflammatory cells into the avascular area, repeated experiments with the C3H mice are needed to show that when there is no evidence of hypoxia, LPS injection does not result in an influx of inflammatory cells into the avascular area. Preliminary investigations (not shown in this report) on P14 control C57Bl6 mice that were not put through OIR were injected with LPS IP at P12 to see if this population entered the retina when no avascular area or hypoxia was present in the retina. No such invasion occurred. This implies that the influx of inflammatory cells into hypoxic retinas is not secondary to an endotoxin-induced uveitis.

In conclusion these results shown that IP injection of LPS at P12 in mice with hypoxic retinas, leads to reduction of hypoxia, even though the central zone is still avascular. This leads to a healthy revascularization of the central zone by P17 without the formation of pathological tufts. It is thought that LPS is triggering an inflammatory response in the retina, which is protecting it from the effects of future ischaemia by

reducing the metabolic demand of the retina, which results in less utilisation of oxygen rendering the tissue less hypoxic.

4.2 Systemic Inflammation induces an invasion of myeloid derived neutrophils and monocyte/macrophages into hypoxic areas of retina.

In attempting to characterise the round-bodied cells, seen in increasing numbers in P14 retina after LPS IP injection at P12, this study confirmed through genetic targeting and immunohistochemistry that they are of myeloid lineage, e.g. macrophages, monocytes or neutrophils, and are non-resident to the retina. Analysis of this cell population, using a myeloid specific panel with flow cytometry, indicates that the invading cell population is predominantly neutrophilic in nature but also includes some inflammatory monocyte/macrophages.

Using the LysMCre GFP reporter model to label cells of the myeloid lineage, meant that the movement of these cells could be tracked at various time points prior to LPS injection and OIR induced hypoxia. At P6 when the retinal vasculature is still developing and the superficial primary plexus is still radiating towards the periphery driven by astrocyte expressed VEGF in response to peripheral hypoxia (Scott et al. 2010), there was no evidence of the round bodied, lectin stained population. This implies that moderate hypoxia alone, without LPS injection, as occurs in the retinal periphery of the developing retina, is not sufficient to cause the same influx of the neutrophils into the retina. However, cells expressing GFP were seen at the vascular front and in the avascular area. These cells had an ameboid appearance unlike the round appearance of the lectin positive cells seen invading the hypoxic area of LPS treated mice retinas and also stained for IBA1, which suggests that they were resident microglia rather than

invading myeloid cells. Similar cells were seen at P10 after 3 days of hyperoxia and at P12 after 5 days of hyperoxia.

The precise origin and cell lineage of microglia is still a matter for debate. Microglial progenitors arise from peripheral mesodermal tissue. The view still commonly held is that tissue-resident mononuclear phagocytes (including microglia) are derived from circulating blood monocytes and these take up residence late in gestation and postnatally. However, microglial progenitors colonise the nervous system primarily during embryonic and fetal periods of development. Recent evidence indicates differences between the lineage of mononuclear phagocytes during the embryonic and fetal period from those in the neonate and adult—mononuclear phagocytes that take up residence within tissues are derived from a lineage of myeloid cells that is independent of the monocyte lineage (Chan et al., 2007).

In the LysMCre model it has been noted that transcription of lysozyme starts early during development, is low but detectable in resident tissue macrophages and can be substantially elevated in response to infectious agents (Clausen *et al.*, 1999). This may explain why GFP is present in the resident population as well as in the invading population seen after LPS injection.

Flow cytometry was able to further separate the incoming myeloid population and show that although there was an increase in "classic" Cd11b+ F4/80+ Ly6C^{hi} inflammatory monocyte macrophages subset, the biggest increase was in the neutrophilic Cd11b+ Ly6G^{hi} subset. In terms of cell counts the number of Cd11b+ F4/80+ Ly6C^{lo} resident monocyte/macrophages showed little change between the three groups. Given that neutrophils are the first cells to be recruited to local site of pathogen invasion in order to provide an immediate defence against infections in

tissues (Kawamoto and Minato, 2004), it is not surprising that they are abundant in LPS injected mice.

Despite having established that the myeloid cells which invade into hypoxic retinas of mice treated systemically with LPS are predominantly neutrophils, these results do not identify whether it is these cells that are modulating the hypoxia in the OIR model or whether the invasion is secondary to the reduction in hypoxia. One possible explanation for the effect LPS has on the hypoxia post vaso-obliteration could be the systemic changes in cytokine expression that result from LPS TLR4 interaction. This may either lead to changes in cytokine expression in the avascular area or this may result in activation of the microglial cells, which despite not changing in number, become activated and induce a hypoxia reducing effect.

To investigate whether cytokine expression in these LPS treated retinas is changed by activation of the neutrophils or the microglia, intracellular cytokine secretion analysis could be performed in future using flow cytometry and the same myeloid panel as used previously.

In conclusion, the invading cell population has been identified as being mostly neutrophilic.

4.3 The invasion of myeloid derived neutrophils and monocyte/macrophages are not responsible for the reduction in hypoxia

Identifying the invading population of cells as being LysM positive neutrophils and inflammatory monocyte/macrophages meant that the invading cells could be targeted. As a result, the infiltrating number of these cells into the retina were successfully reduced through genetic and therapeutic methods. However, despite this reduction in

the invading population, mice treated with LPS still displayed a reduced hypoxic phenotype at P14 after OIR.

In mouse pups that were injected with LPS IP at P12 after 5 days of hyperoxia between P7-12, there was no difference in vascular tortuosity or hypoxia staining between transgenic LysMCreDTA mice and wildtype controls, despite an almost complete depletion of the invading neutrophils and monocyte/macrophages. When the same experiment was tried using the anti-CCR2 MC21 antibody directed against the same inflammatory population, the results were more mixed. MC21 treated retinas displayed a greater avascular EF5 hypoxic area suggesting that the reduction in invading cells resulted in greater hypoxia. However, examination of the retinal arteries showed significant straightening of the vessels implying that hypoxia was reduced. A criticism of this result is the presence of "bleed-through" of a Cd11b stain into the same channel used to assess the EF5 stain, which may have inadvertently affected the results. Although considering that the MC21 treatment should have reduced the number of Cd11b+ cells in the avascular area, it would be expected that the EF5 hypoxic area wold be greater in the wild type mice if this was the case.

Regardless of this, in all the experiments where the invading inflammatory cell population was reduced and LPS treatment was compared to PBS controls, the LPS treatment groups always displayed statistically significant straighter retinal arteries than the PBS control group. There were no statistically significant difference between EF5 hypoxic measures between the PBS and LPS treatment group in all experiments. A criticism of these experiments is the low n-numbers involved. With more mice, the reduction in EF5 hypoxia measures may reach statistical significance. Although in principle, four different methods of depleting/reducing the invading neutrophil and

inflammatory monocyte/macrophage population all resulted in the same results, i.e. depletion of the incoming myeloid cell population is irrelevant to the reduction in hypoxia seen with LPS treatment. This would imply that the cells are drawn to the retina secondary to the reduction in the hypoxia. Possible explanations for this finding may be that LPS triggers a systemic cytokine upregulation, which alters the metabolism of the retina and then chemoattracts the neutrophils and inflammatory monocyte/macrophages. It is also possible that it is in fact the resident microglial population that are activated by LPS and are protective of the retina.

As well as having an effect on circulating myeloid cells, LPS has been shown to activate microglia and can induce transient neuroprotection against ischaemia and stroke (Chen *et al.*, 2012). It was initially hypothesised that intraperitoneal injections of LPS initiating TLR4 signalling through macrophages that are highly enriched in the peritoneal cavity or that LPS diffuses into the bloodstream, where it could stimulate circulating immune cells. An alternate hypothesis would be that the peripheral LPS signal permeates the central nervous system and activates resident microglia within the brain and retina. However, it remains to be determined whether peripherally injected low LPS can directly stimulate microglia or whether it triggers a pathway through cytokine messengers that ultimately lead to microglial activation (Chen *et al.*, 2012). Iba1 has been shown to be upregulated when microglia are activated and immunohistochemistry of the flatmounts consistently highlighted a population of Iba1 positive microglia in the avascular area. Future work looking at depleting the microglial population may provide further insight.

Analysis of the flatmounts failed to show complete depletion of the round-bodied lectin positive cells in the LPS treated retina. The LysMCre model has been reported to

have a deletion efficiency of 83-98% in mature macrophages and near 100% in granulocytes, with 80% in developing macrophages (Clausen *et al.*, 1999). Approximately 86% of Ly6C^{hi} monocytes have been shown to express CCR2 (Saederup *et al.*, 2010) and the MC21 antibody has been shown to delete up to 92% of Ly6C^{hi} CCR2+ monocytes (Liu *et al.*, 2013). Although actual numbers of the non-depleted invading cells weren't quantified in these experiments, it would appear that the level of depletion achieved in each of the experiments was in-line with the levels of expression reported in the literature. To formally assess the exact level of depletion achieved flow cytometry would need to be performed using the same myeloid panel previously described.

Given the incomplete deletion of all the incoming cells it is not possible to definitively rule out the role of these cells in the reduction of retinal hypoxia, as only a small percentage may be needed to reduce the oxygen demand of the retina and reverse the hypoxia. However, it seems unlikely that a metabolic switch in the remaining inflammatory cell population would be sufficient to reduce the metabolic demand of the entire retina. A more plausible explanation would be that other cells in the retina, such as Müller cells or astrocytes, also undergo a metabolic switch in response to LPS activated inflammatory cells or cytokines. It has previously been shown that cultured Müller cells are less susceptible to ischaemia because they obtain ATP mainly from glycolysis and have a low oxygen consumption rate (Winkler et al., 2000). Glial fibrillary acidic protein (GFAP) is known to be upregulated as a response to trauma or ischaemia and GFAP expression can be used as a marker of retinal stress. In preliminary experiments performed in the lab (not shown in this report), GFAP was seen to be upregulated in Müller cells throughout the retina in mice injected with LPS, including

the peripheral vascularised areas. This would suggest that Müller cells are responding to the pro-inflammatory insult induced by LPS and that they may be switching to glycolysis as a result. More work needs to be done to see whether there is cross-talk between the invading neutrophils/monocyte/macrophage population and cells of the retina such as Müller cells.

However, based on the current findings it seems that LPS exerts its hypoxia reducing effects via another mechanism than neutrophil invasion into the hypoxic retina.

4.4 Systemic LPS injection modulates retinal hypoxia and metabolism through cytokine signalling

On examination of the RNA sequencing results it was clear that in the samples analysed there was clear distinction between the samples that had undergone OIR and the age matched control and between the LPS and PBS treated OIR samples. Hypoxic markers were upregulated in both OIR samples compared to the age match control and cytokine and inflammatory markers were upregulated in the LPS injected samples. Also in both OIR groups there appeared to be upregulation of hypoxic factors in the central retina compared to the peripheral retina which correlates with the phenotype seen on retinal flatmounts with the majority of the avascular and hypoxic areas being in the central retina. This validates the methodology used.

However, the data does need to be interpreted with care. Many of the changes between samples when compared as fold changes were relatively small; so looking at individual changes in isolation, unless the fold changes are significantly large, is unlikely to be meaningful. Also, given that only single samples were run for each group, repeated runs with numerous samples would be needed to verify that the results are

true. If further work was to be done using RNA sequencing on a greater number of samples, a more sophisticated method of analysis such as pathway analysis would need to be employed.

Nevertheless, the sequencing data in this study does allow the investigation of trends in certain groups of genes which have similar functions and to pick out genes with large fold changes that may play a role in modulating the hypoxia seen in the OIR model.

The majority of hypoxia markers correlated with upregulation in OIR and downregulation in LPS in the central retina (with the exception of HIF1a, Mt1 and Hmox1). HIF1a was found to be greater in the P14 control than compared to both OIR models, however this can be explained by the fact that hypoxia related changes to HIF1a occur post-translation, so little change in mRNA would be expected. VEGF, although found to be decreased in the central retina after LPS injection, showed only a 5% reduction, which is lower than expected. Preliminary data looking at mRNA levels of VEGF in retinas treated with LPS in OIR showed that LPS significantly reduced VEGF expression when compared with PBS controls (data not shown in the report).

Analysis of the genes involved in retinal metabolism and energy production failed to show any large fold increases between the central retina of LPS treated and PBS treated OIR groups, as was hypothesised. However, of the genes highlighted, Pfkfb3, Hk1 and HK2 were found to be upregulated in the central retina of LPS treated OIR retina when compared to PBS treated retina. Pfkfb3, Hk1 and HK2 are all known to be important in the glycolytic pathway. Although the actual fold change was only 13-15% for both Pfkb3 and Hk1, this could be enough to reduce the metabolic demand of the retina and reduce hypoxia. M1 macrophages that are activated via LPS induced TLR4 signalling induce glycolysis and reduce oxidative metabolism in the mitochondria. By

inducing glycolysis, through the induction of enzymes including PFKFB3, they produce ATP required for biosynthesis as well as maintenance of mitochondrial potential. The maintained mitochondrial potential protects cells from apoptosis and cell death (Garedew et al., 2010).

The analysis of the cytokine and inflammatory genes revealed more impressive fold changes. As expected, the cytokine and inflammatory markers were upregulated in the OIR sample injected with LPS compared to the OIR sample injected with PBS, confirming that LPS stimulation of TLR4 had indeed worked in this sample. Interestingly there seemed to be no differences between central and peripheral retina in the LPS treated group suggesting that any activation by LPS happens throughout the retina and not just in the avascular area.

Analysis of inflammatory cell surface markers appear to correlate with previous investigations in that Cd11b, Csf3rC and Ccr2 were found to be increased in the LPS treated retina and are most likely representing the invading population of neutrophils that had previously been characterised. Interestingly markers of resident microglia such as Iba1 and CXC3R appear to be upregulated in the LPS treated OIR model, which is in contrast to previous findings but may point to the role of microglia activation in this model. Some cytokines that are known to be upregulated by LPS and in OIR were not found in the sequencing database. These included TNFa, Il6 and Il10 to name a few.

The biggest fold changes were noted in Il1β (72 fold increase), CCR1 (16 fold increase), CCL5 (13 fold increase) and CCR2 (13 fold increase).

It has been shown that IL-1β inhibits mitochondrial energy metabolism of retinal neuronal cells and decreased oxygen consumption by nearly half (Abcouwer et al.,

2008). It is possible that IL-1β generated in our LPS injected mice may be contributing to a metabolic switch to glycolysis and saving on oxygen consumption as a result.

4.5 IL1β in ischaemic retinopathy reduces hypoxia and neovascularisation

One of the aims of the RNA sequencing experiments was to find certain cytokines or signals that were upregulated as a result of TLR4 stimulation by LPS, with a view to directly inject suitable candidates directly into the eyes of pups at P12 after hyperoxia, to see if a similar reduction in hypoxia was possible. The two standout cytokines that were found to be upregulated in the LPS treatment group were IL1β and CCL5 and as a result they were selected for intraocular injection.

These intraocular cytokine injection experiments showed that IL1β intraocular injection is able to recreate the hypoxia reducing effects seen in the LPS treatment groups of previous experiments. IL1β also attracted the same population of neutrophils and inflammatory monocyte/macrophages into the avascular areas. CCL5, although found to be upregulated in the RNA sequencing data, was not able to create the same hypoxia reducing effect as IL1β, although some invading inflammatory cells were noted in the avascular areas of these retina. This correlates with the findings from the RNA sequencing data from the LPS treated central retina, in which IL1β demonstrated a 72-fold increase in comparison to the 13-fold increase in CCL5 expression when expression was compared to that of the PBS control central retina.

Systemically, IL1β upregulation results in increased expression of chemokines, cytokines and growth factors, upregulation of adhesion molecules which in turn result in increased leukocyte infiltration. Other downstream effects of IL1β include

alterations in blood flow, platelet activation, decreased neurogenesis and increased angiogenesis (Dammann, 2010; Sobowale *et al.*, 2016).

The finding that IL1β injection in ischaemia can reduce hypoxia and prevent neovascularisation is a novel finding and is contrary to the current literature. Similar to LPS, IL1β has been linked to the worsening of retinal vasculopathies. IL1β is one of the main inflammatory cytokines and has previously been shown to play a role in angiogenesis and promote neovascularisation (Carmi et al., 2009; Lavalette et al., 2011; Olson et al., 2009).

IL1β is a potent regulator of the innate immune response and has been associated with cerebrovascular disease and injury. IL1β has been shown to act as a key driver of the innate immune response to inflammation in the murine brain (Giles *et al.*, 2015). IL1 administration in rats has been shown to exacerbate cerebrovascular ischaemia (Yamasaki *et al.*, 1995). Systemic injection of IL1 prior to cerebral ischaemia reperfusion has been shown to significantly worsen outcomes in both mice and rats (McColl et al., 2007; McColl et al., 2008; Murray et al., 2014). These studies also found increased expression of IL1 in response to ischaemic stroke and that IL1 receptor antagonist has a neuroprotective effect.

In a transient model of retinal ischaemia in rats, IL1β was found to be increasingly expressed by retinal glial cells, endothelial cells and by neutrophils that invade into the retina on reperfusion (Hangai et al., 1995). Retinal microglia have also been shown to highly express IL1β when they become activated in hypoxic conditions (Rivera *et al.*, 2013). In both these studies IL1β upregulation led to a worsening of the hypoxic and neovascular conditions.

In both, the LPS treated and IL1β treated, experiments in this thesis both neutrophil invasion and microglia activation occurred in the avascular retina, but in contrast, there was a reduction in hypoxia and neovascularisation. It has been shown that IL-1β inhibits mitochondrial energy metabolism of retinal neuronal cells and decreased oxygen consumption by nearly half (Abcouwer et al., 2008). It is possible that IL-1β generated in our LPS injected mice may be contributing to a metabolic switch to glycolysis.

M1 macrophages activated by LPS have an increased energy demand in order to respond to tissue injury. It has been shown that they can switch their core metabolism from oxidative phosphorylation to glycolysis (Krawczyk *et al.*, 2010; Rodriguez-Prados *et al.*, 2010). The metabolic changes that occur are similar to those described as the Warburg effect originally described in cancerous cells. In experiments where glycolysis is inhibited LPS-induced IL1β production is found to be suppressed in macrophages. Metabolic mapping of LPS activated macrophages revealed an up regulation in genes responsible for glycolysis and a down-regulation in mitochondrial genes. LPS induced succinate production was also found to stabilise HIF-1α and lead to increased IL1β production during inflammation (Tannahill *et al.*, 2013). Pyruvate kinase M2 (PKM2) has also been shown to modulate IL1β production which in turn results in macrophage polarisation, glycolytic reprogramming and the Warburg effect in LPS activated macrophages **(Figure 4.1)** (Palsson-McDermott *et al.*, 2015).

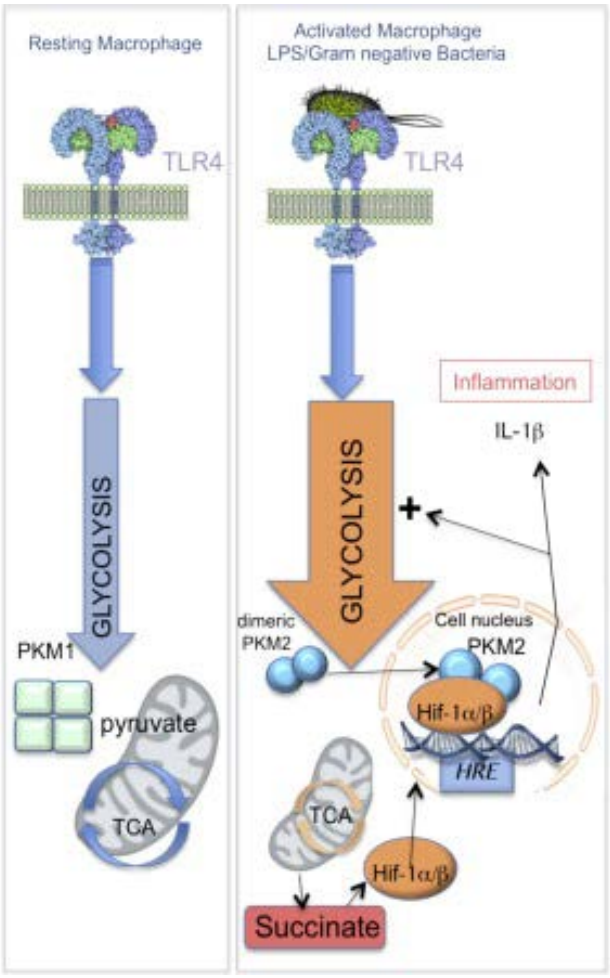

Figure 4.1 – LPS induced glycolytic reprogramming in activated macrophages (Palsson-McDermott *et al.*, 2015)

Endothelial cell metabolism has recently become a novel therapeutic target for treating vascular disease. Glycolysis, fatty acid oxidation, glutamine/asparagine metabolism have emerged as key modulators endothelial cell metabolism which in turn can affect both pathological and physiological angiogenesis. Endothelial cells are highly glycolytic. 6-phosphofructo-2-kinase/fructose-2,6-bisphosphatase 3, a regulator of the glycolytic pathway, has been shown to control vessel sprouting during the angiogenic switch. Given that LPS and IL1β are known to effect endothelial cells it is a

possibility that IL1β could induced a metabolic switch in endothelial cells as it does in macrophages (Draoui, de Zeeuw and Carmeliet, 2017).

Interestingly, just injecting vehicle alone appears to reduce the hypoxic phenotype seen in OIR at P14 to a similar degree as IL1β injection but without the same level of invading inflammatory cells. Rather than contradicting or nullifying the effects of the LPS and IL1β intraocular injections, this finding complements the notion that the stimulation of inflammation within the eye at the time of ischaemia is protective of hypoxia. The intraocular injection of vehicle, which contained 0.1% bovine serum albumin may have caused a mild inflammatory reaction within the eye. This stimulation of the innate immune system within the eye could have been enough to reduce the hypoxia associated with OIR but not enough to trigger the large influx of inflammatory neutrophils/monocytes/macrophages seen with the IL1β and LPS injections. This finding would also further suggest that the invading cells are not responsible for the reduction in hypoxia seen in the cohort. Intravitreal injection of PBS alone has been shown to reduce retinal neovascularization in the mouse OIR model (Maria Vähätupa *et al.*, 2016). This effect however was not seen when the vehicle was injected intraperitoneally, which would suggest a much stronger systemic activation of the immune system is required to result in a retinal phenotype.

Intraocular injections of IL1β were shown to reduce neovascularisation at P17, however, when compared to the initial intraocular LPS injection experiments, the inflammatory response in these retinas was not as severe, despite the reduction in neovascularisation being similar. The LPS intraocular injection also had a systemic effect and resulted in a reduction in neovascularisation in the contralateral non-injected eye, which was not seen in IL1β intraocular injections. This would suggest that

the IL1β injection did not stimulate all of the same pathways as the LPS intraocular injection and that treatment with IL1β was more targeted. However, this may have just been related to the dosing reactivity of the intraocular LPS compared to IL1β. Further studies titrating the doses and effects of IL1β and LPS are needed to further define this effect.

LPS is known to bind to the CD14/TLR4/MD2 receptor complex resulting in the activation of nuclear factor kappaB signalling pathway and subsequent expression of iNOS and pro-inflammatory cytokines such as TNFa and IL1β (Kim et al., 2007). The finding that intraperitoneal injection IL1β results in reduced retinal hypoxia at P14 after OIR would further suggest that ILIβ injection is activating aspects of the same pathway down-stream of LPS-TLR4 binding. Future work is needed to further define if IL1β upregulation after LPS injection is the main cause of retinal protection against hypoxia

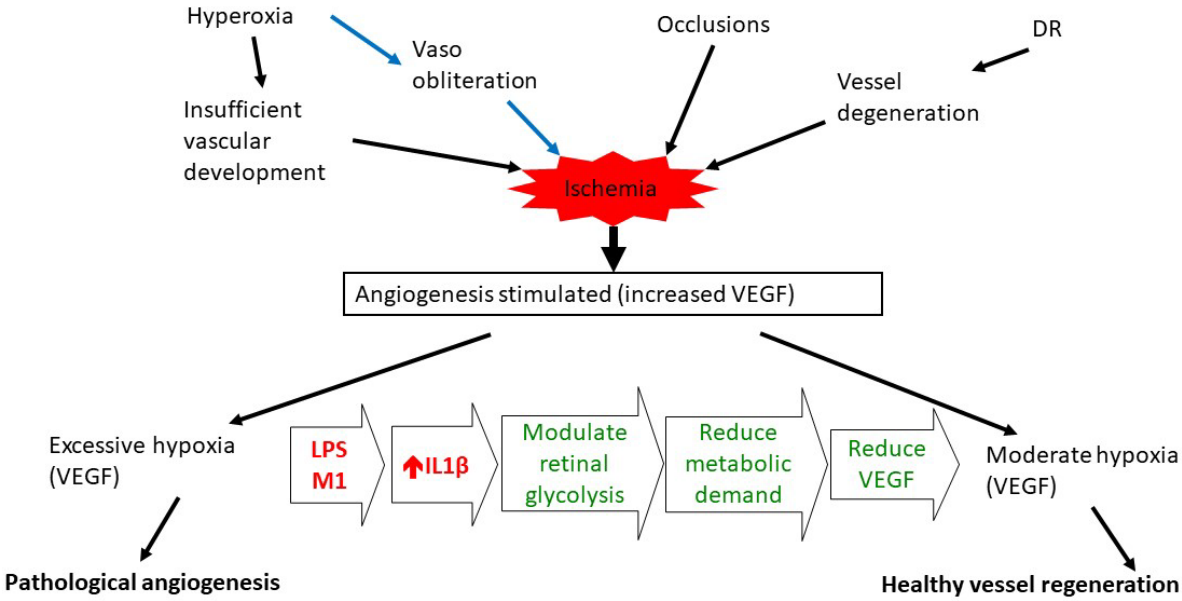

in OIR and if it is, how exactly it is able to modulate oxygen demand in retinal tissue.

Figure 4.2 – Proposed hypothesis: LPS induced IL1β upregulation modulates retinal glycolysis to reduce metabolic demand

4.6 Future Work

Despite the progress made throughout this project there are some issues that need further clarification. Quantification of the infiltrating retina cells is need to assess how successful the immune depletion experiments were.

Firstly, having identified IL1β as a key cytokine involved in the reduction of hypoxia and neovascularisation seen in the LPS treated group undergoing OIR, my next experiment will involve blocking IL1β in LPS treated animals to see whether LPS acts primarily through IL1β. Treatment with Anakinra® (an IL1β receptor antagonist) prior to LPS injection at P12 should be able to answer this question.

Secondly, the exact mechanisms by which IL1β and LPS injected systemically or intraocularly can modulate the oxygen demand of the retina have not been fully answered. The original hypothesis that systemic inflammation activated by either LPS or IL1β results in the retina switching away from mitochondrial respiration towards glycolysis could still explain the reduced oxygen demand and hypoxia seen. Seahorse extracellular flux analyzers have the ability to measure oxygen consumption rate (an indicator of mitochondrial respiration) and extracellular acidification rate (a measure of glycolysis) in tissue. This technique would be able to prove whether LPS treated retinal tissue had a reduced oxygen demand compared to control tissue. As a result, we are working with a collaborator at the Scripps Research Institute, San Diego, USA to perform extracellular flux analysis on retinal tissue taken from mice treated with LPS. Also, in an attempt to investigate the direct effect of IL1β on oxygen demand in retinal tissue in the absence of the invading neutrophil/monocyte/macrophage populations, experiments involving the extracellular flux analysis of ex-vivo retinal tissue exposed to IL1β are planned.

Given that the RNA sequencing data yielded limited information due to the low n-numbers involved, a future set of sequencing is planned with more numbers to compare the central and peripheral retinas of mice undergoing OIR treated with LPS vs IL1β vs vehicle vs age matched controls vs non OIR mice injected with LPS. This should hopefully lead to a better understating of the effect that LPS and IL1β has on other retinal cell types such as Müller cells.

As the OIR model is essentially a hypoxia induced VEGF assay, little work has been done to elucidate the effect IL1β injection has on VEGF in the model. Experiments using an anti-VEGF such as aflibercept may shed some light on this.

Finally, to look at the long-term feasibility of this approach, the time frame of the experiments need to be extended to see if ultimately following IL1β treatment complete healthy retinal re-vascularisation occurs and that normal retinal function is gained. To assess the visual potential of these eyes electroretinograms could be performed.

4.7 Outlook

The findings from this project have shown that activation of the immune cascade can prevent the development of hypoxia in ischaemic retinal tissue by reducing the demand for oxygen rather than increasing the supply of oxygen. Not only is this a novel approach to treating ischaemic retinopathy but these findings imply that cytokines such as IL1β have the potential to regulate tissue oxygen demand. Anti-VEGF therapy is the current mainstay of treatment directed against the neovascular consequences of ischaemic retinopathy. This approach only treats the symptoms of hypoxia induced neovascularisation and not the cause, often requiring repeated treatments. If the exact

mechanism by which IL1β is able to reduce oxygen demand can be elucidated, it is conceivable that intravitreal treatment with a modified IL1β molecule (or a downstream effector), could be given to patients at risk of retinal ischaemia (such as in ROP, diabetic retinopathy or retinal artery occlusion) to protect the retina from the consequent hypoxia and prevent neovascularisation occurring in the first place.

On a broader perspective, moving away from the eye, the findings of this project indicate that systemic injection of IL1β can modulate the oxygen demand in tissue at a distant site away from the site of injection. This implies that the activated immune cascade has a sensing mechanism that targets areas of hypoxia. Therefore, these findings have implications for other diseases where the causative factor is tissue hypoxia such as cerebrovascular disease or cardiovascular disease. An intravenous infusion could therefore be given to a patient at risk of/or during a vascular event to prevent hypoxia in that tissue. This is particular relevant to heart and cerebral disease as direct injection of treatment to the hypoxic tissue isn't readily performed.

4.8 Conclusion

In conclusion, systemic LPS stimulation of TLR4 at P12 in the OIR model prior to hypoxia occurring is protective and has been shown to prevent the typical neovascularisation that occurs at P17. Further investigation found that LPS reduced the level of hypoxia seen at P14, whereas PBS treated controls showed profound hypoxia by way of increased EF5 hypoxia staining and increased arterial vascular tortuosity. Although the exact mechanism by which LPS stimulation of TLR4 reduces retinal hypoxia has yet to be fully confirmed, findings would suggest that stimulation of TLR4 results in reduced oxygen demand in the retina as proliferation of retinal vasculature had been shown to be reduced, while the avascular area remained unchanged when compared with

controls. Therefore, as hypoxia is a balance between oxygen supply and demand, if oxygen supply remained unchanged then LPS must be reducing oxygen demand of the retina. Analysis of the model also identified that LPS injection causes an influx of round bodied inflammatory cells into the retina. Characterisation of these cells determined them to be mostly neutrophils. Furthermore, depletion of the myeloid population did not abrogate the effects of LPS on hypoxia indicators, implying that they were not responsible for the reduction in hypoxia. In an attempt to look for other candidates that may be responsible for the reduction in hypoxia, Il1β was found to be the most upregulated cytokine in the central retina of an LPS treated retina. Following investigations where IL1β was injected, both intraocularly and intraperitoneally a reduction in hypoxia and neovascularisation similar to that seen in LPS injected mice was seen after OIR. This would suggest that LPS binding to TLR4 results in a systemic upregulation of IL1β, which results in upregulation of IL1β in the hypoxic retina of mouse undergoing OIR and prevents hypoxia and the consequent neovascularisation associated with the model.

8. References

Adams, R. H. and Eichmann, A. (2010) 'Axon guidance molecules in vascular patterning.', *Cold Spring Harbor perspectives in biology*. Cold Spring Harbor Laboratory Press, 2(5), p. a001875. doi: 10.1101/cshperspect.a001875.

Aspalter, I. M. *et al.* (2015) 'Alk1 and Alk5 inhibition by Nrp1 controls vascular sprouting downstream of Notch', *Nature Communications*, 6, p. 7264. doi: 10.1038/ncomms8264.

Balkwill, F. and Mantovani, A. (2001) 'Inflammation and cancer: back to Virchow?', *The Lancet*, 357(9255), pp. 539–545. doi: 10.1016/S0140-6736(00)04046-0.

Benedito, R. *et al.* (2009) 'The Notch Ligands Dll4 and Jagged1 Have Opposing Effects on Angiogenesis', *Cell*, 137(6), pp. 1124–1135. doi: 10.1016/j.cell.2009.03.025.

Benedito, R. *et al.* (2012) 'Notch-dependent VEGFR3 upregulation allows angiogenesis without VEGF–VEGFR2 signalling', *Nature*. Nature Research, 484(7392), pp. 110–114. doi: 10.1038/nature10908.

Benoit, M., Desnues, B. and Mege, J.-L. (2008) 'Macrophage polarization in bacterial infections.', *Journal of immunology (Baltimore, Md. : 1950)*, 181(6), pp. 3733–9. Available at: http://www.ncbi.nlm.nih.gov/pubmed/18768823 (Accessed: 12 September 2016).

Bentley, K. *et al.* (2009) 'Tipping the balance: robustness of tip cell selection, migration and fusion in angiogenesis.', *PLoS computational biology*. Public Library of Science, 5(10), p. e1000549. doi: 10.1371/journal.pcbi.1000549.

Brooks, S. E. *et al.* (2001) 'Reduced severity of oxygen-induced retinopathy in eNOS-deficient mice.', *Investigative ophthalmology & visual science*, 42(1), pp. 222–8. Available at: http://www.ncbi.nlm.nih.gov/pubmed/11133872 (Accessed: 3 July 2018).

Caprara, C. *et al.* (2011) 'HIF1A Is Essential for the Development of the Intermediate Plexus of the Retinal Vasculature', *Investigative Opthalmology & Visual Science*. The Association for Research in Vision and Ophthalmology, 52(5), p. 2109. doi: 10.1167/iovs.10-6222.

Carmeliet, P. (2003a) 'Angiogenesis in health and disease', *Nature Medicine*, 9(6), pp. 653–660. doi: 10.1038/nm0603-653.

Carmeliet, P. (2003b) 'Blood vessels and nerves: common signals, pathways and diseases.', *Nature reviews. Genetics*, 4(9), pp. 710–20. doi: 10.1038/nrg1158.

Carmeliet, P. and Jain, R. K. (2011) 'Molecular mechanisms and clinical applications of angiogenesis', *Nature*, 473(7347), pp. 298–307. doi: 10.1038/nature10144.

Carmi, Y. *et al.* (2009) 'The role of macrophage-derived IL-1 in induction and maintenance of angiogenesis.', *Journal of immunology (Baltimore, Md. : 1950)*, 183(7), pp. 4705–14. doi: 10.4049/jimmunol.0901511.

Chan-Ling, T. and Stone, J. (1992) 'Degeneration of astrocytes in feline retinopathy of prematurity causes failure of the blood-retinal barrier.', *Investigative ophthalmology & visual science*, 33(7), pp. 2148–59. Available at: http://www.ncbi.nlm.nih.gov/pubmed/1607225 (Accessed: 1 August 2016).

Chan, W. Y., Kohsaka, S. and Rezaie, P. (2007) 'The origin and cell lineage of microglia: new concepts.', *Brain research reviews*, 53(2), pp. 344–54. doi: 10.1016/j.brainresrev.2006.11.002.

Chang, B. *et al.* (2002) 'Retinal degeneration mutants in the mouse.', *Vision research*, 42(4), pp. 517–25. Available at: http://www.ncbi.nlm.nih.gov/pubmed/11853768 (Accessed: 18 September 2015).

Checchin, D. *et al.* (2006) 'Potential role of microglia in retinal blood vessel formation', *Invest Ophthalmol Vis Sci*, 47(8), pp. 3595–3602. doi: 10.1167/iovs.05-1522.

Chen, Z. *et al.* (2012) 'Lipopolysaccharide-induced microglial activation and neuroprotection against experimental brain injury is independent of hematogenous TLR4.', *The Journal of neuroscience : the official journal of the Society for Neuroscience*, 32(34), pp. 11706–15. doi: 10.1523/JNEUROSCI.0730-12.2012.

Chu, Y., Hughes, S. and Chan-Ling, T. (2001) 'Differentiation and migration of astrocyte precursor cells and astrocytes in human fetal retina: relevance to optic nerve coloboma', *FASEB J*, 15(11), pp. 2013–2015. doi: 10.1096/fj.00-0868fje.

Chu, Z. *et al.* (2013) 'Preliminary study of retinal pathological features in preterm birth pups exposed to an animal model of oxygen-induced retinopathy in mice.', *Graefe's archive for clinical and experimental ophthalmology = Albrecht von Graefes Archiv für klinische und experimentelle Ophthalmologie*, 251(8), pp. 1937–43. doi: 10.1007/s00417-013-2366-8.

Clausen, B. E. *et al.* (1999) 'Conditional gene targeting in macrophages and granulocytes using LysMcre mice', *Transgenic Research*, 8(4), pp. 265–277. doi: 10.1023/A:1008942828960.

Claxton, S. and Fruttiger, M. (2003) 'Role of arteries in oxygen induced vaso-obliteration', *Exp Eye Res*, 77(3), pp. 305–311. doi: 10.1016/S0014-4835(03)00153-2.

Connor, K. M. *et al.* (2007) 'Increased dietary intake of ω-3-polyunsaturated fatty acids reduces pathological retinal angiogenesis', *Nature Medicine*, 13(7), pp. 868–873. doi: 10.1038/nm1591.

Connor, K. M. *et al.* (2009) 'Quantification of oxygen-induced retinopathy in the mouse: a model of vessel loss, vessel regrowth and pathological angiogenesis.', *Nature protocols*. Nature Publishing Group, 4(11), pp. 1565–73. doi: 10.1038/nprot.2009.187.

D'Orazio, T. J. and Niederkorn, J. Y. (1998) 'A novel role for TGF-beta and IL-10 in the induction of immune privilege.', *Journal of immunology (Baltimore, Md. : 1950)*, 160(5), pp. 2089–98. Available at: http://www.ncbi.nlm.nih.gov/pubmed/9498745 (Accessed: 2 July 2018).

Dace, D. S. *et al.* (2008) 'Interleukin-10 promotes pathological angiogenesis by regulating macrophage response to hypoxia during development.', *PloS one*, 3(10), p. e3381. doi: 10.1371/journal.pone.0003381.

Daley, J. M. *et al.* (2008) 'Use of Ly6G-specific monoclonal antibody to deplete neutrophils in mice', *Journal of Leukocyte Biology*, 83(1), pp. 64–70. doi: 10.1189/jlb.0407247.

Dammann, O. (2010) 'Inflammation and retinopathy of prematurity.', *Acta paediatrica (Oslo, Norway : 1992)*, 99(7), pp. 975–7. doi: 10.1111/j.1651-2227.2010.01836.x.

Davies, L. C. and Taylor, P. R. (2015) 'Tissue-resident macrophages: then and now', *Immunology*, 144(4), pp. 541–548. doi: 10.1111/imm.12451.

Dong, A. *et al.* (2009) 'Oxidative stress promotes ocular neovascularization', *Journal of Cellular Physiology*, 219(3), pp. 544–552. doi: 10.1002/jcp.21698.

Dorrell, M. I. *et al.* (2010) 'Maintaining retinal astrocytes normalizes revascularization and prevents vascular pathology associated with oxygen-induced retinopathy', *Glia*, 58(1), pp. 43–54. Available at: http://www.ncbi.nlm.nih.gov/pubmed/19544395.

Dorrell, M. I., Aguilar, E. and Friedlander, M. (2002) 'Retinal vascular development is mediated by endothelial filopodia, a preexisting astrocytic template and specific R-cadherin adhesion', *Invest Ophthalmol.Vis.Sci.*, 43(11), pp. 3500–3510. Available at: http://www.ncbi.nlm.nih.gov/pubmed/12407162.

Downie, L. E. *et al.* (2008) 'AT1 receptor inhibition prevents astrocyte degeneration and restores vascular growth in oxygen-induced retinopathy.', *Glia*, 56(10), pp. 1076–90. doi: 10.1002/glia.20680.

Draoui, N., de Zeeuw, P. and Carmeliet, P. (2017) 'Angiogenesis revisited from a metabolic perspective: role and therapeutic implications of endothelial cell metabolism.', *Open biology*. The Royal Society, 7(12). doi: 10.1098/rsob.170219.

Engerman, R. L. (1976) 'Development of the macular circulation', *Invest Ophthalmol.*, 15(10), pp. 835–840. Available at: http://www.ncbi.nlm.nih.gov/pubmed/824224.

Estrach, S. *et al.* (2011) 'Laminin-binding integrins induce Dll4 expression and Notch signaling in endothelial cells.', *Circulation research*, 109(2), pp. 172–82. doi: 10.1161/CIRCRESAHA.111.240622.

De Filippo, K. *et al.* (2008) 'Neutrophil Chemokines KC and Macrophage-Inflammatory Protein-2 Are Newly Synthesized by Tissue Macrophages Using Distinct TLR Signaling Pathways', *The Journal of Immunology*, 180(6), pp. 4308–4315. doi: 10.4049/jimmunol.180.6.4308.

Fischer, F. *et al.* (2011) 'Activation of retinal microglia rather than microglial cell density correlates with retinal neovascularization in the mouse model of oxygen-induced retinopathy', *Journal of Neuroinflammation*. BioMed Central, 8(1), p. 120. doi: 10.1186/1742-2094-8-120.

Fletcher, E. L. *et al.* (2010) 'The significance of neuronal and glial cell changes in the

rat retina during oxygen-induced retinopathy', *Doc Ophthalmol*. 2009/09/19, 120(1), pp. 67–86. doi: 10.1007/s10633-009-9193-6.

Fruttiger, M., Calver, a R., *et al.* (1996) 'PDGF mediates a neuron-astrocyte interaction in the developing retina', *Neuron*, 17(6), pp. 1117–1131. Available at: http://www.ncbi.nlm.nih.gov/pubmed/8982160.

Fruttiger, M. (2002a) 'Development of the mouse retinal vasculature: angiogenesis versus vasculogenesis.', *Investigative ophthalmology & visual science*, 43(2), pp. 522–7. Available at: http://www.ncbi.nlm.nih.gov/pubmed/11818400 (Accessed: 2 July 2018).

Fruttiger, M., Calver, a R. and Richardson, W. D. (2000) 'Platelet-derived growth factor is constitutively secreted from neuronal cell bodies but not from axons', *Curr.Biol.*, 10(20), pp. 1283–1286. Available at: http://www.ncbi.nlm.nih.gov/pubmed/11069109.

Gardiner, T. A. *et al.* (2005) 'Inhibition of Tumor Necrosis Factor- ␣ Improves Physiological Angiogenesis and Reduces Pathological Neovascularization in Ischemic Retinopathy', 166(2), pp. 637–644.

Gariano, R. F. *et al.* (1996) 'Development of astrocytes and their relation to blood vessels in fetal monkey retina.', *Investigative Ophthalmology & Visual Science*. The Association for Research in Vision and Ophthalmology, 37(12), pp. 2367–2375.

Gautam, N. *et al.* (2001) 'Heparin-binding protein (HBP/CAP37): A missing link in neutrophil-evoked alteration of vascular permeability', *Nature Medicine*, 7(10), pp. 1123–1127. doi: 10.1038/nm1001-1123.

Geissmann, F. *et al.* (2010) 'Development of monocytes, macrophages, and dendritic cells.', *Science (New York, N.Y.)*, 327(5966), pp. 656–661. doi: 10.1126/science.1178331.

Geissmann, F., Jung, S. and Littman, D. R. (2003) 'Blood monocytes consist of two principal subsets with distinct migratory properties.', *Immunity*, 19(1), pp. 71–82. Available at: http://www.ncbi.nlm.nih.gov/pubmed/12871640 (Accessed: 20 September 2015).

Gelfand, M. V *et al.* (2014) 'Neuropilin-1 functions as a VEGFR2 co-receptor to guide developmental angiogenesis independent of ligand binding', *eLife*, 3. doi: 10.7554/eLife.03720.

Gerhardt, H. *et al.* (2003) 'VEGF guides angiogenic sprouting utilizing endothelial tip cell filopodia', *J Cell Biol*, 161(6), pp. 1163–1177. doi: 10.1083/jcb.200302047.

Gerhardt, H. (2008) 'VEGF and endothelial guidance in angiogenic sprouting.', *Organogenesis*. Landes Bioscience, 4(4), pp. 241–6. Available at: http://www.ncbi.nlm.nih.gov/pubmed/19337404 (Accessed: 6 August 2016).

Giles, J. A. *et al.* (2015) 'Requirement for interleukin-1 to drive brain inflammation reveals tissue-specific mechanisms of innate immunity.', *European journal of immunology*, 45(2), pp. 525–30. doi: 10.1002/eji.201444748.

González, H. *et al.* (2014) 'Neuroimmune regulation of microglial activity involved in neuroinflammation and neurodegenerative diseases', *Journal of Neuroimmunology*, 274(1), pp. 1–13. doi: 10.1016/j.jneuroim.2014.07.012.

Gu, X. *et al.* (2002) 'Effects of sustained hyperoxia on revascularization in experimental retinopathy of prematurity', *Investigative Ophthalmology and Visual Science*, 43(2), pp. 496–502.

Halder, S. K. *et al.* (2013) 'Retinal cell type-specific prevention of ischemia-induced damages by LPS-TLR4 signaling through microglia.', *Journal of neurochemistry*, 126(2), pp. 243–60. doi: 10.1111/jnc.12262.

Hamilton, T. A. *et al.* (2014) 'Myeloid Colony-Stimulating Factors as Regulators of Macrophage Polarization', *Frontiers in Immunology*, 5. doi: 10.3389/fimmu.2014.00554.

Hangai, M. *et al.* (1995) 'Interleukin-1 gene expression in transient retinal ischemia in the rat.', *Investigative ophthalmology & visual science*, 36(3), pp. 571–8. Available at: http://www.ncbi.nlm.nih.gov/pubmed/7890488 (Accessed: 15 September 2016).

Hellström, M. *et al.* (2007) 'Dll4 signalling through Notch1 regulates formation of tip cells during angiogenesis.', *Nature*, 445(7129), pp. 776–80. doi: 10.1038/nature05571.

Higgins, R. D. *et al.* (1999) 'Diltiazem reduces retinal neovascularization in a mouse model of oxygen induced retinopathy.', *Current eye research*, 18(1), pp. 20–7. Available at: http://www.ncbi.nlm.nih.gov/pubmed/10075199 (Accessed: 3 July 2018).

Hirota, S. *et al.* (2015) 'Neuropilin-1 balances β8 integrin-activated TGFβ signaling to control sprouting angiogenesis in the brain.', *Development (Cambridge, England)*, (November). doi: 10.1242/dev.113746.

Hong, H. K. *et al.* (2014) 'Neonatal systemic inflammation in rats alters retinal vessel development and simulates pathologic features of retinopathy of prematurity.', *Journal of neuroinflammation*, 11, p. 87. doi: 10.1186/1742-2094-11-87.

de Hoz, R. *et al.* (2016) 'Retinal Macroglial Responses in Health and Disease.', *BioMed research international*, 2016, p. 2954721. doi: 10.1155/2016/2954721.

Huxlin, K. R., Sefton, A. J. and Furby, J. H. (1992) 'The origin and development of retinal astrocytes in the mouse', *J Neurocytol.*, 21(7), pp. 530–544. Available at: http://www.ncbi.nlm.nih.gov/pubmed/1500949.

Ilg, R. C., Davies, M. H. and Powers, M. R. (2005) 'Altered retinal neovascularization in TNF receptor-deficient mice.', *Current eye research*, 30(11), pp. 1003–13. doi: 10.1080/02713680500330355.

Ishida, S. *et al.* (2003) 'Leukocytes mediate retinal vascular remodeling during development and vaso-obliteration in disease', *Nat Med*, 9(6), pp. 781–788. doi: 10.1038/nm877.

Ivanova, A. *et al.* (2005) 'In vivo genetic ablation by Cre-mediated expression of

diphtheria toxin fragment A.', *Genesis New York NY 2000*. Wiley-Liss, 43(3), pp. 129–135. Available at: http://discovery.ucl.ac.uk/132225/.

Jakobsson, L. *et al.* (2010) 'Endothelial cells dynamically compete for the tip cell position during angiogenic sprouting.', *Nature cell biology*, 12(10), pp. 943–53. doi: 10.1038/ncb2103.

Kasai, A. *et al.* (2008) 'Retardation of retinal vascular development in apelin-deficient mice.', *Arteriosclerosis, thrombosis, and vascular biology*, 28(10), pp. 1717–22. doi: 10.1161/ATVBAHA.108.163402.

Katsumoto, A. *et al.* (2014) 'Ontogeny and functions of central nervous system macrophages.', *Journal of immunology (Baltimore, Md. : 1950)*, 193(6), pp. 2615–21. doi: 10.4049/jimmunol.1400716.

Kawamoto, H. and Minato, N. (2004) 'Myeloid cells.', *The international journal of biochemistry & cell biology*, 36(8), pp. 1374–9. doi: 10.1016/j.biocel.2004.01.020.

Kim, C. B., D'Amore, P. A. and Connor, K. M. (2016) 'Revisiting the mouse model of oxygen-induced retinopathy', *Eye and brain*. NIH Public Access, 8, p. 67. doi: 10.2147/eb.s94447.

Kim, J.-B. *et al.* (2007) 'Inhibition of LPS-induced iNOS, COX-2 and cytokines expression by poncirin through the NF-kappaB inactivation in RAW 264.7 macrophage cells.', *Biological & pharmaceutical bulletin*, 30(12), pp. 2345–51. Available at: http://www.ncbi.nlm.nih.gov/pubmed/18057724 (Accessed: 15 September 2016).

Kim, J. *et al.* (2011) 'Semaphorin 3E-Plexin-D1 signaling regulates VEGF function in developmental angiogenesis via a feedback mechanism', *Genes & Development*, 25(13), pp. 1399–1411. doi: 10.1101/gad.2042011.

Kim, S. *et al.* (2013) 'ERG Immunohistochemistry as an Endothelial Marker for Assessing Lymphovascular Invasion', *Korean Journal of Pathology*, 47(4), p. 355. doi: 10.4132/KoreanJPathol.2013.47.4.355.

Kim, S. J. and Kim, H. M. (2017) 'Dynamic lipopolysaccharide transfer cascade to TLR4/MD2 complex via LBP and CD14.', *BMB reports*. Korean Society for Biochemistry and Molecular Biology, 50(2), pp. 55–57. doi: 10.5483/BMBREP.2017.50.2.011.

Koch, C. J. (2002) '[1] Measurement of absolute oxygen levels in cells and tissues using oxygen sensors and 2-nitroimidazole EF5', *Methods in Enzymology*, 352, pp. 3–31. doi: 10.1016/S0076-6879(02)52003-6.

Kociok, N. *et al.* (2006) 'Pathological but not physiological retinal neovascularization is altered in TNF-Rp55-receptor-deficient mice.', *Investigative ophthalmology & visual science*, 47(11), pp. 5057–65. doi: 10.1167/iovs.06-0407.

Krawczyk, C. M. *et al.* (2010) 'Toll-like receptor-induced changes in glycolytic metabolism regulate dendritic cell activation', *Blood*, 115(23), pp. 4742–4749. doi: 10.1182/blood-2009-10-249540.

Kubota, Y. *et al.* (2008) 'Leukemia inhibitory factor regulates microvessel density by

modulating oxygen- dependent VEGF expression in mice', *The Journal of Clinical Investigation*, 118(7), pp. 2393–2403. doi: 10.1172/JCI34882DS1.

Kubota, Y. *et al.* (2009) 'M-CSF inhibition selectively targets pathological angiogenesis and lymphangiogenesis.', *The Journal of experimental medicine*, 206(5), pp. 1089–1102. doi: 10.1084/jem.20081605.

Lange, C. *et al.* (no date) 'Kinetics of retinal vaso-obliteration and neovascularisation in the oxygen-induced retinopathy (OIR) mouse model', *Graefe's Archive for Clinical and Experimental Ophthalmology*. Springer-Verlag, 247(9), pp. 1205–1211. doi: 10.1007/S00417-009-1116-4.

Larrivée, B. *et al.* (2009) 'Guidance of vascular development: lessons from the nervous system.', *Circulation research*, 104(4), pp. 428–41. doi: 10.1161/CIRCRESAHA.108.188144.

Larrivée, B. *et al.* (2012) 'ALK1 Signaling Inhibits Angiogenesis by Cooperating with the Notch Pathway', *Developmental Cell*, 22(3), pp. 489–500. doi: 10.1016/j.devcel.2012.02.005.

Lavalette, S. *et al.* (2011) 'Interleukin-1β inhibition prevents choroidal neovascularization and does not exacerbate photoreceptor degeneration.', *The American journal of pathology*, 178(5), pp. 2416–23. doi: 10.1016/j.ajpath.2011.01.013.

Lee, J. and Dammann, O. (2012) 'Perinatal infection, inflammation, and retinopathy of prematurity.', *Seminars in fetal & neonatal medicine*, 17(1), pp. 26–9. doi: 10.1016/j.siny.2011.08.007.

Liu, J. *et al.* (2013) 'Myeloid Cells Expressing VEGF and Arginase-1 Following Uptake of Damaged Retinal Pigment Epithelium Suggests Potential Mechanism That Drives the Onset of Choroidal Angiogenesis in Mice', *PLoS ONE*. Edited by F. Sennlaub. Public Library of Science, 8(8), p. e72935. doi: 10.1371/journal.pone.0072935.

Lobov, I. B. *et al.* (2007) 'Delta-like ligand 4 (Dll4) is induced by VEGF as a negative regulator of angiogenic sprouting.', *Proceedings of the National Academy of Sciences of the United States of America*, 104(9), pp. 3219–3224. doi: 10.1073/pnas.0611206104.

Lu, B. *et al.* (1998) 'Abnormalities in monocyte recruitment and cytokine expression in monocyte chemoattractant protein 1-deficient mice.', *The Journal of experimental medicine*. Rockefeller University Press, 187(4), pp. 601–8. doi: 10.1084/jem.187.4.601.

Mack, M. *et al.* (2001) 'Expression and Characterization of the Chemokine Receptors CCR2 and CCR5 in Mice', *The Journal of Immunology*. American Association of Immunologists, 166(7), pp. 4697–4704. doi: 10.4049/jimmunol.166.7.4697.

Magaud, J. P. *et al.* (1989) 'Double immunocytochemical labeling of cell and tissue samples with monoclonal anti-bromodeoxyuridine.', *Journal of Histochemistry & Cytochemistry*. SAGE Publications, 37(10), pp. 1517–1527. doi: 10.1177/37.10.2476478.

Maria Vähätupa *et al.* (2016) 'Intravitreal injection of PBS reduces retinal neovascularization in the mouse oxygen-induced retinopathy model', in *ARVO 2016 Annual Meeting*. Seattle, WA, USA.

McCarty, J. H. (2009) 'Integrin-mediated regulation of neurovascular development, physiology and disease.', *Cell adhesion & migration*. Landes Bioscience, 3(2), pp. 211–5. Available at: http://www.ncbi.nlm.nih.gov/pubmed/19372738 (Accessed: 15 August 2016).

McColl, B. W., Rothwell, N. J. and Allan, S. M. (2007) 'Systemic inflammatory stimulus potentiates the acute phase and CXC chemokine responses to experimental stroke and exacerbates brain damage via interleukin-1- and neutrophil-dependent mechanisms.', *The Journal of neuroscience : the official journal of the Society for Neuroscience*, 27(16), pp. 4403–12. doi: 10.1523/JNEUROSCI.5376-06.2007.

McColl, B. W., Rothwell, N. J. and Allan, S. M. (2008) 'Systemic inflammation alters the kinetics of cerebrovascular tight junction disruption after experimental stroke in mice.', *The Journal of neuroscience : the official journal of the Society for Neuroscience*, 28(38), pp. 9451–62. doi: 10.1523/JNEUROSCI.2674-08.2008.

McCracken, J. M. and Allen, L.-A. H. (2014) 'Regulation of Human Neutrophil Apoptosis and Lifespan in Health and Disease', *Journal of Cell Death*, 7, p. JCD.S11038. doi: 10.4137/JCD.S11038.

McGown, C. C. *et al.* (2011) 'ROCK induced inflammation of the microcirculation during endotoxemia mediated by nitric oxide synthase.', *Microvascular research*, 81(3), pp. 281–8. doi: 10.1016/j.mvr.2011.02.003.

Medina, R. J. *et al.* (2011) 'Myeloid angiogenic cells act as alternative M2 macrophages and modulate angiogenesis through interleukin-8.', *Molecular medicine Cambridge Mass*, 17(9–10), pp. 1045–55. doi: 10.2119/molmed.2011.00129.

Medzhitov, R. (2013) 'Pattern recognition theory and the launch of modern innate immunity.', *Journal of immunology (Baltimore, Md. : 1950)*, 191(9), pp. 4473–4. doi: 10.4049/jimmunol.1302427.

Medzhitov, R. and Janeway, C. A. (1997) 'Innate immunity: the virtues of a nonclonal system of recognition.', *Cell*, 91(3), pp. 295–8. Available at: http://www.ncbi.nlm.nih.gov/pubmed/9363937 (Accessed: 2 July 2018).

Möllers, B. *et al.* (1992) 'The mouse M-lysozyme gene domain: identification of myeloid and differentiation specific DNasel hypersensitive sites and of a 3'-cis acting regulatory element', *Nucleic Acids Research*, 20(8), pp. 1917–1924. doi: 10.1093/nar/20.8.1917.

Movat, H. Z. *et al.* (1987) 'Acute inflammation in gram-negative infection: endotoxin, interleukin 1, tumor necrosis factor, and neutrophils.', *Federation proceedings*, 46(1), pp. 97–104. Available at: http://www.ncbi.nlm.nih.gov/pubmed/3542580 (Accessed: 2 July 2018).

Moya, I. M. *et al.* (2012) 'Stalk Cell Phenotype Depends on Integration of Notch and Smad1/5 Signaling Cascades', *Developmental Cell*, 22(3), pp. 501–514. doi:

10.1016/j.devcel.2012.01.007.

Mudhar, H. S. *et al.* (1993) 'PDGF and its receptors in the developing rodent retina and optic nerve.', *Development (Cambridge, England)*, 118(2), pp. 539–52. Available at: http://www.ncbi.nlm.nih.gov/pubmed/8223278.

Murdock, J. L. and Núñez, G. (2016) 'TLR4: The Winding Road to the Discovery of the LPS Receptor.', *Journal of immunology (Baltimore, Md. : 1950)*, 197(7), pp. 2561–2. doi: 10.4049/jimmunol.1601400.

Murray, K. N. *et al.* (2014) 'Systemic inflammation impairs tissue reperfusion through endothelin-dependent mechanisms in cerebral ischemia.', *Stroke*, 45(11), pp. 3412–9. doi: 10.1161/STROKEAHA.114.006613.

Muzumdar, M. D. *et al.* (2007) 'A global double-fluorescent Cre reporter mouse.', *Genesis (New York, N.Y. : 2000)*, 45(9), pp. 593–605. doi: 10.1002/dvg.20335.

Nakamura-Ishizu, A. *et al.* (2012) 'The formation of an angiogenic astrocyte template is regulated by the neuroretina in a HIF-1-dependent manner', *Developmental Biology*, 363(1), pp. 106–114. doi: 10.1016/j.ydbio.2011.12.027.

Nauseef, W. M. (2007) 'How human neutrophils kill and degrade microbes: an integrated view', *Immunological Reviews*, 219(1), pp. 88–102. doi: 10.1111/j.1600-065X.2007.00550.x.

O'Neill, L. A. J. (2006) 'How Toll-like receptors signal: what we know and what we don't know.', *Current opinion in immunology*, 18(1), pp. 3–9. doi: 10.1016/j.coi.2005.11.012.

O'Neill, L. A. J. (2008) 'When signaling pathways collide: positive and negative regulation of toll-like receptor signal transduction.', *Immunity*, 29(1), pp. 12–20. doi: 10.1016/j.immuni.2008.06.004.

Okabe, K. *et al.* (2014) 'Neurons limit angiogenesis by titrating VEGF in retina', *Cell*. Elsevier Inc., 159(3), pp. 584–596. doi: 10.1016/j.cell.2014.09.025.

Olson, J. L. *et al.* (2009) 'Intravitreal anakinra inhibits choroidal neovascular membrane growth in a rat model', *Ocular Immunology and Inflammation*, 17(3), pp. 195–200. doi: 10.1080/09273940802710705.

Palsson-McDermott, E. M. *et al.* (2015) 'Pyruvate kinase M2 regulates Hif-1α activity and IL-1β induction and is a critical determinant of the warburg effect in LPS-activated macrophages.', *Cell metabolism*, 21(1), pp. 65–80. doi: 10.1016/j.cmet.2014.12.005.

Pardali, E., Goumans, M.-J. and ten Dijke, P. (2010) 'Signaling by members of the TGF-β family in vascular morphogenesis and disease', *Trends in Cell Biology*, 20(9), pp. 556–567. doi: 10.1016/j.tcb.2010.06.006.

Pierce, E. A., Foley, E. D. and Smith, L. E. (1996) 'Regulation of vascular endothelial growth factor by oxygen in a model of retinopathy of prematurity', *Arch.Ophthalmol.*, 114(10), pp. 1219–1228. Available at: http://www.ncbi.nlm.nih.gov/pubmed/8859081.

Pitulescu, M. E. *et al.* (2010) 'Inducible gene targeting in the neonatal vasculature and analysis of retinal angiogenesis in mice', *Nat.Protoc.* Nature Publishing Group, 5(9), pp. 1518–1534. doi: nprot.2010.113 [pii];10.1038/nprot.2010.113 [doi].

Poltorak, A. *et al.* (1998) 'Defective LPS signaling in C3H/HeJ and C57BL/10ScCr mice: mutations in Tlr4 gene.', *Science (New York, N.Y.)*. American Association for the Advancement of Science, 282(5396), pp. 2085–8. doi: 10.1126/science.282.5396.2085.

Potente, M., Gerhardt, H. and Carmeliet, P. (2011) 'Basic and therapeutic aspects of angiogenesis.', *Cell*. Elsevier, 146(6), pp. 873–87. doi: 10.1016/j.cell.2011.08.039.

Powner, M. B. *et al.* (2012) 'Visualization of gene expression in whole mouse retina by in situ hybridization', *Nature Protocols*. Nature Publishing Group, 7(6), pp. 1086–1096. doi: 10.1038/nprot.2012.050.

Prame Kumar, K., Nicholls, A. J. and Wong, C. H. Y. (2018) 'Partners in crime: neutrophils and monocytes/macrophages in inflammation and disease.', *Cell and tissue research*, 371(3), pp. 551–565. doi: 10.1007/s00441-017-2753-2.

Prince, L. R. *et al.* (2011) 'The role of TLRs in neutrophil activation', *Current Opinion in Pharmacology*, 11(4), pp. 397–403. doi: 10.1016/j.coph.2011.06.007.

Provis, J. M. *et al.* (1997) 'Development of the human retinal vasculature: cellular relations and VEGF expression', *Exp.Eye Res.*, 65(4), pp. 555–568. Available at: http://www.ncbi.nlm.nih.gov/pubmed/9464188.

Rehaume, L. M. and Hancock, R. E. W. (2008) 'Neutrophil-derived defensins as modulators of innate immune function.', *Critical reviews in immunology*, 28(3), pp. 185–200. Available at: http://www.ncbi.nlm.nih.gov/pubmed/19024344 (Accessed: 2 July 2018).

Ricklin, D. *et al.* (2010) 'Complement: a key system for immune surveillance and homeostasis.', *Nature immunology*, 11(9), pp. 785–97. doi: 10.1038/ni.1923.

Risau, W. (1997) 'Mechanisms of angiogenesis', *Nature*, 386(6626), pp. 671–674. doi: 10.1038/386671a0.

Risau, W. and Flamme, I. (1995) 'Vasculogenesis', *Annual Review of Cell and Developmental Biology*, 11(1), pp. 73–91. doi: 10.1146/annurev.cb.11.110195.000445.

Ritter, M. R. *et al.* (2006) 'Myeloid progenitors differentiate into microglia and promote vascular repair in a model of ischemic retinopathy', *Journal of Clinical Investigation*. American Society for Clinical Investigation, 116(12), pp. 3266–3276. doi: 10.1172/JCI29683.

Rivera, J. C. *et al.* (2013) 'Microglia and interleukin-1β in ischemic retinopathy elicit microvascular degeneration through neuronal semaphorin-3A.', *Arteriosclerosis, thrombosis, and vascular biology*, 33(8), pp. 1881–91. doi: 10.1161/ATVBAHA.113.301331.

Rodriguez-Prados, J.-C. *et al.* (2010) 'Substrate Fate in Activated Macrophages: A

Comparison between Innate, Classic, and Alternative Activation', *The Journal of Immunology*, 185(1), pp. 605–614. doi: 10.4049/jimmunol.0901698.

Rose, S., Misharin, A. and Perlman, H. (2012) 'A novel Ly6C/Ly6G-based strategy to analyze the mouse splenic myeloid compartment.', *Cytometry. Part A : the journal of the International Society for Analytical Cytology*, 81(4), pp. 343–50. doi: 10.1002/cyto.a.22012.

Rotschild, T. *et al.* (1999) 'Dexamethasone reduces oxygen induced retinopathy in a mouse model.', *Pediatric research*, 46(1), pp. 94–100. Available at: http://www.ncbi.nlm.nih.gov/pubmed/10400141 (Accessed: 3 July 2018).

Saederup, N. *et al.* (2010) 'Selective chemokine receptor usage by central nervous system myeloid cells in CCR2-red fluorescent protein knock-in mice.', *PloS one*, 5(10), p. e13693. doi: 10.1371/journal.pone.0013693.

Sakimoto, S. *et al.* (2012) 'A role for endothelial cells in promoting the maturation of astrocytes through the apelin/APJ system in mice', *Development*, 139(7), pp. 1327–1335. doi: 10.1242/dev.072330.

Sapieha, P. *et al.* (2012) 'Eyeing central neurons in vascular growth and reparative angiogenesis.', *Blood*. American Society of Hematology, 120(11), pp. 2182–94. doi: 10.1182/blood-2012-04-396846.

Schnitzer, J. (1987) 'Retinal astrocytes: their restriction to vascularized parts of the mammalian retina', *Neurosci.Lett.*, 78(1), pp. 29–34. Available at: http://www.ncbi.nlm.nih.gov/pubmed/3614770.

Scott, A. *et al.* (2010) 'Astrocyte-derived vascular endothelial growth factor stabilizes vessels in the developing retinal vasculature.', *PloS one*, 5(7), p. e11863. doi: 10.1371/journal.pone.0011863.

Scott, A., Powner, M. B. and Fruttiger, M. (2014) 'Quanti fi cation of vascular tortuosity as an early outcome measure in oxygen induced retinopathy (OIR)', *Experimental Eye Research*. Elsevier Ltd, 120, pp. 55–60. doi: 10.1016/j.exer.2013.12.020.

Selvam, S., Kumar, T. and Fruttiger, M. (2018) 'Retinal vasculature development in health and disease.', *Progress in retinal and eye research*, 63, pp. 1–19. doi: 10.1016/j.preteyeres.2017.11.001.

Semenza, G. L. (2001) 'Hypoxia-inducible factor 1: control of oxygen homeostasis in health and disease.', *Pediatric research*, 49(5), pp. 614–7. doi: 10.1203/00006450-200105000-00002.

Sharma, J. *et al.* (2003) 'Ibuprofen improves oxygen-induced retinopathy in a mouse model.', *Current eye research*, 27(5), pp. 309–14. Available at: http://www.ncbi.nlm.nih.gov/pubmed/14562167 (Accessed: 3 July 2018).

Siemerink, M. J. *et al.* (2013) 'Endothelial tip cells in ocular angiogenesis: potential target for anti-angiogenesis therapy.', *The journal of histochemistry and cytochemistry : official journal of the Histochemistry Society*. Histochemical Society,

61(2), pp. 101–15. doi: 10.1369/0022155412467635.

Silva, M. T. (2010) 'When two is better than one: macrophages and neutrophils work in concert in innate immunity as complementary and cooperative partners of a myeloid phagocyte system', *Journal of Leukocyte Biology*, 87(1), pp. 93–106. doi: 10.1189/jlb.0809549.

Silva, M. T. and Correia-Neves, M. (2012) 'Neutrophils and Macrophages: the Main Partners of Phagocyte Cell Systems', *Frontiers in Immunology*, 3. doi: 10.3389/fimmu.2012.00174.

Silvestre-Roig, C., Hidalgo, A. and Soehnlein, O. (2016) 'Neutrophil heterogeneity: implications for homeostasis and pathogenesis.', *Blood*, 127(18), pp. 2173–81. doi: 10.1182/blood-2016-01-688887.

De Smet, F. *et al.* (2009) 'Mechanisms of Vessel Branching: Filopodia on Endothelial Tip Cells Lead the Way', *Arteriosclerosis, Thrombosis, and Vascular Biology*. Lippincott Williams & Wilkins, 29(5), pp. 639–649. doi: 10.1161/ATVBAHA.109.185165.

Sobowale, O. A. *et al.* (2016) 'Interleukin-1 in Stroke: From Bench to Bedside.', *Stroke*, 47(8), pp. 2160–7. doi: 10.1161/STROKEAHA.115.010001.

Soehnlein, O. *et al.* (2008) 'Neutrophil secretion products pave the way for inflammatory monocytes.', *Blood*, 112(4), pp. 1461–71. doi: 10.1182/blood-2008-02-139634.

Stahl, A. *et al.* (2010) 'The mouse retina as an angiogenesis model', *Investigative Ophthalmology and Visual Science*, 51(6), pp. 2813–2826. doi: 10.1167/iovs.10-5176.

Stevenson, L. *et al.* (2010) 'Reduced Nitro-oxidative Stress and Neural Cell Death Suggests a Protective Role for Microglial Cells in TNFα $^{-/-}$ Mice in Ischemic Retinopathy', *Investigative Opthalmology & Visual Science*. The Association for Research in Vision and Ophthalmology, 51(6), p. 3291. doi: 10.1167/iovs.09-4344.

Stone, J. *et al.* (1995) 'Development of retinal vasculature is mediated by hypoxia-induced vascular endothelial growth factor (VEGF) expression by neuroglia', *J.Neurosci.*, 15(7 Pt 1), pp. 4738–4747. Available at: http://www.ncbi.nlm.nih.gov/pubmed/7623107.

Stone, J. *et al.* (1996) 'Roles of vascular endothelial growth factor and astrocyte degeneration in the genesis of retinopathy of prematurity', *Investigative Ophthalmology and Visual Science*, 37(2), pp. 290–299.

Stone, J. and Dreher, Z. (1987) 'Relationship between astrocytes, ganglion cells and vasculature of the retina', *J.Comp Neurol.*, 255(1), pp. 35–49. Available at: http://www.ncbi.nlm.nih.gov/pubmed/3819008.

Stout, R. D. and Suttles, J. (2004) 'Functional plasticity of macrophages: reversible adaptation to changing microenvironments.', *Journal of leukocyte biology*, 76(3), pp. 509–13. doi: 10.1189/jlb.0504272.

Suchting, S. *et al.* (2007) 'The Notch ligand Delta-like 4 negatively regulates endothelial tip cell formation and vessel branching.', *Proceedings of the National*

Academy of Sciences of the United States of America, 104(9), pp. 3225–30. doi: 10.1073/pnas.0611177104.

Tammela, T. *et al.* (2008) 'Blocking VEGFR-3 suppresses angiogenic sprouting and vascular network formation.', *Nature*, 454(7204), pp. 656–60. doi: 10.1038/nature07083.

Tan, S. M. *et al.* (2013) 'Lack of the Antioxidant Glutathione Peroxidase-1 (GPx1) Exacerbates Retinopathy of Prematurity in Mice', *Investigative Opthalmology & Visual Science*. The Association for Research in Vision and Ophthalmology, 54(1), p. 555. doi: 10.1167/iovs.12-10685.

Tannahill, G. M. *et al.* (2013) 'Succinate is an inflammatory signal that induces IL-1β through HIF-1α.', *Nature*. NIH Public Access, 496(7444), pp. 238–42. doi: 10.1038/nature11986.

Thompson, A. A. R. *et al.* (2014) 'Hypoxia-inducible factor 2α regulates key neutrophil functions in humans, mice, and zebrafish.', *Blood*, 123(3), pp. 366–76. doi: 10.1182/blood-2013-05-500207.

Tomlins, S. A. *et al.* (2005) 'Recurrent Fusion of TMPRSS2 and ETS Transcription Factor Genes in Prostate Cancer', *Science*, 310(5748), pp. 644–648. doi: 10.1126/science.1117679.

del Toro, R. *et al.* (2010) 'Identification and functional analysis of endothelial tip cell-enriched genes.', *Blood*, 116(19), pp. 4025–33. doi: 10.1182/blood-2010-02-270819.

Tremblay, S., Miloudi, K., Chaychi, S., Favret, S., Binet, F., Polosa, A., *et al.* (2013) 'Systemic inflammation perturbs developmental retinal angiogenesis and neuroretinal function.', *Investigative ophthalmology & visual science*. The Association for Research in Vision and Ophthalmology, 54(13), pp. 8125–39. doi: 10.1167/iovs.13-12496.

Trinchieri, G. and Sher, A. (2007) 'Cooperation of Toll-like receptor signals in innate immune defence.', *Nature reviews. Immunology*, 7(3), pp. 179–90. doi: 10.1038/nri2038.

Trollmann, R. and Gassmann, M. (2009) 'The role of hypoxia-inducible transcription factors in the hypoxic neonatal brain.', *Brain & development*, 31(7), pp. 503–9. doi: 10.1016/j.braindev.2009.03.007.

Uemura, A. *et al.* (2006) 'Tlx acts as a proangiogenic switch by regulating extracellular assembly of fibronectin matrices in retinal astrocytes', *J.Clin.Invest*, 116(2), pp. 369–377. Available at: http://www.ncbi.nlm.nih.gov/pubmed/16424942.

Watanabe, T. and Raff, M. C. (1988) 'Retinal astrocytes are immigrants from the optic nerve', *Nature*, 332(6167), pp. 834–837. Available at: http://www.ncbi.nlm.nih.gov/pubmed/3282180.

Weidemann, A. *et al.* (2010) 'Astrocyte hypoxic response is essential for pathological but not developmental angiogenesis of the retina', *Glia*. Wiley Subscription Services, Inc., A Wiley Company, 58(10), p. NA-NA. doi: 10.1002/glia.20997.

West, H., Richardson, W. D. and Fruttiger, M. (2005) 'Stabilization of the retinal vascular network by reciprocal feedback between blood vessels and astrocytes', *Development*, 132(8), pp. 1855–1862. doi: 10.1242/dev.01732.

Wilson, C. M. *et al.* (2008) 'Computerized analysis of retinal vessel width and tortuosity in premature infants.', *Investigative ophthalmology & visual science*, 49(8), pp. 3577–85. doi: 10.1167/iovs.07-1353.

Witmer, A. N. *et al.* (2003) 'Vascular endothelial growth factors and angiogenesis in eye disease.', *Progress in retinal and eye research*, 22(1), pp. 1–29. Available at: http://www.ncbi.nlm.nih.gov/pubmed/12597922 (Accessed: 15 August 2016).

Wu, W.-K. *et al.* (2010) 'IL-10 regulation of macrophage VEGF production is dependent on macrophage polarisation and hypoxia.', *Immunobiology*. Elsevier, 215(9–10), pp. 796–803. doi: 10.1016/j.imbio.2010.05.025.

Wynn, T. A. and Vannella, K. M. (2016) 'Macrophages in Tissue Repair, Regeneration, and Fibrosis.', *Immunity*, 44(3), pp. 450–462. doi: 10.1016/j.immuni.2016.02.015.

Yamasaki, Y. *et al.* (1995) 'Interleukin-1 as a pathogenetic mediator of ischemic brain damage in rats.', *Stroke*, 26(4), p. 676–80; discussion 681. doi: 10.1161/01.str.26.4.676.

Yamashiro, S. *et al.* (2001) 'Phenotypic and functional change of cytokine-activated neutrophils: inflammatory neutrophils are heterogeneous and enhance adaptive immune responses.', *Journal of leukocyte biology*, 69(5), pp. 698–704. Available at: http://www.ncbi.nlm.nih.gov/pubmed/11358976 (Accessed: 2 July 2018).

Yang, W.-J. *et al.* (2015) 'Semaphorin-3C signals through Neuropilin-1 and PlexinD1 receptors to inhibit pathological angiogenesis.', *EMBO molecular medicine*, 7(10), pp. 1267–1284. doi: 10.15252/emmm.201404922.

Yoshida, S. *et al.* (2003) 'Role of MCP-1 and MIP-1 ␣ in retinal neovascularization during postischemic inflammation in a mouse model of retinal neovascularization Abstract : Macrophages are important partici- pants in neovascularization . This study was de- ischemic retinopathy , p', 73(January), pp. 137–144. doi: 10.1189/jlb.0302117.Journal.

Zarkada, G. *et al.* (2015) 'VEGFR3 does not sustain retinal angiogenesis without VEGFR2.', *Proceedings of the National Academy of Sciences of the United States of America*, 112(3), pp. 761–6. doi: 10.1073/pnas.1423278112.